Development Of A Multiplex Sensing Platform For The Accurate And
Rapid Diagnosis Of Sepsis

A thesis submitted in accordance with the conditions

governing candidates for the degree of

Doctor Philosophiae in Cardiff University

By

Nikolaos Demertzis

M.Sc.

March 31st, 2020

Welsh School of Pharmacy and Pharmaceutical Sciences

Cardiff University

Acknowledgements

The present work describes a journey full of adventures and discoveries "Odyssey" and this single page is the minimum thing I can do to express my gratitude to people that marked this journey.

I have to personally thank all the people working at School who made me feel as a part of this large society. I would like to personally thank the technical staff who were always there to help and cover the lab's needs. I would like to also thank colleagues for all the quality times we spent in and out of the University's walls.

I would like to express my gratitude to all the members of the Bowen Lab of this three-year long era. Firstly, I have to thank Vibha for the introduction in electrochemistry and Andreas for the quality chats through the breaks. I really enjoyed working with all students who stepped in and supported the ongoing projects. Ben, Max, Sarah, Clare, Dilraj, Chalina and Natalie, it's my turn now to say a big thanks for everything you've made during your presence in the Lab. Each and everyone of you changed the Lab's mood in a very positive way. My biggest thanks goes to Mafalda, for all the collaboration, support and laughs we had throughout her time in Cardiff.

I would also like to personally thank all the previous collaborators and mentors who never stopped supporting me throughout my studies and continued to build up stronger relations.

Lastly and most importantly, I have to express my thanks to Dr Jenna Bowen. Thanks for believing in me, for making a dream come true, for helping me reach my own "Ithaka". The present work wouldn't exist if she didn't make the call to bring me to the UK and work in the lab and Cardiff University. Jenna undoubtedly belongs to the closed group of people I call mentor and I am sure that this collaboration has marked me for the rest of my life.

Summary

Sepsis derives from an uncontrolled response of the host immune system to a pathogenic insult. The complex, rapidly evolving nature of the condition makes diagnosis difficult, and to date a single 'gold-standard' biomarker has not been reported. An increasing number of studies suggest that monitoring of a panel of biomarkers, ideally at point-of-care, is needed. The present study therefore focused on the development of a multiplex biosensing platform targeting lipopolysaccharide (LPS), c-reactive protein (CRP), and procalcitonin (PCT).

The study designed a series of electrochemical sensors targeting the three selected biomarkers. Whilst all systems employed aptamers as the recognition element, a hybrid system combining aptamer and molecular imprinting technology was also developed for LPS. Following optimisation of sensor design, electrochemical impedance spectroscopy was used to evaluate performance (binding affinity (K_d), sensitivity, selectivity and dynamic range).

Aptasensors were developed for all markers with varying degrees of success. Whilst the optimised aptasensors for LPS and CRP demonstrated good performance, the PCT aptasensor showed poor stability. Despite these issues however, a limit of detection (LOD) of ~ 25 pg/ml was achieved. LODs for LPS and CRP were 100 and 250 fg/ml respectively. The use of a hybrid imprinting approach further enhanced the performance of the LPS detection system, taking the LOD down to 1 fg/ml whilst also increasing binding capacity.

Although aptamer-based sensing systems have been described for LPS and CRP, to the best of our knowledge, this is the first report of a such a system targeting PCT. The hybrid imprinting strategy exploited in the study has previously been demonstrated for prostate specific antigen, however this is the first report of such an approach being used for non-protein targets. The recognition of such molecules using conventional imprinting approaches has been largely unsuccessful; the method described herein should be translatable to other biologically relevant targets.

Table of Contents

List of Figures

Chapter 1

Chapter 2

Chapter 3

Chapter 5

List of Tables

Chapter 1

Table 1.1: Potential biomarkers being used for the detection of sepsis in clinical studies as presented by Pierrakos et al. Biomarkers marked with * have shown sensitivity and specificity more than 90%. aPTT: activated partial thromboplastin time; ARDS: acute respiratory distress syndrome; CRP: C-reactive protein; DIC: disseminated intravascular coagulopathy; EA: elastase alpha 1-proteinase inhibitor; ELAM: endothelial leukocyte adhesion molecule; G-CSF: granulocyte colony-stimulating factor; IP: interferon-induced protein; LBP: lipopolysaccharide-binding protein; MCP:

General Introduction

1.1 Project Overview

Sepsis is a life-threatening condition, defined as an "organ dysfunction caused by a dysregulated host response to infection" (1). It is a complex, rapidly evolving condition resulting from uncontrolled and prolonged activation of host immune system due to pathogenic insult (2,3). Pathogen and host immune mediators act together to induce an exaggerated and catastrophic systemic immune response completely unequal to the initial infection. Despite the fact that the sepsis incidents may have been decreased over the years (from 60 million cases in 1990 to ~ 50 million cases in 2017), the mortality rates are still high, with one out of five deaths globally linked to the condition (4).

The condition's complexity impedes the rapid and definitive diagnosis, as clinicians try to detect sepsis by combining non-specific physiological and laboratory anomalies (5). The lack of a gold standard in sepsis diagnosis is quite obvious when one considers that more than 170 potential biomarkers have been reported in the literature. To date, no sepsis-specific marker exists and it is widely accepted that a panel of markers will be needed in order to achieve the requisite clinical specificity and sensitivity (6).

This project was focused on the development of a multiplex sensing platform, capable of detecting both pathogen-associated and host immune markers. Therefore, the biomarkers of choice were lipopolysaccharide (LPS), c-reactive protein (CRP) and procalcitonin (PCT).

Lipopolysaccharide (LPS), also known as endotoxin, is the major pathogenic determinant of Gram-negative bacteria and is ubiquitously associated with sepsis as a consequence of endogenous stores (7). To date, the most commonly used method to detect LPS is the Limulus Amoebocyte Lysate (LAL) assay. However, LPS is hard to recover from clinical samples and the sample matrix itself has a profound effect on the LAL assay, making existing detection methods unreliable diagnostic tools (8). One of the project's key objectives was to develop an electrochemical impedance sensor capable of sensitive, direct detection of LPS. The first intention was to develop an aptasensor capable of detecting the molecule in low concentrations. The aptasensor will rely on the chemistry of self-assembled monolayers (SAM), however it is largely uncertain if the system's sensitivity will be enough to determine LPS' clinical cut-off during the progression to septic response. The ultimate goal was the generation of a hybrid recognition system, integrating aptamer and molecular imprinting technologies. This theory builds upon the

group's recent success in developing a similar system for the detection of prostate specific antigen (PSA), where a low picomolar limit of detection was achieved (9).

C-reactive protein (CRP) is one of the most common markers of systemic inflammation and has been used in the diagnosis of sepsis for many years (10–12). Despite CRP's lack of specificity, the biomarker remains in routine use in clinical care to continuously monitor the patients' condition (13). For this reason, the development of a CRP biosensor would be a considerable part of the platform.

Procalcitonin (PCT) is considered as an important biomarker for the determination of bacterial infections, allowing differentiation from viral infections or other illnesses of non-infective origin (14). PCT was first characterised as a sepsis marker in 1993 (15). Since then, the biomarker has been proposed by numerous studies as a highly prognostic biomarker for sepsis, but its efficiency is controversial (16–18).

1.2 History of sepsis

Sepsis was first described more than 3000 years ago, with numerous reports found throughout human history. The very first report describing sepsis comes from ancient Egypt (19). In 1862, the American dealer Edwin Smith, purchased a papyrus at Luxor. The so-called Edwin Smith papyrus was written in around 1600 BC and appears to be a copy of an older manuscript that was prepared in 3000 BC. The Edwin Smith papyrus reported 48 cases of traumatic lesions from wounds, fractures and dislocations in different parts of the body, along with their symptoms, progression, prognosis and treatment. The association between sepsis and wound healing was described both directly and indirectly; fever was reported as a secondary phenomenon in 5 cases where the person was suffering from a wound, while the 47th case describes the flesh of an open wound on the shoulder turning black.

The word sepsis derives from the original Greek word "σήψις" (sipsis), describing the decay or the putrefaction of the human body (20). The word could be also used to describe the decomposition of animal or vegetable organic matter. The word σήψις derives from the verb σήπω (sipo) which means "I rot" (20). The verb can be found for the very first time in Homer's Iliad; Priam goes to the Greek camp to find Achilles and begs to take

Hector's corpse. Prior to meeting, Priam asks a Greek soldier where Hector's body is and the second replies (lines 411-415):

ὦ γέρον οὔ πω τόν γε κύνες φάγον οὐδ᾽ οἰωνοί,	No, old man, dogs and birds haven't eaten him,
ἀλλ᾽ ἔτι κεῖνος κεῖται Ἀχιλλῆος παρὰ νηῒ αὔτως ἐν κλισίῃσι· δυωδεκάτη δέ οἱ ἠὼς κειμένῳ, οὐδέ τί οἱ χρὼς *σήπεται*, οὐδέ μιν εὐλαὶ	your son lies unharmed next to Achilles' ship, inside the hut. 12 days have passed since (your son) lies in this state, and his body neither *rots* nor the worms that eat all
ἔσθουσ᾽, αἵ ῥά τε φῶτας ἀρηϊφάτους κατέδουσιν.	the dead due to war have touched him

Sepsis was introduced as a medical concept many years later by Hippocrates (460-370 B.C.), as one can find the term in "*Corpus Hippocraticum*", used interchangeably with the word σηπεδών (sipedon / sepidon) (20). Σηπεδών had the definition of the decay of webs (Epidemic. B. 2,2, Prorret. I. 99). Hippocrates tried to treat the infection and sepsis by applying a mixture of myrrh (resin deriving from trees of the genus *Commiphora*), wine and inorganic salts on wounds (21). Other distinguished Greek polymaths such as Aristotle, Plutarch and Galen (Roman physician of Greek origin) used the word σήψις as first defined by Hippocrates. In fact, the Greeks described pepsis (digestion) and sepsis as two stages of "breakdown" (22). Two centuries later, Marcus Terentius Varro (116 B.C. –27 B.C.) in "*De re rustica libri III*" noted that "small creatures, invisible to the eye, fill the atmosphere, and breathed through the nose cause dangerous diseases" (21).

However, the most accurate description of sepsis came from Niccolo Machiavelli (1469–1527), as in 1513 he described sepsis as 'hectic fever, at its inception, is difficult to recognize but easy to treat; left unattended it becomes easy to recognize and difficult to treat' (23). A few decades later (1546), Hieronymus Fracastorius established the germ theory in his *''De contagione et contagiosis morbis''*(24).

Significant progress has been made to further understand the development of infection during the 17th century. Francisco Redi (1626–1697) conducted experiments to refute the spontaneous generation of infection, by observing the putrefaction of meat (21). The century's milestone belongs to Anthony van Leeuwenhoek (1632–1723), who managed to build a compound microscope and described bacteria for the very first time, using the term "animalcules", in 1674 (25). Following van Leeuwenhoek's landmark observations, the 19th century can be described as the era that saw microbiology flourish. Scientists such as Joseph Lister, Ignaz Semmelweiss, Louis Pasteur and Robert Koch worked on the origin and development of infectious diseases, providing important information about the etiopathogenesis of septic responses (24) .

The discovery of early antibiotics appears in 1905. Until then, the therapy for infectious diseases was strictly empiric. Paul Erlich (1845–1915), discovered a compound containing arsenic (salvarsan) that was able to kill *Treponema pallidum*, without affecting the host. This later became the standard treatment of syphilis (24). A few decades later, a British doctor, Alexander Flemming (1881-1955), who served during World War I, observed that many of the soldiers died from profound infectious phenomena and sepsis. These observations triggered his interest to discover a cure for infections. In 1928, Flemming discovered, by accident, the famous anti-microbial penicillin and cemented a brand new era of drug discovery (26).

Although the clinical definition of sepsis has changed over the years, the condition remains notoriously difficult to identify and diagnose. Nowadays, sepsis is the leading cause of death in non-coronary intensive care units worldwide. Its mortality rates can reach up to 50%, with one out of two/three hospital deaths being related to sepsis (27,28).

1.3 Etiopathogenesis and progression epidemiology of Sepsis

1.3.1 Immunopathogenesis of sepsis

As previously described, sepsis develops in the presence of an infection and can be characterised as extremely complex (1). It involves pro-inflammatory and anti-inflammatory processes combined with humoral and cellular reactions and circulatory abnormalities (6,29,30). This complexity gives rise to a number of non-specific symptoms, thus making the condition difficult to diagnose.

The molecular background of the immunopathogenesis of sepsis is well established and has been described extensively by Cohen (2002) and Russel (2006) amongst others (31–33). Sepsis destabilises the normal equilibrium between procoagulant and anticoagulant mechanisms, inflammatory pathways and activates the complement system. Figure 1.1 shows the key molecules of the immune response that lead to the pathogenesis of sepsis. In the first instance, cell wall components of pathogens bind to pattern-recognition receptors (e.g. toll-like receptors, TLRs) on the surface of immune cells (33). These pathogen-associated molecular patterns are unique to each membrane component and therefore, they interact with different TLRs (34). For example, the peptidoglycan of Gram-positive bacteria and lipopolysaccharide (LPS) of Gram-negative bacteria bind to TLR-2 and TLR-4, respectively (35). These interactions trigger the activation of a number of intracellular signal-transduction pathways.
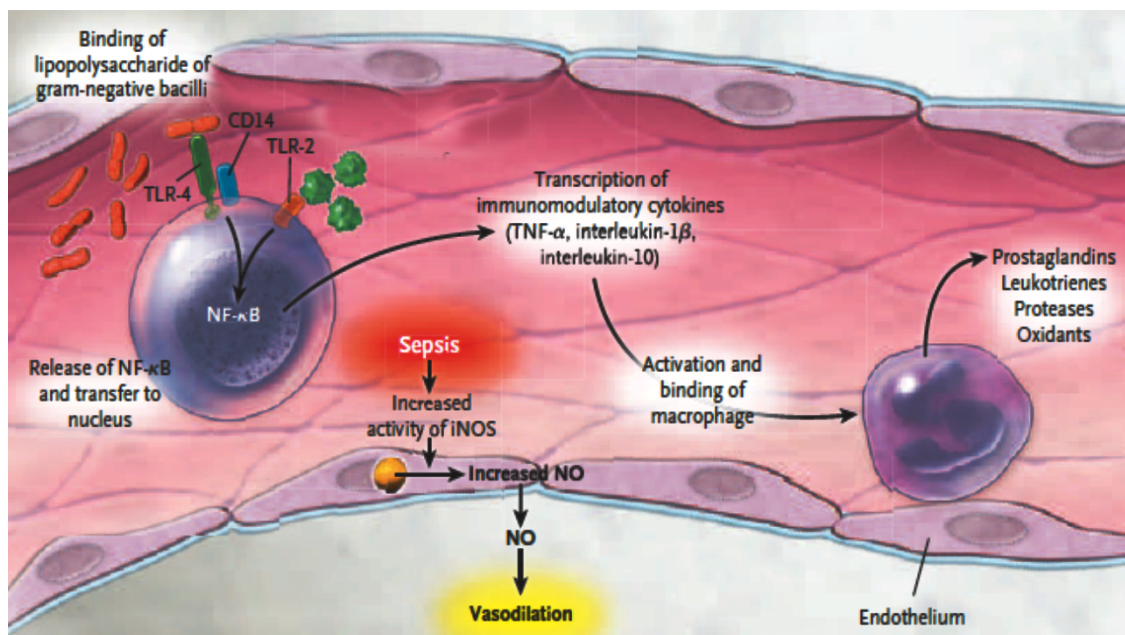
Figure 1.1: The pathophysiology of sepsis (33). Cell wall components (e.g. LPS) bind on pattern recognition receptors on the surface of immune cells, triggering the activation of intracellular signal-transduction pathways. High levels of Nitric Oxide (NO) lead to vasodilation and consequently the release of cell lysis mediators such as proteases, oxidants, prostaglandins and leukotrienes.

The initiation of this cascade results in the activation of the cytosolic nuclear factor κB (NF-κB), that subsequently relocates to the nucleus and increases the transcription rates

of cytokines such as tumor necrosis factor α (TNF-α), interleukin-1β, and interleukin-10 (36). It is well established that TNF-α and interleukin-1β are pro-inflammatory cytokines that activate the adaptive immune response, however they can also cause both direct and indirect host injury (37). On the other hand, Interleukin-10 is an anti-inflammatory cytokine that can suppress the macrophage activity (38).

Moreover, the activity of nitric oxide synthase (iNOS) is increased during sepsis, elevating the levels of nitric oxide (NO) (39). NO is known to be a potent vasodilator. Cytokines can activate endothelial cells by up-regulating adhesion receptors. However, endothelial cells can be potentially injured by the same molecules, as they induce neutrophils, monocytes, macrophages, and platelets, which bind to the cells. This results in the release of mediators such as proteases, oxidants, prostaglandins and leukotrienes; their role is to increase the cell membrane permeability and then promote cell lysis (33). The procoagulant-anticoagulant equilibrium is unbalanced as the cytokines regulate the activation of the coagulation cascade.

The coagulation cascade is also initiated as part of the septic response, as the endothelium has been activated in order to increase the expression of tissue factor (33). The activation of factors Va and VIIIa leads to the formation of thrombin-α, converting fibrinogen to fibrin (40,41). As a result, the fibrin binds to platelets, which adhere to endothelial cells and they develop microvascular thrombi, amplifying the injury's effect. These thrombi have the potential to cause distal ischemia and tissue hypoxia by microvascular obstruction, often meaning that patients need to undergo amputations (33).

On the contrary, molecules such as protein C and S diminish coagulation by favouring fibrinolysis and removal of microthrombi. More precisely, thrombin-α binds to thrombomodulin on the surface of endothelial cells, increasing dramatically the protein C activation (42) (Figure 1.2). Then, the activated protein C forms a complex with its co-factor protein S, leading to the suppression of the factors Va and VIIIa and decreasing the plasminogen-activator inhibitor 1 (PAI-1) synthesis (40,41,43).
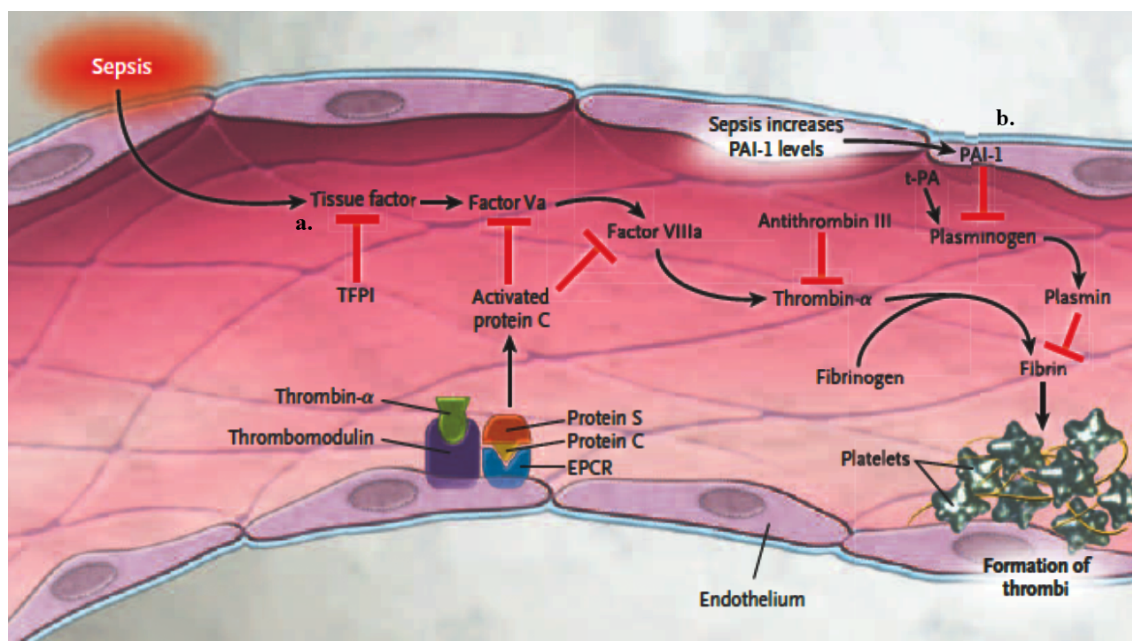
Figure 1.2: The release of cytokines regulates the activation of the coagulation cascade during sepsis (33). a) The activated factors Va and VIIIa lead to the formation of thrombin-α and b, converting fibrinogen to fibrin. The signal transduction remains at high levels due to the decrease of protein C levels. b) Sepsis increases the PAI-1 levels, inhibiting fibrinolysis.

However, data shows that sepsis increases the synthesis of PAI-1 and decreases protein C levels (or anticoagulants in general) via the presence of LPS and TNF-α (44,45). The protein C pathway is further disrupted due to the decrease of the endothelial protein C receptor (EPCR) expression. Moreover, LPS and TNF-α regulate positively the PAI-1 levels resulting in the inhibition of fibrinolysis. The consequences of the changes in coagulation caused by sepsis are increased levels of biomarkers that indicate disseminated intravascular coagulation and widespread organ dysfunction (33).

1.3.2 Epidemiology of sepsis

The worldwide incidence of sepsis reached an estimated 48.9 million cases in 2017 (4). However, this number may be much higher due to under-diagnosis of the condition (46). The prevalence of severe sepsis is 90.4 cases per 100,000 people in European Union. This proportion is relatively high when compared to the development of other diseases such as breast cancer (58 cases per 100,000 people). In the USA, the reported cases of sepsis per

100,000 people are more than stroke, myocardial infarction, and lung, breast and prostate cancer combined (47) (Figure 1.3).
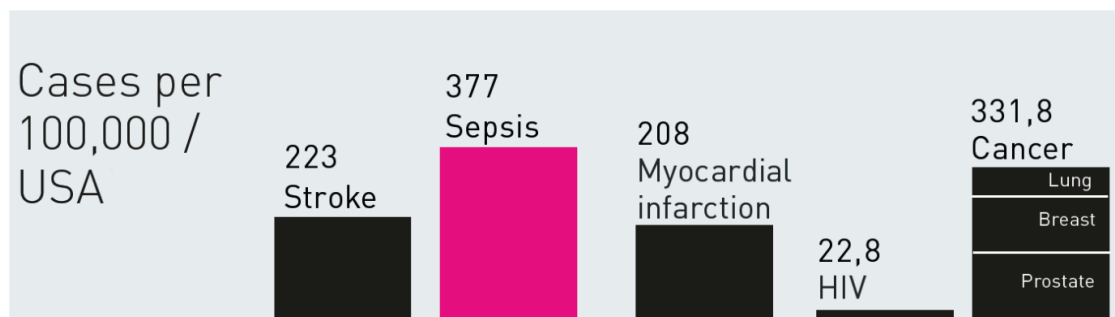
Figure 1.3: Prevalence of Sepsis in Cases per 100,000 people in USA (48).

Sepsis is reported as a leading cause of death in hospitals of the United States of America; it accounted for five times as many deaths as heart disease in 2013 (49). In the United Kingdom, more than 250,000 people are reported to suffer from sepsis per year and approximately 44,000 patients lose their lives (50). In addition, sepsis is responsible for more deaths per year in the UK when compared to other conditions, such as bowel or breast cancer (51).

Due to an increasingly ageing population and the ever-growing issue of antimicrobial resistance, sepsis is not going away (52,53). It appears that the advantages of modern medicine are not enough to counter the increasing rates of sepsis. More precisely, hospitalisations due to sepsis incidents have doubled over the last decade (53,54). International and national surveys highlight the fact that 20-40% of septic patients admitted to intensive care units, developed sepsis outside the hospital (55). The incidence of patients developing sepsis after surgery trebled during the period 1997 – 2006 (47).

Although sepsis is non-discriminatory in nature, meaning that it is a global healthcare problem, in the Western World (UK, Europe, North America, Australasia) deaths related to sepsis generally sit below 10 % according to epidemiologic data provided by Rudd *et al.* (4). On the other hand, more than 25 % (sometimes as high as 65%) of deaths are related to sepsis in central and South Africa (Figure 1.4).
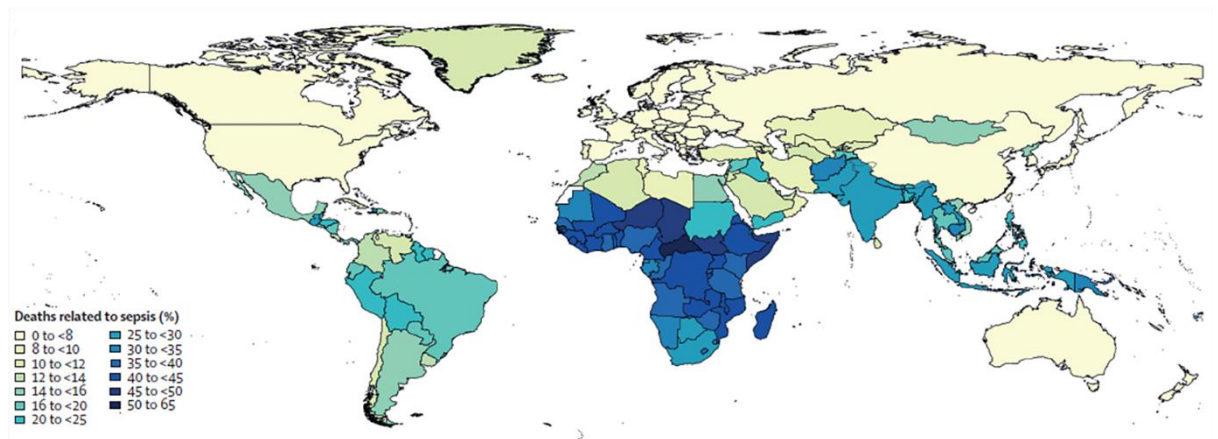
Figure 1.4: World map showing the deaths related to sepsis (%) across countries (epidemiologic data of 2017) (4).

The United States Government spent approximately $14.6 billion in 2008 on treating people hospitalised with sepsis. From 1997 to 2008, the costs for treating septic patients increased annually by 11.9% (on average) (56). However, the costs related to long-term hospitalisations are still unknown. According to data deriving from Europe, a typical septic episode is estimated to cost around 25,000 €. The UK sepsis Trust estimates that hospitalisations cost the NHS in England approximately £2.5 billion per year, while the average cost of care corresponds to £20,000 per patient. In addition to that, considering the loss of life years, the human cost of sepsis is incalculable (57).

Despite sepsis being a leading cause of death worldwide, the research funds being spent for its treatment and diagnosis are small when compared to other conditions (47). In 2011, state-funded research for management of sepsis amounted to ~ $91 million, while that spent on researching HIV was around $2.9 billion. This cost difference is enormous, since the prevalence of HIV equals to only 22.8 cases per 100,000 people in USA and Europe (Figure 1.5).
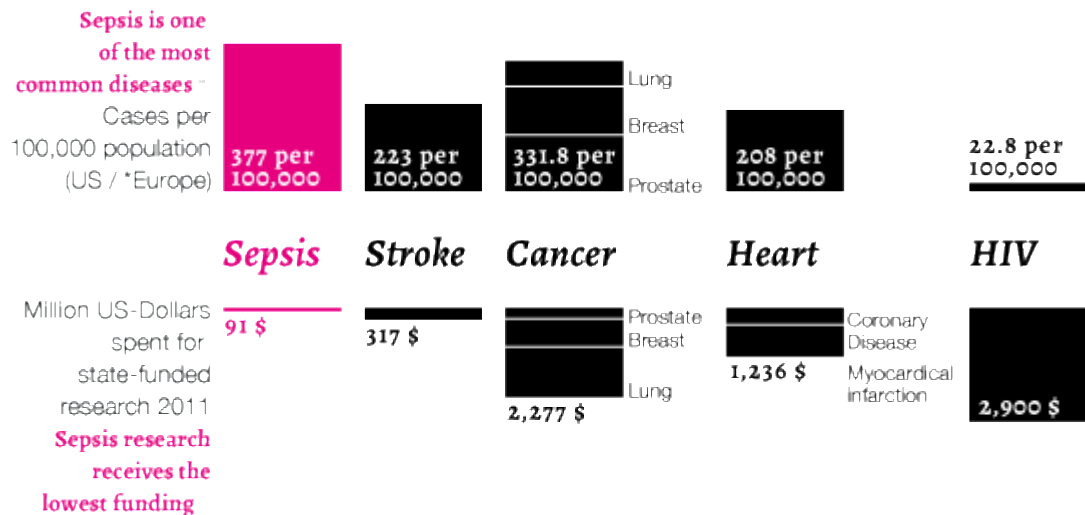
Figure 1.5 Prevalence of sepsis, stroke, cancer, heart diseases and AIDS in Europe and USA, in comparison to million US $ spent for state-funded research in 2011 (48).

1.3.3 Clinical presentation of sepsis

In 1989, Bone *et al* proposed the term 'sepsis syndrome' to describe critically ill patients who showed clinical and laboratory signs of severe infection (58,59). In order to diagnose the systemic inflammation during sepsis, the patients had to present with at least two of the following signs: elevated heart rate, elevated respiration rate, decreased blood pressure, hyper- or hypothermia and leukocytosis or leukopenia (60). This state was later defined as the 'Systemic Inflammatory Response Syndrome' (SIRS).

A consensus was created, three years later, to further develop the concept of sepsis and SIRS. The aim was to divide sepsis into stages and discriminate between infectious and sterile / non-infectious causes of systemic inflammation (61). There is a chain that starts from infection, progresses to sepsis and then to severe sepsis. The end of this chain leads to the most catastrophic stage of the septic shock, when mortality rates as high as 50% are not uncommon (Figure 1.6) (60).

According to Figure 1.5, SIRS may follow a wide variety of clinical insults such as: infection, pancreatitis, ischemia, multiple trauma, tissue injury, hemorrhagic shock, or immune-mediated organ injury (60). The next stage is the development of sepsis as a systemic response to infection (60). The current stage shows similarities to SIRS, as 2 of

the SIRS signs must be diagnosed. However, there is a crucial detail that discriminates the two sides: sepsis must result from an infection.

The condition progresses to severe sepsis when the patient shows all the symptoms from the previous stage combined with dysfunction of at least one remote organ (59). Finally, the patient proceeds to septic shock, demonstrating the symptoms of severe sepsis plus hypotension despite adequate fluid resuscitation (60).
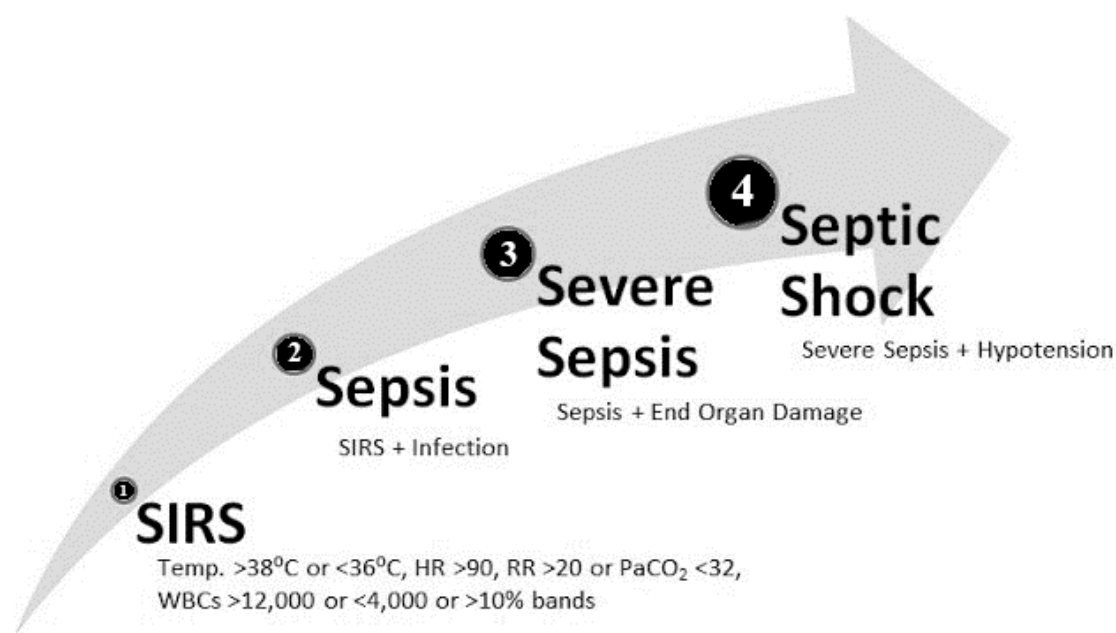
Figure 1.6: The four stages of the sepsis continuum (62). *According to the incident severity, the patient presents with at least two symptoms indicative of systemic inflammation (SIRS) (1). Once an infection is identified as the cause of these SIRS symptoms, the patient is diagnosed as having sepsis (2). If sepsis progresses to the point at which organ damage is present, the patient is said to be suffering from severe sepsis (3). The final stage is septic shock (4) where the patient is profoundly hypotensive despite adequate fluid resuscitation.*

The division of sepsis into discrete stages set some serious obstacles regarding its diagnosis and treatment. The accurate diagnosis and timely clinical evaluation of each patient is crucial to allow initiation of effective treatment. It is worth noting that it is sometimes difficult to get a definitive diagnosis of infection, with culture negative sepsis being relatively common (63).

In early 2016, the Society of Critical Care Medicine and the European Society of Intensive Care Medicine released a consensus statement (Sepsis 3.0) which redefined the clinical syndrome of sepsis (1). The new diagnostic criteria excluded the concept of SIRS from the diagnosis and, in recognition of the diagnostic delay conferred by waiting for positive confirmation of an infection, changed the wording to "*known or suspected infection."* A quick Sequential Organ Failure Assessment (qSOFA) score threshold of ≥ 2 was introduced for the purposes of prioritising patients; a qSOFA score ≥ 2 suggests the patient is at higher risk of a poorer outcome. This move has raised some controversy from physicians who expressed their concerns as the SOFA's widespread application is likely to cost patient lives (61).

Since sepsis derives from an infection, the biomarkers that have been used for its diagnosis are non-specific (6). The main diagnostic tool is blood cultures that need time and are not always accurate, providing false negative results (64). A delay in diagnosis may lead to significant increase in mortality rates. However even if the patient survives, their quality of life is often impaired. Sepsis shows a devastating effect in physical (insomnia, dysphagia), psychological (post traumatic distress syndrome) and cognitive (memory, concentration) aspects (65). Sepsis survivors are prone to develop new infections, requiring further hospital readmissions (66). In fact, up to 63 % of the patients will be re-hospitalised within the first year of survival (67). Beside the increased morbidities, up to 60 % of survivors die within the first 3 years after the septic response (68). Apart from the detrimental loss of the quality of life, it can be referred that the healthcare systems have to manage a huge amount costs, deriving from the number of days each patient remains in the intensive care unit of a hospital. Regarding the present diagnostic standards, the need to develop an accurate and sensitive tool is urgent.

1.4 Sepsis biomarkers

According to the above information, biomarkers play a very important role in the diagnostic process; ideally they should not only be able to indicate the presence sepsis but also provide information with regard to severity / prognosis (6,69,70). It is highly desirable if a potential biomarker can discriminate between systemic and local infections. However, its exact role to the management of septic patients remains undefined, due to the non-specific nature of signs and symptoms (71).

The literature reports 178 potential biomarkers for the diagnosis of sepsis (6); 18 have been evaluated in experimental studies only, 58 in both experimental and clinical studies and 101 in clinical studies only. Despite the biomarker abundance, only 34 of have been used specifically for the diagnosis of sepsis (Table 1.1). The vast majority of biomarkers (if not all of them) displayed on the table below are upregulated during the development of sepsis. Only a few exceptions such as troponin (used to diagnose myocardial dysfunction), are not connected with the biochemical cascade due to the immune response. If one considers their specificity and sensitivity, only five of the demonstrated biomarkers report convincing values (6).

Sepsis Biomarker	Outcome
aPTT	High negative predictive value
CD11b	Higher values in neonates with sepsis than in those with possible infection
CD25*	Distinguished between sepsis and SIRS
CD64*	Low sensitivity and specificity to distinguish between viral and bacterial infections
Complement (C3, C4, C5a)	Distinguished between sepsis and SIRS
EA complex	Diagnosis of sepsis, increased earlier than CRP
ELAM-1 (cellular and soluble)	Increased in trauma patients with sepsis compared with no sepsis
Endocan	Distinguished between sepsis and SIRS
E-Selectin (cellular and soluble)	Distinguished between sepsis and SIRS
Fibrin degradation products	High negative predictive value
Gas6	Higher values in patients with severe sepsis compared with patients with organ failure but no sepsis
G-CSF	Distinguished between sepsis and SIRS
Gelsolin	Higher in septic patients compared with patients without sepsis
IL-1 receptor antagonist	Early diagnosis of sepsis before symptoms in newborns
IL-8	Higher in septic neutropenic patients compared with febrilneutropenic patients without sepsis
IL-10	Higher in septic shock compared with cardiogenic shock
IL-12*	Diagnosis of sepsis in pediatric patients
IL-18	Distinguished between Gram-positive and Gram-negative sepsis. Higher in trauma patients with sepsis than in those without
IP-10*	Early diagnosis of sepsis in newborns
Laminin	Distinguished between Candida sepsis and bacterial sepsis
LBP	Distinguished between Gram-positive sepsis and Gram-negative

MCP-1	Distinguished between sepsis and SIRS in neutropenicpediatric patients
NO, nitrate, nitrite	Higher in septic shock compared with cardiogenic shock
Osteopontin	Distinguished between sepsis and SIRS
PAI-1	Higher in patients with sepsis and DIC compared with no-septic patients with DIC
Pentraxin 3	Distinguished between septic shock and SIRS
Peptidoglycan	Higher in postoperative patients with infection compared with no-infected postoperative patients
pFN	Distinguished between sepsis and SIRS
PLA2-II (soluble)*	Distinguished between bacteremic and non-bacteremic infections
Serum lysozyme (activity)	Distinguished between sepsis and organ rejection in transplanted patients
ST2 (soluble)	Higher in septic patients compared with those with no sepsis
Surfactant protein (A, B, C, D)	Early diagnosis of ARDS in septic patients
3 TREM-1 (soluble)	Distinguished between sepsis and SIRS, diagnosed pneumonia
Troponin	Diagnosis of myocardial dysfunction in septic patients

*Table 1.1: Potential biomarkers being used for the detection of sepsis in clinical studies as presented by Pierrakos et al. Biomarkers marked with * have shown sensitivity and specificity more than 90%. aPTT: activated partial thromboplastin time; ARDS: acute respiratory distress syndrome; CRP: C-reactive protein; DIC: disseminated intravascular coagulopathy; EA: elastase alpha 1-proteinase inhibitor; ELAM: endothelial leukocyte adhesion molecule; G-CSF: granulocyte colony-stimulating factor; IP: interferon-induced protein; LBP: lipopolysaccharide-binding protein; MCP: monocyte chemotactic protein; NO: nitric oxide; PAI: plasminogen activator inhibitor; pFN: plasma fibronectin; PLA2: phospholipase A2; SIRS: systemic inflammatory response syndrome; TREM: triggering receptor expressed on myeloid cells (6).*

Beyond the typical markers of infection and inflammation, there is little consensus on the clinical usefulness of other markers under investigation, meaning that groups often focus on their preferred marker of interest. For instance, Nupponen *et al.* demonstrated that CD11b's levels can show whether a patient has sepsis or just SIRS (72). Nuutila *et al.* and Cardelli *et al.* showcased CD64 as a potential biomarker, due to its high specificity and sensibility to distinguish between viral and bacterial infections (73,74). In addition to CD64, Rintala *et al.* showed that the soluble for of PLA-II can discriminate bacterial from non-bacterial infections (75). Il-12 seems to be a helpful biomarker to detect sepsis in paediatric patients, but the reported results do not apply for older groups (76). Interferon gamma-induced protein 10 (IP-10) has shown interesting results in neonates (77).

Despite the apparently positive results, none of these markers are in routine clinical use at the time of writing. Instead, clinicians tend to use standard clinical blood tests (white blood cell count, liver function tests, lactate and electrolytes), which require analysis in centralised laboratories meaning that results are often not available for a number of hours / days, depending on the test of interest. C Reactive Protein (CRP) has been used to help in the diagnosis of sepsis for many years (78,79). However, CRP has been highly criticised for its low specificity as biomarker (80). Researchers have proposed procalcitonin (PCT) as a better alternative. It seems that PCT is a more specific and prognostic marker, yet its efficiency is controversial (81–83). Furthermore, PCT tests are relatively expensive and therefore many health boards will only allow tests to be requested by critical care clinicians. Both CRP and PCT are currently tested for centrally, rather than utilising point-of-care technologies. The role of endotoxin (LPS) in sepsis has been extensively described in the literature. Despite its importance, LPS is not a frequently measured biomarker, due to a number of limitations associated with current testing methods. More information about endotoxin, CRP and PCT, as well as the current testing methodologies is provided in Chapters 2 and 4 respectively.

1.5 Aptamers

Aptamers are synthetic single stranded (ss) oligonucleotide molecules (84). The term results from the conjugation of the Latin word "*aptus*" (= to fit) with the Greek word "*μέρος*" (= meros, part). Aptamers can be either DNA or RNA sequences and demonstrate biorecognition properties similar to that of antibodies, targeting a wide variety of molecules, ranging from small ions to proteins (85). Some papers demonstrate that aptamers can even recognise whole cells (86).

The use of aptamers has been extensively described in the fields of (bio-)analysis, diagnostics and therapeutics (87). Aptamers are 20-50 nucleotide long sequences, flanked by two conserved primer binding sites (88). These sites, apart from being used for PCR amplification purposes, are also characteristic to the generated library. Despite their relatively small molecular weight (5 to 30 kDa), aptamers can display large surface areas that confer a high level of affinity to their targets (89). These molecules can interact via hydrogen bonding, structure compatibility, stacking of aromatic rings, electrostatic and hydrophobic interactions and van der Waals forces (88).

Aptamers are derived from an *in vitro* selection process, called SELEX (**S**ystematic **E**volution of **L**igands by **EX**potential enrichment) (88). The process was first described in 1990 by the independent works of Tuerk & Gold and Ellington & Szostak (90,91). According to Figure 1.7, the classic SELEX process consists of four stages. The first stage describes the development of an oligonucleotide library containing up to 10^{15} unique sequences (90). Each molecule is a randomly generated sequence. The oligonucleotide library is then incubated with the target molecule, during the selection stage. On completion of this stage, the unbound molecules are removed by a variety of washing steps, while the bound are amplified by PCR (reverse transcription PCR in the case of RNA aptamers). This activity generates a new, smaller group of sequences capable of binding to the target. However, the level of affinity and specificity remains rather ambiguous, thus the newly formed group proceeds to a second selection round. This process is repeated multiple times with only the molecules demonstrating increasingly high affinity proceeding to the next stage. At the end of the selection stages the aptamers are sequenced and their properties further explored and evaluated.
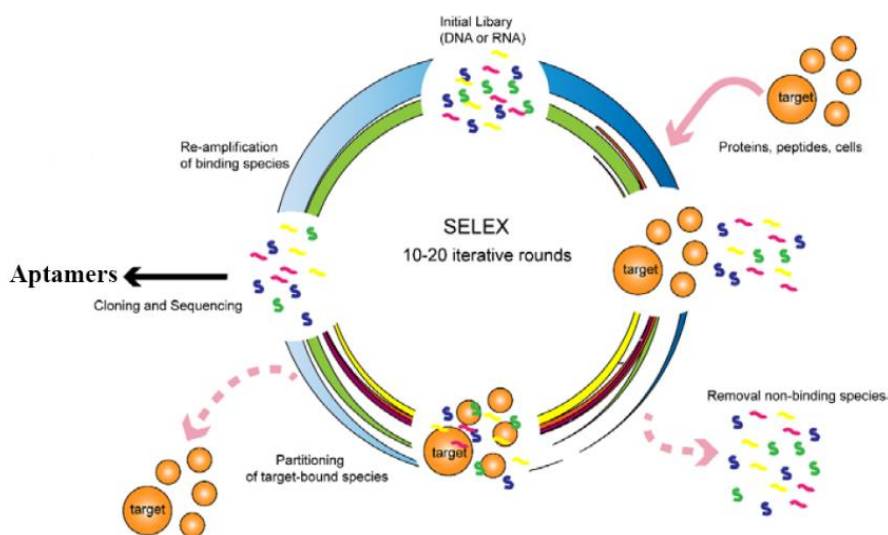
Figure 1.7: The conventional SELEX process for the generation of DNA & RNA libraries (88). The initial library of oligonucleotides is challenged with the target molecules. The bound molecules are sorted from the unbound ones during the washing process. This process is repeated multiple times until the molecule(s) with highest affinity are cloned and sequenced.

Due to its nature, the SELEX process is time-consuming; it takes weeks to months to generate sequences with high specificity towards the target. Furthermore, as the process starts with a vast number of random oligonucleotide sequences, it is possible that none of these possess the desired biorecognition properties. To overcome these problems, the SELEX method has been modified by various approaches. For example, negative or counter SELEX, combining capillary electrophoresis or microfluidics with SELEX or by using whole cells as targets so that the target is presented in its native conformation (88). However, tweaking the SELEX process will not solve all the problems; the process is still reliant on *in vitro* approaches and therefore, their functionality in *in vivo* settings has to be further elucidated.

Low dissociation constants (K_d), in the range of micro- to picomolar, are typically observed with aptamer recognition systems (92). The affinities observed are therefore highly comparable to antibodies but aptamers possess a number of significant advantages (Table 2.1) (88). Antibodies are highly immunogenic, while aptamers record miniscule humoral responses. In addition to that, antibodies are targeting only immunogenic molecules, while aptamers can recognise a wide range of targets. Antibodies are produced *in vivo*, therefore they are extremely costly, unstable and their generation takes ~ 6 months. On the other hand, aptamers are produced *in vitro* and as a result, they are low cost, stable and faster to develop. Due to their oligonucleotide properties, aptamers are easier to modify.

Features	Antibodies	Aptamers
Immunogenicity	High	No humoral response
Potential Targets	Immunogenic molecules	Wide range of targets
Production	*In vivo*	*In vitro*
Cost	High	Low
Stability	Unstable	Highly stable
Generation Time	~ 6 months	~ 3-7 weeks
Modification	Limited	Facile

Table 1.2: The use of aptamers demonstrates a series of advantages over antibodies (88).

Aptamers may also find future application as novel therapeutics. Pegaptanib (Macugen; Pfizer / Eyetech) was the first ever aptamer-drug to receive FDA / EMA approval for market release (89). However, as of late June 2019, pegaptanib has been withdrawn from the European Union at the request of PharmaSwiss, the current market-authorisation holder (93). A number of other aptamer-based therapies have failed in clinical trials, suggesting there is still some way to go in order to realise their full therapeutic potential (94).

1.5.1 Aptasensors

The easily accessible 5' and 3' primers of the oligonucleotide sequences provide a relatively straight-forward route for chemically modifying the aptamer; various functional groups can be readily attached / conjugated using facile chemistry approaches, without (probably) interrupting the 3D structure. This has led to the development of a range of aptamer-based biosensors, so called aptasensors.

The development of aptasensors relies on the utilisation of various detection methodologies (95). These methods can be divided into two groups. Initially, the label free biosensing systems are using technologies such as quartz crystal microbalance (QCM) measurements and surface plasmon resonance (SPR). On the other hand, methods requiring the use of labels utilise electrochemistry, fluorescence and chemiluminescence (27–32). Electrochemical systems have also been used to develop label-free assays using electrochemical impedance spectroscopy (EIS) (95,100).

The approach to construct an electrochemical aptasensor can follow two different ways. The first relies on the direct immobilization of aptamer onto a surface (101). This is usually achieved by using aptamers to which thiol functionality has been introduced. Under these circumstances, the method often includes the use of alkanethiols to spatially resolve neighbouring aptamers to avoid steric hindrance effects. Molecules such as 6-mercaptohexanol (MCH), mercaptoundecanoic acid (MUA) and cysteamine are frequently used for this purpose, assuming that gold electrodes will be employed for the development of the biosensor (101). Thiols may also bind on surfaces comprised of materials such as silver, platinum, palladium and semiconductors (102). Different types of electrodes, such as glassy carbon and silica, demand the use of molecules with different

properties to achieve the immobilisation. For instance, silanes can be immobilised on oxides such as silicon dioxide (SiO_2) or indium tin oxide (ITO) (102).

The second approach relies on the coating of the electrode by generating either a thin polymer film containing specific functional groups to facilitate further attachment or depositing a self-assembled monolayer of molecules to which recognition molecules can be attached using N-(3-dimethylaminopropyl)-N-ethylcarbodiimide hydrochloride (EDC) / N-hydroxy-succinimide (NHS) (or other) chemistry.

EDC/NHS chemistry relies on the use of a carbon chain that will add distance between the site of recognition and the working electrode. In this approach, the aptamer must be modified with either an amine or carboxylic acid. A short carbon-chain carboxythiol (in the case of amine modified aptamers) or aminothiol (in the case of carboxy-modified sequences) such as mercaptopropionic acid (MPA) or cysteamine, is used to generate a self-assembled monolayer at the surface of the gold electrode (103). The carboxylic acid group is activated by EDC and NHS, forming an amine reactive ester, which facilitates the immobilization of the aptamer. An example of an amine-modified aptamer being immobilised to a carboxy-functionalised SAM is provided in Figure 1.8.
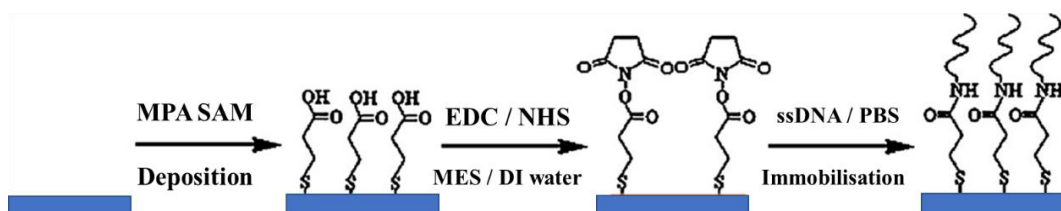
Figure 1.8: Fabrication of a biosensor using EDC/NHS chemistry to immobilise an aptamer on a mercaptopropionic acid (MPA) self-assembled monolayer (SAM) (103).

There are advantages and disadvantages to both approaches with regard to sensor development. In the first case, aptamer and alkanethiol are directly attached to the gold surface. Although this is perhaps the most straight-forward approach, it is possible that the gold surface might not be fully covered, and its bare areas might give rise to non-specific binding via hydrophobic interactions. A backfilling process with alkanethiol following surface modification with aptamer might help ameliorate this. Direct

conjugation of aptamers to the surface may also restrict their conformations, affecting overall recognition performance.

On the other hand, when utilising the EDC/NHS approach it is less likely that areas of the gold surface will be found to be exposed, since the sensor development starts with the deposition of an alkanethiol SAM to which the aptamer becomes anchored. Providing a 'spacer' between the electrode surface and the aptamer can sometimes be beneficial in terms of encouraging conformational flexibility. However, the deposition of an increased mass on the working electrode coupled with the increased distance between the surface and the recognition element may result in a less sensitive biosensing system.

In both cases, sensitivity is the key factor affected by the chemistry behind these two strategies. The present project will focus on the optimisation of direct immobilisation of aptamer and spacer molecules on the working electrode. Electrochemical impedance spectroscopy (EIS) will be used to monitor and characterise the development of the sensors, as well as to evaluate the binding performance of the optimised system.

1.6 Electrochemistry background

1.6.1 Electrochemistry Fundamentals

This section describes the information needed to understand the background behind the measurement acquisition and method development, with respect to electrochemical biosensing. A classic electrochemical cell is utilised in all measurements, which can either develop electrical energy from chemical reactions or catalyse chemical reactions through the supply of electrical energy (104).

The electrochemical cell consists of three electrodes: a working electrode (WE), a reference electrode (RE) and a counter electrode (CE) (Figure 1.9). In most cases, the interest is focused on reactions taking place within the setup and specifically at the working electrode. In order to solely focus on the changes resulting from the chemical phenomena within the system, all the other cell components must be fixed. Therefore, the reference electrode - the system's main indicator of these changes in terms of charge - is made up of phases having essentially constant composition. There are many types of reference electrodes, but for this study, a silver-silver chloride (Ag/AgCl) electrode has

been utilised (105). The current going through the reference electrode should be equal to zero under ideal circumstances, avoiding any electrode polarisation. The current supply can only go via the working and counter (or auxiliary) electrode (105). The counter electrode may be of any type, as far as its physical / chemical properties do not affect the behaviour of the working electrode and chemical reactions. For this study, a counter electrode made from Platinum (Pt) has been used.
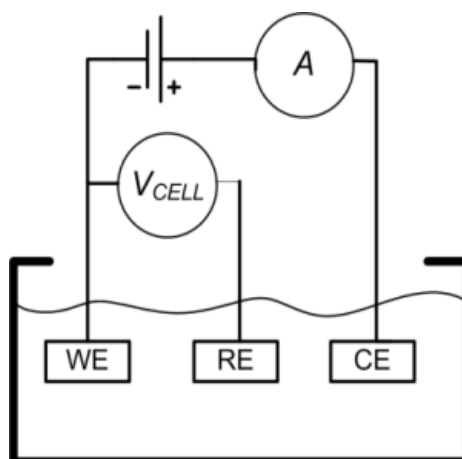
Figure 1.9: An electrochemical cell consists of a three-electrode setup: the working electrode (WE), reference electrode (RE) and the counter electrode (CE) (106).

The most commonly used materials to develop a working electrode surface are gold, platinum, carbon and mercury (107). Gold disc electrodes (Figure 1.10) demonstrate good electrochemical inertness and are easy to fabricate into many forms. However, they show limitations due to gold's oxidation in some areas of the positive potential range. When the gold surface is electrochemically activated, molecules containing thiols, amines or those possessing general hydrophobic properties can bind to it, developing self-assembled monolayers (SAMs).

Figure 1.10: A working electrode with a 2mm diameter gold surface (108).

1.6.2 Cyclic Voltammetry (CV)

Electrochemical activation is achieved using Cyclic Voltammetry (CV), in which the potential of the working electrode is swept linearly as a function of time and the resulting current is measured. In a CV experiment, the potential of the working electrode is ramped in the opposite direction after the end of the sweep, thus returning to the initial potential. A plot of current versus voltage provides the so-called 'Cyclic Voltammogram', an example of which is shown in Figure 1.11 (109–111).
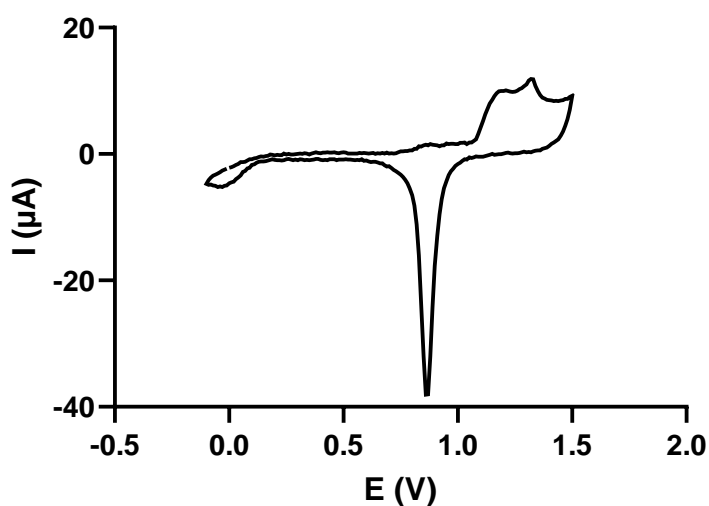
Figure 1.11: Cyclic voltammogram of the bare gold electrode subjected to electropolishing between 0 V and 1.5 V.

Cyclic Voltammograms demonstrate a material-specific profile due to the development of unique peaks in the oxidation and reduction currents. Since gold is the surface of choice, its voltammogram will be further analysed. Three consecutive oxidation peaks are apparent between 1.35 – 1.5 V, whilst a single reduction peak appears in the region of 1.0 – 0.8 V when the scanning potential returns to its initial point. The sharpness of each individual peak is indicative to the surface cleanliness and presence of impurities / residues.

Both the anode and cathode of the above cyclic voltammogram demonstrate a flat area that corresponds to double layer charging. The oxidation peaks recorded during the application of the anodic current correspond to the formation of the gold oxide. The number of the peaks (3 in total) shows the complexity of the reaction, since the gold atoms comprising the surface can be discriminated into 3 categories: bulk lattice atoms (Au^0), with small influence on the oxidation reaction, regular surface atoms (Au^*), able to show higher activity than the bulk ones and finally displaced surface atoms (Au^{**}), showing the highest activity (112). These three forms do not characterise a specific state of the gold surface, as it tends to be quite heterogeneous during the whole process. It is easy to understand that Au^* and Au^{**} can proceed into the oxidation process, as demonstrated on Figure 1.12.

$$Au^* + H_2O \longrightarrow Au^{\delta+}.OH^{\delta-} + H^+ + e^-$$

$$HO^{\delta-}.Au^{\delta+}$$
$$+ 2H_2O - 2H^+ - 2e^-$$

$$+3H^+ + 3e^-$$

$$Au^{**} + 3H_2O \longleftarrow Au(OH)_3$$
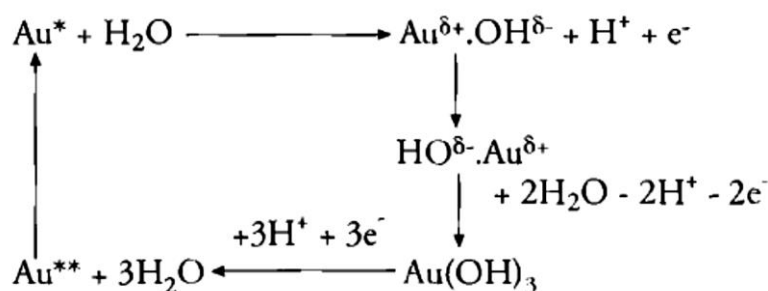
Figure 1.12: The formation of gold oxide during Cyclic Voltammetry. Both regular (Au*) and displaced (Au**) surface atoms can participate in the reaction with water, giving gold oxide as final product (112).

More precisely, the Au^{**} atoms can be spontaneously altered into Au^* ones before entering the oxidation process. However, the rest of the process cannot be regarded as straightforward, since the formed dipoles between $Au^{\delta+}$ and $OH^{\delta-}$ need to be converted into a more stable reactive oxygen species, such as the $Au(OH)^3$, or AU_2O_3. As a result,

the formation of gold oxide takes place into 3 distinctive steps, as referred from the peaks on the voltammogram.

The forms of the generated species can be more than one (i.e. oxides, hydroxides, and hydrous oxides) (113). Therefore, the term oxide is widely used for convenience reasons. In addition to that, the anodic profile of each individual surface may differ, due to reasons such as different approaches in the electrode cleaning process, presence of impurities and electrode history (usage) (113).

Figure 1.13 shows how the response observed changes upon modification of the electrode's surface, when an oscillating potential between -0.1 and 0.4 V is applied, using 10 mM $[Fe(CN)_6]^{3-/4-}$ as a redox probe. This pattern may change according to the physical properties of the molecules bound on the surface (9). CV will be used throughout the development process as proof of modification or interaction with the biomarker of interest.
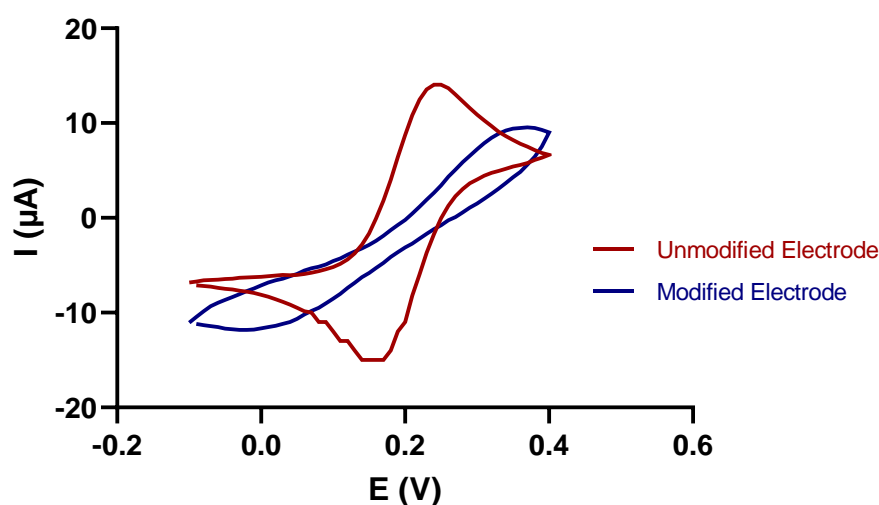
Figure 1.13: Cyclic Voltammograms obtained prior and after electrode modification. The unmodified bare gold surface (red) demonstrates a characteristic pattern that changes following surface modification (blue), depending on the physical properties of the molecules bound on it.

1.6.3 Electrochemical Impedance Spectroscopy (EIS)

Electrochemical Impedance Spectroscopy (EIS) tracks the changes of an electrode or electrolyte interface by applying a oscillating potential as a function of frequency (114). EIS relies on the transfer kinetics of charge that take place in a redox probe e.g. a solution

of potassium ferricyanide / ferrocyanide $[Fe(CN)_6]^{3-/4-}$. Data from EIS is presented as either Bode or Nyquist plots, which are analysed to determine changes in impedance (111).

Electrical impedance is defined as the ratio between the difference of the applied potential (ΔV) and the current (I) that flows through the system (115). This relationship is described by Ohm's law, as shown in Equation 1.1 and shows similarities to the description of resistance. Impedance is a general parameter used to describe the circuit's ability to resist the electron flow. However, unlike resistance, the term is not limited by the determination of the two variables participating in Ohm's law.

$$Z = \frac{\Delta V}{I}$$
<div align="right">Equation 1.1</div>

The dominant elements used to characterise passive electrical circuits are resistance, capacitance and inductance (116). All three terms are displaying unique characteristics, as they explain different physical phenomena. More presicely, resistance shows the opposition of a specific point within the electrical circuit towards the current flow. On the other hand, capacitance is the ability of a certain material to contain electrical charge / energy. Inductance is caused by magnetic fields generated by electric currents and shows the opposition towards these currents. Therefore, a component of the under-characterisation circuit can belong to only one group.

Considering all the above information, impedance is equal to resistance when focusing on a pure resistor. The observation relies on the fact that impedance displays zero lag between the current and the potential phase.

On the other hand, capacitance describes the ability of a component to store charge (electrons) (Equation 1.2). Unlike resistors, a capacitor displays a lag of -90° between current and potential, resulting in zero real impedance. The system is only described by the imaginary impedance which is frequency (ω) dependent (Equation 1.2). Therefore, one can refer that real impedance is behaving like a resistor, while the imaginary one is behaving like a capacitor.

$$Z_{Capacitor} = \frac{1}{j\omega C} \qquad\qquad \text{Equation 1.2}$$

A Nyquist plot is generated from the resulting real and imaginary impedances occurring as a result of the application of a number of frequencies through the system. As per Figure 1.14, the real impedance (Z_{real}) is plotted on X axis, while the Y axis refers to the imaginary impedance values ($Z_{imaginary}$). The $Z_{imaginary}$ is described by negative values (117).
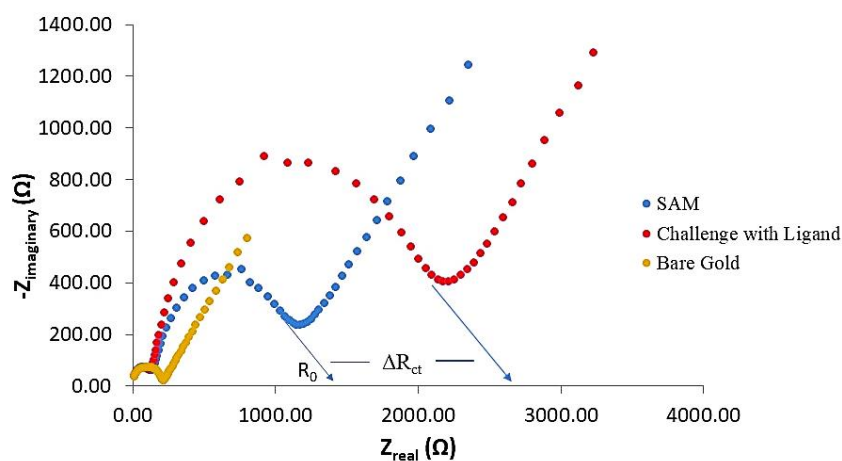
Figure 1.14: A typical Nyquist plot acquired during EIS. Data obtained from real impedance is on the x axis, while y axis describes the imaginary impedance. The plot intercepts the x axis by extrapolation at two points; the one is located in high frequencies and shows the solution resistance (R_s), while the other is appearing in low frequencies and shows the charge transfer resistance (R_{ct}). Warburg impedance can also be observed at low frequencies and is used to understand diffusion processes that take place in the circuit. When running these experiments, a difference in R_{ct} is recorded (ΔR_{ct}), between the initial reading of a recognition surface (R_0, here a self-assembled monolayer, SAM) and the final reading, after incubation with ligand.

The use of equivalent circuits has been employed to investigate the best possible curve fit for the generated impedance spectra and to extract data relating to changes in impedance. The present study develops systems comprising either resistors or capacitors to determine changes in impedance, since a inductive response is not a frequent phenomenon at low frequencies (118).

Most electrochemical systems utilise Randle's equivalent circuit to get the optimal fit of the previously mentioned Nyquist plots. The yellow curve presented on the Nyquist plot in Figure 1.14 represents the type of data generated from a bare metal (i.e. gold) experiencing activation polarization. The plot intercepts the x axis at two points. The Solution Resistance (R_s) is found by utilising the high frequency data, while the value for the Charge Transfer Resistance (R_{ct}) is defined by low frequency data (117). It is important to notice that the readings begin by applying high frequencies (left part of the plot) and moving towards the low ones (right part of the plot). The R_{ct} values would normally be defined as the difference between the two intercepts.

$\Delta Rct_{\%}$ is calculated for all the acquired measurements following incubation with biomarkers / further modifications that might change the impedance observed for a particular electrode, according to equation 1.3:

$$\%\Delta R_{ct} = \frac{Rct_{final} - Rct_{baseline}}{Rct_{baseline}} \, 100 \qquad \text{Equation 1.3}$$

Where:

Rct_{final}   *: The Rct measured following the electrode incubation / modification*

$Rct_{baseline}$ *: The Rct measured to determine the electrode's background prior to*
                modification / incubation with target analyte

Apart from R_{ct} and R_s, the Randle's equivalent circuit comprises a further two components. The first one deals with the constant phase element (CPE), representing the distribution of reactivity in impedance response within the equivalent electrical circuits (119). It is mainly used to bridge the deviation observed between the actual and ideal response. The impedance of a blocking electrode is then expressed as per equation 1.4:

$$Z_{(\omega)} = R_e + \frac{1}{(j\omega)^\alpha Q} \qquad \text{Equation 1.4}$$

Equation 1.4 includes the terms of Reynolds number (R_e) and the independent values of α and the CPE coefficient (Q). α stands for an exponent that adopts values within the range of [0,1] (120). This exponent is preferably treated as an empirical constant and affects the units of Q (119). More precisely, when α equals 1, the system behaves as a "pure capacitor", forcing Q to adopt units of capacitance and stand for the interface's capacitance. On the contrary, when $\alpha \neq 1$, Q is utilised to describe a response fitting to a heterogeneous surface or continuously distributed time constants for charge-transfer reactions. Q's values are proportional to the active area.

The second element is the Warburg impedance, used to understand the diffusion processes that are affected by the Faradaic currents applied during the experiments. The Warburg impedance is connected in series with the R_{ct} and depends on the concentration of redox markers and frequency (121). This element can be barely observed when the frequencies are high.

None of the existing models can perfectly describe the physics of experimental data obtained from real experiments (119). Consequently, the system of choice will be based upon the data obtained during the experiment and the degree of fit to the particular equivalent circuit model. The need to develop a standard rule to characterise biomolecular surfaces and interfaces is apparent.

The present study utilised the model $R_s((R_{ct}W)Q_{dl})$ to fit the experimental data (Figure 1.15). The determination of the double layer CPE coefficient (Q_{dl}) provided a constant good fit to the obtained data, retaining the balance between capacitive and resistive elements of the systems. Despite the model's ability to fit data collected from insulators, it was decided to change the Q_{dl} to the double layer Capacitance (C_{dl}), thus modifying the model to $R_s((R_{ct}W)C_{dl})$ when analysing data generated by non-conducting bulk polymers.
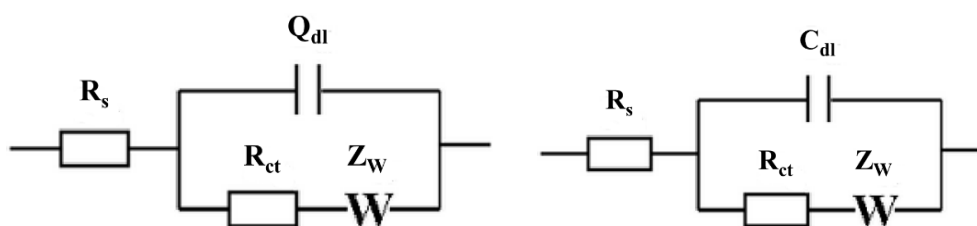
Figure 1.15: The Randle's equivalent circuits used for the analysis of EIS circuits. R_s is the resistance due to solution. R_s is connected in series with resistance due to charge transfer (R_{ct}) and double layer CPE coefficient (Q_{dl}) (left image). The Q_{dl} is replaced by double layer capacitance (C_{dl}), in the presence of insulators (right image). The Warburg impedance (Z_W) is always connected in series with R_{ct}, defining the system's diffusion process.

1.6.4 Chronocoulometry (CC)

Chronocoulometry is an electrochemical method capable of measuring the changes in charge (coulomb). The variable is dependent on time and is applied to determine various features of modified working electrodes (122). The present study used chronocoulometry to estimate the number of aptamers bound on the gold surface and consequently, the number of active binding sites, able to capture the targeted molecules.

Chronocoulometry is a controlled potential method and is divided into two steps. The initial step introduces a potential at which no electrolysis takes place (initial E). The second step involves the sudden change in potential that oxidises / reduces molecules present in the solution phase (ruthenium hexamine (RuHex) in the present study). This potential is held for pre-determined period of time. The present study applied this potential for either 250 ms or 500 msec, depending on the phase of the experimental process, aiming to oxidise as much as RuHex as possible.

The experiments may utilise single or double steps to determine the differences in charge (Q) (34). The experiments are performed twice; with and without the presence of RuHex. In the marker's absence, data is collected and $Q_{dl} = f(t^{1/2})$ plotted by extrapolating the 2nd half-period of the pulse, in which the oxidation potential is applied. RuHex is then introduced to the solution and the same process repeated, to obtain the total charge (Q_{total}). RuHex penetrates the DNA's backbone and changes the charge within the system (123). The reaction is extremely fast, meaning there is no need for pre-incubation. The charge

(Q_{ss}) corresponding to RuHex electrostatically bound to surface-confined ssDNA is calculated as per Equation 1.5:

$$Q_{ss} = Q_{total} - Q_{dl}$$

Equation 1.5

Following the determination of Q_{ss}, the surface density of the aptamer is calculated (Γ_{ss}) using Equation 1.6:

$$\Gamma ss = \frac{Q_{ss} N_A}{nFA} \frac{z}{m}$$

Equation 1.6

Where:

n = the number of electrons in the reaction

A = the surface area of the working electrode

m = the number of nucleotides in the aptamer sequence

z = the charge of the redox molecules

N_A = Avogadro's number

Here, it is important to mention that despite the same symbol (Q_{dl}), the charge due to double layer and double layer CPE coefficient (as in the equivalent circuit) are two different parameters.

1.7 Scope of Thesis

The scope of this project was to develop a multiplex electrochemical platform for the rapid and accurate diagnosis of sepsis. In order to achieve these goals, aptamer and hybrid molecular imprinting technologies have been employed to develop label-free bioassays for three biomarkers: lipopolysaccharide (LPS), C-reactive protein (CRP) and procalcitonin (PCT). The development of the aptasensors and the hybrid recognition

system along with their electrochemical characterisation and deployment is described in Chapters 2 – 4 of this thesis.

It is clear there is not a single biomarker that can be treated as a "gold standard" for the accurate diagnosis of sepsis. CRP is one of the most widely used clinical biomarkers for the diagnosis and monitoring of septic patients, despite its questionable sensitivity / specificity. For this reason, CRP can easily justify its place in the electrochemical multiplex platform this project aims to develop. PCT seems to be a better marker when compared to CRP, especially when it comes to prognosis. However, current commercial PCT tests are rather expensive and so testing, certainly within the NHS, is limited to those patients who are critically ill. Development of low-cost PCT sensor, using the electrochemical sensing approach described herein, would allow more widespread testing. A vast number of publications highlight the role of LPS in the development of sepsis. To date, quantitative detection of LPS from clinical samples has proved difficult using the commercially available, regulatory approved, LAL-based assays. Therefore, this project aims to develop a novel cost-effective, highly specific, sensitive and robust electrochemical sensor, targeting LPS. This project will showcase the full story starting from the optimisation of the recognition properties of a simple aptasensor, to the development of a hybrid apta-MIP system capable of detecting LPS at very low levels.

The use of artificial oligonucleotides (aptamers) that can bind a broad range of targets with high affinity and specificity has been increasingly attracting the interest of the research society. These molecules can be utilised as recognition elements in the development of biosensors for all three biomarkers of interest. An extensive literature review shows a wide selection of aptamers for both LPS and CRP, while the options regarding PCT are limited. Chapters 2 (LPS) and 4 (CRP and PCT) extensively explore the development and optimisation of these aptasensor systems.

Despite the fact that the surface chemistry of the aptasensor development has the potential to be quite simple in its application, it may lack the sensitivity needed for the detection of changes in the LPS levels during sepsis. Therefore, electropolymers have been employed to enable development of a hybrid recognition system utilising a molecular imprinting approach (a so-called apta-MIP, Figure 1.16). Chapter 3 covers the screening process of various electropolymerisable monomers such as dopamine and aminophenylboronic acid and the development of the hybrid system.

Immobilisation of LPS-aptamer complex on the gold surface

Development of a polymer to a similar height of the complex

Removal of LPS to expose the hybrid binding sites
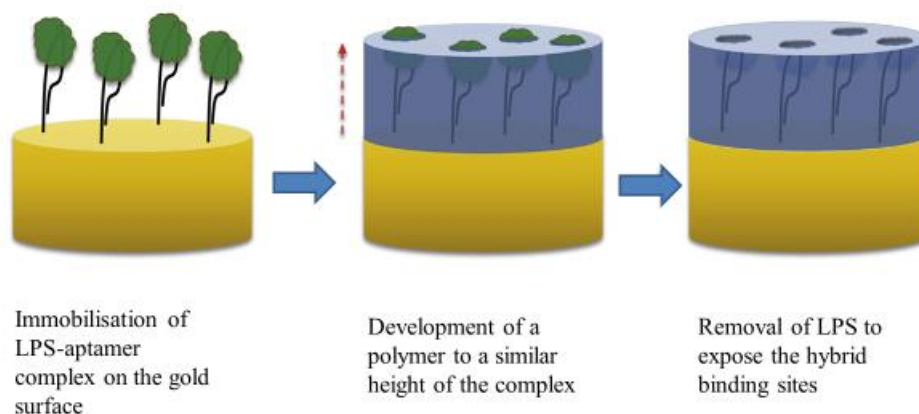
Figure 1.16: The development of a hybrid apta-MIP sensor. Polymerisation around an immobilised aptamer-LPS complex with subsequent removal of LPS, leaves behind an aptamer-lined imprinted site capable of recognising LPS (9).

Upon completion of their development, the biosensors have been challenged with clinical samples, to investigate their ability to detect their target analytes in more complex sample matrices.

Finally, Chapter 5 provides a general discussion of the project providing insight into future perspectives, applications and suggestions to continue building up on the project's significant results.

1.8 Bibliography

1.   Singer M, Deutschman CS, Seymour CW, Shankar-Hari M, Annane D, Bauer M,
        et al. The Third International Consensus Definitions for Sepsis and Septic Shock
        (Sepsis-3). JAMA [Internet]. 2016 Feb 23 [cited 2017 Apr 21];315(8):801.
        Available from:
        http://jama.jamanetwork.com/article.aspx?doi=10.1001/jama.2016.0287

2.   Bhan C, Dipankar P, Chakraborty P, Sarangi PP. Role of cellular events in the
        pathophysiology of sepsis. Inflamm Res [Internet]. 2016 Nov 8 [cited 2019 Jun
        22];65(11):853–68. Available from:
        http://www.ncbi.nlm.nih.gov/pubmed/27392441

3.   Delano MJ, Ward PA. The immune system's role in sepsis progression,
        resolution, and long-term outcome. Immunol Rev [Internet]. 2016 [cited 2019
        Jun 22];274(1):330–53. Available from:
        http://www.ncbi.nlm.nih.gov/pubmed/27782333

4.   Rudd KE, Johnson SC, Agesa KM, Shackelford KA, Tsoi D, Kievlan DR, et al.
        Global, regional, and national sepsis incidence and mortality, 1990–2017:
        analysis for the Global Burden of Disease Study. Lancet. 2020 Jan
        18;395(10219):200–11.

5.   Gül F, Arslantaş MK, Cinel İ, Kumar A. Changing Definitions of Sepsis. Turkish
        J Anaesthesiol Reanim [Internet]. 2017 Jun [cited 2019 Jun 22];45(3):129–38.
        Available from: http://www.ncbi.nlm.nih.gov/pubmed/28752002

6.   Pierrakos C, Vincent J-L. Sepsis biomarkers: a review. Crit Care [Internet]. 2010
        [cited 2017 Apr 21];14(1):R15. Available from:
        http://www.ncbi.nlm.nih.gov/pubmed/20144219

7.   Opal SM. Endotoxins and Other Sepsis Triggers. In: Endotoxemia and Endotoxin
        Shock [Internet]. Basel: KARGER; 2010 [cited 2019 Jun 22]. p. 14–24.
        Available from: http://www.ncbi.nlm.nih.gov/pubmed/20519895

8.   Marshall JC, Foster D, Vincent J-L, Cook DJ, Cohen J, Dellinger RP et al.
        Diagnostic and prognostic implications of endotoxemia in critical illness: results
        of the MEDIC study. J Infect Dis. 2004;190(3):527–34.

9.   Jolly P, Tamboli V, Harniman RL, Estrela P, Allender CJ, Bowen JL. Aptamer-MIP hybrid receptor for highly sensitive electrochemical detection of prostate specific antigen. Biosens Bioelectron [Internet]. 2016;75:188–95. Available from: http://dx.doi.org/10.1016/j.bios.2015.08.043

10.   Nargis W, Ibrahim M, Ahamed BU. Procalcitonin versus C-reactive protein: Usefulness as biomarker of sepsis in ICU patient. Int J Crit Illn Inj Sci [Internet]. 2014 Jul [cited 2017 Nov 27];4(3):195–9. Available from: http://www.ncbi.nlm.nih.gov/pubmed/25337480

11.   Póvoa P, Teixeira-Pinto AM, Carneiro AH. C-reactive protein, an early marker of community-acquired sepsis resolution: a multi-center prospective observational study. Crit Care [Internet]. 2011 [cited 2017 Nov 23];15(4):R169. Available from: https://www.ncbi.nlm.nih.gov/pmc/articles/PMC3387609/

12.   Schmit X, Vincent JL. The Time Course of Blood C-reactive Protein Concentrations in Relation to the Response to Initial Antimicrobial Therapy in Patients with Sepsis. Infection [Internet]. 2008 Jun 10 [cited 2017 Nov 23];36(3):213–9. Available from: http://link.springer.com/10.1007/s15010-007-7077-9

13.   Clyne B, Olshaker JS. The C-reactive protein. J Emerg Med [Internet]. 1999 Nov 1 [cited 2017 Nov 27];17(6):1019–25. Available from: http://www.sciencedirect.com/science/article/pii/S0736467999001353?via%3Dihub

14.   Baruti Gafurri Z, Pacarizi H, Zhubi B, Begolli L, Topciu V. The importance of determining procalcitonin and C reactive protein in different stages of sepsis. Bosn J basic Med Sci [Internet]. 2010 Feb [cited 2017 Nov 30];10(1):60–4. Available from: http://www.ncbi.nlm.nih.gov/pubmed/20192933

15.   Assicot M, Gendrel D, Carsin H, Raymond J, Guilbaud J, Bohuon C. High serum procalcitonin concentrations in patients with sepsis and infection. Lancet (London, England) [Internet]. 1993 Feb 27 [cited 2017 Dec 1];341(8844):515–8. Available from: http://www.ncbi.nlm.nih.gov/pubmed/8094770

16.   Nakamura A, Wada H, Ikejiri M, Hatada T, Sakurai H, Matsushima Y, et al. Efficacy of procalcitonin in the early diagnosis of bacterial infections in a critical

care unit. Shock [Internet]. 2009 Jun [cited 2017 Nov 27];31(6):587–92. Available from: http://www.ncbi.nlm.nih.gov/pubmed/19060784

17. Luzzani A, Polati E, Dorizzi R, Rungatscher A, Pavan R, Merlini A. Comparison of procalcitonin and C-reactive protein as markers of sepsis. Crit Care Med [Internet]. 2003 Jun [cited 2017 Nov 27];31(6):1737–41. Available from: http://www.ncbi.nlm.nih.gov/pubmed/12794413

18. Tang BM, Eslick GD, Craig JC, McLean AS. Accuracy of procalcitonin for sepsis diagnosis in critically ill patients: systematic review and meta-analysis. Lancet Infect Dis [Internet]. 2007 Mar [cited 2017 Nov 27];7(3):210–7. Available from: http://www.ncbi.nlm.nih.gov/pubmed/17317602

19. Botero JSH, Pérez MCF. The History of Sepsis from Ancient Egypt to the XIX Century. IntechOpen [Internet]. 2012; Available from: http://dx.doi.org/10.5772/51484

20. Geroulanos S, Douka ET. Historical perspective of the word "sepsis." Intensive Care Med [Internet]. 2006 Nov 27 [cited 2019 Jun 22];32(12):2077–2077. Available from: http://link.springer.com/10.1007/s00134-006-0392-2

21. Funk DJ, Parrillo JE, Kumar A. Sepsis and Septic Shock: A History. Vol. 25, Critical Care Clinics. 2009. p. 83–101.

22. Majno G. The ancient riddle of (Sepsis). J Infect Dis [Internet]. 1991 [cited 2020 Dec 22];163(5):937–45. Available from: https://pubmed.ncbi.nlm.nih.gov/2019770/

23. Martin GS. Sepsis, severe sepsis and septic shock: Changes in incidence, pathogens and outcomes. Vol. 10, Expert Review of Anti-Infective Therapy. 2012. p. 701–6.

24. Thurston AJ. Of blood, inflammation and gunshot wounds: the history of the control of sepsis. Aust N Z J Surg [Internet]. 2000 Dec [cited 2019 Oct 21];70(12):855–61. Available from: http://www.ncbi.nlm.nih.gov/pubmed/11167573

25. Vincent JL, Abraham E. The last 100 years of sepsis. Vol. 173, American Journal of Respiratory and Critical Care Medicine. 2006. p. 256–63.

26.   Sir Alexander Fleming - Biographical [Internet]. [cited 2019 Oct 27]. Available from: https://www.nobelprize.org/prizes/medicine/1945/fleming/biographical/

27.   Rhee C, Jones TM, Hamad Y, Pande A, Varon J, O'Brien C, et al. Prevalence, Underlying Causes, and Preventability of Sepsis-Associated Mortality in US Acute Care Hospitals. JAMA Netw open. 2019 Feb 1;2(2):e187571.

28.   Liu V, Escobar GJ, Greene JD, Soule J, Whippy A, Angus DC, et al. Hospital deaths in patients with sepsis from 2 independent cohorts. JAMA - J Am Med Assoc. 2014;312(1):90–2.

29.   Hotchkiss RS, Karl IE. The pathophysiology and treatment of sepsis. Vol. 348, New England Journal of Medicine. 2003. p. 138–50.

30.   Gullo A, Bianco N, Berlot G. Management of severe sepsis and septic shock: challenges and recommendations. Crit Care Clin [Internet]. 2006 Jul [cited 2019 Oct 27];22(3):489–501, ix. Available from: http://www.ncbi.nlm.nih.gov/pubmed/16893735

31.   Lever A, Mackenzie I. Sepsis: Definition, epidemiology, and diagnosis. Vol. 335, British Medical Journal. 2007. p. 879–83.

32.   Cohen J. The immunopathogenesis of sepsis. Vol. 420, Nature. 2002. p. 885–91.

33.   Russell J a. Sepsis Drugs. N Engl J Med [Internet]. 2006 Oct 19 [cited 2019 Oct 27];355(16):1699–713. Available from: http://www.ncbi.nlm.nih.gov/pubmed/17050894

34.   Modlin RL, Brightbill HD, Godowski PJ. The toll of innate immunity on microbial pathogens. N Engl J Med [Internet]. 1999 Jun 10 [cited 2019 Oct 27];340(23):1834–5. Available from: http://www.ncbi.nlm.nih.gov/pubmed/10362831

35.   Mogensen TH. Pathogen recognition and inflammatory signaling in innate immune defenses. Vol. 22, Clinical Microbiology Reviews. 2009. p. 240–73.

36.   Brown MA, Jones WK. NF-kappaB action in sepsis: the innate immune system and the heart. Front Biosci [Internet]. 2004 May 1 [cited 2019 Oct 27];9:1201–17. Available from: http://www.ncbi.nlm.nih.gov/pubmed/14977537

37.   Dinarello CA. Proinflammatory cytokines. Chest. 2000 Aug 1;118(2):503–8.

38.   Mosser DM, Zhang X. Interleukin-10: New perspectives on an old cytokine. Vol.
        226, Immunological Reviews. NIH Public Access; 2008. p. 205–18.

39.   López A, Lorente JA, Steingrub J, Bakker J, McLuckie A, Willatts S, et al.
        Multiple-center, randomized, placebo-controlled, double-blind study of the nitric
        oxide synthase inhibitor 546C88: effect on survival in patients with septic shock.
        Crit Care Med [Internet]. 2004 Jan [cited 2019 Oct 27];32(1):21–30. Available
        from: http://www.ncbi.nlm.nih.gov/pubmed/14707556

40.   Walker FJ, Sexton PW, Esmon CT. The inhibition of blood coagulation by
        activated Protein C through the selective inactivation of activated Factor V.
        Biochim Biophys Acta [Internet]. 1979 Dec 7 [cited 2019 Oct 27];571(2):333–
        42. Available from: http://www.ncbi.nlm.nih.gov/pubmed/508770

41.   Fulcher CA, Gardiner JE, Griffin JH, Zimmmerman TS. Proteolytic inactivation
        of human factor VIII procoagulant protein by activated human protein C and its
        analogy with factor V. Blood. 1984;63(2):486–9.

42.   Esmon CT. Structure and functions of the endothelial cell protein C receptor.
        Vol. 32, Critical care medicine. 2004.

43.   van Hinsbergh VW, Bertina RM, van Wijngaarden A, van Tilburg NH, Emeis JJ,
        Haverkate F. Activated protein C decreases plasminogen activator-inhibitor
        activity in endothelial cell-conditioned medium. Blood [Internet]. 1985 Feb [cited
        2019 Oct 27];65(2):444–51. Available from:
        http://www.ncbi.nlm.nih.gov/pubmed/3917696

44.   Creasey AA, Reinhart K. Tissue factor pathway inhibitor activity in severe
        sepsis. Crit Care Med [Internet]. 2001 Jul [cited 2019 Oct 27];29(7 Suppl):S126-
        9. Available from: http://www.ncbi.nlm.nih.gov/pubmed/11445747

45.   Liaw PCY, Esmon CT, Kahnamoui K, Schmidt S, Kahnamoui S, Ferrell G, et al.
        Patients with severe sepsis vary markedly in their ability to generate activated
        protein C. Blood [Internet]. 2004 Dec 15 [cited 2019 Oct 27];104(13):3958–64.
        Available from: http://www.ncbi.nlm.nih.gov/pubmed/15319291

46.   Daniels R. Surviving the first hours in sepsis: getting the basics right (an

intensivist's perspective). J Antimicrob Chemother [Internet]. 2011 Apr [cited 2019 Oct 27];66 Suppl 2:ii11-23. Available from: http://www.ncbi.nlm.nih.gov/pubmed/21398303

47.   World Sepsis Day Factsheet.

48.   Toolkits — World Sepsis Day - September 13 [Internet]. [cited 2020 Apr 13]. Available from: https://www.worldsepsisday.org/toolkits

49.   Hall MJ, Levant S, DeFrances CJ. Trends in inpatient hospital deaths: National Hospital Discharge Survey, 2000-2010. NCHS Data Brief. 2013;(118):1–8.

50.   The UK Sepsis Trust. The Sepsis Manual.

51.   Bowen JL. Detection of Lipopolysaccharide Pyrogens by Molecularly Imprinted Polymers. 2011.

52.   Angus DC, Linde-Zwirble WT, Lidicker J, Clermont G, Carcillo J, Pinsky MR. Epidemiology of severe sepsis in the United States: Analysis of incidence, outcome, and associated costs of care. Crit Care Med. 2001;29(7):1303–10.

53.   International Organizations Declare Sepsis a Global Medical Emergency [Internet]. [cited 2019 Oct 27]. Available from: https://www.prnewswire.com/news-releases/international-organizations-declare-sepsis-a-global-medical-emergency-104142073.html

54.   Kumar G, Kumar N, Taneja A, Kaleekal T, Tarima S, McGinley E, et al. Nationwide trends of severe sepsis in the 21st century (2000-2007). Chest [Internet]. 2011 [cited 2019 Oct 27];140(5):1223–31. Available from: http://www.embase.com/search/results?subaction=viewrecord&from=export&id=L362918069

55.   Yeh RW, Sidney S, Chandra M, Sorel M, Selby J V, Go AS. Population trends in the incidence and outcomes of acute myocardial infarction. N Engl J Med [Internet]. 2010 Jun 10 [cited 2019 Oct 27];362(23):2155–65. Available from: http://www.ncbi.nlm.nih.gov/pubmed/20558366

56.   Hall MJ, Williams SN, DeFrances CJ, Golosinskiy A. Inpatient care for septicemia or sepsis: a challenge for patients and hospitals. NCHS Data Brief. 2011;(62):1–8.

57.   Vincent JL, Sakr Y, Sprung CL, Ranieri VM, Reinhart K, Gerlach H, et al. Sepsis in European intensive care units: Results of the SOAP study. Crit Care Med. 2006;34(2):344–53.

58.   Balk RA, Bone RC. The septic syndrome. Definition and clinical implications. Crit Care Clin [Internet]. 1989 Jan [cited 2019 Oct 27];5(1):1–8. Available from: http://www.ncbi.nlm.nih.gov/pubmed/2647221

59.   Bone RC, Balk RA, Cerra FB, Dellinger RP, Fein AM, Knaus WA, et al. Definitions for sepsis and organ failure and guidelines for the use of innovative therapies in sepsis. In: Chest. 1992. p. 1644–55.

60.   Reinhart K, Bauer M, Riedemann NC, Hartog CS. New approaches to sepsis: Molecular diagnostics and biomarkers. Clin Microbiol Rev. 2012 Oct;25(4):609–34.

61.   Simpson SQ. New Sepsis Criteria: A Change We Should Not Make. Chest [Internet]. 2016 [cited 2019 Oct 27];149(5):1117–8. Available from: http://www.ncbi.nlm.nih.gov/pubmed/26927525

62.   Bhatt N. Sepsis From EMS to ER to ICU What we need to be doing [Internet]. [cited 2020 Apr 13]. Available from: https://www.piedmont.org/media/file/PAR-CME-EMS-Bhatt-SEPSIS.pdf

63.   Phua J, Ngerng WJ, See KC, Tay CK, Kiong T, Lim HF, et al. Characteristics and outcomes of culture-negative versus culture-positive severe sepsis. Crit Care [Internet]. 2013 Sep 12 [cited 2020 Apr 13];17(5):R202. Available from: http://ccforum.biomedcentral.com/articles/10.1186/cc12896

64.   Szakmany T. Size of sepsis in Wales - Health Research Authority [Internet]. Critical Care Medicine. 2015 [cited 2019 Oct 27]. Available from: https://www.hra.nhs.uk/planning-and-improving-research/application-summaries/research-summaries/size-of-sepsis-in-wales/

65.   Umberger RA, Thomas SP. Survivor But Not Fully Recovered. Dimens Crit Care Nurs [Internet]. 2019 Nov 1 [cited 2020 Mar 20];38(6):317–27. Available from: http://journals.lww.com/10.1097/DCC.0000000000000381

66.   Prescott HC, Angus DC. Enhancing recovery from sepsis: A review. Vol. 319,

JAMA - Journal of the American Medical Association. American Medical Association; 2018. p. 62–75.

67.   Prescott HC, Langa KM, Liu V, Escobar GJ, Iwashyna TJ. Increased 1-year healthcare use in survivors of severe sepsis. Am J Respir Crit Care Med. 2014 Jul 1;190(1):62–9.

68.   Schuler A, Wulf DA, Lu Y, Iwashyna TJ, Escobar GJ, Shah NH, et al. The impact of acute organ dysfunction on long-term survival in sepsis. Crit Care Med [Internet]. 2018 [cited 2020 Mar 20];46(6):843–9. Available from: http://www.ncbi.nlm.nih.gov/pubmed/29432349

69.   Atkinson AJ, Colburn WA, DeGruttola VG, DeMets DL, Downing GJ, Hoth DF, et al. Biomarkers and surrogate endpoints: Preferred definitions and conceptual framework. Vol. 69, Clinical Pharmacology and Therapeutics. 2001. p. 89–95.

70.   Marshall JC, Reinhart K, International Sepsis Forum. Biomarkers of sepsis. Crit Care Med [Internet]. 2009 Jul [cited 2019 Oct 27];37(7):2290–8. Available from: http://www.ncbi.nlm.nih.gov/pubmed/19487943

71.   Dellinger RP, Levy MM, Carlet JM, Bion J, Parker MM, Jaeschke R, et al. Surviving Sepsis Campaign: International guidelines for management of severe sepsis and septic shock: 2008. Intensive Care Med. 2008 Jan;34(1):17–60.

72.   Nupponen I, Andersson S, Järvenpää AL, Kautiainen H, Repo H. Neutrophil CD11b expression and circulating interleukin-8 as diagnostic markers for early-onset neonatal sepsis. Pediatrics. 2001;108(1).

73.   Nuutila J, Hohenthal U, Laitinen I, Kotilainen P, Rajamäki A, Nikoskelainen J, et al. Simultaneous quantitative analysis of FcgammaRI (CD64) expression on neutrophils and monocytes: a new, improved way to detect infections. J Immunol Methods [Internet]. 2007 Dec 1 [cited 2019 Oct 28];328(1–2):189–200. Available from: http://www.ncbi.nlm.nih.gov/pubmed/17905303

74.   Cardelli P, Ferraironi M, Amodeo R, Tabacco F, De Blasi RA, Nicoletti M, et al. Evaluation of neutrophil CD64 expression and procalcitonin as useful markers in early diagnosis of sepsis. Int J Immunopathol Pharmacol [Internet]. [cited 2019 Oct 28];21(1):43–9. Available from:

http://www.ncbi.nlm.nih.gov/pubmed/18336730

75.   Rintala EM, Aittoniemi J, Laine S, Nevalainen TJ, Nikoskelainen J. Early
       identification of bacteremia by biochemical markers of systemic inflammation.
       Scand J Clin Lab Invest [Internet]. 2001 [cited 2019 Oct 28];61(7):523–30.
       Available from: http://www.ncbi.nlm.nih.gov/pubmed/11763410

76.   Sherwin C, Broadbent R, Young S, Worth J, McCaffrey F, Medlicott NJ, et al.
       Utility of interleukin-12 and interleukin-10 in comparison with other cytokines
       and acute-phase reactants in the diagnosis of neonatal sepsis. Am J Perinatol
       [Internet]. 2008 Nov [cited 2019 Oct 28];25(10):629–36. Available from:
       http://www.ncbi.nlm.nih.gov/pubmed/18850512

77.   Ng PC, Li K, Chui KM, Leung TF, Wong RPO, Chu WCW, et al. IP-10 is an
       early diagnostic marker for identification of late-onset bacterial infection in
       preterm infants. Pediatr Res [Internet]. 2007 Jan [cited 2019 Oct 28];61(1):93–8.
       Available from: http://www.ncbi.nlm.nih.gov/pubmed/17211148

78.   Schmit X, Vincent JL. The time course of blood C-reactive protein
       concentrations in relation to the response to initial antimicrobial therapy in
       patients with sepsis. Infection [Internet]. 2008 Jun [cited 2019 Oct
       27];36(3):213–9. Available from:
       http://www.ncbi.nlm.nih.gov/pubmed/18463788

79.   Póvoa P, Coelho L, Almeida E, Fernandes A, Mealha R, Moreira P, et al. C-
       reactive protein as a marker of infection in critically ill patients. Clin Microbiol
       Infect [Internet]. 2005 Feb [cited 2019 Oct 27];11(2):101–8. Available from:
       http://www.ncbi.nlm.nih.gov/pubmed/15679483

80.   Clyne B, Olshaker JS. The C-reactive protein. J Emerg Med [Internet]. [cited
       2019 Oct 28];17(6):1019–25. Available from:
       http://www.ncbi.nlm.nih.gov/pubmed/10595891

81.   Tang BMP, Eslick GD, Craig JC, Mclean AS, South N. 2007 lancet infect dis
       review Accuracy of procalcitonin for sepsis diagnosis in critically ill.pdf.
       2007;7(March).

82.   Luzzani A, Polati E, Dorizzi R, Rungatscher A, Pavan R, Merlini A. Comparison

of procalcitonin and C-reactive protein as markers of sepsis. Crit Care Med [Internet]. 2003 Jun [cited 2019 Oct 28];31(6):1737–41. Available from: http://www.ncbi.nlm.nih.gov/pubmed/12794413

83.   Nakamura A, Wada H, Ikejiri M, Hatada T, Sakurai H, Matsushima Y, et al. Efficacy of procalcitonin in the early diagnosis of bacterial infections in a critical care unit. Shock [Internet]. 2009 Jun [cited 2019 Oct 28];31(6):586–91. Available from: http://www.ncbi.nlm.nih.gov/pubmed/19060784

84.   What is an Aptamer? - Aptamers and SELEX - Base Pair Biotechnologies [Internet]. [cited 2020 Jan 19]. Available from: https://www.basepairbio.com/what-is-an-aptamer/

85.   Song S, Wang L, Li J, Zhao J, Fan C. Aptamer-based biosensors. Trend Anal Chem [Internet]. 2008 [cited 2019 Nov 4];27:108–17. Available from: http://www.elsevier.com/locate/trac

86.   Yoon S, Armstrong B, Habib N, Rossi JJ. Blind SELEX approach identifies RNA aptamers that regulate EMT and inhibit metastasis. Mol Cancer Res. 2017 Jul 1;15(7):811–20.

87.   Thiviyanathan V, Gorenstein DG. Aptamers and the next generation of diagnostic reagents. Vol. 6, Proteomics - Clinical Applications. NIH Public Access; 2012. p. 563–73.

88.   Zhuo Z, Yu Y, Wang M, Li J, Zhang Z, Liu J, et al. Recent advances in SELEX technology and aptamer applications in biomedicine. Vol. 18, International Journal of Molecular Sciences. MDPI AG; 2017.

89.   Morita Y, Leslie M, Kameyama H, Volk DE, Tanaka T. Aptamer therapeutics in cancer: Current and future. Vol. 10, Cancers. MDPI AG; 2018.

90.   Tuerk C, Gold L. Systematic evolution of ligands by exponential enrichment: RNA ligands to bacteriophage T4 DNA polymerase. Science (80-). 1990;249(4968):505–10.

91.   Ellington AD, Szostak JW. In vitro selection of RNA molecules that bind specific ligands. Nature. 1990;346(6287):818–22.

92.   Brody EN, Gold L. Aptamers as therapeutic and diagnostic agents. J Biotechnol

[Internet]. 2000 Mar [cited 2019 Nov 7];74(1):5–13. Available from: http://www.ncbi.nlm.nih.gov/pubmed/10943568

93.   Macugen | European Medicines Agency [Internet]. [cited 2019 Nov 7]. Available from: https://www.ema.europa.eu/en/medicines/human/EPAR/macugen

94.   Zhou J, Rossi J. Aptamers as targeted therapeutics: Current potential and challenges. Vol. 16, Nature Reviews Drug Discovery. Nature Publishing Group; 2017. p. 181–202.

95.   Hong P, Li W, Li J. Applications of aptasensors in clinical diagnostics. Vol. 12, Sensors. Multidisciplinary Digital Publishing Institute (MDPI); 2012. p. 1181–93.

96.   Zayats M, Huang Y, Gill R, Ma CA, Willner I. Label-free and reagentless aptamer-based sensors for small molecules. J Am Chem Soc [Internet]. 2006 Oct 25 [cited 2020 Mar 21];128(42):13666–7. Available from: http://www.ncbi.nlm.nih.gov/pubmed/17044676

97.   Wang X, Zhou J, Yun W, Xiao S, Chang Z, He P, et al. Detection of thrombin using electrogenerated chemiluminescence based on Ru(bpy)32+-doped silica nanoparticle aptasensor via target protein-induced strand displacement. Anal Chim Acta [Internet]. 2007 Aug 29 [cited 2020 Mar 21];598(2):242–8. Available from: http://www.ncbi.nlm.nih.gov/pubmed/17719898

98.   Rupcich N, Nutiu R, Li Y, Brennan JD. Entrapment of fluorescent signaling DNA aptamers in sol-gel-derived silica. Anal Chem [Internet]. 2005 Jul 15 [cited 2020 Mar 21];77(14):4300–7. Available from: http://www.ncbi.nlm.nih.gov/pubmed/16013839

99.   Willner I, Zayats M. Electronic Aptamer-Based Sensors. Angew Chemie Int Ed [Internet]. 2007 Aug 27 [cited 2020 Mar 21];46(34):6408–18. Available from: http://doi.wiley.com/10.1002/anie.200604524

100.   Ostatná V, Vaisocherová H, Homola J, Hianik T. Effect of the immobilisation of DNA aptamers on the detection of thrombin by means of surface plasmon resonance. Anal Bioanal Chem [Internet]. 2008 Jul [cited 2020 Mar 21];391(5):1861–9. Available from:

http://www.ncbi.nlm.nih.gov/pubmed/18481050

101.   Zuo MY, Chen LJ, Jiang H, Tan L, Luo ZF, Wang YM. Detecting endotoxin with a flow cytometry-based magnetic aptasensor. Anal Biochem. 2014 Dec 1;466:38–43.

102.   Mandler D, Kraus-Ophir S. Self-assembled monolayers (SAMs) for electrochemical sensing [Internet]. Vol. 15, Journal of Solid State Electrochemistry. Springer; 2011 [cited 2020 Sep 2]. p. 1–24. Available from: https://link.springer.com/article/10.1007/s10008-011-1493-6

103.   Su W, Lin M, Lee H, Cho MS, Choe WS, Lee Y. Determination of endotoxin through an aptamer-based impedance biosensor. Biosens Bioelectron. 2012 Feb 15;32(1):32–6.

104.   Zolin L. Electrochemical Power Sources. In: Large-scale Production of Paper-based Li-ion Cells. Springer; 2017. p. 3–11.

105.   Bard AJ, Faulkner L. Introduction and overview of electrode processes. In: Electrochemical Methods, Fundamentals and Applications. 2nd ed. John Wiley and Sons Inc.; 2001. p. 1–43.

106.   Punter J, Colomer-Farrarons J, Ll. P. Bioelectronics for Amperometric Biosensors. In: State of the Art in Biosensors - General Aspects. InTech; 2013. p. 241–74.

107.   Honeychurch KC. Printed thick-film biosensors. In: Printed Films: Materials Science and Applications in Sensors, Electronics and Photonics. Elsevier Ltd.; 2012. p. 366–409.

108.   PS101 Gold Working Electrode - PalmSens [Internet]. [cited 2020 Apr 13]. Available from: https://www.palmsens.com/product/ps101/

109.   Prodromidis MI. Impedimetric immunosensorsâ€"A review. Electrochim Acta. 2009;

110.   Heinze J. Cyclic Voltammetry—"Electrochemical Spectroscopy". New Analytical Methods(25). Angew Chemie Int Ed English [Internet]. 1984 Nov [cited 2020 Jan 21];23(11):831–47. Available from: http://doi.wiley.com/10.1002/anie.198408313

111. Nicholson RS, Shain I. Theory of Stationary Electrode Polarography. Single Scan and Cyclic Methods Applied to Reversible, Irreversible, and Kinetic Systems. Anal Chem [Internet]. 1964 Apr [cited 2020 Jan 21];36(4):706–23. Available from: https://pubs.acs.org/doi/abs/10.1021/ac60210a007

112. Burke LD, Nugent PF. The electrochemistry of gold: I. The redox behaviour of the metal in aqueous media. Gold Bull [Internet]. 1997 [cited 2020 Sep 13];30(2):43–53. Available from: https://link.springer.com/article/10.1007/BF03214756

113. Cherevko S, Topalov AA, Zeradjanin AR, Katsounaros I, Mayrhofer KJJ. Gold dissolution: Towards understanding of noble metal corrosion. RSC Adv [Internet]. 2013 Oct 7 [cited 2020 Sep 13];3(37):16516–27. Available from: https://pubs.rsc.org/en/content/articlehtml/2013/ra/c3ra42684j

114. Bard AJ, Faulkner L. Techniques based on concepts of impedance. In: Electrochemical Methods, Fundamentals and Applications. 2nd ed. John Wiley and Sons Inc.; 2001. p. 368–416.

115. Barbero G, Lelidis I. Analysis of Warburg's impedance and its equivalent electric circuits. Phys Chem Chem Phys. 2017 Sep 20;19(36):24934–44.

116. Orazem ME, Tribollet B. Electrical circuits. In: Electrochemical Impedance Spectroscopy. John Wiley and Sons Inc.; 2008. p. 61–72.

117. Mitton DB, Wallace SL, Cantini NJ, Bellucci F, Thompson GE, Eliaz N, et al. The correlation between substrate mass loss and electrochemical impedance spectroscopy data for a polymer-coated metal. J Electrochem Soc. 2002 Jun;149(6).

118. Napporn TW, Holade Y, Kokoh B, Mitsushima S, Mayer K, Eichberger B, et al. Electrochemical Measurement Methods and Characterization on the Cell Level. In: Fuel Cells and Hydrogen. Elsevier; 2018. p. 175–214.

119. Orazem ME, Tribollet B. Time-Constant Dispersion. In: Electrochemical Impedance Spectroscopy. John Wiley and Sons Inc.; 2008. p. 233–63.

120. Koklu A, Sabuncu AC, Beskok A. Rough Gold Electrodes for Decreasing Impedance at the Electrolyte/Electrode Interface. Electrochim Acta. 2016 Jul

1;205:215–25.

121. Jorcin JB, Orazem ME, Pébère N, Tribollet B. CPE analysis by local electrochemical impedance spectroscopy. In: Electrochimica Acta. 2006. p. 1473–9.

122. Bott AW, Heineman WR. Current Separations: Chronocoulometry. In 2004 [cited 2020 Feb 2]. p. 121–6. Available from: www.currentseparations.com

123. Zhang J, Song S, Wang L, Pan D, Fan C. A gold nanoparticle-based chronocoulometric DNA sensor for amplified detection of DNA. Nat Protoc [Internet]. 2007 Nov [cited 2017 Mar 26];2(11):2888–95. Available from: http://www.nature.com/doifinder/10.1038/nprot.2007.419

Development of LPS

aptasensor

2.1 Introduction

2.1.1 General overview

The use of artificial oligonucleotides (aptamers) to bind a broad range of targets with high affinity and specificity, has been increasingly attracting the interest of the research society. Aptamers can be designed to detect a large variety of different targets, from small ions and to whole cells, making them important diagnostic tools.

The ease of aptamer modification and general manipulation due to its nucleotide nature are properties that make it a desirable component of biosensors. The aim of the present chapter was to take advantage of these properties and develop an easy to use, low cost aptasensor to accurately and rapidly detect LPS.

A number of anti-LPS aptamer sequences can be found in the literature. The sequence with the highest reported affinity was selected for use in this study. Recognising that optimal sensor performance relies on appropriate presentation of the aptamer at the electrode surface, screening of alkanethiol molecules that can be used to space the aptamers and minimise the risk of steric interference when the system is challenged with the target analyte, was undertaken. Thiolated molecules, containing different functional groups (-OH, -NH$_2$, -COOH) were selected and the level of interaction between these and LPS was evaluated prior to the generation of mixed aptamer / alkanethiol self-assembled monolayers being developed and tested. Following optimisation, the aptasensor was characterised in terms of sensitivity, dynamic range and specificity, with comparison to LPS assays either available commercially or reported in the literature.

2.1.2 Endotoxin

The discovery of the role of endotoxin in infectious diseases is one of the most long, yet exciting stories in Microbiology. Very early physicians credited the mechanistic cause of death to the presence of "*μιάσματα*" (:miasmata; small creatures that pollute, singular: miasma) or "*contagions*" (deriving from the Latin verb *contigere*; touch). Despite the presence of these two distinct theories, true endotoxins were not discovered until ~ 2,000 years later by Richard Pfeifer (1858-1955) (1).

Following Pfeifer's work, Eugenio Centanni established the relationship between endotoxins and the development of fever due to bacterial presence (2). Centanni noted that the endotoxins were inseparable from the bacterial cell wall and named them pyrogens. However, the molecule's structure remained unclear until the middle of the 20th century. At this time, endotoxin was found to consist of lipid and polysaccharide regions and thus the molecule was named lipopolysaccharide (3).

2.1.2.1 Lipopolysaccharide structure

Lipopolysaccharide (LPS) consists of three different regions: Lipid A, Core Regions and O-specific Antigen (Figure 2.1) (4). The contribution of all regions to its three-dimensional structure is equal, while Lipid A is the most influential part in terms of toxicity *in vivo* (5).
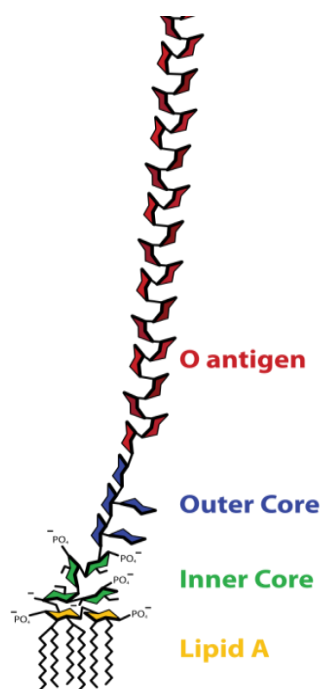
Figure 2.1: Structure of Lipopolysaccharide (6).

Lipopolysaccharide occupies ~ 75 % of the surface area of the outer membrane of Gram-negative bacteria (7); Lipid A is located inside the lipid bilayer of the membrane, while the core and O-specific antigen regions extend outwards from the cell (Figure 2.2).
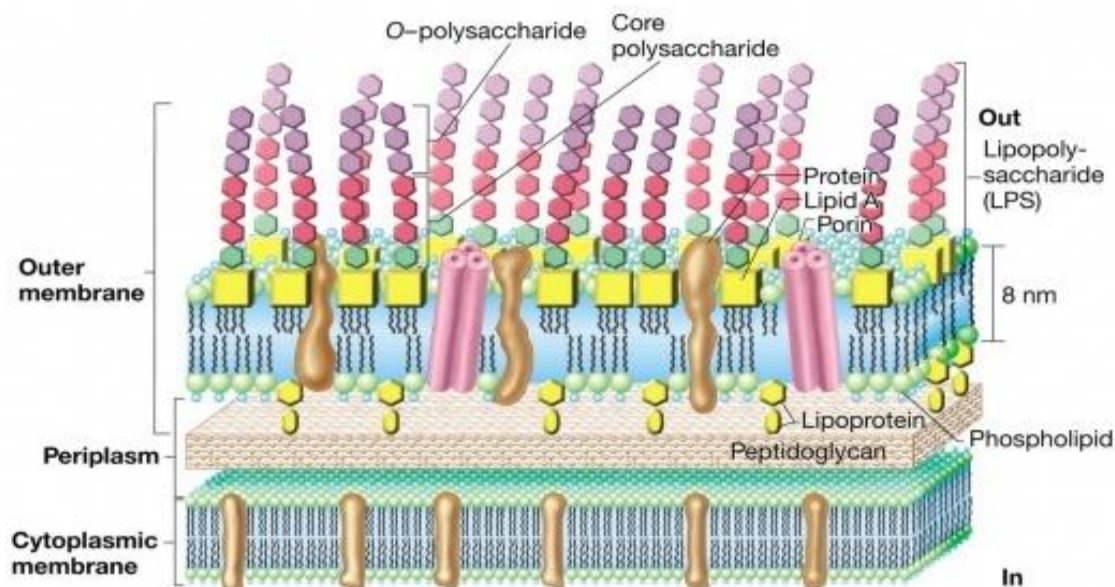
Figure 2.2: Conformation of LPS in the outer membrane of Gram-negative bacteria (8). *Lipid A is represented by the yellow squares sitting in the outer membrane, whilst the green and pink hexagons relate to the core sugars and the purple hexagons the O-antigen.*

2.1.2.1.1 Lipid A

The Lipid A portion consists of two glucosamine units, connected with a β(1→6) linkage with one phosphate group on each carbohydrate (under normal circumstances) (9). Fatty acids (acyl chains) are attached to these units, making this region highly hydrophobic (yellow area in Figure 2.1).

The biosynthetic pathway of Lipid A has been determined over 30 years ago (10). The involved genes, encoding the enzymes that monitor the pathway, are present in a single copy in the bacterial genome. As one would expect, these DNA regions are highly conserved (11). In fact, Lipid A is one of the most preserved regions of LPS.

Lipid A is vital for Gram-negative bacteria as it anchors LPS and stabilises the outer membrane (Figure 2.2). However, it is widely believed that this region is the 'endotoxic centre' of LPS. Literature reports that synthetic Lipid A and its analogues are capable of triggering the same response as the wild type Lipid A (11,12). Moreover, the effect of Lipid A's molecular conformation on toxicity has been associated with particular Gram-negative bacteria strains. *In vivo* studies have shown that when the asymmetric hexaacyl lipid A is attached to a phosphorylated disaccharide, a conical shape is formed, which is the potent conformation in terms of toxicity (13,14). This conformation is more active than the cylindrical shape, producing the most dynamic pro-inflammatory reaction, following its recognition by TLR4 (15,16). On the contrary, changes in that conformation such as switching the number of acyl chains, may lead to the reduction of Lipid A's biological activity (7).

2.1.2.1.2 Core Regions

The core oligosaccharide (OS) region is a short chain of approximately 10 sugar residues, located in the centre of the molecule (Figure 2.1). Unlike Lipid A, this region shows high diversity even between strains of the same species (16). The core regions are bound to lipid A and its formation consists of two sub-regions: the inner and outer core.

The inner core comprises L-(D)-glycero-D-(L)-manno-heptose and 3-deoxy-D-manno-octulosonic acid (KDO) residues (17). The phosphorylation of KDOs and inner core sugars results in an accumulation of negative charge. This phenomenon is crucial for the

cell viability as LPS stabilises the outer membrane via interaction with divalent cations. This interaction can determine the molecule's three-dimensional conformation and thus the core regions can influence the endotoxic activity of Lipid A (18).

The outer core contains hexoses (glucose, galactose, glucosamine) that bind to repeating units of O antigen (O-PS) (16). These O-PS units may vary in composition, stereochemistry and even in the sequence of O-glycosidic linkages between bacterial strains, providing a specific O-serotype. The outer core is significantly more variable than the inner LPS region (19).

2.1.2.1.3 O-antigen

The O-antigen, also known as O-polysaccharide and O-side-chain, consists of a repetitive glycan polymer (5). Its composition is characteristic to bacterial strains. As described in the previous section, the O-antigen is attached to the core region, comprising the outer molecular domain. It is the potential target for recognition by host antibodies, however its variability shows protective effects from an activated innate immune system (20).

LPS exists in a variety of forms, depending on the presence and repetitions of the O-antigen. For instance, the binding of the O-antigen to core lipid A results in the formation of "smooth" LPS (also known as S-type LPS). LPS is described as "rough" LPS (R-type LPS) when it lacks an O-antigen. The attachment of one repeating unit to lipid A results in the conformation of SR-LPS (core-plus-one repeating unit) (21–23). On the other hand, regarding the conformation of the outer core region, LPS can be further characterised as either "uncapped" or "capped". The "capped" core contains attached O-antigen repeating units due to modifications in the outer core region, in contrast to the 'uncapped' one which is lacking these units (22). "Rough" LPS is more hydrophobic than the "smooth", making it more vulnerable to hydrophobic antibiotics (24).

2.1.3 The role of LPS in sepsis

According to the definition and etiopathogenesis of sepsis, a Gram-negative bacterial infection is enough to trigger the exaggerated immune cascade. Numerous reports showcase the resistance of Gram-negative strains against antimicrobial formulations and

these have increase steadily through time (25,26). As previously reported, the emergence of multi-drug resistant pathogens, in an ageing population, with an increased number of immuno-compromised patients in combination with uncontrolled use of antibiotics, means that the incidence of sepsis is increasing at rate of ~ 10% each year (27).

LPS is abundant on the bacterial wall of Gram-negative bacteria and it is ubiquitously implicated in the development of the septic response. It is well established that LPS has the potential to stimulate the immune response (28). High levels of LPS have been found in a highly heterogeneous population of patients at the time of their admission to Intensive Care Units and has been associated with high mortality rates (78). Despite the high prevalence of LPS in blood, studies have demonstrated that not all of these infections are developed due to the presence of Gram-negative bacteria (29,30).

In fact, the divergent rates between Gram-negative bacterial infection and the prevalence of LPS indicate that the latter derives from other sources apart from a real-time invasion of the pathogen. The concomitant use of antibiotics could influence this observation. In addition to that, the indigenous flora of the gastrointestinal tract gives rise to a large store of LPS (estimated to be up to 25 grams) (29). This endogenous store of LPS can become translocated in to the bloodstream in the case of sepsis since during the pro-inflammatory stages of the condition blood is diverted from the gut to more valuable organs or even the tissue where the "problem" is located, which can cause loss of integrity of the GI barrier secondary to ischaemia (31).

The translocation of both LPS and bacteria from the gut to other tissues has been linked with splanchnic hyperfusion (29). Once LPS enters the circulation, the permeability of the vascular endothelium becomes elevated, facilitating LPS entry into the tissue and magnifying the inflammation. The enhanced oedema results in decreased blood volume leading to hypotension and tissue ischaemia. The gut mucosal barrier is further disrupted, allowing the influx of endogenous LPS into systemic circulation thus amplifying the problem (32).

The review authored by Munford describes the fate of endotoxin once it successfully translocates from the GI tract to the blood stream (33). All the studies suggest that bloodborne LPS is rarely found free. The study of Roth *et al.* demonstrated that more than 2/3 of the free LPS incubated with citrated human blood was bound on High Density

Lipoprotein (HDL) (34). In fact, a small portion of LPS, corresponding to less than 5 % can be found attached on cell membranes – most of them are platelets (34).

According to the previous statement, it can be referred that LPS is capable of binding to a large variety of molecules, from lipoproteins to components of the immune response, such as the soluble CD14 (35,36). A carrier protein named LPS binding protein (LBP), transfers circulating LPS and facilitates its recognition by mononuclear phagocytes through binding to pattern recognition receptors (PRRs), formed by CD14, Toll-like receptor 4 and the accessory protein MD2 (Figure 2.3) (37). The cascade gets initiated and the LPS signal is transduced to the cell nucleus, leading to the expression of a complex network of cytokines and inflammatory mediators (38). The organ systems most affected are the brain, heart, kidneys, liver and lungs, resulting to low mental alertness, myocardial depression, acute renal and hepatic failure and respiratory distress syndromes (39).
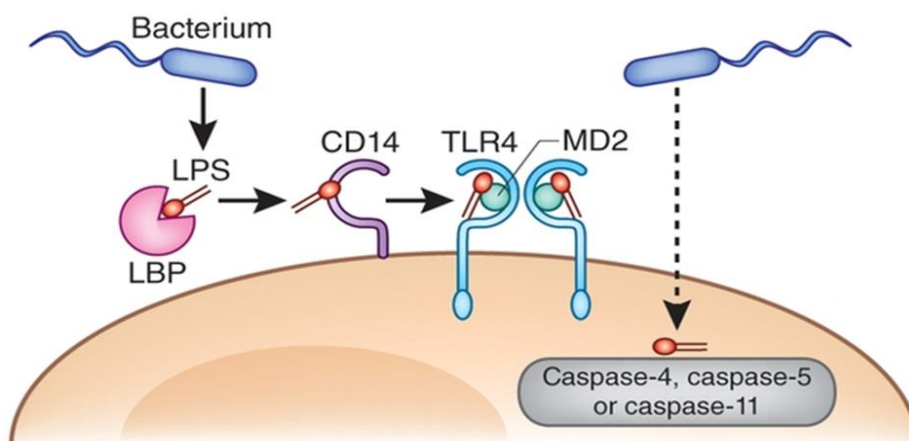
Figure 2.3: Recognition of LPS by PRRs, formed by CD14, TLR4 and the accessory protein MD2 (37). *The carrier protein LBP transfers circulating LPS and facilitates its recognition by mononuclear phagocytes.*

The *in vivo* activity of LPS - in terms of the signal transduction - is antagonised by the enzyme alkaline phosphatase and bactericidal permeability–increasing protein (40). Therefore, the involved biological mechanisms in the recognition of LPS are rather complex. Since LPS is often complexed with a wide variety of biomolecules, existing detection methods are unreliable when it comes to analysing clinical samples (29).

It can be referred that patients with high levels of LPS show more symptoms and are more susceptible to develop severe sepsis. Consequently, the prevalence of LPS characterizes a high-risk subpopulation of critically ill patients. Studies confirm that the approach of neutralizing LPS in sepsis was beneficial for patients, however any interference is quite possible to harm patients whose infection is caused by non-Gram negative organisms (41,42). The continuous monitoring of such a highly potent stimulator of the immune response can be proved quite beneficial. High levels of endotoxin may indicate early or even advanced stages of endotoxaemia leading to sepsis. However, the detection of LPS in clinical samples is quite challenging, for a number of reasons explained in the later stages of the present chapter. A diagnostic assay capable of rapidly and efficiently detecting endotoxin from clinical samples has the potential to not only help identify those patients suffering from severe endotoxemia, but also to stratify patients into treatment groups.

2.1.4 Lipopolysaccharide Detection Methods

The rabbit pyrogen test (RPT), introduced in the 1940's, was the first method reported for the detection of endotoxin (43,44). The test relied on the monitoring of the febrile response of a rabbit following injection of the under-examination formulation. If the rise in the rabbit's temperature fell outside of previously established limits, the solution was considered to contain high levels of endotoxin. There are many drawbacks associated with this method of pyrogen testing including the need for live animals, low throughput, high cost and inability to test a number of medicines, for example, those associated with severe toxicity or that modulate temperature response (45). The RPT's limit of detection is ~ 0.5 Endotoxin Units (EU) / ml (46). For reference, 1 EU is equal to approximately 0.1 ng of LPS.

As a consequence of these shortcomings, the rabbit pyrogen test was largely substituted by the Limulus amoebocyte lysate (LAL) assay, a method developed by Levin and Bang, in the 1960's (47,48). The assay relies on monitoring the coagulation reaction of haemocytes from the horseshoe crab, *Limulus polyphemus*, when exposed to endotoxin (49). Factor C is a key molecule in the development of the clotting cascade; its activation by LPS in turn activates Factor B. The final outcome of this cascade is the conversion of coagulogen into the insoluble coagulin (Figure 2.4). The coagulation based assay (the so-

called 'gel-clot' method) has a limit of detection of 0.03 EU/ml (46).The LAL assay is easier to perform compared to the rabbit pyrogen test, more amenable to testing high sample numbers and doesn't require the use of live animals. However the method remains susceptible to potential interference from drugs and other test substances (50,51). In addition, false positive results can be seen as a consequence of fungal contamination (52). (1→3)-β-glucan is a component of the fungal cell wall that interacts with factor G, resulting in the activation of clotting enzymes in the amoebocyte cells, as is the case with endotoxin (Figure 2.4) (51). Whilst the LAL assay demonstrates adequate performance in the testing of pharmaceutical products, its use in clinical studies is limited due to the poor recovery of endotoxin from biological fluids (53). Furthermore, several components of human blood directly interfere with the clotting cascade.
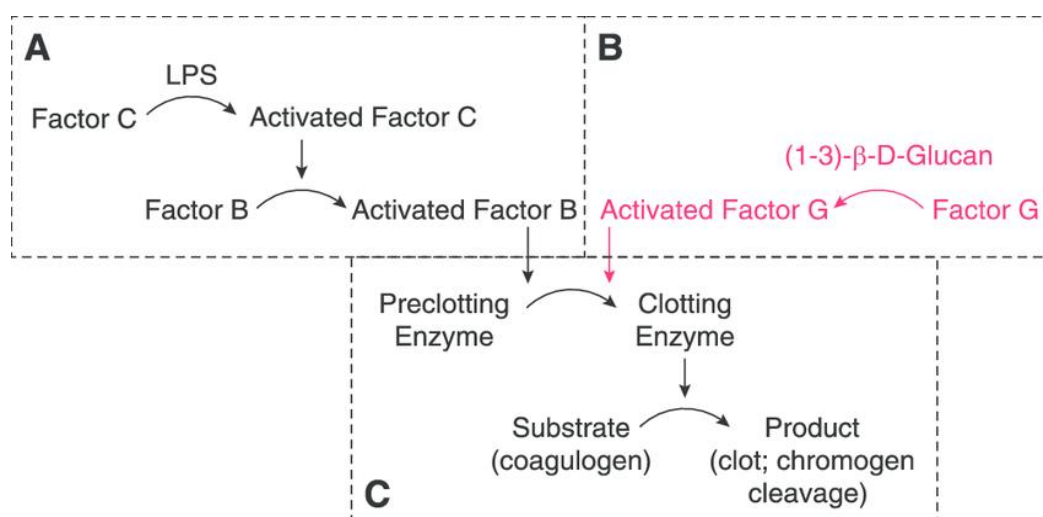
Figure 2.4: The LAL assay (31). *LPS activates factor C, thus initiating the coagulation cascade (A). The activated Factor B participates in the successful modification of the clotting enzyme that converts the coagulogen to the insoluble coagulin (C). Activation by (1→3)-β-glucan via Factor G can also lead to the activation of the pre-clotting enzyme, causing the same outcome and providing false positive results (B).*

For years, the LAL assay was the only practical method for direct detection of endotoxin. However, the Pharmacopoeia refers to another two assays, suitable to detect endotoxin: the monocyte activation test (MAT) and the recombinant Factor C (rFC) based endotoxin assay (54,55). The MAT assay was developed in 1995, while the rFc assay is more recent, first being published in 2010 (46).

The MAT assay was introduced by both the Food and Drug Administration (FDA) and European Medicines Agency (EMA) as a humane alternative method to the RPT (54). The method relies on the quantification of the pro-inflammatory cytokine IL-1β, produced by the direct exposure of human blood cells (monocytes) to the test material (56,57). The MAT assay claims to be highly sensitive, being able to detect down to 10 pg/ml (46). Studies demonstrated that the sensitivity level can be lowered even more, when cryopreserved blood is used (58). The most commonly used sources of monocytes are human whole blood, peripheral blood mononuclear cells and monocytic cell lines (56). Although promising results have been demonstrated, the method tends to be inconsistent due to the nature of human blood and requires an overnight incubation of the test material with monocytes prior to analysing the cell supernatant using a standard ELISA (46). As a consequence, it has not been widely adopted as a testing method.

A zymogen-based electrochemical sensor was developed comprising a recombinant factor C (rFC) (59). Initially, the inactive proenzyme rFC (zymogen) displays two main domains: the LPS binding domain and the enzyme region. The proenzyme is activated to protease from the interaction with endotoxin, which then subsequently hydrolyses a synthetic peptide (46,59). Finally, one of the reaction's products is detected electrochemically. The sensor can detect as little as 1 EU/ml, when the reaction time reaches 3 hours (46). A decrease in incubation time results in less sensitive results e.g. 5 EU/ml following a 1-hour incubation.

The above principal of detection has been applied to generate a modified form of an ELISA, called EndoLISA (60). More specifically, Grallert *et al.* employed the use of a bacteriophage receptor protein with high affinity towards the LPS core regions to slectviely bind LPS to the surface microwell plate. This allows the facile removal of all the other components belonging to the test solution through washing. The next step involves the activation of rFc in the exact same fashion described above. The study reports a broad range of detection, satisfactory sensitivity as well as fewer false results generated by either the presence of β-glucans (positive) or inhibitory constituents of the test solution (negative). It is however, a time-consuming assay to perform.

None of the previously described assays are routinely used to analyse clinical samples. Spectral Diagnostics recently developed the Endotoxin Activity Assay (EEA) (61). The method relies on the priming of human neutrophils by LPS-antibody complexes.

Subsequently, a chemiluminescent response is generated via the oxidation of luminol. The assay is used to provide semi-quantitative data with regard to LPS concentrations (low, intermediate or high) in clinical samples (62).

Despite LPS being implicated in the pathophysiology of sepsis and a number of other inflammatory conditions, to date an inexpensive, reliable and efficient clinical test is lacking.

2.2   Materials and Methods

2.2.1 Reagents and apparatus

A number of aptamers able to bind to lipopolysaccharide have been reported in the literature (63,64). According to Kim *et al.*, the aptamer with the highest affinity has the sequence (64):

5'- CTT CTG CCC GCC TCC TTC CTA GCC GGA TCG CGC TGG CCA GAT GAT ATA AAG GGT CAG CCC CCC AGG AGA CGA GAT AGG CGG ACA CT - 3'

This aptamer was therefore selected to be the biorecognition component in the current study. Thiol functionality was introduced at the 5' end via along with a C_6 spacer. The aptamer was purchased from Sigma-Aldrich (UK) and stored at -20 ºC prior to use. All alkanethiols [6-mercaptohexanol (MCH), 11-mercaptoundecanoic acid (MUA), 4,4-dithiodibutiric acid (DTBA)] and reducing agents [Tris (2-carboxyethyl) phosphine hydrochloride (TCEP)] were purchased from Sigma-Aldrich (UK) and stored at ambient conditions. Water and ethanol were of HPLC grade and purchased from Fisher Scientific, UK. Sulphuric acid was also purchased from Fisher Scientific (UK), while hydrogen peroxide was obtained from Sigma-Aldrich (UK). Lipopolysaccharide from *E. coli*, lipoteichoic acid and (1→3)-β-D glucan were purchased from Sigma-Aldrich (UK). The LPS used for the experimental process is conjugated to FITC label, thus, an average molecular weight of 5,289 g/mol has been used, relying on numbers provided from Pubchem (65,66). Despite the fact that the conjugation performance is rather poor (only 2-10 μg of FITC can be found in 1 mg of LPS, according to manufacturer), the study considered the molecule's molecular weight in the final calculation; the impact of adding the FITC's molecular weight is insignificant, mainly due to the fact that LPS shows a wide variety of molecular weights (15).

Polishing kits and electrochemistry accessories (Faraday's cage, 2 mm diameter gold disc working electrodes, teflon caps and Pt-wire counter electrodes) were purchased from CH Instruments (UK). Salt bridges and reference electrodes were purchased from Basi Analytical Instruments (UK). Potassium ferrocyanide [$K_4Fe(CN)_6$] was obtained from Fisher Scientific (UK) and potassium ferricyanide [$K_3Fe(CN)_6$] was purchased from Sigma-Aldrich (UK). The MultiWE32 Potensiostat was purchased from Ivium Technologies (The Netherlands).

2.2.2. Methods

2.2.2.1 Aptamer handling

All aptamer batches were aliquoted (100 μM) in TE buffer (10 mM Tris, 1 mM EDTA) pH 7.5 and kept in a non-defrosting, -20 °C freezer, for maximum long-term stability (67). Prior to use, aptamers were diluted to 10 μM in 10 mM PBS pH 7.4 (1X) enriched with 1 mM MgCl$_2$ (herein referred to as "Folding Buffer") (68). Subsequently, the aptamer solution was immersed in a waterbath to heat the aptamer to 90-95 °C for 5 minutes (69). This results in disruption of inter- and intramolecular bonds within or between neighbouring aptamer molecules. All solutions were allowed to cool to room temperature so that the aptamers can form the appropriate 3D conformation to recognize the ligands.

Thiolated aptamers must be reduced immediately prior to use, as their thiols are oxidized by manufacturers to retain molecular stability (37, 39). An aqueous solution of 1 mM TCEP (tris(2-carboxyethyl)phosphine) in TE buffer (10 mM Tris, 1 mM EDTA) enriched with 100 mM NaCl (herein referred to as "immobilisation buffer") has been used to activate the aptamer thiol groups and facilitate immobilisation on the gold surface.

2.2.2.2 Cleaning of gold working electrodes

The first step of the experimental process deals with the polishing and extensive cleaning of the gold disc of the working electrode (WE) (70). This ensures that the surface is free from residues that might interfere with the deposition of molecules, leading to either uneven distribution of thiolated molecules at the surface, non-specific binding with the target molecule or increased background impedance.

The electrode was immersed in a beaker with HPLC grade water and sonicated for five minutes. The polishing pad was soaked with 0.05 μm particle alumina slurry and the face of the electrode was carefully rubbed against the polishing pad by making a figure of 8 pattern for five minutes. On completion of the polishing process, the WEs were first rinsed with distilled water to remove the alumina particles, and then with ethanol. The WEs were subsequently immersed in ethanol and subjected to sonication for 5 minutes. Sonication was repeated after replacing the ethanol with HPLC grade water. Finally, the WEs were immersed in piranha solution (3:1 ratio of Sulphuric Acid: Hydrogen Peroxide) for 8-10 minutes, rinsed and placed into a beaker with HPLC grade water (71).

2.2.2.3 Electrochemical activation of gold working electrodes

A 10 ml solution of 0.5 M Sulfuric acid was prepared. The salt bridge was rinsed with distilled water inside and outside, filled with 10 mM PBS pH 7.4. The salt bridge was then placed in the beaker. The reference electrode (RE) was rinsed with HPLC grade water and placed inside the salt bridge. The working electrode (WE) and platinum counter electrode (CE) were rinsed with HPLC grade water and placed into the beaker, forming a 3-electrode setup. All electrodes were connected to the potensiostat and Cyclic Voltammetry was performed until there were no changes observed between consecutive voltammograms (~25 cycles) (72). The potential ranged from 0 to 1.5 V and the scan rate was equal to 100 mV/sec (73).

Following electrochemical activation, the WEs were rinsed with HPLC water and dried with nitrogen.

2.2.2.4 Development of self-assembled monolayers (SAMs)

Once it was ensured that the gold surfaces are free from molecular residues, working solutions containing an appropriate ratio of aptamer and alkanethiol were applied on the gold surfaces.

During the development and optimisation of the aptasensor, various ratios of anti-LPS aptamer and alkanethiols [mercaptohexanol (MCH), mercaptoundecanoic acid (MUA) and dithiodibutyric acid (DTBA)] were explored. All components were dissolved in immobilisation buffer pH 7.4 containing 100mM NaCl (74). The final aptamer concentration never exceeded 1 μM. Owing to the poor aqueous solubility of DTBA, a solution containing buffer / ethanol (50:50) was used for all systems using this alkanethiol; higher ethanol levels have the potential to damage the aptamer (75). Consequently, the final concentration of TCEP was 0.5 mM. The WEs were immersed in 100 μL of the prepared mix (aptamers and alkanethiols) and incubated either overnight at 2-8 °C, or for an hour under ambient conditions.

2.2.2.5 Aptasensor Characterisation

2.2.2.5.1 Electrochemical impedance spectroscopy

The acquisition process of the electrochemical impedance spectrum can be divided into two parts. Firstly, there is a small pre-treatment period – lasting 30 seconds - in which a potential of 0.2 V is applied. The potensiostat then applies 61 frequencies. More precisely, the impedance spectra were captured upon the application of a frequency range starting from 10 kHz to 100 mHz, with a 10 mV a.c. voltage superimposed on a bias d.c. voltage of 0.2 V versus and Ag / AgCl reference electrode, in a solution containing 10 mM $[Fe(CN)_6^{3-/4-}]$ | 10 mM PBS pH 7.4.

EIS responses of each SAM (alkanethiol +/- anti-LPS aptamer) were recorded at least three times to determine baseline impedance.

2.2.2.5.2 Evaluation of binding performance

Blank measurements were obtained prior to any characterisation process, with a minimum of 3 readings, separated with a time gap equal to the one of the incubation process. Each SAM was challenged with various concentrations of lipopolysaccharide from *E. coli* O111:B4. Each WE was incubated with 100 μL of LPS in 10 mM PBS pH 7.4 (concentrations vary). EIS was used to measure changes in impedance at the electrode/electrolyte interface resulting from the LPS interaction with the SAM. Before each recording, the electrodes were rinsed with 10mM PBS pH 7.4 to remove any loosely associated LPS.

2.2.2.5.3 Specificity Studies

Specificity studies were performed using (1→3)-β-glucan (GLU) and lipoteichoic acid (LTA) as pathogen-associated cross-reactants.

A 1 mg/ml stock solution of GLU was prepared in 1 % NaCl. The solution was heated for 5 minutes at 65 °C to overcome solubility problems and then allowed to cool to room temperature. The stock solution was diluted to produce concentrations of 1, 50 and 100 pg/ml using 10 mM PBS pH 7.4.

A stock solution of LTA (1 mg/ml) was prepared in 10 mM PBS pH 7.4. The stock solution was diluted to produce concentrations of 1, 50 and 100 pg/ml using 10 mM PBS pH 7.4.

The aptasensor was challenged with each of the cross-reactants in the same manner as described for LPS.

2.2.2.5.4 Chronocoulometry

Chronocoulometry has been employed to determine the number of aptamers bound to the surface of the gold WEs. The method was extracted from the paper of Zhang *et al.* with slight modification (70). To a 10 ml beaker, 6 ml of 10 mM Tris-HCl (pH 7.4) (electrochemistry buffer) was added and a teflon cap holding the reference and counter electrode was placed on top of the beaker. The beaker was placed inside the Faraday cage. The electrochemistry buffer was degassed with oxygen-free nitrogen prior to any experimentation for 10 minutes. A small tube was also fitted in the cap to provide a gentle continuous flow of nitrogen into the system.

The WE was added to the beaker and chronocoulometry was performed by applying the following parameters:

Initial potential: 0.2 V

Final potential: -0.5 V

Number of steps: 2

Pulse width: 0.25 s

Sample interval: 0.002

Sensitivity (C or A/V): 5e–5 A/V.

The data were collected and $Q_{dl} = f(t^{1/2})$ was plotted.

Subsequently, 60 µL of 10 mM $[Ru(NH_3)_6]^{3+}$ (dissolved in HPLC grade water) was injected into the solution and the same process repeated. The number of molecules bound on the surface was calculated as per the instructions provided in section 1.6.4 (Electrochemistry Fundamentals, Chronocoulometry).

The use of two steps is to get a better understanding of the surface's behaviour when interacting with the solutions and currents required from chronocoulometry. The first application period operates as a precondition of the interface and gives an opportunity to observe the reaction. On the other hand, the application of the second pulse ensures that all the ruthenium molecules are oxidised, providing better and clearer results when compared to the first period. This can also allow a comparison between the results of the two pulses, showing signs of repeatability. Nevertheless, the second period of application is being used to perform all calculations

2.3   Results and discussion

2.3.1   Electrochemical activation of WEs

It is vital that the gold surface of the WE is free from residues that might interfere with the formation of the SAM or even in the binding of LPS. Cyclic Voltammetry is a useful tool to enable evaluation and monitoring of the gold surface throughout the cleaning and functionalisation processes.

When performing CV on a gold WE, there are three consecutive oxidation peaks apparent in the cyclic voltammogram (Figure 2.5), appearing in the region of 1.35 – 1.5 V, while the sole reduction peak is evident between 1.0 – 0.8 V (73). The sharpness of each peak is indicative of the extent to which the gold surface is free from residues (73). As is evident from Figure 2.11, the resolution of oxidation and reduction peaks increases as the number of CV cycles increase. No further improvement in resolution is observed above 25 cycles.
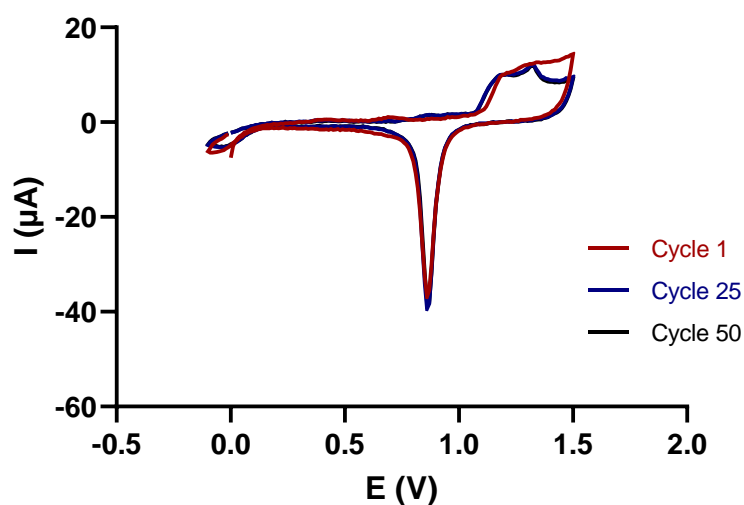
Figure 2.5: Cyclic voltammograms obtained after the cleaning of WEs. The resolution of the oxidation and reduction peaks improve between cycles 1 - 25, with little / no difference observed between cycles 25 - 50.

2.3.2   Development of an aptasensor for recognition of LPS

2.3.2.1 Evaluation of aptamer performance

The aptamer sequence employed in the current study has been extracted from the literature, and as such, its ability to interact with LPS, with reported nanomolar affinity,

has already been demonstrated (64). Although Kim *et al.* also used electrochemical transduction methodologies in their study, it was important that a baseline level of performance was established for the aptamer in this study given the desire to integrate with a molecular imprinting approach, described in Chapter 3.

In the first instance, an aptamer-only SAM system was explored. Improper folding, failure to anchor to or non-specific / non-orientated attachment to the gold surface of the working electrode could all impact on the overall recognition / binding performance of the system. For example, it is well established that amines in the DNA backbone are able to form weak bonds with gold, therefore interfering with the molecule's coordination on the surface (76). Subsequently, this leads to sub-optimal orientation of the aptamer sequence (Figure 2.6).
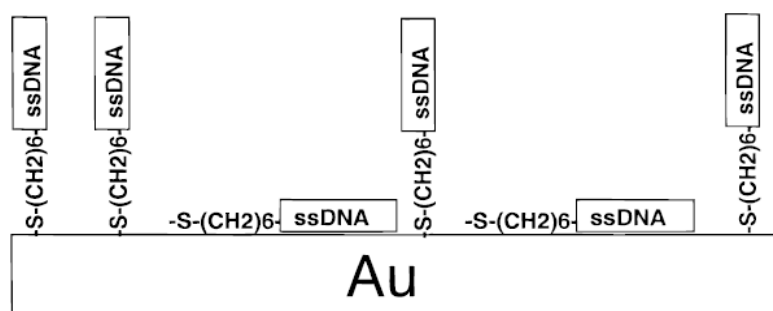
Figure 2.6: Representation of a thiolated aptamer (ssDNA) on gold. The thiol groups can form bonds with bare gold and present the aptamer in its presumed optimal configuration / orientation. However, the nitrogen containing nucleotide bases are also able to interact with gold, forming weaker bonds and forcing the molecule to "lie down" on the surface (76).

Electrochemically cleaned and activated WEs were incubated with 1 μM aptamer in immobilisation buffer overnight at 2-8 °C (n=4). Following incubation, electrodes were rinsed with 10 mM PBS pH 7.4 to remove any non-chemisorbed aptamers and then challenged with 10, 100 and 1,000 pg/ml of LPS (Figure 2.7).

Prior to any data presentation and analysis, it is worth noted that in this development stage, corresponding to the initial project experiments, a number of kinks can be observed in the spectra. These kinks are mainly located the higher frequencies and are point specific, according to the independent experiments and individual modified electrodes. The kinks deal with the wrong (higher) estimation of the imaginary impedance, due to

random interference of the environment. These issues were fixed during the project progression. Nevertheless, the data integrity is undisputed, since the spectra can provide accurate information about the system and the modified monolayers.
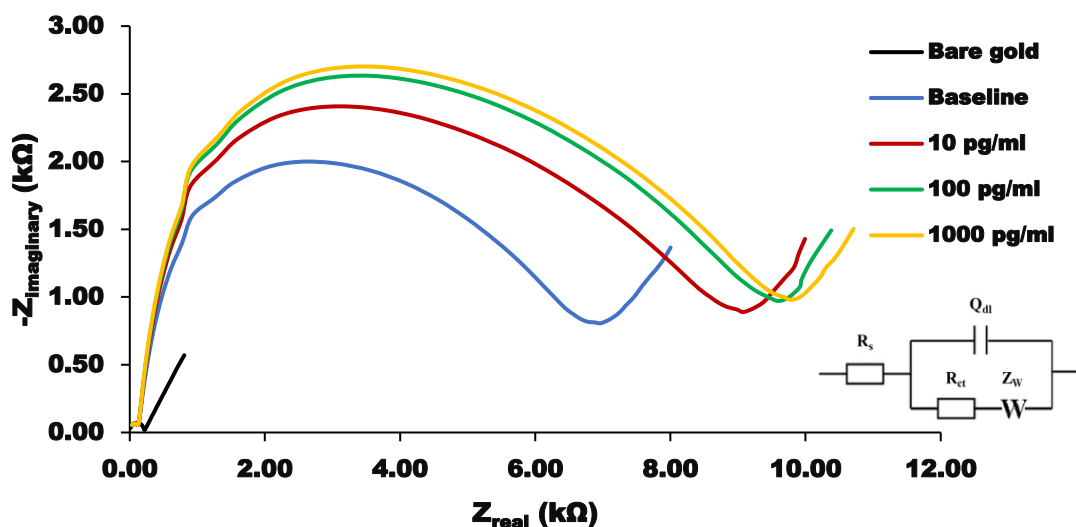
Figure 2.7: Development and characterisation of an aptamer-only SAM. The SAM recorded impedances are around ~ 6.5 kΩ. Increases in impedance are shown following incubation with a variety of concentrations of LPS (10, 100 and 1000 pg/ml). According to experimental data, the equivalent circuit that fits the curve is the $R_s((R_{ct}W)Q_{dl})$.

Following the electrode modification, EIS responses were acquired at least three times to determine the stability of the monolayer. The recorded measurements were averaged and described as the monolayer's "baseline" (blue curve, Figure 2.7). The aptamer forms a relatively stable SAM, with an impedance of ~ 6.5 kΩ. Consecutive readings show a small and stable increase in impedance possibly as aptamers rearrange at the surface of the electrode. This 'noise' diminishes with consecutive readings, and the addition of alkanethiols to the SAM in subsequent experiments will likely result in more stable SAMs. An increase in impedance of ~ 3 kΩ was observed on addition of 10 pg/ml of LPS. However, the observed signal following incubation with 1,000 pg/ml is similar to the one of 100 pg/ml, suggesting saturation of the system.

As described in Chapter 1, the equivalent circuit that has been employed to describe the system and obtain the R_{ct} values is $R_s((R_{ct}W)Q_{dl})$. All spectra demonstrate the Warburg impedance, which is more profound at lower impedances (diagonal lines with 45° slope

at end of semi-circle, Figure 2.7). In addition to that, the Q_{dl} value is the component of choice used to describe the metal / solution interface and characterises the oligonucleotide SAMs. R_s is the impedance recorded in higher frequencies due to solution, while R_{ct} is the charge transfer resistance. It should be noted that the data obtained from each spectrum provide a satisfactory fit when using $R_s((R_{ct}W)Q_{dl})$.

In an aptamer only SAM, a disordered surface and/or steric hindrance may negatively impact target binding. In the study by Kim *et al.* they report linearity over the range of 0.01 to 1 ng/ml (64). The results from the current study, suggest saturation is achieved ~ 100 pg/ml. Improved performance may be achieved through the use of alkanethiols as spacer or backfilling / blocker molecules. Such an approach is routinely used in the development of electrochemical sensors (77). The ease and convenience of developing a SAM on working electrodes allows opportunity to experiment with alkanethiols displaying different functional groups and to also vary the ratios of aptamers and spacer molecules, in an effort to maximise the performance of the system.

2.3.2.2 Screening of alkanethiols as spacer molecules

The nature of the target molecule i.e. LPS, is a key factor when considering which alkanethiols to investigate. LPS is a strongly negatively charged molecule due to a high degree of phosphorylation of the sugar molecules that make up the core and O-antigen regions. Therefore, positively charged alkanethiols such as cysteamine, were avoided as it was thought likely that a high degree of non-specific binding would be observed. Also, the aptamer itself is negatively charged and therefore solution phase complexation may have also been a problem.

Keeping the above information in mind, the alkanethiols chosen for evaluation were mercaptohexanol (MCH), mercaptoundecanoic acid (MUA) and 4,4-dithiodibutyric acid (DTBA). Both acids are negatively charged, while MCH is expected to be neutral at physiological pH values, which is the current working environment (78–80). A negatively charged SAM could potentially interfere with target binding through electrostatic repulsion. It was hoped though, that by modifying the length of the carbon chain, the organisation of the self-assembled monolayer could be optimised along with the binding performance.

Figure 2.8 shows the impedances developed by each alkanethiol. The impedances are related to the length and the charge of each molecule participating in the SAM formation. MCH shows the lowest impedances, as it contains 5 carbon atoms and a hydroxyl group providing a mild negative charge. Therefore, the monolayers created by MCH are lightly packed. On the other hand, DTBA displays 8 carbons, comprising 2 butyric acids connected via a disulfide. The disulfide is reduced once the molecule interacts with the gold surface and creates a mercaptobutanoic acid. The negative charge of the carboxyl group is bigger than the ones observed from MCH, resulting in a better packing. The biggest impedances are recorded with MUA, which contains 11 carbon atoms, adding the biggest amount of mass on the electrode.
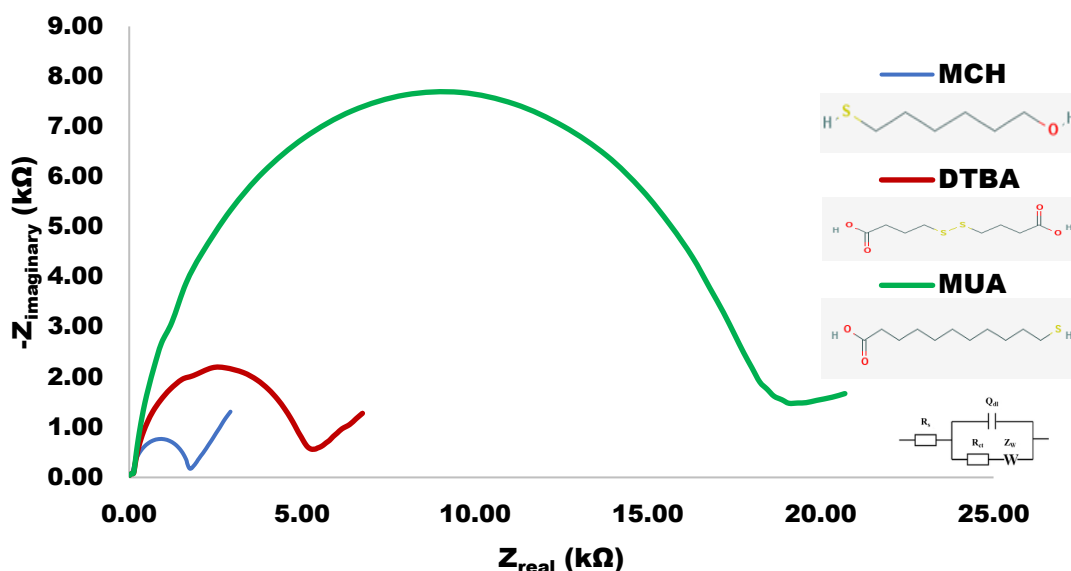
Figure 2.8: Self Assembled Monolayers of 6-mercaptohexanol (MCH), 4,4-dithiodibutyric acid (DTBA) and 11-mercaptoundecanoic acid (MUA). The molecular structures were obtained from sources (78–80).

A screening process was undertaken to determine the most suitable alkanethiol for the SAM development. The ideal candidate should be able to show minimum binding to LPS, in an attempt to avoid obtaining results vastly influenced by non-specific binding events. Alkanethiol only SAMs (n = 3) were challenged with 10, 100 and 1000 pg/ml of LPS to assess the degree of interaction (Figure 2.9).
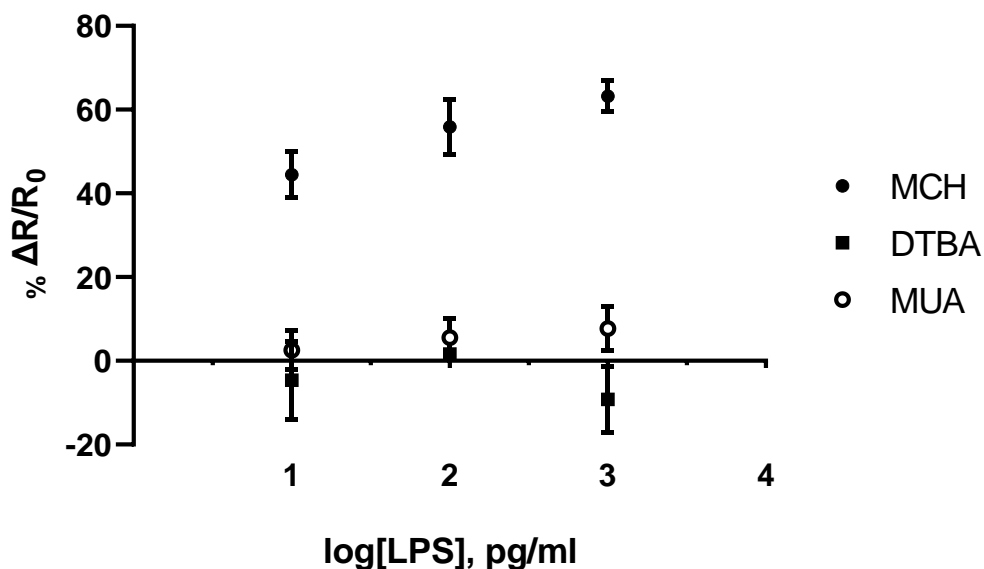
Figure 2.9: MCH, DTBA, MUA SAMs were challenged with LPS concentrations ranging from 10 to 1000 pg/ml. MCH shows strong interaction with LPS, while the negatively charged MUA and DTBA molecules show minimal binding.

MCH is the most common alkanethiol used in the development of recognition surfaces and specifically biosensors. Kim *et al.* employ the use of MCH to examine the aptamer's overall performance (64). However, in the current study results show that MCH displays significant non-specific interaction with LPS; a 44.49 % change in R_{ct} values was observed when the MCH SAM was incubated with a solution containing 10 pg/ml LPS, with further increases in R_{ct} observed for 100 pg/ml (55.90 %) and 1000 pg/ml (63.21%). It was therefore decided, that MCH would not be taken forward in the development of the aptasensor.

On the other hand, the carboxylic acid containing alkanethiols showed promising results. MUA and DTBA have 11 and 4 carbons between the thiol and carboxylic acid groups respectively, meaning that the SAMs formed by each will be quite different. Furthermore, as the name suggests, DTBA is a molecule containing two carboxylic acid groups connected via a disulphide. This disulphide is reduced at the gold surface, forming a gold-sulphur bond, leaving the carboxy-terminated propyl chains at the surface (81). The packing of short carbon-chain molecules is better, as large molecules are prone to leave gaps on the electrode surface, especially when repulsive forces between same functional groups exist.

The interaction between MUA and LPS is minimal, with all recorded changes in impedance falling below 10 %. The recorded impedances when challenging the DTBA SAM with LPS did not really deviate from the baseline value (Figure 2.9). Both carboxythiols were therefore taken forward for further evaluation.

2.3.2.3 Evaluation of mixed aptamer / alkanethiol SAMs

Mixed SAMs comprising aptamer and MUA in ratio 1:10 were developed and challenged with LPS. The results obtained were promising; a concentration dependent increase in R_{ct} values was observed (Figure 2.10). Each electrode was challenged with 10, 100, 1000 pg/ml LPS (n = 3).
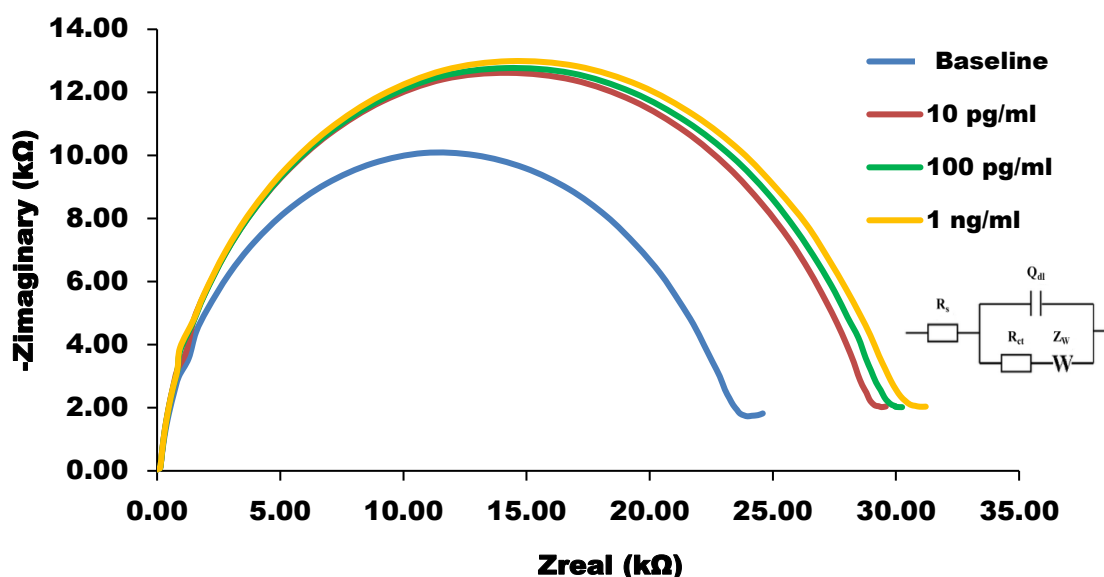
Figure 2.10: EIS results obtained from a mixed aptamer / MUA (1:10) SAM. The Nyquist plots suggest that the aptamer is still able to bind to LPS however, the relative change on addition of increasing concentrations of LPS is small.

An expected increase in baseline impedance was observed when comparing the MUA-only SAM (~ 18 kΩ) to the mixed aptamer:MUA layer (~ 24 kΩ). MUA is not expected to antagonise immobilisation of the aptamer on the gold surface but provide some level of spacing and organisation via steric and electrostatic effects. The mixed SAM retains the ability recognise LPS, however the relative change in impedance with increasing

concentrations of LPS is small; the difference in impedance between 10 pg/ml and 1000 pg/ml is only ~ 2 kΩ (Figure 2.10). This would suggest that the sensor would lack the necessary sensitivity to be useful in practice, where accurate, quantitative results would be required.

It was hypothesised that the length of the carbon chain in MUA might mean that the carboxylic acid group is close to the aptamer binding site, therefore either limiting the diffusion of LPS into the site (due to repulsive effects) or preventing the optimal binding conformation from being adopted. For this reason, MUA was considered an unsuitable spacer molecule for the sensor development.

The same experimental approach was followed to produce a mixed aptamer/DTBA SAM. As each molecule of DTBA has two carboxylic acid groups, then a ratio of 1:5 aptamer: DTBA was employed in the first instance. During the screening experiments, very little interaction between DTBA modified surfaces and LPS was observed (Figure 2.9). This means that any interaction between the aptamer/DTBA SAM and LPS will be due to the aptamer's presence. The Nyquist plots obtained following the incubation with 10 pg/ml and 100 pg/ml show a better resolution when compared to the results of 1:10 MUA-based mixed SAM. The difference in impedance observed when the system is challenged with 1000 pg/ml is not that much different to the impedance observed with 100 pg/ml (Figure 2.11). In fact, the aptamer / DTBA mixed SAM's overall response is similar to what was observed with the aptamer only SAM. This suggests that the aptamer / DTBA ratio requires further optimization.
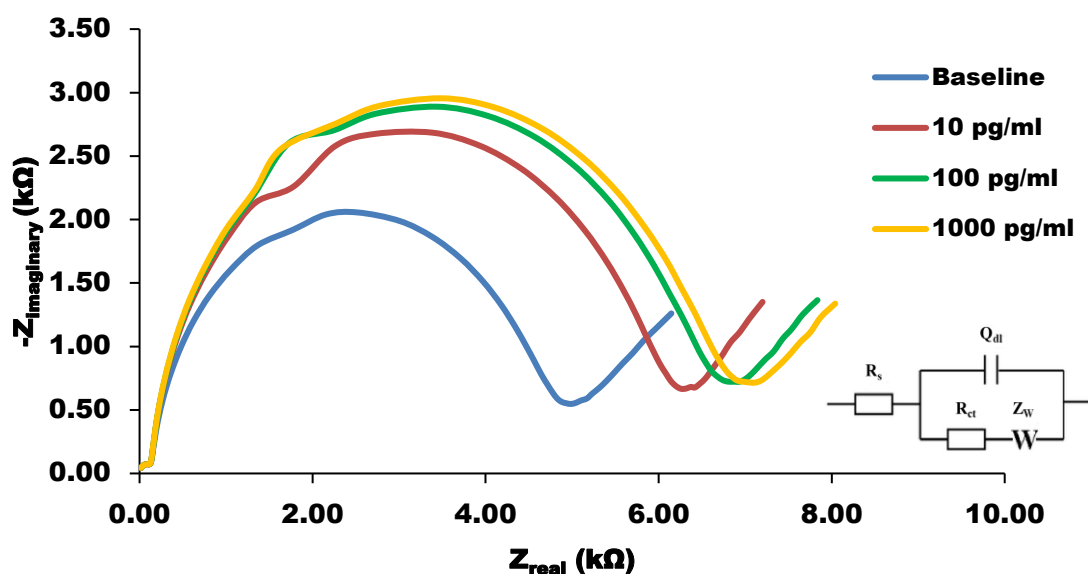
Figure 2.11: EIS results obtained from aptamer / DTBA SAM. The Nyquist plots suggest that the increase of the curves is correlated to the increase of LPS concentration. However, the ratio between DTBA and aptamer is not ideal since there is not a proper distinction between 10 and 50 pg/ml and 100 and 1000 pg/ml.

A screening process was undertaken to examine the best working ratio between the aptamer and DTBA. As the disulphide bond in DTBA reduces at the gold surface to form two mercaptobutanoic acid groups, an equimolar ratio of DTBA : aptamer should result in two "spacer" molecules per aptamer. The ratios explored are therefore expressed as molar ratios as well as aptamer : spacer ratios (Table 2.1). In all cases the aptamer concentration remained constant at 1 μM, while the DTBA concentration was varied.

Sensor	Aptamer : spacer ratio	Aptamer : DTBA molar ratio
1	1:1	2:1
2	1:10	1:5
3	1:25	1:12.5
4	1:50	1:25
5	1:75	1:32.5
6	1:100	1:50

Table 2.1: Examined ratios between aptamer and DTBA.

All SAMs were challenged with 0.1, 1, 10 and 50 pg/ml LPS to observe their overall performance (n = 1) (Figure 2.12). Sensor 1 displayed the same attributes as the aptamer only SAM (section 2.3.2.1, Figure 2.7). The aptamer dominates as there is insufficient spacer molecules and so the same steric hindrance effects are apparent, and the overall binding efficiency is reduced. Similar results were obtained for Sensor 2 (1:10), indicating that the DTBA concentration needs to be increased further.
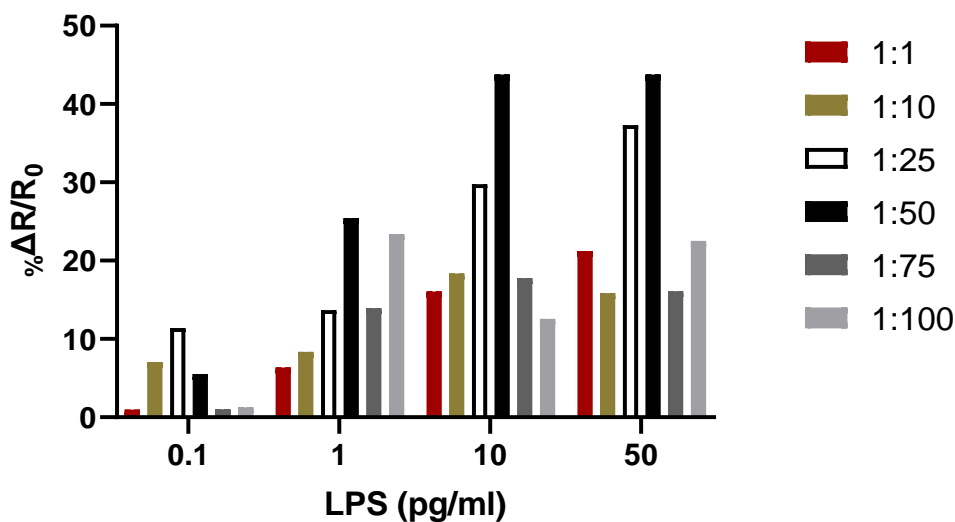
Figure 2.12: Screening of mixed aptamer : DTBA SAMs of varying ratios. Each SAM was challenged with 0.1, 1, 10 and 50 pg/ml LPS. Sensors 3 (1:25) and 4 (1:50) demonstrated the best performance over the concentration range tested.

A similar pattern was observed with sensors 5 (1:75) and 6 (1:100), however the reasons are quite different from the previous cases. Here, it is likely that the number of aptamers bound on the gold surface is insufficient, such that the surface is predominantly composed of DTBA. The lack of active binding sites significantly reduces the SAMs' ability to bind LPS. The SAMs are less responsive to the lowest concentrations, with very little change in impedance recorded following incubation with 0.1 pg/ml LPS.

Promising results were observed during the evaluation of sensors 3 (1:25) and 4 (1:50). Both cases delivered stable consecutive baseline readings. All spectra obtained after the incubation with LPS are above the baseline, indicating a good interaction between the aptamers and LPS. The sensitivity of sensor 3 is ambiguous, as the sensor failed to show significant changes in R_{ct} between the incubation with 1 and 10 pg/ml. These values might be fixed by repeating the experiment with a greater number of replicates. Sensor 4 (1:50) on the other hand showed better discrimination at the lower concentrations, with little difference between 10 and 50 pg/ml observed. The response to 0.1 pg/ml with Sensor 4 was however lower than that seen with Sensor 3. The sweet spot was considered likely somewhere in between the two systems, and so a ratio of 1:40 aptamer:spacer (1:20 aptamer:DTBA) was employed in subsequent experiments.

In other words, despite the fact that the screening process was performed with one individual electrode per monolayer, the results can divide the SAMs into 3 distinctive groups, depending on the spacer's presence. Initially, sensors 1 and 2 show similar results, lower to those of 3 and 4. The second group shows a peak in response, indicating a zone that the SAM is likely to perform at its best. The signal of sensors 5 and 6 drops in levels similar to those of the one belonging to the first group (sensors 1 and 2). The connection of each peak corresponding to the response due to the presence of LPS is developing a Gaussian-like bell-shaped curve, minimising the risks of avoiding the use of three individuals per monolayer.

2.3.3 LPS aptasensor characterisation

Having attempted to optimise the aptamer : DTBA ratio in the preceding experiments, the performance of the final system was characterised. The following performance characteristics were evaluated:

    a. Stability, reproducibility and sensitivity

    b. Detection range (binding kinetics)

    c. Determination of active binding sites

    d. System specificity

2.3.3.1 Sensor stability, reproducibility and sensitivity

Stability and sensitivity are two features that influence each other. For this reason, these properties will be examined together. A sensor showing stable and reproducible readings will allow detection of relatively small changes in impedance associated with the interaction between the aptamer and LPS. This is one of the keys factors to unlock the maximum recognition potential and create a useful and competitive sensor.

Multiple replicates of the aptasensors were generated to determine the reproducibility (n=3). As a baseline, the mixed aptamer / DTBA SAM results in an average impedance of 31.3 kΩ, with a standard deviation (SD) of 0.699 (CV of 2.24%). From a biosensing / diagnostics perspective a CV (Coefficient of Variation) of < 5% (intra-assay) or <10% (inter-assay) is deemed acceptable, although it does vary with analyte and assay methodology (82). The values of standard deviation are considered as the system's noise. Therefore, a response would be considered significant only if the ΔR_{ct} value due to incubation with the target is higher that ~2.1 kΩ (3 x SD).

The aptasensor was subsequently challenged with low concentrations of LPS (0.1, 0.5, 1, 5, 10, 15 and 20 pg/ml, n = 4 for each concentration) to determine the sensitivity of the system and to allow calculation of the limit of detection. The results are presented in Figure 2.13. The aptasensor was shown to be capable of detecting the lowest concentration (100 fg/ml), as an increase in R_{ct} of > 3 kΩ was recorded. The ΔR_{ct} value is significantly higher than 3 x signal / noise ratio. A further increase in impedance was observed following incubation of the aptasensor with 0.5 pg/ml LPS. However, the relatively high standard deviations mean that these two responses are not statistically significant (two tailed student's t-test, p = 0.8506). The same observation applies when considering the response to 0.5 and 1 pg/ml LPS. The linearity of response over the range of 1 to 20 pg/ml is satisfactory, with an R^2 of 0.9863.
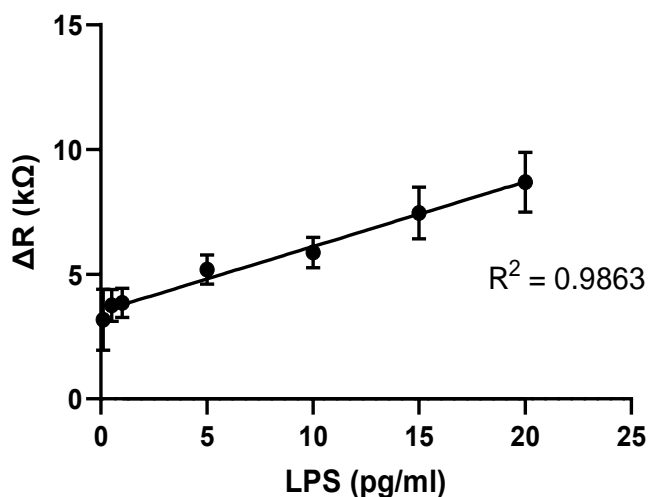
Figure 2.13: The aptasensor was challenged with 0.1, 0.5, 1, 5, 10, 15 and 20 pg/ml, to determine its sensitivity. A LOD of 100 fg/ml was determined, with good linearity demonstrated between 1 and 20 pg/ml, ($R^2 = 0.9863$).

These results that are quite interesting when compared to those found in other studies that use the same aptamer. As discussed before, Kim *et al.* demonstrate an LOD of 10 pg/ml (64). Despite the fact that Su *et al.* used the EDC/NHS approach to immobilise the aptamer to the WE, the dynamic range of the sensor also starts from 1 pg/ml. Both aptasensors are shown to behave similarly when challenged with solutions containing less than 1 pg/ml LPS (25).

Bai *et al.* have developed an electrochemical aptasensor that relies on an enzymatic recycling strategy to develop a three-way DNA junction (83). A graphene and toluidine blue nanohybrid was developed during the study. The nanohybrid was also decorated with gold nanoparticles to amplify the signal from the aptasensor. The nanohybrid's LOD was determined to be 8.7 fg/ml. However, the process of developing the aptasensor is laborious compared to the current study.

Su *et al.* developed an impedance biosensor comprising aptamer-conjugated gold nanoparticles (AuNPs), deposited on gold electrodes (84). The study describes the optimisation process to maximise the sensor's performance, focusing on the limitations affecting the aptamer's coupling to the nanoparticles and ability to recognise LPS. The aptasensor can detect as little as 5 pg/ml with a total reaction time of 10 minutes.

Wang *et al.* used differential pulse voltammetry to obtain the results generated by a sandwich-type electrochemical LPS aptasensor (85). The study used EDC/NHS chemistry to modify mercaptopropionic acid (MPA) and immobilise the aptamer on gold disc WEs. MCH was the alkanethiol of choice to block the remaining space on the modified surface. The study employs the use of Cu / Au nanoparticles fabricated by copper ions and L-cysteine, to enhance signal generation. The sensor's LOD is reported to be 33 fg/ml. Despite the promising results, the assay requires incubation at 37 $^{\circ}$C for 60 minutes.

Posha *et al.* developed a highly sensitive gold cluster mediated electrochemical LPS aptasensor that lacks any additional signal amplification strategy (86). The study modified the aptamer with an amino group at the 5' end. The gold working electrodes were covered with electrochemically synthesised gold atomic clusters. Immobilisation of the aptamer was facilitated via the 5' amine forming charge-neutral interactions with weak covalent bonds. Using this approach Posha *et al.* report an impressive LOD of 7.94 zM, with a dynamic range of 0.01 aM to 1pM (based on their assumption that 1EU/ml = 100 pM).

One of the latest studies reporting the development of an LPS aptasensor belongs to Yuan *et al.*(87). The study describes the development of a voltammetric biosensor, utilising the LPS aptamer and a functionalised graphene and molybdenum disulfide composite as a new nanocarrier. The nanocomposite displays properties such as high electrical conductivity and a large specific surface area that can greatly increase the binding of the electroactive toluidine blue (TB). The excessive loading of toluidine blue results in easier electron transfer between TB and the working electrode in an attempt to amplify the signal. Gold nanoparticles are then applied on the top of TB to immobilise the thiolated LPS aptamer. The sensor's LOD was reported to be 30.1 fg/ml.

According to data provided from the above studies, the newly developed aptasensor demonstrates positive features. The direct immobilisation of the aptamer via the 5' thiol group, provides an extremely easy and fast way to develop a SAM with the alkanethiol of choice. In fact, the total experimental time prior to sensor characterisation and challenge with LPS can be as little as 1½ hours, since overnight incubation at 2-8 $^{\circ}$C can be substituted with an hour incubation under ambient conditions. With the exception of the study by Kim *et al.* and Su *et al.*, all other protocols are a lot more time consuming and require more complex approaches (64,88).

The current aptasensor has been shown to have a LOD of 100 fg/ml, which is similar to that reported by Yuan *et al*. (87). Although better LODs are reported by Posha *et al.*, Bai *et al.* and Wang *et al.,* the process required to either develop these sensors or detect LPS (or both) are significantly more complicated.

2.3.3.2 Detection range (binding kinetics)

The next step of sensor characterisation involves the investigation of the detection range. The determination of the sensor's dynamic range is another key aspect in the developmental process. It has already been established that the sensor starts to provide significant responses following incubation with 1 pg/ml LPS; a small part of the linear response can be observed in Figure 2.13 (1 – 20 pg/ml).

In order to determine the dynamic range, the aptasensor was challenged with a wide range of LPS concentrations, ranging from 100 fg/ml (the current LOD) to 100 ng/ml (n=3). Figure 2.14 shows the aptasensor responses as a function of log LPS concentrations. ΔR_{ct} instead of $_\%\Delta R/R_0$ values are plotted on the y axis, since the differences in baseline impedance between the individual replicate SAMs are minimal ($\bar{x} = 27.2$ kΩ, SD = 2.39).

The results form a characteristic curve that follows the rules of sigmoid functions, as expected. In other words, low concentrations (at or below LOD) will generate similar responses. Then, the linear part of the curve starts to form as the applied concentrations fall within the detection range of the sensor. A plateau is observed at higher concentrations, as the sensor becomes saturated with little / no active binding sites (aptamers) available to interact with the target molecules.
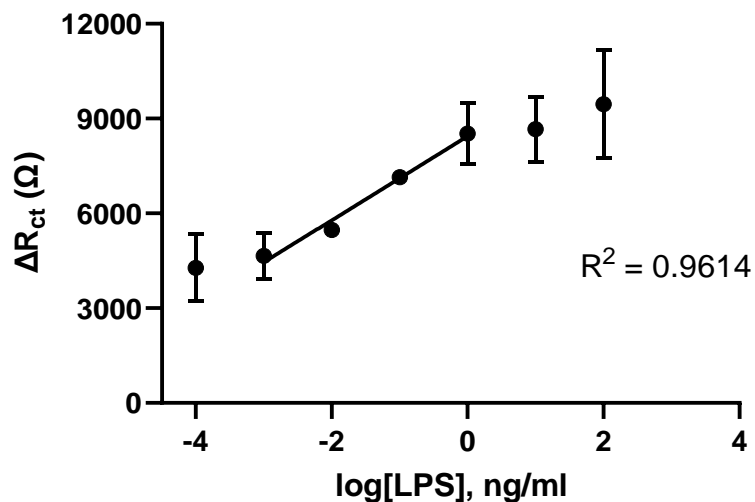
Figure 2.14: The aptasensor was challenged with a variety of LPS concentrations, ranging from 100 fg/ml to 100 ng/ml to determine its dynamic range. The sensor shows a linear response between 1 pg/ml and 1 ng/ml (R^2 = 0.9614).

According to data acquisition, the sensor's detection range appears to fall between 1 pg/ml and 1 ng/ml. However, more data points are required across this range to better characterise the binding kinetics of the system. The aptasensor was therefore challenged with further concentrations of LPS; the results are shown in Figure 2.15.

In order to generate parameters indicative of binding performance such as a dissociation constant (K_d) the LPS concentration has been converted to pM from ng/ml. It is reminded that the present study used 5,289 g/mol as the molecular weight of LPS (section 2.2.1).
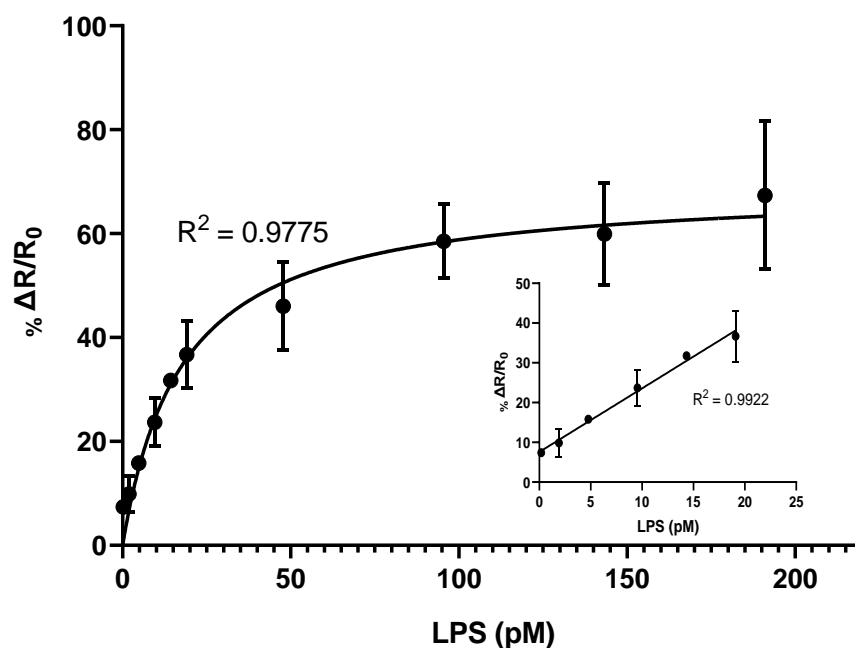
Figure 2.15: The aptasensor was challenged with a variety of LPS concentrations, ranging from 0.2 pM (1 pg/ml) to 200 pM (1 ng/ml) to determine its dynamic range. The sensor shows an apparent K_d of 17.62 pM (92.25 pg/ml) and a linear range between 0.2 and 20 pM (1 pg/ml and 100 pg/ml, R^2 = 0.9922).

As per Figure 2.13, linearity starts at ~ 0.2 pM (1 pg/ml) and the curve reaches a plateau at ~100 pM (500 pg/ml). Graphpad Prism (Version 8) was used to determine the appropriate kinetic model to fit the aptasensor's data. The one site – specific binding model (Langmuir) has been selected, since it is assumed that only one type of binding site exists (aptamer) and that the binding stoichiometry between aptamer and LPS is 1:1. Indeed, the fit is satisfactory, with an R^2 of 0.9775. Using this model, an apparent K_d of 17.62 pM (92.25 pg/ml) has been determined. The sensor's maximum response is determined at 69.19 %. A strong linear dose-dependent relationship is evident over the range of 1 to 100 pg/ml (0.2 to 20 pM), (R^2 = 0.9922).

Taking into consideration the binding performance and ease of development, the current system is competitive when compared to the other reported aptasensors (Table 2.2).

Aptasensor Chemistry	Linear Range	Reference
SH-Aptamer / MCH	0.01 to 1 ng/ml	62
EDC /NHS, NH_2 - Aptamer	1 pg/ml to 1 ng/ml	25
Nanocomposite with Au NPs/TB, SH-Aptamer	10 fg/ml to 50 ng/ml	81
Au NP modified electrode, Aptamer	0.01 to 10.24 ng/ml	82
NH_2 - Aptamer modified electrode with modified Au NPs	0.05 to 1 pg/ml and 1 to 10 pg/ml	83
Gold / Gold atomic clusters, NH_2-Aptamer	0.01 aM to 1 pM	84
Nanocomposite with TB, SH-Aptamer	50 fg/ml to 200 ng/ml	85
SH-Aptamer / DTBA	1 pg/ml to 100 pg/ml	Present study

Table 2.2: Comparison of the linear range across LPS aptasensors reported in the literature.

2.3.3.3 Determination of active binding sites

Chroncoulometry has been used to provide an estimation of the active binding sites (aptamers) on the surface of the WE following immobilisation of the mixed SAM. The use of control (DTBA SAMs) is not needed, as RuHex binds specifically in the nucleic acid's backbone (70,89).

Measurements were obtained before and after the addition of RuHex, to determine the Γ_0. Subsequently, the number of nucleotides can be determined by following the formula indicated in the description of electrochemistry fundamentals (section 1.6.4).

One set of electrodes was used to perform the experiment. The analysis revealed an approximate surface density of 6.4 x 10^{14} molecules/cm^2. In other words, the aptasensor displayed 6.63 x 10^{10} aptamer molecules, given the 3.14 x 10^{-2} cm^2 surface area of the working electrodes (diameter of 2 mm). Keeping in mind the stoichiometry of the binding reaction between aptamer and LPS is 1:1, then the same number of LPS molecules would be needed to fully saturate the aptasensor. This corresponds to 583 pg of LPS. Since 100 μL of sample is applied on to the surface of the electrode for each challenge, that would mean that a sample of ~ 5 ng/ml would saturate the aptasensor. However, it should be appreciated that 100% occupancy is unrealistic, given the fact that the system is under equilibrium and that as LPS binds to the immobilised aptamers, the surface becomes

increasingly crowded. Since LPS is also negatively charged, it is likely that repulsive effects also increase as the number of LPS bound to the sensor increases. It is therefore likely that this value is likely to be at least 5 – 10 fold less in practice. Experimental data presented in Figure 2.15, suggest that a maximum response is observed at an LPS concentration of ~ 500 pg/ml (~ 100 pg applied dose), which is supportive of the data obtained via chronocoulometry.

2.3.3.4 System specificity

The final and most crucial stage to confirm the functionality of the aptasensor involves investigating the specificity of the recognition system. It is well established that the LAL assay - the main method to detect LPS in pharmaceutical products – has issues with specificity, with false positive results seen in the presence of (1→3)-β-glucans (GLU) (9). The aptasensor was challenged with 1, 50 and 100 pg/ml of LPS, GLU and lipoteichoic acid (LTA, the main component of the membranes of Gram-positive bacteria), to assess the specificity of the system. The schematic representation of LTA and GLU can be seen on Figure 2.16. More information about their structure can be found on the next chapter since their interaction with both the aptamer and imprinted site will be examined in detail.

Figure 2.16: Schematic representations of Lipoteichoic acid (top) and (1→3)-β-glucan (bottom) (90,91)

The results are shown in Figure 2.17 (n = 3). The developed aptasensor demonstrates remarkable results, clearly favouring interaction with LPS. Both LTA and GLU showed minimal interaction with the aptasensor, generating impedances within the noise of the baseline readings.

Figure 2.17: The aptasensor was challenged with 1, 50 and 100 pg/ml of LPS, LTA and GLU. The aptamer is clearly favouring the binding of LPS, while other saccharides fail to interact with the generated SAM.

Other studies utilising the current aptamer have not focused on evaluating the interference from other pathogen associated molecular patterns (GLU and LTA). They decided to show the aptamer's selectivity to LPS by challenging with other components of commonly found in clinical samples, recording minimal responses. More precisely, Posha *et al.,* Yuan *et al.* and Bai *et al.* challenged their sensors with compounds that are abundant in plasma; (bovine) serum albumin, ascorbic acid, dopamine and glucose (83,86,87). It is important to highlight that glucose is one of the sugars that make up the polysaccharide region of LPS, thus it is very important that the aptamer should be able not to interact with the specific molecule (57). Indeed, the results of the studies focused on glucose. showed limited interaction, further cementing the specificity of the aptamer to LPS. Su *et al.* show minimal interaction following challenge of the aptasensor with (bovine) serum albumin, RNA and pDNA (25). The other study by Su *et al.* demonstrate selectivity using pDNA, RNA, BSA, glucose and sucrose (84). Interestingly, Wang et al. decided to challenge their aptasensor with epinephrine, cholesterol, glucose and uric acid (85).

2.3.4 LPS aptasensor regeneration

The ability to regenerate the aptasensor was also explored. It will be vital in follow-on studies where an aptamer-MIP hybrid system is developed (Chapter 3), that LPS can be removed from the aptamer without adversely affecting the ability of the system to rebind

the target. Literature is rather poor in this area, as only the study by Su *et al.* demonstrates evidence of sensor regeneration (25). Their aptasensor was shown to be regenerated by incubating the electrodes in PBS pH 4 for 10 min followed by several washes with PBS pH 7.4. The system could be regenerated twice before its overall performance was affected.

In the current study, a variety of approaches other than changing pH were explored. The ultimate objective is to increase the number of times the sensors can be regenerated before becoming unresponsive. A broad range of papers suggest the application of surfactants such as Triton X to remove and detach LPS from biological preparations (e.g. recombinant proteins) (92–94). However, Triton-X proved to be too harsh in the current study; application of the aforementioned surfactant destabilised the aptasensor rendering it dysfunctional. Jang *et al.* suggest the application of 0.5 % of Tween 20 followed by ultrafiltration to remove LPS from bacterial cell homogenate (95). Using 0.5% Tween 20 proved to be damaging to the aptasensor, however Tween at a concentration of 0.05% was shown to efficiently regenerate the aptasensor following a 5-minute incubation (Figure 2.18).
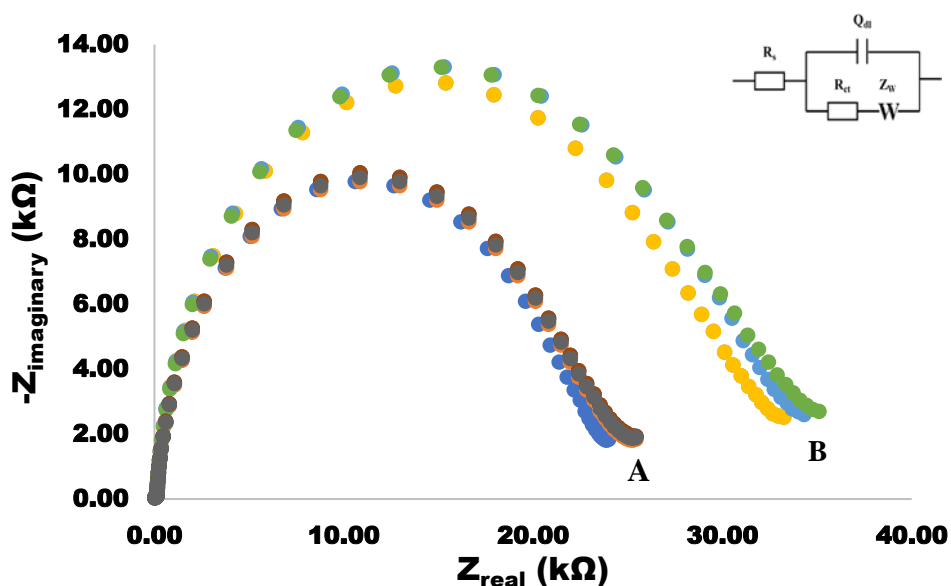
Figure 2.18: The aptasensor was challenged with 50 pg/ml and then the SAM was washed by immersion in a solution containing 0.05 % TWEEN 20. A. Impedances corresponding to baseline (blue circle) and 3 consecutive washes. B. Impedances corresponding to repeat challenge with 50 pg/ml LPS following washes (yellow = initial response, before wash).

Following immersion in 0.05% Tween, the recorded responses are similar to that of the initial SAM (Figure 2.18). Washing after incubation with 10 mM PBS pH 7.4 was used to ensure complete removal of Tween prior to re-challenge with LPS. Tween is known to interfere with the detection of LPS in the LAL assay through the formation of aggregates (96). It was therefore deemed important that all traces of Tween were removed from the aptasensor. On incubation in Tween, impedances were initially observed to increase returning to the initial baseline value of the mixed SAM following washes with 10 mM PBS pH 7.4. It was shown that the aptasensor could be regenerated up to three times with little effect on performance.

2.4   Conclusions

The present chapter discussed the successful development of an LPS aptasensor. Despite the fact that the aptamer of choice has been used for the development of a number of aptasensors, the developmental approach is different and less complex; the aptamer is directly bound on gold, minimising the distance between the site of interaction and the rest of the circuit (working electrode). This results in the minimisation of noise and a drastic reduction in preparation time, establishing a facile laboratory routine.

The developed aptasensor is highly specific to LPS, according to data collected and presented in the current study. The lack of interaction with glucan and lipoteichoic acid provides a competitive edge over the current 'gold-standard' LAL assay. The present study is the only one that demonstrates the challenge with other pathogen associated molecular patterns, as all other studies use plasma components. The present chapter has also demonstrated the successful regeneration of the aptasensor, adding a significant piece of information to the literature.

The developed aptasensor showed an LOD of 100 fg/ml, while its linear range was shown to span 1 to 100 pg/ml. Therefore, the aptasensor is competitive when compared to the other LPS sensing system described in the literature, although it is recognised that it does not demonstrate the best results.

Studies have reported that LPS concentrations in sepsis samples are ~ 110 pg/ml (97,98). This sits at the top the sensor's dynamic range, meaning that dilution is likely to be necessary. The development of a more sensitive system, with a larger dynamic range is therefore desirable. The ability to use the aptamer in a hybrid molecular imprinting approach in order to achieve this, is explored in the next Chapter.

2.5   Bibliography

1.   Beutler B, Rietschel ET. Rietschel_Beutler_Innate Immune Sensing and Its
        Roots-the Story of Endotoxin_Nat Rev_2003. 2003;3(February).

2.   Funk DJ, Parrillo JE, Kumar A. Sepsis and Septic Shock: A History. Vol. 25,
        Critical Care Clinics. 2009. p. 83–101.

3.   Parija SC. Textbook of Microbiology and Immunology. 3rd ed. Elsevier RS;
        2016. 640 p.

4.   Rietschel ET, Brade H, Brade L, Brandenburg K, Schade U, Seydel U, et al.
        Lipid A, the endotoxic center of bacterial lipopolysaccharides: relation of
        chemical structure to biological activity. Prog Clin Biol Res [Internet]. 1987
        [cited 2019 Oct 29];231:25–53. Available from:
        http://www.ncbi.nlm.nih.gov/pubmed/3588622

5.   Caroff M, Karibian D. Structure of bacterial lipopolysaccharides. Vol. 338,
        Carbohydrate Research. Elsevier BV; 2003. p. 2431–47.

6.   Lipopolysaccharide - Wikipedia [Internet]. [cited 2020 Dec 22]. Available from:
        https://en.wikipedia.org/wiki/Lipopolysaccharide

7.   Lerouge I, Vanderleyden J. O-antigen structural variation: mechanisms and
        possible roles in animal/plant-microbe interactions. FEMS Microbiol Rev
        [Internet]. 2002 Mar [cited 2019 Oct 29];26(1):17–47. Available from:
        http://www.ncbi.nlm.nih.gov/pubmed/12007641

8.   Madigan MT, Martinko J. Cell Structure/Function. In: Brock biology of
        microorganisms. 11th ed. Pearson Prentice Hall, Inc; 2006.

9.   Raetz CRH, Guan Z, Ingram BO, Six DA, Song F, Wang X, et al. Discovery of
        new biosynthetic pathways: The lipid A story. Vol. 50, Journal of Lipid
        Research. 2009.

10.   Reitschel ET, Kirikae T, Shade FU, Mamat U, Schmidt G, Loppnow H, et al.
        Bacterial endotoxin: Molecular relationships of structure to activity and function.
        Vol. 8, FASEB Journal. 1994. p. 217–25.

11.   Raetz CRH, Whitfield C. Lipopolysaccharide Endotoxins. Annu Rev Biochem.

2002 Jun;71(1):635–700.

12.   Rietschel ET, Brade H, Brade L, Brandenburg K, Schade U, Seydel U, et al. Lipid A, the endotoxic center of bacterial lipopolysaccharides: relation of chemical structure to biological activity. Prog Clin Biol Res. 1987;231:25–53.

13.   Zahringer U, Lindner B, Rietschel ET. Molecular Structure of Lipid A, The Endotoxic Center of Bacterial Lipopolysaccharides. In: Advances in Carbohydrate Chemistry and Biochemistry. 1994. p. 211–76.

14.   Seydel U, Schromm AB, Blunck R, Brandenburg K. Chemical structure, molecular conformation, and bioactivity of endotoxins. Chem Immunol [Internet]. 2000 [cited 2019 Oct 29];74:5–24. Available from: http://www.ncbi.nlm.nih.gov/pubmed/10608079

15.   Steimle A, Autenrieth IB, Frick JS. Structure and function: Lipid A modifications in commensals and pathogens. Vol. 306, International Journal of Medical Microbiology. Elsevier GmbH; 2016. p. 290–301.

16.   Netea MG, Van Deuren M, Kullberg BJ, Cavaillon JM, Van Der Meer JWM. Does the shape of lipid A determine the interaction of LPS with Toll-like receptors? Vol. 23, Trends in Immunology. Elsevier; 2002. p. 135–9.

17.   Tsujimoto H, Gotoh N, Nishino T. Diffusion of macrolide antibiotics through the outer membrane of Moraxella catarrhalis. J Infect Chemother [Internet]. 1999 Dec [cited 2019 Oct 29];5(4):196–200. Available from: http://www.ncbi.nlm.nih.gov/pubmed/11810516

18.   Heinrichs DE, Yethon JA, Whitfield C. Molecular basis for structural diversity in the core regions of the lipopolysaccharides of Escherichia coli and Salmonella enterica. Vol. 30, Molecular Microbiology. 1998. p. 221–32.

19.   Bertani B, Ruiz N. Function and Biogenesis of Lipopolysaccharides. EcoSal Plus. 2018 Feb 8;8(1).

20.   Kintz E, Heiss C, Black I, Donohue N, Brown N, Davies MR, et al. Salmonella enterica serovar Typhi lipopolysaccharide O-antigen modification impact on serum resistance and antibody recognition. Infect Immun. 2017 Apr 1;85(4).

21.   Ooi CE, Weiss J, Doerfler ME, Elsbach P. Endotoxin-neutralizing properties of

the 25 kD N-terminal fragment and a newly isolated 30 kD C-terminal fragment of the 55-60 kD bactericidal/permeability-increasing protein of human neutrophils. J Exp Med [Internet]. 1991 Sep 1 [cited 2019 Oct 29];174(3):649–55. Available from: http://www.ncbi.nlm.nih.gov/pubmed/1875165

22.   Opal SM, Palardy JE, Marra MN, Fisher CJ, McKelligon BM, Scott RW. Relative concentrations of endotoxin-binding proteins in body fluids during infection. Lancet (London, England) [Internet]. 1994 Aug 13 [cited 2019 Oct 29];344(8920):429–31. Available from: http://www.ncbi.nlm.nih.gov/pubmed/7520106

23.   Schromm AB, Brandenburg K, Loppnow H, Moran AP, Koch MH, Rietschel ET, et al. Biological activities of lipopolysaccharides are determined by the shape of their lipid A portion. Eur J Biochem [Internet]. 2000 Apr [cited 2019 Oct 29];267(7):2008–13. Available from: http://www.ncbi.nlm.nih.gov/pubmed/10727940

24.   Haziot A, Rong GW, Bazil V, Silver J, Goyert SM. Recombinant soluble CD14 inhibits LPS-induced tumor necrosis factor-alpha production by cells in whole blood. J Immunol [Internet]. 1994 Jun 15 [cited 2019 Oct 29];152(12):5868–76. Available from: http://www.ncbi.nlm.nih.gov/pubmed/7515917

25.   Arias CA, Murray BE. Antibiotic-resistant bugs in the 21st century--a clinical super-challenge. N Engl J Med [Internet]. 2009 Jan 29 [cited 2019 Oct 28];360(5):439–43. Available from: http://www.ncbi.nlm.nih.gov/pubmed/19179312

26.   Velkov T, Thompson PE, Nation RL, Li J. Structure-activity relationships of polymyxin antibiotics. Vol. 53, Journal of Medicinal Chemistry. 2010. p. 1898–916.

27.   Hall MJ, Williams SN, DeFrances CJ, Golosinskiy A. Inpatient care for septicemia or sepsis: a challenge for patients and hospitals. NCHS Data Brief. 2011;(62):1–8.

28.   Sampath VP. Bacterial endotoxin-lipopolysaccharide; structure, function and its role in immunity in vertebrates and invertebrates. Vol. 52, Agriculture and Natural Resources. Elsevier B.V.; 2018. p. 115–20.

29. Marshall JC, Foster D, Vincent J-L, Cook DJ, Cohen J, Dellinger RP, et al. Diagnostic and prognostic implications of endotoxemia in critical illness: results of the MEDIC study. J Infect Dis [Internet]. 2004 Aug 1 [cited 2019 Oct 28];190(3):527–34. Available from: http://www.ncbi.nlm.nih.gov/pubmed/15243928

30. Opal SM, Scannon PJ, Vincent JL, White M, Carroll SF, Palardy JE, et al. Relationship between plasma levels of lipopolysaccharide (LPS) and LPS-binding protein in patients with severe sepsis and septic shock. J Infect Dis [Internet]. 1999 Nov [cited 2019 Oct 28];180(5):1584–9. Available from: http://www.ncbi.nlm.nih.gov/pubmed/10515819

31. Munford RS. Endotoxemia-menace, marker, or mistake? J Leukoc Biol. 2016 Oct;100(4):687–98.

32. Van Leeuwen PAM, Boermeester MA, Houdijk APJ, Ferwerda CC, Cuesta MA, Meyer S, et al. Clinical significance of translocation. In: Gut. 1994.

33. Munford RS. Endotoxemia-menace, marker, or mistake? J Leukoc Biol [Internet]. 2016 Oct [cited 2020 Sep 7];100(4):687–98. Available from: /pmc/articles/PMC5014740/?report=abstract

34. Roth RI, Levin FC, Levin J. Distribution of bacterial endotoxin in human and rabbit blood and effects of stroma-free hemoglobin. Infect Immun [Internet]. 1993 [cited 2020 Sep 7];61(8):3209–15. Available from: https://pubmed.ncbi.nlm.nih.gov/8335351/

35. Murch O, Collin M, Hinds CJ, Thiemermann C. Lipoproteins in inflammation and sepsis. I. Basic science. Vol. 33, Intensive Care Medicine. 2007. p. 13–24.

36. Lloyd-Jones KL, Kelly MM, Kubes P. Varying Importance of Soluble and Membrane CD14 in Endothelial Detection of Lipopolysaccharide. J Immunol. 2008 Jul 15;181(2):1446–53.

37. Zipfel C. A new receptor for LPS. Vol. 16, Nature Immunology. Nature Publishing Group; 2015. p. 340–1.

38. Raetz CRH, Ulevitch RJ, Wright SD, Sibley CH, Aihao S, Nathan CF. Gram-negative endotoxin: an extraordinary lipid with profound effects on eukaryotic

signal transduction1.

39.   Rosenfeld Y, Shai Y. Lipopolysaccharide (Endotoxin)-host defense antibacterial peptides interactions: role in bacterial resistance and prevention of sepsis. Biochim Biophys Acta [Internet]. 2006 Sep [cited 2019 Oct 28];1758(9):1513–22. Available from: http://www.ncbi.nlm.nih.gov/pubmed/16854372

40.   Poelstra K, Bakker WW, Klok PA, Kamps JAAM, Hardonk MJ, Meijer DKF. Dephosphorylation of endotoxin by alkaline phosphatase in vivo. Am J Pathol. 1997 Oct;151(4):1163–9.

41.   McCloskey R V., Straube RC, Sanders C, Smith SM, Smith CR. Treatment of septic shock with human monoclonal antibody HA-1A: A randomized, double-blind, placebo-controlled trial. Ann Intern Med. 1994 Jul 1;121(1):1–5.

42.   Ziegler EJ, Fisher CJ, Sprung CL, Straube RC, Sadoff JC, Foulke GE, et al. Treatment of Gram-Negative Bacteremia and Septic Shock with HA-1A Human Monoclonal Antibody against Endotoxin. N Engl J Med [Internet]. 1991 [cited 2019 Oct 29];324(7):429–36. Available from: http://www.ncbi.nlm.nih.gov/pubmed/1988827

43.   Welch H, Calvery HO, McClosky WT, Price CW. Method of preparation and test for bacterial pyrogen. J Am Pharm Assoc (Scientific ed). 1943 Mar;32(3):65–9.

44.   Tsujimoto H, Gotoh N, Nishino T. Diffusion of macrolide antibiotics through the outer membrane of Moraxella catarrhalis. J Infect Chemother. 1999;5(4):196–200.

45.   McClosky WT, Price CW, Van Winkle W, Welch H, Calvery HO. Results of first U. S. P. Collaborative study of pyrogens. J Am Pharm Assoc (Scientific ed). 1943 Mar;32(3):69–73.

46.   Dullah EC, Ongkudon CM. Current trends in endotoxin detection and analysis of endotoxin–protein interactions. Crit Rev Biotechnol [Internet]. 2017 Feb 17 [cited 2020 Feb 23];37(2):251–61. Available from: https://www.tandfonline.com/doi/full/10.3109/07388551.2016.1141393

47.   Levin J, Bang FB. Clottable protein in Limulus; its localization and kinetics of its coagulation by endotoxin. Thromb Diath Haemorrh. 1968 Mar 31;19(1):186–97.

48.   Charles River Laboratories. EndosafeTimes: In vitro products and services newsletter. 2017;13(1):1–8.

49.   Levin J, Bang FB. The role of endotoxin in the extracellular coagulation of limulus blood. Bull Johns Hopkins Hosp. 1964 Sep;115:265–74.

50.   Iwanaga S, Miyata T, Tokunaga F, Muta T. Molecular mechanism of hemolymph clotting system in Limulus. Thromb Res. 1992 Oct 1;68(1):1–32.

51.   Nachum R, Shanbrom E. Rapid detection of Gram-negative bacteriuria by Limulus amoebocyte lysate assay. J Clin Microbiol [Internet]. 1981 Jan [cited 2020 Jan 19];13(1):158–62. Available from: http://www.ncbi.nlm.nih.gov/pubmed/7462410

52.   Wong J, Zhang Y, Patidar A, Vilar E, Finkelman M, Farrington K. Is Endotoxemia in Stable Hemodialysis Patients an Artefact? Limitations of the Limulus Amebocyte Lysate Assay and Role of (1→3)-β-D Glucan. Jha V, editor. PLoS One [Internet]. 2016 Oct 20 [cited 2020 Jan 19];11(10):e0164978. Available from: http://dx.plos.org/10.1371/journal.pone.0164978

53.   Hausmann MJ, Yulzari R, Lewis E, Saisky Y, Douvdevani A. Gel clot LAL assay in the initial management of peritoneal dialysis patients with peritonitis: A retrospective study. Nephrol Dial Transplant. 2000;15(5):680–3.

54.   Franco E, Garcia-Recio V, Jiménez P, Garrosa M, Girbés T, Cordoba-Diaz M, et al. Endotoxins from a pharmacopoeial point of view. Vol. 10, Toxins. MDPI AG; 2018.

55.   Piehler M, Roeder R, Blessing S, Reich J. Comparison of LAL and rFC Assays—Participation in a Proficiency Test Program between 2014 and 2019. Microorganisms [Internet]. 2020 Mar 16 [cited 2020 Apr 1];8(3):418. Available from: https://www.mdpi.com/2076-2607/8/3/418

56.   Schindler S, Von Aulock S, Daneshian M, Hartung T. Development validation and applications of the monocyte activation test for pyrogens based on human whole blood. Vol. 26, Altex. 2009. p. 265–77.

57.   Hartung T, Wendel A. Detection of Pyrogens using human whole blood. ALTEX [Internet]. 1995 [cited 2020 Mar 31];12(2):70–5. Available from:

http://www.ncbi.nlm.nih.gov/pubmed/11178418

58.   Hasiwa N, Daneshian M, Bruegger P, Fennrich S, Hochadel A, Hoffmann S, et al. Report evidence for the detection of non-endotoxin pyrogens by the whole blood monocyte activation test. ALTEX. 2013;30(2):169–208.

59.   Inoue KY, Ino K, Shiku H, Matsue T. Electrochemical detection of endotoxin using recombinant factor C zymogen. Electrochem commun. 2010 Aug;12(8):1066–9.

60.   Grallert H, Leopoldseder S, Schuett M, Kurze P, Buchberger B. EndoLISA®: a novel and reliable method for endotoxin detection. Nat Methods. 2011 Oct 29;8(10):iii–v.

61.   Novitsky TJ. Limitations of the Limulus amebocyte lysate test in demonstrating circulating lipopolysaccharides. In: Annals of the New York Academy of Sciences. Blackwell Publishing Inc.; 1998. p. 416–21.

62.   EAA for CLINICANS | Spectral Medical Inc [Internet]. [cited 2020 Jan 19]. Available from: https://spectraldx.com/eaa-for-clinicans/#eaa-researchers

63.   Ying GQ, Zhu FF, Yi Y, Chen JS, Mei JF, Zhang YL, et al. Selecting DNA aptamers for endotoxin separation. Biotechnol Lett [Internet]. 2015 Aug 1 [cited 2020 Apr 4];37(8):1601–5. Available from: http://www.ncbi.nlm.nih.gov/pubmed/25896682

64.   Kim SE, Su W, Cho M, Lee Y, Choe WS. Harnessing aptamers for electrochemical detection of endotoxin. Anal Biochem [Internet]. 2012;424(1):12–20. Available from: http://dx.doi.org/10.1016/j.ab.2012.02.016

65.   Lipopolysaccharide | C205H366N3O117P5 - PubChem [Internet]. [cited 2020 Mar 3]. Available from: https://pubchem.ncbi.nlm.nih.gov/compound/Lipopolysaccharide

66.   Fluorescein-5-isothiocyanate | C21H11NO5S - PubChem [Internet]. [cited 2020 Apr 4]. Available from: https://pubchem.ncbi.nlm.nih.gov/compound/18730

67.   Oligonucleotide Handling & Stability | Sigma-Aldrich [Internet]. [cited 2020 Jan 21]. Available from: https://www.sigmaaldrich.com/technical-documents/articles/biology/handling-guidelines-for-dna-and-rna-

oligonucleotides.html

68.   Aptamer Best Practices: Handling and Storage [Internet]. [cited 2020 Jan 21].
        Available from: www.basepairbio.com

69.   Jolly P, Tamboli V, Harniman RL, Estrela P, Allender CJ, Bowen JL. Aptamer-
        MIP hybrid receptor for highly sensitive electrochemical detection of prostate
        specific antigen. Biosens Bioelectron [Internet]. 2016 Jan 15 [cited 2017 Apr
        21];75:188–95. Available from:
        http://linkinghub.elsevier.com/retrieve/pii/S0956566315303699

70.   Zhang J, Song S, Wang L, Pan D, Fan C. A gold nanoparticle-based
        chronocoulometric DNA sensor for amplified detection of DNA. Nat Protoc
        [Internet]. 2007 Nov [cited 2017 Mar 26];2(11):2888–95. Available from:
        http://www.nature.com/doifinder/10.1038/nprot.2007.419

71.   Fischer LM, Tenje M, Heiskanen AR, Masuda N, Castillo J, Bentien A, et al.
        Gold cleaning methods for electrochemical detection applications. Microelectron
        Eng. 2009 Apr;86(4–6):1282–5.

72.   Su W, Lin M, Lee H, Cho M, Choe W-S, Lee Y. Determination of endotoxin
        through an aptamer-based impedance biosensor. Biosens Bioelectron [Internet].
        2012 [cited 2017 Apr 25];32(1):32–6. Available from:
        http://www.sciencedirect.com/science/article/pii/S0956566311007536

73.   Ma W, Ying Y-L, Qin L-X, Gu Z, Zhou H, Li D-W, et al. Investigating electron-
        transfer processes using a biomimetic hybrid bilayer membrane system. Nat
        Protoc [Internet]. 2013 Feb 7 [cited 2017 Dec 1];8(3):439–50. Available from:
        http://www.nature.com/doifinder/10.1038/nprot.2013.007

74.   Zhang J, Song S, Wang L, Pan D, Fan C. A gold nanoparticle-based
        chronocoulometric DNA sensor for amplified detection of DNA. 2007;

75.   Piškur J, Rupprecht A. Aggregated DNA in ethanol solution. Vol. 375, FEBS
        Letters. 1995. p. 174–8.

76.   Herne TM, Tarlov MJ. Characterization of DNA Probes Immobilized on Gold
        Surfaces. J Am Chem Soc [Internet]. 1997 Sep [cited 2020 Jan
        21];119(38):8916–20. Available from:

https://pubs.acs.org/doi/10.1021/ja9719586

77.   Radi A-E. Electrochemical Aptamer-Based Biosensors: Recent Advances and Perspectives. Res Int J Electrochem. 2011;2011:17.

78.   11-Mercaptoundecanoic acid | C11H22O2S - PubChem [Internet]. [cited 2020 Jan 25]. Available from: https://pubchem.ncbi.nlm.nih.gov/compound/543502#section=Structures

79.   6-Mercapto-1-hexanol | C6H14OS - PubChem [Internet]. [cited 2020 Jan 25]. Available from: https://pubchem.ncbi.nlm.nih.gov/compound/6-Mercapto-1-hexanol

80.   4,4'-Dithiodibutyric acid | C8H14O4S2 - PubChem [Internet]. [cited 2020 Jan 25]. Available from: https://pubchem.ncbi.nlm.nih.gov/compound/76196

81.   Dilimon VS, Rajalingam S, Delhalle J, Mekhalif Z. Self-assembly mechanism of thiol, dithiol, dithiocarboxylic acid, disulfide and diselenide on gold: An electrochemical impedance study. Phys Chem Chem Phys. 2013 Oct 21;15(39):16648–56.

82.   Precision indicates how closely a test result is reproduced [Internet]. [cited 2020 Apr 14]. Available from: http://www.clinlabnavigator.com/precision.html

83.   Bai L, Chai Y, Pu X, Yuan R. A signal-on electrochemical aptasensor for ultrasensitive detection of endotoxin using three-way DNA junction-aided enzymatic recycling and graphene nanohybrid for amplification. Nanoscale. 2014 Mar 7;6(5):2902–8.

84.   Su W, Kim S-E, Cho M, Nam J-D, Choe W-S, Lee Y. Selective detection of endotoxin using an impedance aptasensor with electrochemically deposited gold nanoparticles. Innate Immun [Internet]. 2013 Aug 19 [cited 2020 Apr 4];19(4):388–97. Available from: http://www.ncbi.nlm.nih.gov/pubmed/23165992

85.   Wang N, Dai H, Sai L, Ma H, Lin M. Copper ion-assisted gold nanoparticle aggregates for electrochemical signal amplification of lipopolysaccharide sensing. Biosens Bioelectron. 2019 Feb 1;126:529–34.

86.   Posha B, Nambiar SR, Sandhyarani N. Gold atomic cluster mediated

electrochemical aptasensor for the detection of lipopolysaccharide. Biosens Bioelectron. 2018 Mar 15;101:199–205.

87.   Yuan Y, Li L, Zhao M, Zhou J, Chen Z, Bai L. An aptamer based voltammetric biosensor for endotoxins using a functionalized graphene and molybdenum disulfide composite as a new nanocarrier. Analyst. 2019 Feb 21;144(4):1253–9.

88.   Su W, Lin M, Lee H, Cho MS, Choe WS, Lee Y. Determination of endotoxin through an aptamer-based impedance biosensor. Biosens Bioelectron. 2012 Feb 15;32(1):32–6.

89.   Satjapipat M, Sanedrin R, Zhou F. Selective desorption of alkanethiols in mixed self-assembled monolayers for subsequent oligonucleotide attachment and DNA hybridization. Langmuir. 2001 Nov 27;17(24):7637–44.

90.   Finkelman MA. (1→3)-ß-D-Glucan: Pharmaceutical Contaminant and Biological Response Modifier. Am Pharm Rev [Internet]. 2016 [cited 2020 Sep 13];(The Review of American Pharmaceutical Business & Technology). Available from: https://www.americanpharmaceuticalreview.com/Featured-Articles/190861-1-3-D-Glucan-Pharmaceutical-Contaminant-and-Biological-Response-Modifier/

91.   Malanovic N, Lohner K. Gram-positive bacterial cell envelopes: The impact on the activity of antimicrobial peptides. Biochim Biophys Acta - Biomembr. 2016 May 1;1858(5):936–46.

92.   Liu S, Tobias R, McClure S, Styba G, Shi Q, Jackowski G. Removal of endotoxin from recombinant protein preparations. Clin Biochem. 1997 Aug;30(6):455–63.

93.   Szermer-Olearnik B, Boratyński J. Removal of endotoxins from bacteriophage preparations by extraction with organic solvents. PLoS One. 2015 Mar 26;10(3).

94.   de Oliveira Magalhães P, Lopes AM, Mazzola PG, Rangel-Yagui C, Penna TCV, Pessoa A. Methods of endotoxin removal from biological preparations: A review. Vol. 10, Journal of Pharmacy and Pharmaceutical Sciences. 2007. p. 388–404.

95.   Jang H, Kim HS, Moon SC, Lee YR, Yu KY, Lee BK, et al. Effects of protein concentration and detergent on endotoxin reduction by ultrafiltration. BMB Rep [Internet]. 2009 Jul 31 [cited 2017 Dec 1];42(7):462–6. Available from:

http://www.ncbi.nlm.nih.gov/pubmed/19643046

96.   Schwarz H, Gornicec J, Neuper T, Parigiani MA, Wallner M, Duschl A, et al.
        Biological activity of masked endotoxin. Sci Rep. 2017 Mar 20;7(1):1–11.

97.   Kaser A, Ludwiczek O, Waldenberger P, Jaschke W, Vogel W, Tilg H.
        Endotoxin and its binding proteins in chronic liver disease: the effect of
        transjugular intrahepatic portosystemic shunting. Liver Int [Internet]. 2002 Oct
        [cited 2020 Feb 1];22(5):380–7. Available from:
        http://doi.wiley.com/10.1034/j.1600-0676.2002.01666.x

98.   Marshall JC, Walker PM, Foster DM, Harris D, Ribeiro M, Paice J, et al.
        Measurement of endotoxin activity in critically ill patients using whole blood
        neutrophil dependent chemiluminescence. Crit Care. 2002;6(4):342–8.

Development of LPS apta - MIP

3.1 Introduction

3.1.1. General overview

The present chapter will build upon the successful development of the LPS aptasensor described in Chapter 2. The developed system demonstrated satisfactory results so far, however an attempt to increase the observed sensitivity and dynamic range will be deployed. To achieve this, a hybrid imprinting strategy will be employed where the aptamer from Chapter 2 will be incorporated into the binding site of a molecularly imprinted polymer to generate a so-called apta-MIP system.

The term molecular imprinting was first introduced by Linus Pauling in the 1940s, describing molecular recognition through the formation of molecule specific cavities within a synthetic material. Since this early demonstration, molecular imprinting technology has received much attention as a method capable of producing cost-effective, robust, tailor-made artificial recognition elements, not dissimilar to antibodies.

Although there are a range of ways to develop a MIP, the methodology used is often governed by the final intended application. For example, bulk polymers have often been used as stationary phases for use in chromatographic separations. The present study focuses its interest on the polymerisation of electroactive monomers, as this allows for the development of biorecognition matrices directly at the surface of an electrochemical transduction platform.

The aim of this chapter is to develop a hybrid sensor, by bringing together aptamer and molecular imprinted technologies. The study begins with the screening of potential electroactive monomers for their ability to non-specifically interact with LPS. Following a narrowing of the pool of potential monomers, a number of conventional MIPs have been produced to enable final selection of the monomer to take forward into the hybrid imprinting studies. The final apta-MIP has been characterised in terms of sensitivity, dynamic range and specificity as per the aptasensor in Chapter 2. There are very few reports in the literature of such an approach being employed, indeed this is the first report of an apta-MIP being developed for a non-protein target. As a consequence, the results have been contextualised with reference to more typical MIP systems and other assays (electrochemical and wider) targeting LPS.

3.1.2. Molecularly Imprinted polymers

Linus Pauling introduced the term "molecular imprinting" in the 1940s, when proposing the development of natural antibodies in the presence of specific antigens whose role was to behave as template molecules (1). This approach lead to the development of template-induced interaction centres located in antibodies, with the final outcome being highly selective antibodies (2). However, the first to generate synthetic imprinted materials was Polyakov and his co-workers, when attempting to synthesise silica gel and use its adsorption properties to imprint dyes (2,3). Despite Polyakov's early efforts, Linus Pauling's contribution to the field is still considered more impactful as in his second publication focused on molecular imprinting, he described molecular recognition through the formation of specific cavities within a synthetic material that eventually resemble the binding site of an enzyme (4) (Figure 3.1).
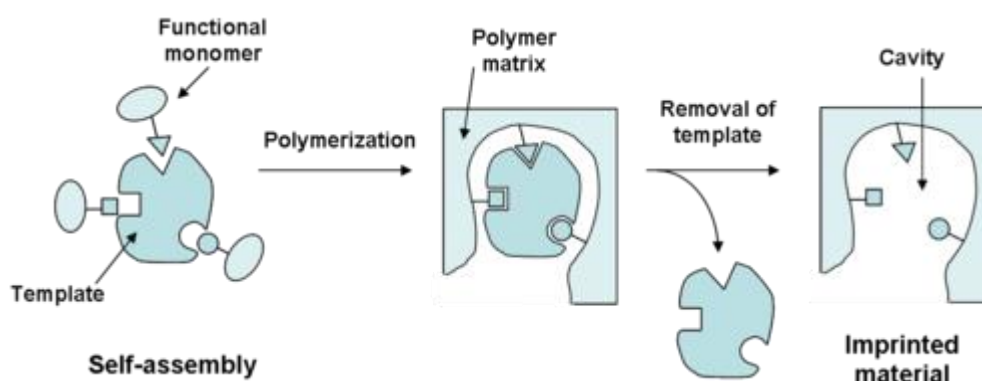
Figure 3.1: Schematic representation of the molecular imprinting process (5).

Research in the field of molecularly imprinted polymers bloomed during the 1950s, with a focus on materials capable of separating enantiomers (2). Notable works of this decade belong to Patrikeev, who worked with silica gels and bacteria; silica gel that had been incubated with bacteria (imprinted) facilitated bacterial growth to a greater extent when compared to control (non-imprinted) gels (6).

The work of Wulff and Mosbach in the 1970s and 80s were fundamental in extending the application of the technology to organic materials, using the covalent and non-

covalent molecular assembly approaches that are still used today to generate synthetic recognition materials (7,8).

MIPs are often referred to as robust, cost effective alternatives to antibodies (9). Whilst recognition of small molecules from non-aqueous sample matrices is impressive, application in the detection of biomolecules still suffers from a number of shortcomings.

The construction of truly biomimetic materials remains a great challenge for a number of reasons. Most importantly, typical developmental processes that rely on free radical initiated polymerisation are largely uncontrolled, producing multiple heterogeneous binding sites, resulting in poor reproducibility and low binding capacities (9,10). Other reasons have to deal with the size, complexity conformational flexibility and environmental sensitivity of macromolecular targets such as proteins; conventional imprinted polymers display poor recognition capabilities outside of organic media (11). Traditional bulk polymers (essentially 'chunks' of polymer that is ground and sieved to a powder) display a network of binding sites distributed throughout the polymer particles. Removal of template from, and diffusion to, more deeply located binding sites is hindered, especially when considering larger molecular templates.

Despite the aforementioned limitations, some decisive steps have been made towards the careful fabrication and optimisation of imprinted systems for the recognition of biologically important molecules. Epitope imprinting, most successful demonstrated through the work of the Shea group, uses small, well-defined epitopic sequences as template molecules to realise the recognition of the larger parent molecule (12). Epitope imprinting approaches have often been integrated with the surface imprinting of polymer films. Polymerisation at a surface, rather than freely in solution, is thought to result in the development of more homogenous, surface confined, binding sites that are more freely accessible for both template removal and rebinding (13).

The present study relies on combining a surface imprinting approach with a hybrid recognition system. The hybrid approach first described by Allender and Bowen, relies on the use of biological recognition elements e.g. peptides, aptamers etc. as "super monomers" when creating molecularly imprinted polymers (14). Dechtrirat *et al.* have since described a 'hybrid' approach using mannose to detect concanavalin A (15). More recently the Bowen group demonstrated the successful development of an apta-

MIP for the sensitive electrochemical detection of prostate specific antigen (16). The main advantage of using a hybrid system to bring about the recognition of biologically important macromolecules, such as LPS in the present study, is that it allows synthetic polymeric materials to efficiently recognise target molecules in physiologically relevant environments, whilst the methods used to generate such systems result in more homogenous binding sites that are readily accessible by the target. This often manifests itself as an increase in apparent affinity and binding capacity.

3.1.3. Surface imprinting and electroactive monomers

Whilst the literature reports a wide variety of methods for the development of a MIP, the majority rely on classic, free-radical initiated, polymer chemistry that occurs in solution to produce either chunks of polymer deriving from nano/microparticles (17). As described earlier, the use of surface imprinting approaches demonstrates a number of advantages over more traditional methods when it comes the development of systems for macromolecular templates (Figure 3.2).
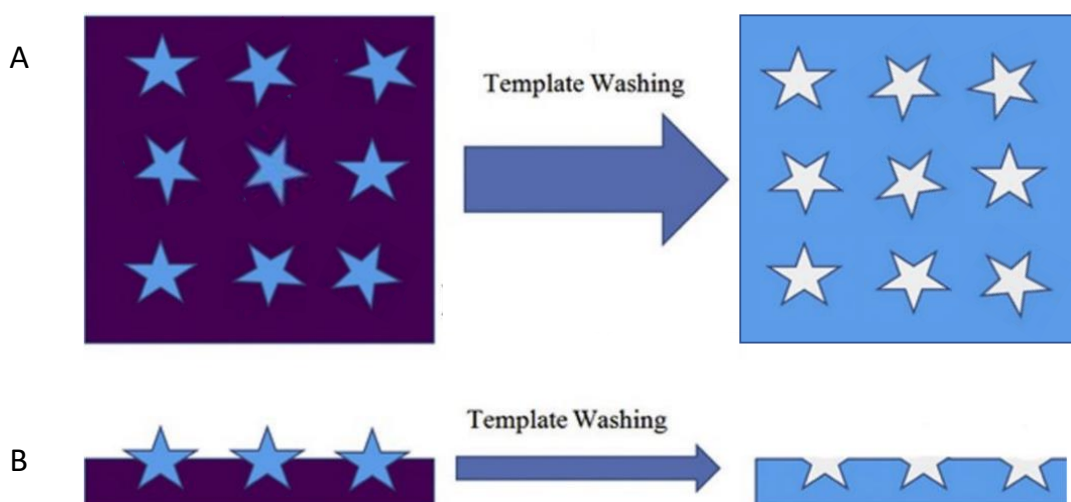
Figure 3.2: Development of molecularly imprinted polymers using A. Traditional bulk methods and B. surface imprinting approaches. Binding sites in bulk produced MIPs are distributed throughout the polymer network, and the uncontrolled nature of polymerisation results in a more heterogeneous population of imprinted sites. On the other hand, surface imprinting approaches rely in growth of a polymer around surface immobilised templates such that a more homogenous population of imprinted sites are formed at the surface of the polymer allowing facile removal and binding of the template molecule (18).

Surface imprinting can be achieved by employing a wide variety of strategies, such as the use of initiators on supporting matrices and combined surface imprinting with controlled living free radical polymerisation (19,20). However, the present study focuses on the use of electropolymerisation to develop the recognition systems directly at the surface of the transduction platform. This obviously relies on the use of electroactive monomers.

Controlled polymerisation of electroactive monomers can be achieved by employing one of three electrochemical methodologies described as galvanostatic (constant current), potentiostatic (constant potential), or most commonly potentiodynamic conditions (scanning/cycling or sweeping potential) (21). The resultant polymers can either be conducting or nonconducting, with conducting polymers further discriminated into electronically (ECPs), proton and ion conducting polymers (22–24). The present study focuses on the development of ECPs. Some examples of conducting (e.g. poly-aminophenylboronic acid / PAPBA, polypyrrole / PPy) and nonconducting (e.g. polyphenol, polyaminophenol) polymers are shown in Figure 3.3. Polydopamine (PDA) and polyaminobenzoic acid (PABA) are also considered to be nonconducting monomers (16,25) .
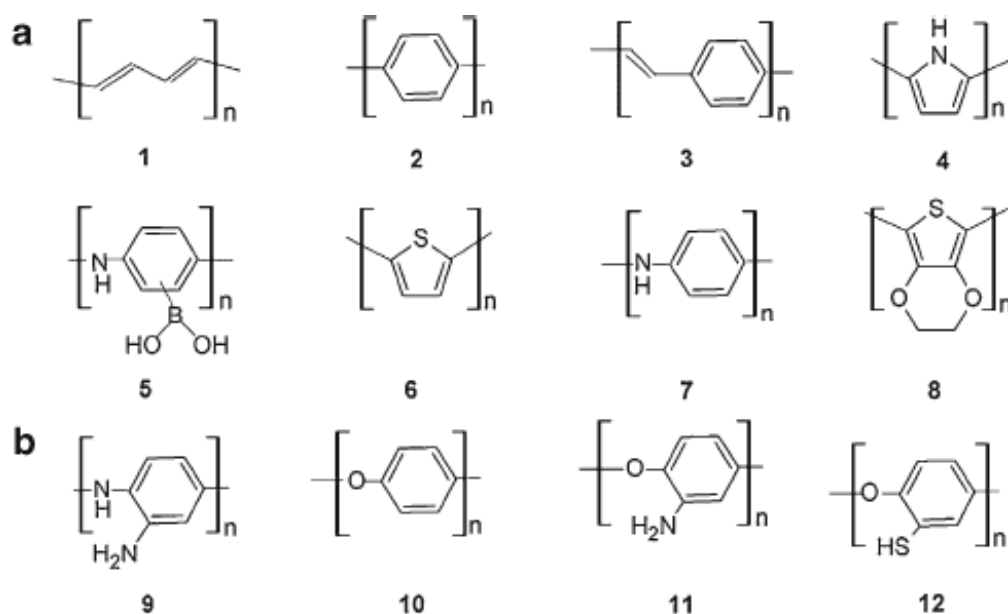
Figure 3.3: Structure of some of the most common electropolymers. Group a demonstrates electronically conducting polymers such as 1. Polyacetylene, 2. polyphenylene, 3. polyphenylenevinylene, 4. polypyrrole, 5. poly(aminophenylboronic acid), 6. polythiophene, 7. polyaniline, and 8. polyethylenedioxythiophene. Group b presents nonconducting polymers such as 9. polyphenylenediamine, 10. polyphenol, 11. polyaminophenol and 12. polythiophenol.

Electronically Conducting polymers (ECPs) display electronic properties similar to those of metals, without losing their conventional organic identity. The appearance of these electrochemical properties is based on the conjugated π-electron backbones (21). More specifically, neighbouring sp^2 hybridised carbon atom centres form the backbones of ECPs. Each centre donates one valence electron to reside in a p_z atomic orbital, which finds itself in an orthogonal position to three σ bonds. These bonds are developed by the presence of other p orbitals, whose electrons interact with adjacent centres to finally form the conjugated π orbitals. The conductivity depends on the high mobility of these electrons, allowing currents to surpass the polymer mass (22).

On the other hand, nonconducting polymers demonstrate a completely different formation. The valence electrons are found in sp^3 hybridised atomic orbitals that heavily support covalent bonds. These electrons exhibit low mobility resulting in the development of an insulator. The developed films are thin and self-controlling by the increasing impedances during electropolymerisation (21).

3.1.4. Selecting the candidate electroactive monomers

A wide selection of electroactive monomers, along with techniques to deposit them on the surface of interest, has been reported in the literature (Table 3.1). Therefore, the first and probably most crucial stage of the present study was to identify the best candidate monomer for the development of the hybrid imprinting system. In order to initially narrow the selection to a manageable group of monomers that can be taken forward into screening studies, consideration of the target molecule (LPS) and its physicochemical properties is needed.

As described in Chapters 1 & 2, lipopolysaccharide is a molecule containing a lipid region and an abundance of sugars in the core and O-antigen regions. A good number of studies have focused on the generation of polymers that interact with sugars such as glucose. Many rely on creation of a permeable polymer film to entrap glucose oxidase and determine glucose levels (26). ul Haque *et al.* used aniline to develop such a sensor, as this monomer produces a polymer of high porosity, thus allowing glucose to permeate through the polymer network and reach the enzyme (27). 3-aminophenol has been used in much the same way, with a study by Dawei *et al.* demonstrating an amperometric sensor by entrapping glucose oxidase in the electropolymer (28).

The presence of sugars means that LPS contains diols. Monomers containing boronic acid – e.g. aminophenylboronic acid (APBA) - have been extensively demonstrated as ideal when targeting molecules displaying such functionality (29). Furthermore, APBA has been shown to be an effective monomer when imprinting whole bacterial membranes (30). Incubation with *E. coli* resulted in an increase in impedance of ~ 40%. Given the high density of LPS in the outer membrane of Gram-negative bacteria, such as *E. coli*, it is likely that the APBA polymer is interacting with the saccharide portion of the molecule.

Dopamine (DA) is a popular electroactive monomer. Its structure offers the opportunity to create hydrogen bonds with target molecules. A patent describing the development of a MIP chip targeting LPS using SPR sensing relies on the formation of polydopamine (PDA) (31). This is one of the very few examples of molecular imprinting technology being successfully used to specifically target LPS.
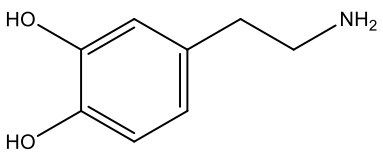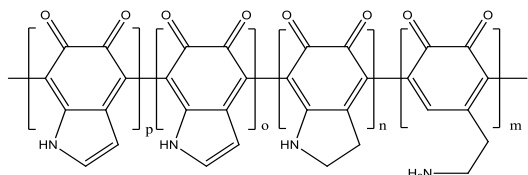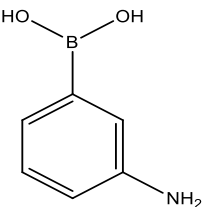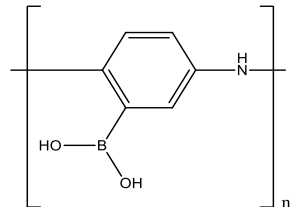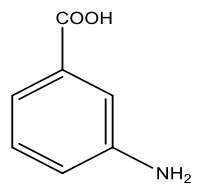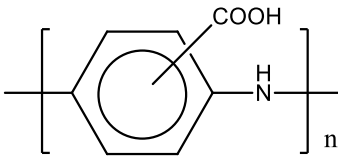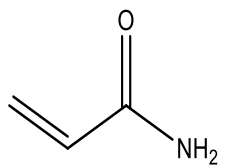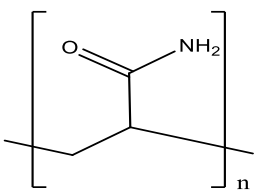
Ogawa *et al.* attempted to develop lipid A-imprinted polymer hydrogels that selectively recognize lipopolysaccharides, using vinylpyrrolidone and acrylamide (32). Altintas *et al.* also tried to developed a nano-MIP for the ultrasensitive detection of LPS, using acrylamide as one of the potential monomers with ambiguous results (33). The conditions required to bring about the electropolymerisation of acrylamide involve the application of potentials ranging from -1 to 1.8 V (34). It is well established that the reductive desorption of thiolated molecules occurs between -0.9 and -1.5 V, reaching a peak around -1.4 V (35). Consequently, acrylamide is unlikely to be compatible with the apta-MIP system under development in the current study.

There is little in the literature with regard to the use of 3-aminobenzoic acid (ABA) for the recognition of LPS and related molecules. However, polyaminobenzoic acid (PABA) appears to offer a good opportunity to develop hydrogen bonds with the templates, similar to DA. An example of work undertaken using ABA is described in a study by Sriwichai *et al.*, where this monomer was used to develop a thin polymeric film to create a label-free immunosensor targeting human immunoglobulin G (IgG) (25).

The list of potential candidates closes with the addition of squaramides and thiophenes. Squaramides have been shown to be excellent monomers for the recognition of negatively charged targets (36). However, these monomers are not naturally

electropolymerisable, requiring further chemical modification to be able to polymerise in this manner. On the other hand, modified versions of thiophenes are able to interact with diols (37). Again, although an electropolymerisation approach is feasible, the monomers are not commercially available, rather they must be synthesised in the lab in a time-consuming process.

Considering all of the above information, it was anticipated that polydopamine (PDA) and polyaminophenylboronic acid (PAPBA) would demonstrate the best performance in the screening studies. Aniline (ANI) and aminobenzoic acid (ABA) were also selected for evaluation.

Name	Monomer	Justification	Electropolymerisation	Method
Dopamine (DA)		a. Hydrogen Bonding b. Seems to interact with sugars efficiently		Using CV: -0.5 – 0.5 V E step: 10 mV Scan rate: 20 mV/sec
3-aminophenyl-boronic acid (APBA)		a. Interaction with Sugars b. Imprinting Bacterial Surfaces as a whole		Using CV: -0.2 – 0.7 V E step: 10 mV Scan rate:100 mV/sec
3-aminobenzoic acid (ABA)		Hydrogen Bonding		Using CV: -0.2 to 0.9 V (10 mA), E step: 10 mV Scan rate: 20 mV/sec
Acrylamide (AA)		Interaction with Lipid A		Potential sweep: -1 – 1.8 V E step: 10 mV Scan rate:20 mV/sec
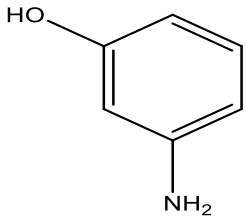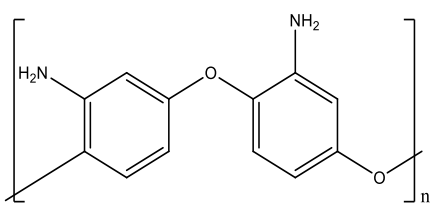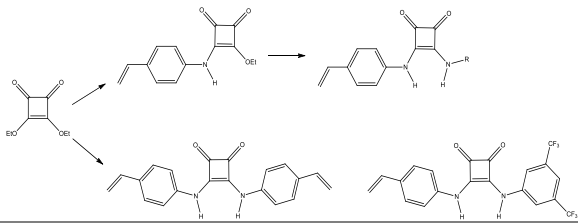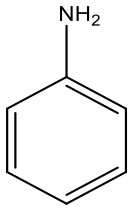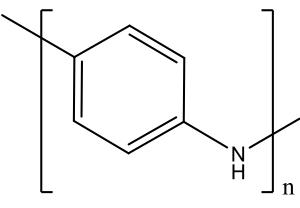
3-Aminophenol	HO—〇—NH₂	a. Interaction with sugars (Glucose) b. Formation of amperometric biosensors	(polymer structure)	Using CV: -0.2 – 1.6 V E step: 10 mV Scan rate: 50 mV/sec
Squaramides	(reaction scheme)	Interaction with anions	N/A	Unknown
Aniline	NH₂—〇	a. Interaction with sugars (Glucose) b. Formation of amperometric biosensors	(polymer structure)	Using CV: -0.2V to +0.85V E step: 10 mV Scan rate: 100 mV/sec

Table 3.1: Candidate electroactive monomers for the apta-MIP development and their polymerisation products.

3.2 Materials and Methods

General electrochemical approaches

The experimental process described in this chapter has common parts with the one described in Chapter 2. Mechanical polishing and electrochemical activation of gold electrodes are fundamental parts of the experimental process and are always used in the preparation of the electrochemical sensors. Additionally, the preparation of redox probes / solutions for use in CV, EIS and chronocoulometry remains the same. For this reason, methodological descriptions for these processes will not be duplicated in this section.

3.2.1. Materials

All monomers (aniline, dopamine, 3-aminobenzoic acid, 3-aminophenylboronic acid) and Sodium fluoride (NaF) were purchased from Sigma-Aldrich (UK) and stored at ambient conditions.

All other reagents including the aptamer, solvents etc have already been described in Chapter 2 along with details of the equipment used.

3.2.2. Methods

3.2.2.1 Monomer screening – electropolymerisation and challenge with LPS

Prior to any polymerisation process, the WEs were polished and cleaned as previously described in Chapter 2. A solution containing one of the candidate monomers was prepared and degassed with nitrogen. The solution was either stored at 2-8 ^{o}C if not used immediately or transferred to a beaker containing the three-electrode setup.

A 5 mM solution of dopamine (DA) in 10mM PBS pH 7.4 was prepared. The applied potential was cycled from -0.5 to 0.5 V with a step of 10 mV and a scan rate of 20 mV/sec. The number of cycles of cyclic voltammetry was varied (16).

A 4mM solution of aniline in 0.1M HCl was prepared and polymerised with successive cyclic voltammetric sweeps in which the applied potential is swept between -0.2V to +0.85V with a step of 10 mV, at a scan rate of 100mV/sec (27).

A 50mM solution of 3-amino benzoic acid (ABA) was prepared in 0.5 M H_2SO_4. The applied potential was cycled between -0.2 and 0.9 V, with a step of 10 mV and a scan rate of 20 mV/sec (25).

A 50 mM solution of 3-aminophenylboronic acid (APBA) was prepared in 100 mM PBS pH 5.0 enriched with 120 mM NaF. The applied potential was cycled from -0.2 to 0.7 V with a step of 10 mV and scan rate of 50 mV/sec (38).

Following polymerisation, the modified electrodes were immediately immersed into 10 mM [Fe(CN)$_6^{3-/4-}$] | 10 mM PBS pH 7.4 and allowed to stabilise. CV and EIS were used to confirm growth of a polymer layer. Once a stable baseline reading had been obtained, polymers were incubated with 10, 20 and 50 pg/ml of LPS, with EIS being used to monitor the interaction with the polymer surface.

3.2.2.2 Polymer washing / regeneration

The non-imprinted polymers generated through the methods outlined in 3.2.2.1 (10 cycles of CV) were incubated with 50 pg/ml LPS and analysed by EIS. The electrodes were subsequently immersed in a solution containing 0.05 % TWEEN 20 for 5 minutes followed by 10 mM PBS pH 7.4 for another 5 minutes. The electrodes were then stored in 10 mM [Fe(CN)$_6^{3-/4-}$] 10 mM PBS pH 7.4 and left to stabilise, before performing EIS again. The same approach was used to wash both conventionally imprinted polymers and hybrid recognition (apta-MIP) systems.

3.2.2.3 Surface Imprinting – generation of conventional MIPs

In order to develop a conventional MIP, bare WEs were submerged in a 50 pg/ml solution of LPS dissolved in HPLC water for an hour under ambient conditions to allow deposition of LPS at the electrode surface. The electrodes were rinsed with 10 mM PBS pH 7.4 to remove any non-chemisorbed LPS, before undergoing electropolymerisation with the monomer of choice. The polymer(s) were subsequently washed, as described in 3.2.2.2 and then challenged with 10, 20 and 50 pg/ml of LPS. EIS was used to determine MIP binding performance.

3.2.2.4 Hybrid imprinting strategy - Generation of apta-MIPs

Following the protocol described in Chapter 2, 10 μM of freshly thawed anti-LPS aptamer was incubated with 10 μM LPS in folding buffer for 45 minutes to allow complex formation. The aptamer-LPS complex was diluted to 1 μM and incubated with 1 mM TCEP in immobilisation buffer for 5 minutes. The solution was then applied to the WEs overnight at 2-8 ℃.

Subsequently the WEs were washed with 10 mM PBS pH 7.4 to remove any loosely associated complexes and were then immersed in a degassed monomer solution. The monomers advanced in this stage are dopamine (5 mM) and 3-aminophenylboronic acid (50 mM). The polymerisation process has followed the protocol described in section 3.2.2.1.

The number of CV cycles were varied to control polymer layer thickness. The hybrid apta-MIPs were washed as described in 3.2.2.2 before being challenged with LPS at a variety of concentrations to determine their performance using EIS.

3.2.2.5 Sensor characterisation

As described in Chapter 2, cyclic voltammetry and EIS was used to characterise the apta-MIP and assess its performance as a sensor for LPS. The methodological approach is the same as detailed in Section 2.2.5, and so will not be repeated here.

3.2.2.5.1 Chronocoulometry

The method described in Section 2, with slight modification, was used to estimate the number of aptamers immobilised on the surface of the WE. Reagents and concentrations remain the same, however the pulse has changed to 500 ms from 250 ms. The larger pulse time has consequently dropped the experimental periods to 1 period instead of 2. The system set-up therefore displays the following parameters:

Initial potential: 0.2 V

Final potential: -0.5 V

Number of steps: 1

Pulse width: 0.5 s

Sample interval: 0.002

Sensitivity (C or A/V): 5e–5 A/V.

WEs were modified with the aptamer – LPS complex, to mimic the surface coordination during the development of the apta-MIP. Chronocoulometry was then performed in the presence and absence of LPS. LPS was removed by washing with Tween / PBS as detailed in 3.2.2.2.

3.2.2.5.2 Specificity Studies

Specificity studies were performed using (1→3)-β-glucan (GLU) and lipoteichoic acid (LTA) as pathogen-associated cross-reactants. The apta-MIP was also challenged with human serum albumin (HSA).

A 1 mg/ml stock solution of GLU was prepared in 1 % NaCl. The solution was heated for 5 minutes at 65 °C to overcome solubility problems and then allowed to cool to room temperature. The stock solution was diluted to produce concentrations ranging from 1 fg/ml to 100 pg/ml using 10 mM PBS pH 7.4.

A stock solution of LTA (1 mg/ml) was prepared in 10 mM PBS pH 7.4. The stock solution was diluted to produce concentrations ranging from 1 pg/ml to 1000 pg/ml.

For the studies involving HSA, solutions of 0.5, 5, 500 and 5,000 μg / ml of HSA dissolved in 10 mM PBS pH 7.4 were prepared.

The apta-MIP system was challenged with each of the cross-reactants in the same manner as described for LPS.

3.2.2.5.3 Recovery of LPS from spiked serum

Human serum (obtained following informed consent), spiked to produce a final concentration of 1 ng/ml LPS, was used in this study. Samples for testing were prepared by taking 100 μL of the spiked sample and mixing with 200 μL of 3.75 % v/v HCl (final concentration 2.5 %). The sample was then heated at 100 °C for 3 minutes, before being allowed to cool to room temperature and mixed with an equal volume of 5 % NaOH. The

sample was then diluted with 10 mM PBS pH 7.4 to obtain an LPS concentration of 100 pg/ml. This sample was further diluted to a concentration of 10 fg/ml using 10 mM PBS pH 7.4 A blank sample was prepared in the same manner, using non-spiked serum. EIS was used to evaluate the response of the apta-MIP.

3.3 Results and discussion

3.3.1. Monomer screening – electropolymerisation and challenge with LPS

Four monomers were screened during this study as outlined in the introduction to this Chapter. In the screening experiments, polymers were grown in the absence of LPS to generate non-imprinted polymer surfaces that could subsequently be incubated with LPS to assess degree of interaction. For each monomer, three replicates were prepared and tested. The number of cycles of polymerisation was varied up to a maximum of 10 to allow exploration of polymer growth. It was assumed, based on previous work of the group, that 10 cycles were sufficient to ensure growth of a complete polymer layer at the surface of the working electrode (16).

Figures 3.4 and 3.5 show the voltammograms obtained following polymerisation of each of the under-examination monomers. Each monomer generates a characteristic CV profile that can be confirmed from other studies (16,25,27,38). According to the literature, the generated polymers can be divided into conducting - polyaminophenylboronic acid (PAPBA) and polyaniline (PANI), (Figure 3.4) - and nonconducting - polydopamine (PDA) and polyaminobenzoic acid (PABA), Figure 3.5.
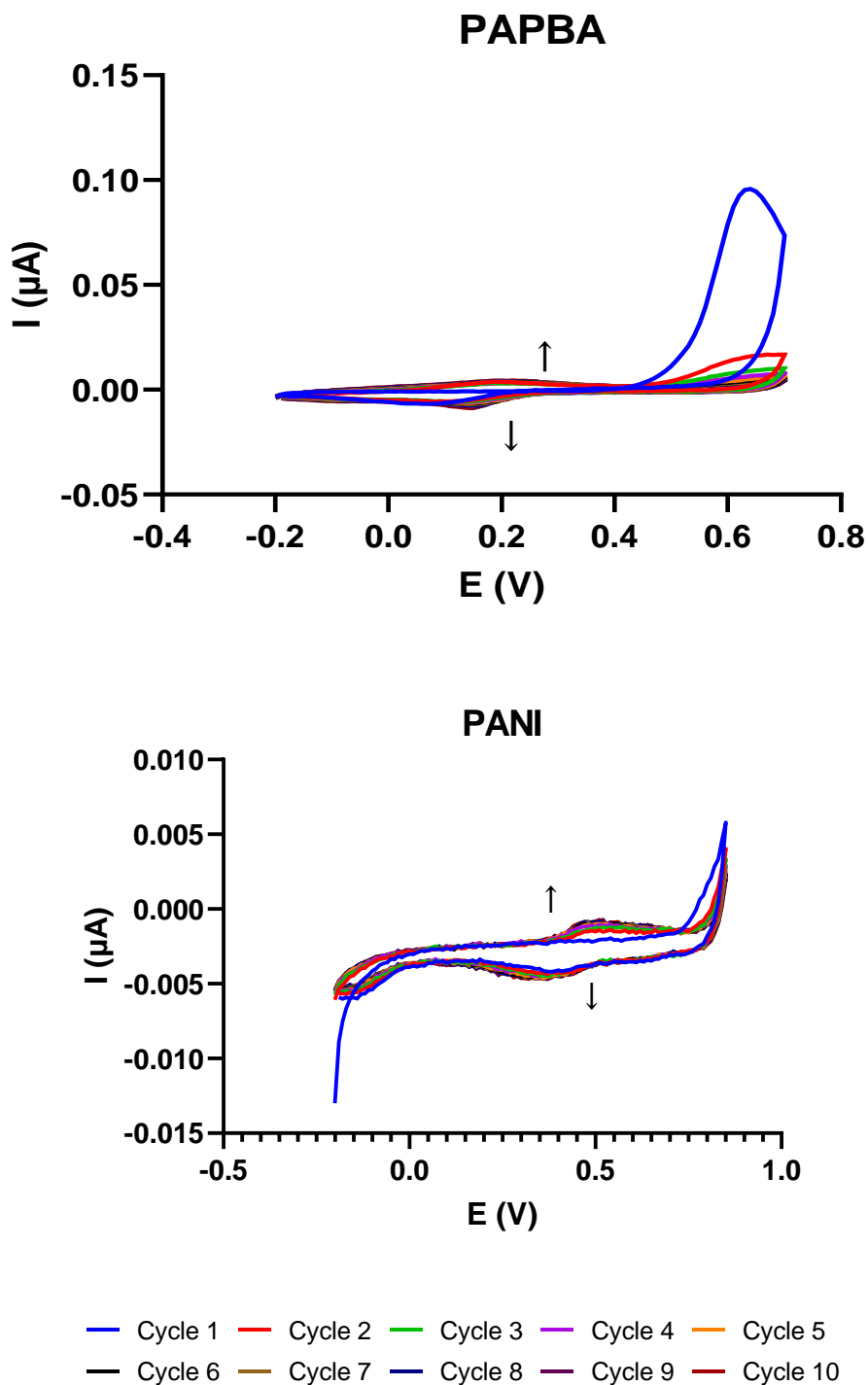
Figure 3.4: Voltammograms obtained following various cycles of polymerisation. Both PAPBA (top) and PANI (bottom) are conducting in nature, as evidenced by the increasing redox peaks on the voltammogram (indicated by arrows).
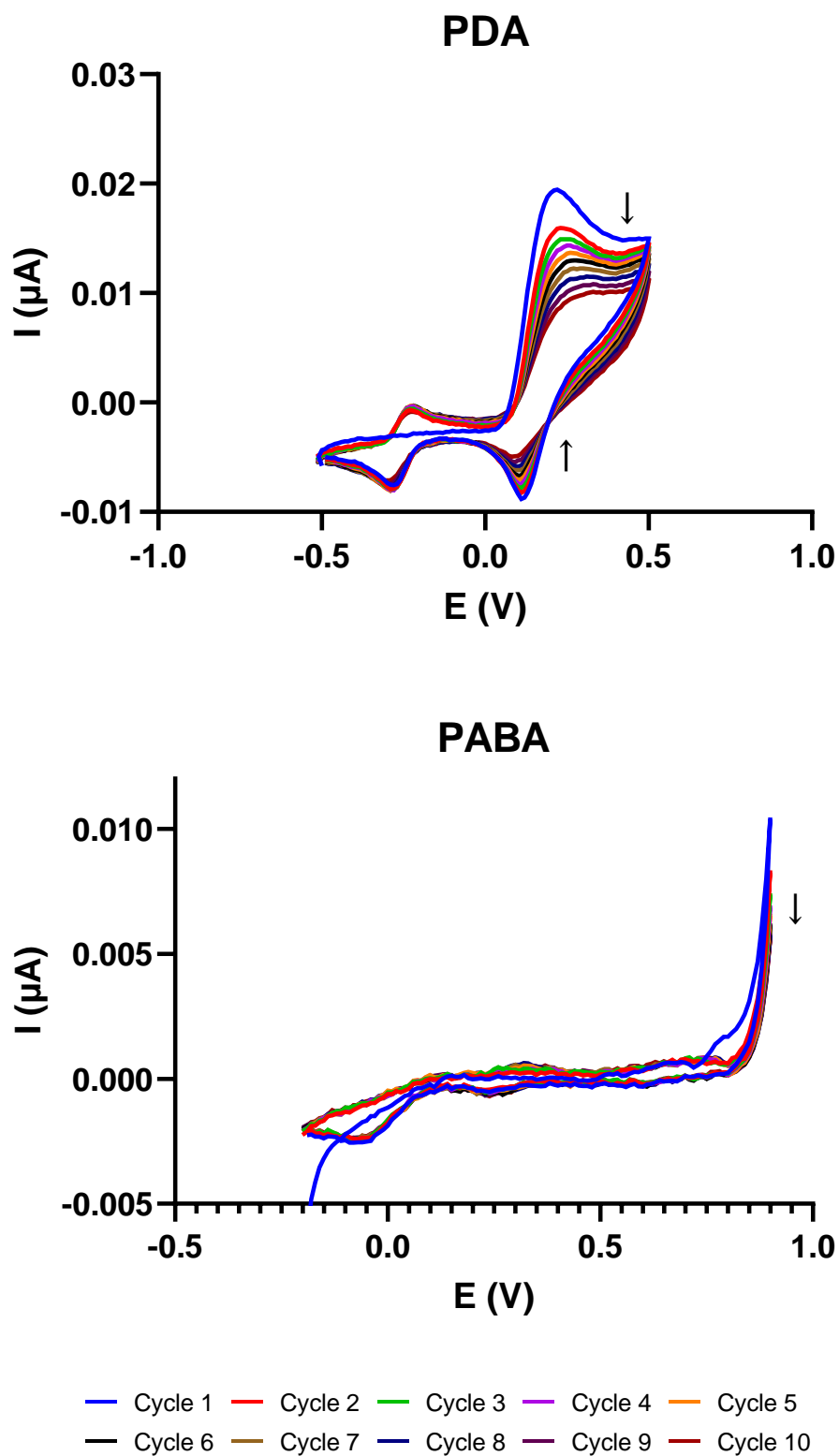
Figure 3.5: Voltammograms obtained following various cycles of polymerisation. Both PDA (top) and PABA (bottom) are non-conducting in nature, as evidenced by the decreasing current as the number of cycles increase (indicated by arrows).

PAPBA and PANI are conducting polymers (22). Focusing on the PAPBA voltammogram, the two peaks at ~ 0.2 V, one in the cathodic and one in the anodic current, are increasing. However, a significant reduction in peak current is observed at ~0.6V. A closer look at the polymer's structure provides an explanation for this (Figure 3.6); there is no direct conjugation between the π-systems of the two aromatic rings, rather the amino group serves as a bridge, with the *n* electrons being shared between neighbouring monomers (38). This results in a constant decrease in current during the polymerisation process, as the available free surface of the WE decreases (38).

Aminophenylboronic acid   Poly - aminophenylboronic acid
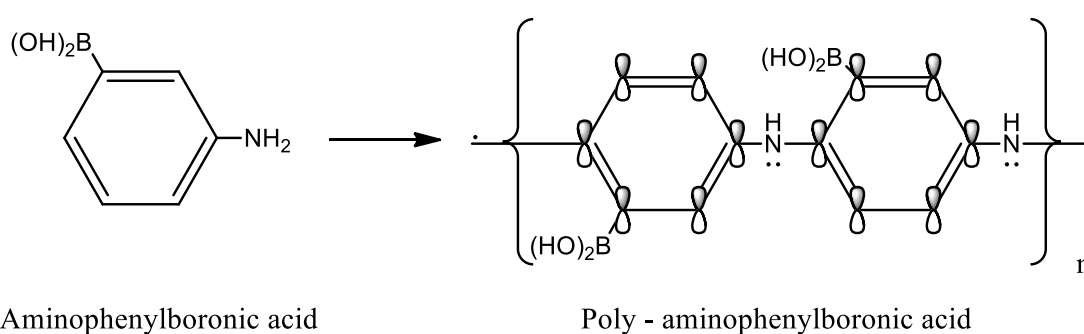
Figure 3.6: APBA conversion to PAPBA. During polymerisation, there is no direct conjugation between the π-systems of the two aromatic rings, but the central NH bridging group is common to both adjacent residues (38).

Given the structural analogy between aminophenylboronic acid and aniline (phenylamine, no boronic acid group), it is unsurprising that the formation of the PANI polymer reveals an almost identical pattern in the resultant voltammogram. According to the literature, the electropolymerisation of APBA proceeds by a mechanism that is characteristic to aniline (39). Both polymers utlise the amino group as a bridge between neighbouring monomers, with no direct conjugation between the π-systems of the two aromatic rings.

The voltammogram corresponding to PANI in Figure 3.4 may lack the peak at around 0.3 V, showing the conversion of the different redox forms [between leucomeraldine (fully reduced) and emeraldine salt state (half oxidised)] as displayed in the study of Belarb *et al.* (40,41). However, there's clear evidence of the peak corresponding to the polymer's further oxidation and anion doping process, at 0.5 V. The peak located at the end of the half cycle shows the conversion of the other two oxidised states of PANI [between

emeraldine salt (metallic state, the base is a half oxidised form) and pernigraniline state (fully oxidised)] (40,41).

On the other hand, PDA and PABA are nonconducting monomers, thus both behave as insulators (16,42). Consequently, the application of each consecutive polymerisation cycle results in a decrease in the general area under curve; the signal becomes flatter, with loss of characteristic redox peaks and the current begins to approach zero. In the voltammogram for PDA, several distinct features are noted. Peaks at ~ 0.1 and 0.3 V decrease with increasing number of cycles, whilst an oxidation peak at -0.2V appears in the second cycle (Figure 3.5, top). More precisely, the voltammogram shows the presence / formation of two redox couples (43). Initially, the anodic peak at ~ 0.2 V shows the presence of dopamine in the solution, while the one at 0.12 V corresponds to the formation of dopaminequinone. The other two peaks show the redox couple of leucodopaminechrome (at -0.21 V) and dopaminechrome (-0.28 V). The reactions shown in Figure 3.7 suggest that the polymerisation of dopamine includes both electrochemical and chemical reactions.
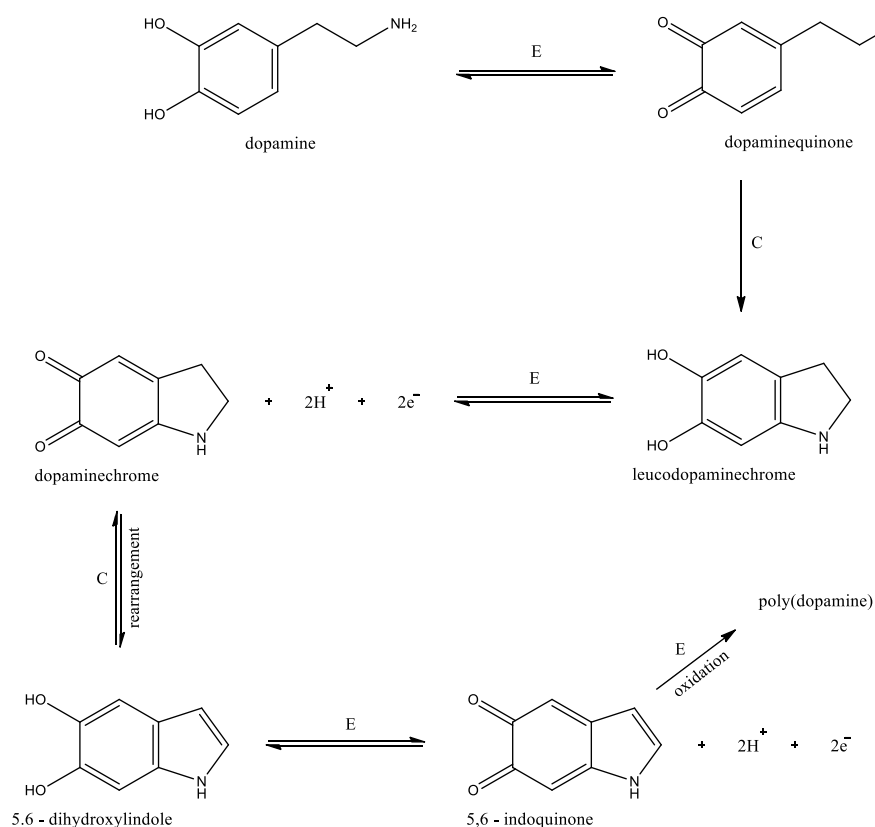
Figure 3.7: Electropolymerisation of dopamine proceeds via the formation of a number of different intermediates that are evident in the voltammogram. The polymerisation process includes both chemical (C) and electrochemical reactions (E) (43).

121

A similar observation applies to the PABA voltammogram. PABA's area under curve is already significantly smaller when compared to the starting points of the other polymers, indicative of its strong insulating properties. Although it is difficult to identify distinctive redox peaks, the peak current at 0.9 V can be seen to be constantly decreasing as the number of cycles increases (Figure 3.5, bottom). To date, the exact mechanism of 3-aminobenzoic acid remains unidentified. However, it is proposed that the electropolymerisation process would follow – or be similar to - that of aniline, since the only difference in structure is the substitution of the amine group with a carboxylic acid (44).

The differing nature of the generated polymers impacts on the data analysis and the simulation of equivalent circuits. Data obtained from the conducting polymers fit a charge based equivalent circuit best, and therefore a $R_s((R_{ct}W)Q_{dl})$ circuit was used to analyse data from PAPBA and PANI based systems. On the other hand, nonconducting polymers behave more like a capacitor and so data generated by PABA and PDA systems were analysed using the $R_s((R_{ct}W)C)$ circuit, as discussed in Chapter 1 (Section 1.6.3).

Following stabilisation and determination of a baseline signal from all polymer systems, each polymer was challenged with 10, 20 and 50 pg/ml LPS and the degree of interaction analysed using EIS (Figures 3.8 and 3.9).

The results obtained following incubation of LPS with PABA and PANI surfaces are shown in Figure 3.8.
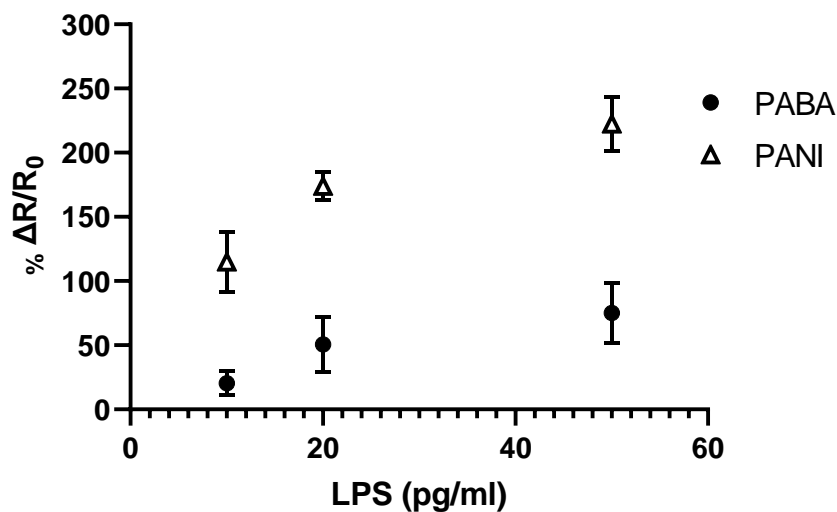
Figure 3.8: EIS responses of PABA (•) and PANI (Δ) when challenged with 10, 20 and 50 pg/ml of LPS (n=3). PANI is a porous polymer, allowing LPS penetrate to its inner core, resulting in high ΔR values. PABA shows promising results when incubated with 10 pg/ml.

PANI has been extensively used in studies focused on the development of glucose permeable materials (26). The high porosity of aniline based polymer systems is perhaps what contributes to the large changes in impedance observed upon addition of LPS (45). Even at the lowest concentration of 10 pg/ml, PANI produces a ΔR of more than 100%. Further increases are observed with higher concentrations of LPS. Although LPS is a larger molecule than glucose, nanoscale pores within the polymer structure would potentially allow easy diffusion of the molecule throughout the PANI modified surface. It was hypothesised that the porous nature of this polymer would result in a high degree of non-specific interaction when challenged with more complex biological matrices, and for this this reason it was dropped from the present study.

PABA showed a change in ΔR values of around 20 % when incubated with 10 pg/ml. ΔR values were further increased after the application of higher LPS concentrations. Two out of three electrodes showed high changes in impedance, averaging ~ 63 and ~ 86 % following incubation with 20 and 50 pg/ml LPS respectively, whilst the third electrode recorded much smaller changes of 10 % (10 pg/ml) and 53 % (50 pg/ml). PABA showed the biggest variance in response across replicates when compared to the other polymers, with the responses obtained from 20 and 50 pg/ml showing a standard deviation of more

than 20 %. PABA's somewhat ambiguous responses, exclude the polymer from further evaluation in the present study.

The results obtained with PAPBA and PDA are shown in Figure 3.9. As outlined in Section 3.1.4, aminophenylboronic acid was selected as a monomer since boronic acid has been shown to interact strongly with diol groups typically found in saccharides (46,47).
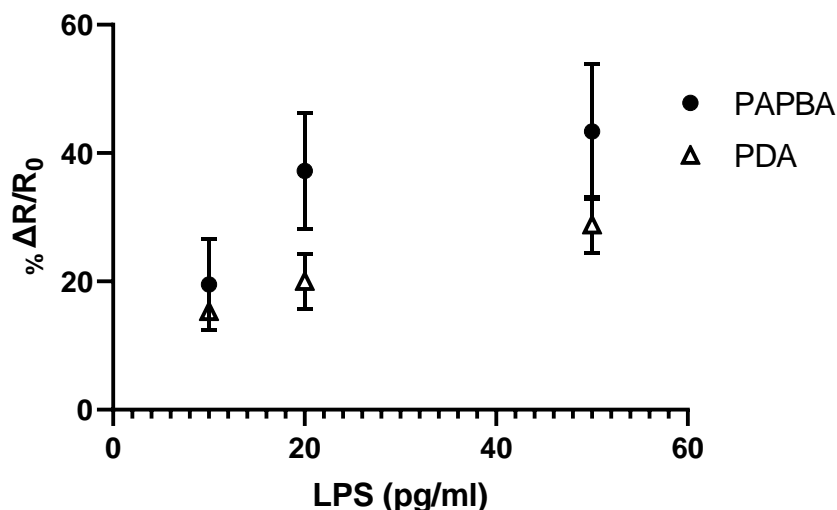
Figure 3.9: EIS responses of PAPBA (•) and PDA (Δ) when challenged with 10, 20 and 50 pg/ml of LPS (n=3). Both polymers are interacting with LPS in a satisfactory level, since they are not displaying phenomena of massive chemisorption with the target.

As in the case of PABA, a change of ~ 20% is observed in the ΔR values following incubation of PAPBA modified electrodes with 10 pg/ml of LPS, which further increases with introduction of higher concentrations of LPS. Although the standard deviation of the responses was higher than would be desirable (~ 10 % for 50 pg/ml) it was recognised that as a screening experiment, only three repeats had been performed. Further evaluation was warranted as the boronic acid functionality maybe advantageous further down the line in terms of minimising non-specific binding with other sample components.

When evaluating the PDA modified electrodes, a similar ΔR to that observed with PABA and PAPBA was achieved following incubation with 10 pg/ml LPS. Although the response increased with higher concentrations of LPS, the ΔR changes observed following incubation with 20 and 50 pg/ml LPS are smaller than those seen with the PAPBA modified electrodes. Still, PDA produced the second best ΔR_{ct} values when

challenged with LPS. Therefore, the following sections will investigate the potential of both PAPBA and PDA to bind and eventually imprint endotoxin.

All the examined polymers showed a tendency to plateau, with smaller than expected responses observed following incubation with 50 pg/ml (Figures 3.7 and 3.8). Although it is recognised that only three concentrations, repeated in triplicate, have been tested the profile is somewhat expected. The present investigation only focuses on non-specific interactions; no specific recognition elements (e.g. aptamer) or imprinted sites are present in the polymer surface. Therefore, once LPS has assembled to cover most of the polymer surface, the response will saturate. This sort of response is commonly seen with control (non-imprinted) polymers in molecular imprinting studies. Introduction of imprinted sites not only serves to increase affinity and/or specificity but also shows an improved binding capacity.

3.3.2. Regeneration of non-imprinted polymers (NIPs)

Chapter 2 described the development of a washing method to allow regeneration of the aptamer surface. As the current Chapter is focused on developing a hybrid imprinting strategy, it is important that the washing step not only disrupts the aptamer-LPS complex, but also disfavours LPS interaction with the polymer surface. This must be achieved without damaging or removing the apta-MIP surface.

APBA forms boronate esters on interaction with diols, which are pH and solvent dependent (46). Previous studies have used low pH conditions to regenerate APBA via hydrolysis of the ester group (30). Golabi *et al.* and Springsteen & Wang demonstrate that PAPBA and phenylboronic acid modified electrodes could be regenerated by incubating in phosphate solutions at pH 2.2 to remove the bound molecules (fructose) and regain the boronic groups' functionality (30,46). Such acidic conditions may prove detrimental to the aptamer used in the current study. Badhulica and co-workers have demonstrated that boronate esters can be regenerated by exposure to less acidic conditions (pH 5), which is more likely to provide an "aptamer-friendly" solution (48).

Jolly, Tamboli *et al.* demonstrated that a PDA-based apta-MIP could be regenerated by overnight immersion of electrodes in a solution containing 5% v/v acetic acid and 5% w/v sodium dodecyl sulphate (SDS) in purified water (16). This shows that PDA based hybrid systems are resistant to such acidic conditions. The residual acid was removed by

rinsing with water and detergent before restabilising the apta-MIP in measurement buffer (10 mM PBS (pH 7.4) containing 10 mM [Fe (CN)6]$^{3-/4-}$ and 0.05% v/v Tween 20).

Chapter 2 demonstrated that treatment of aptamer only surfaces with 0.05 % v/v Tween 20 is a safe and simple way to remove bound LPS. It was therefore decided to use this as starting point for washing the polymer surfaces. Both APBA and PDA modified electrodes (n=1) were incubated with 50 pg/ml LPS, allowing plenty of time for LPS to bind (Figure 3.10). EIS was performed and the spectra recorded before and after incubation with LPS, and then again following the wash process. Initially, following the wash step, larger impedances were recorded, possibly as a consequence of the surfactant becoming entrapped within a hydrated polymer. Storing the electrodes in 10 mM PBS (pH 7.4) containing 10 mM [Fe (CN)6]$^{3-/4-}$ for 2 days was shown to bring the impedances back down to the baseline value, demonstrating that LPS had been successfully removed. Although impedances were shown to be slightly lower following washing for both polymer systems, this is likely a consequence of removal of loosely associated polymer / unpolymerised monomer. The study by Jolly *et al*., used AFM to show that polymer thickness decreased following washing (16).
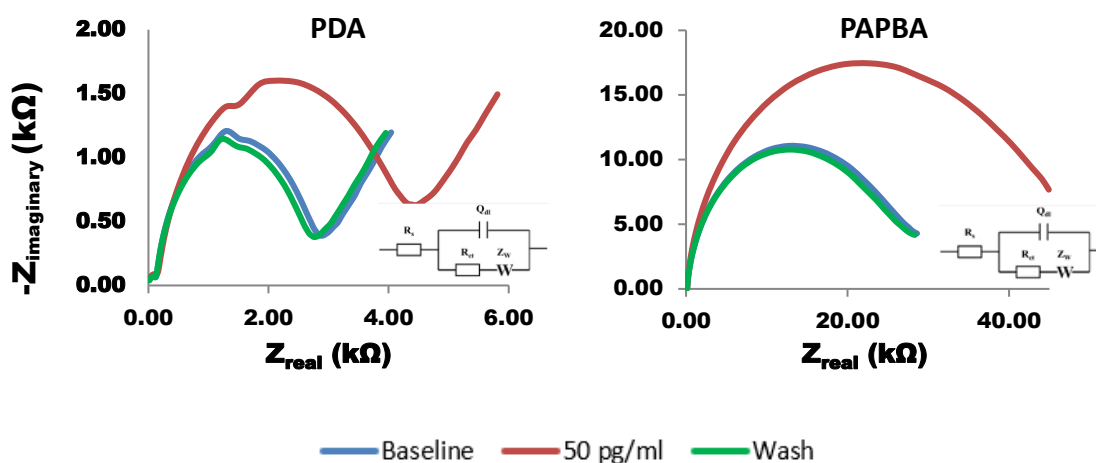
Figure 3.10: EIS responses of PDA (left) and PAPBA (right) following their incubation with LPS and washing with 0.05 % Tween. Wash conditions successfully regenerate both polymer surfaces as the spectra obtained after washing are similar to that of the baseline response.

3.3.3. Development of PDA and PAPBA molecularly imprinted systems

Having narrowed down the candidate monomers to dopamine and aminophenylboronic acid, the next step was to produce 'conventional' molecularly imprinted systems using LPS as the template molecule. Both PDA and PAPBA imprinted systems were generated and evaluated in order to make the final choice of monomer to take forward to the hybrid imprinting approach.

A SAM consisting of LPS only was developed by incubating the working electrodes with 50 pg/ml LPS. The hydrophobic regions of LPS are capable of interacting with the gold surface of the WEs, providing impedances of ~ 2 – 2.5 kΩ. Non-chemisorbed LPS was removed by rinsing the electrodes with 10mM PBS pH 7.4 before immersion in the monomer solution of choice. In this study, 10 polymerisation cycles were used to develop the molecularly imprinted polymers. It is important that a sufficient polymer layer is grown to allow imprinting of LPS, but that significant overgrowth is prevented to avoid permanent entrapment of the template molecule. Based on the group's recent success using PDA to imprint prostate specific antigen (PSA), 13 polymerisation cycles were shown to produce a polymer of ~ 10 nm thickness (10). These values were reported in the presence of the aptamer, although small changes between MIPs and NIPs were noted. Given LPS is smaller than PSA, it was thought that a polymer of similar thickness would allow for the efficient imprinting and subsequent removal of LPS. Following polymer growth, the electrodes were washed with 0.05 % Tween and 10 mM PBS pH 7.4. EIS was used to confirm template removal (average of 2 – 2.5 kΩ reduction in impedance observed) before the electrodes were re-challenged with 10, 20 & 50 pg/ml LPS (Figure 3.11).
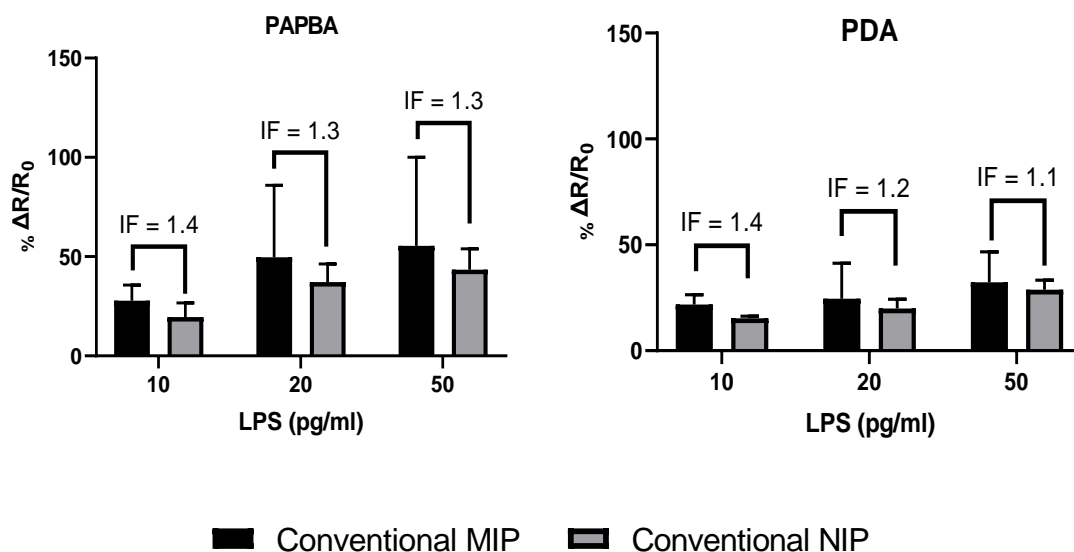
Figure 3.11: EIS responses of PDA and PAPBA conventional MIPs and NIPs, following incubation with LPS (n=3). Imprinting factors (IF) are shown above each pair of bars (MIP response / NIP response).

Both imprinted systems show a modest improvement in response when compared to their non-imprinted counterparts. A significant difference between MIP and NIP was not anticipated given the inherent difficulty in imprinting molecules such as LPS, as described in section 3.1.2. Figure 3.11 shows that the PAPBA MIP and NIP demonstrate higher changes in impedance when compared to the PDA polymers. However, when considering the imprinting factor (IF, equation 3.1) little difference between the two polymer systems was noted, especially when the standard deviations are taken into consideration. (49).

$$IF = \frac{MIP\ Response}{NIP\ Response} \qquad \text{Equation 3.1}$$

Although a MIP-based SPR sensor targeting LPS has been reported using PDA, the interactions between the polymer and target molecule are relatively non-specific when compared to the preference of boronic acid groups to interact strongly with diol

containing molecules (31). For this reason, it was decided to proceed with APBA as the monomer of choice.

3.3.4. Development of the PAPBA apta-MIP hybrid system

Having created non-imprinted and conventionally imprinted PAPBA surfaces, the next stage of the study was to develop the hybrid recognition system, incorporating the anti-LPS aptamer in the imprinted sites. Following the deposition of the LPS-aptamer complex on the surface of the WE as described in Section 3.2.2.3, the working electrodes were immersed in APBA solution and cyclic voltammetry was used to bring about polymer growth around the immobilised complex (Figure 3.12). Removal of LPS, whilst leaving behind the aptamer, creates the LPS-specific, aptamer-lined binding pockets at the sensor surface.
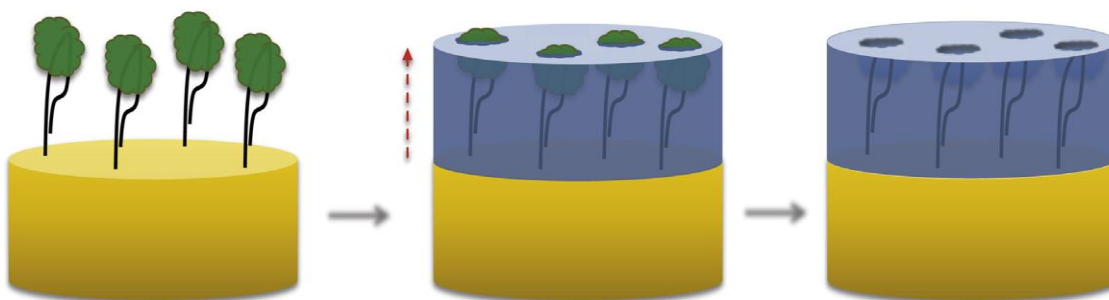
Figure 3.12: Apta-MIP development. Initially the aptamer-template complex is bound on the gold surface. Then, the monomer of choice is electropolymerized around the complex to create the template specific imprint. Finally, the template is removed from the material and the system is ready to be challenged (16).

Polymer thickness is a key aspect in the development of an efficient apta-MIP hybrid system. In the case of insufficient growth of the polymer, it was hypothesised that the system would behave similarly to a conventional aptasensor, with negligible contribution from the polymer to the recognition of the target. On the other hand, overgrowth of the complex will result in a system which performs like the non-imprinted control as the aptamer will be buried by polymer, unable to interact efficiently with the target.

As mentioned before, it was assumed that any polymer obtained after the application of ~ 10 cycles would be sufficient to start providing results of a hybrid sensor. The above statement is based on a previous work of the group, in which 13 polymerisation cycles

provided the hybrid site with maximum recognition towards the targeted biomarker (Prostate Specific Antigen – PSA) (16).

In an attempt to investigate the above hypotheses, the number of polymerisation cycles were varied from 4 to 10. The reproducibility of the polymers generated after the application of a low amount of cycles can be characterised as rather poor. The polymerisation process demands a minimum amount of 4 cycles to develop a hybrid sensor in which the polymer does not ware off, essentially living a completely bare aptamer after the application of EIS measurements. This observation can be confirmed from the general CVs displayed on Figure 3.5, since the shape of the voltammograms 1 to 3 is rapidly changing. For each cycle three repeats were prepared, and the recognition performance evaluated by incubating the electrodes with 10, 20 and 50 pg/ml of LPS (Figure 3.13).
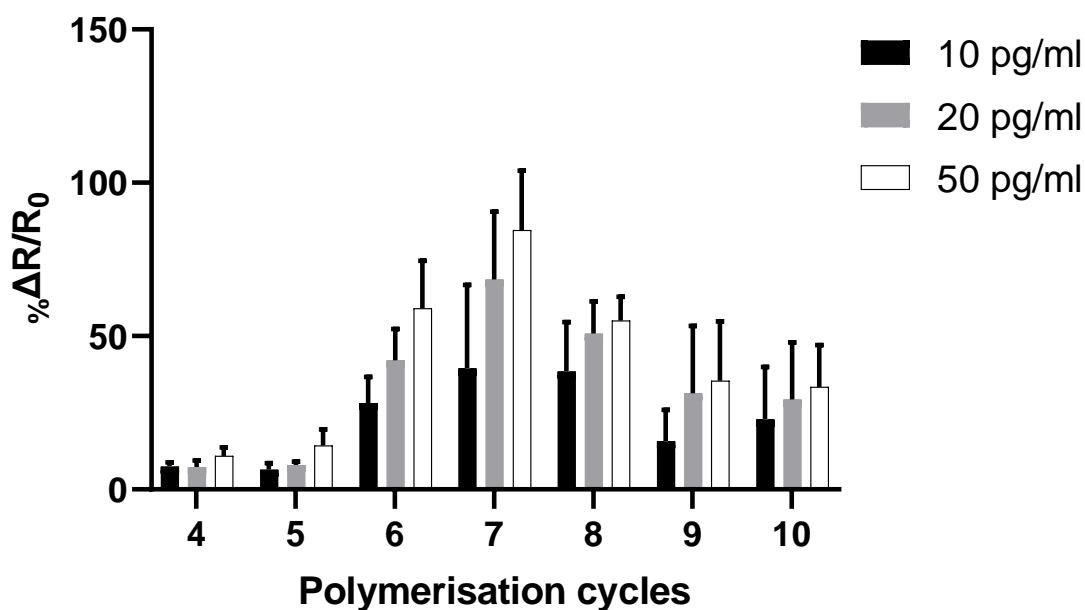
Figure 3.13: Dose-response graphs of the apta-MIP as a function of the number of polymerisation cycles when challenged with 10, 20 & 50 pg/ml LPS. The apta-MIP maximum performance is achieved when APBA is polymerised for 7 cycles.

As shown in Figure 3.13, the performance of the hybrid system is strongly dependent upon the number of polymerisation cycles. When either 4 or 5 polymerisation cycles were used, relatively small changes in impedances were observed. It would appear that these number of cycles are not enough to allow creation of aptamer lined imprinted sites, rather

the aptamer is still mainly responsible for the recognition of LPS. In addition to that, the small and random amount of polymer formed around the aptamers would initially provide baseline readings with high variability. A comparison between the responses seen after 5 cycles and the conventional aptasensor described in Chapter 2 is provided in Figure 3.14 A. Regarding the response after the application of 10 and 50 pg/ml, the two systems perform similarly, with the aptasensor somewhat outperforming the hybrid system.

At the opposite end, when more than 8 polymerisation cycles are used, performance of the hybrid system starts to decline. This is likely a consequence of incomplete removal of LPS following the initial creation of the imprinted sites as the polymer overgrows the surface-immobilised complex. Subsequent re-challenge with LPS means that LPS is largely only able to interact with the polymer surface, as a consequence of the overgrowth, and so performance is similar to that seen with the non-imprinted polymer surfaces (Figure 3.14 B).
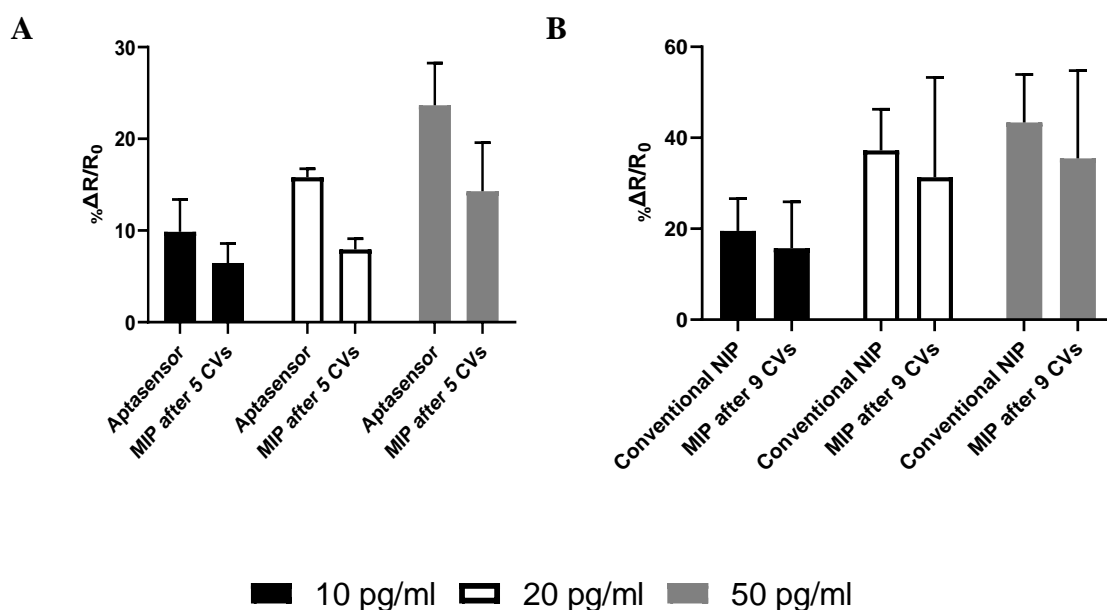
Figure 3.14: The dose-response performances of the aptasensor and apta-MIP generated after 5 polymerisation cycles are similar, since the polymer film does not effectively capture the aptamer-LPS complex to create the binding site (A). On the other hand, the responses of conventional NIP and the apta-MIP generated after 9 CVs are almost identical, since the polymer film overgrows the binding site (B).

Cycles 6, 7 and 8 demonstrate much improved responses, with peak performance observed following 7 cycles of polymerisation. It is hypothesised that this system has

sufficient polymer growth to enable efficient capture of the aptamer-LPS complex that, on removal of LPS, results in the formation of a imprinted site which is lined with the aptamer held in a preferred binding conformation.

A hybrid NIP system was also developed. The developmental process was the same as that used in the generation of the hybrid MIP, with one significant change in the protocol; following immobilisation of the aptamer-LPS complex on the electrode surface, LPS is immediately washed away to leave just the aptamer on the surface. This strategy was employed to try and ensure that the amount of aptamers / coordination on the gold surface would be the same in both hybrid systems, as differences in the aptamer density would likely affect polymer growth / thickness. Nevertheless, it is recognised that the absence of LPS in the SAM possibly provides some additional space for the polymer growth. Readings obtained from hybrid NIP showed an astonishingly low binding performance (Figure 3.15). A possible explanation relies on the fact that the polymer "locks" the aptamers conformation in a way that both materials are blocked from binding LPS. Perhaps the aptamer binding site is covered to the extent that LPS cannot interact, while any exposed aptamer possesses sufficient negative charge to inhibit binding to the PAPBA surface.

Figure 3.15 summarises the performance of the systems developed so far (apta-MIP, apta-NIP, conventional MIP, conventional NIP and aptasensor). It is clear that the hybrid system outperforms all of the other sensors. Interestingly, the conventional MIP system (no aptamer) shows a better response than the aptasensor, however the response seen with the apta-MIP is greater than the sum of the two individual parts (MIP and aptasensor) suggesting a synergistic effect.
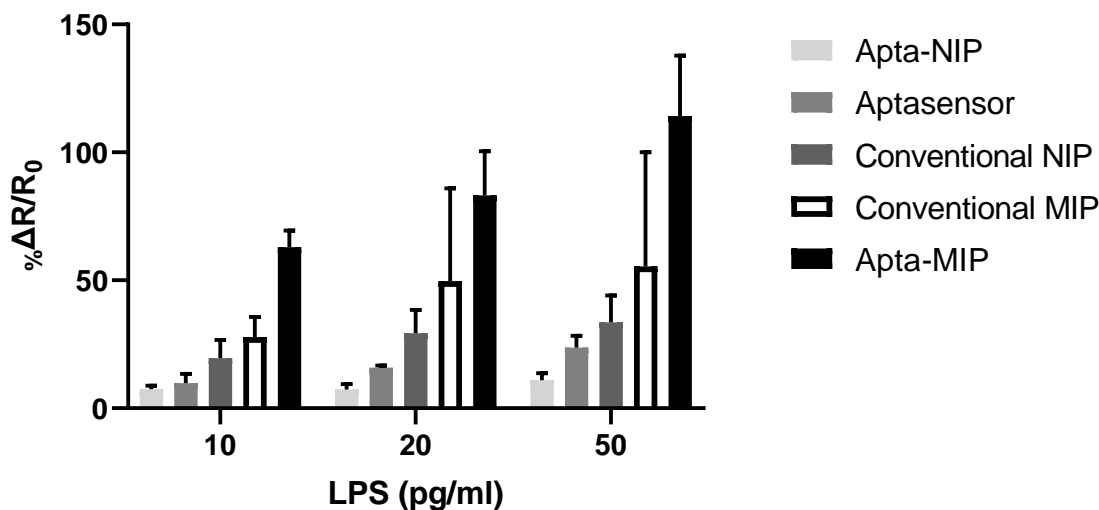
Figure 3.15: Comparison of the changes in ΔR between the generated systems (optimised apta-MIP, apta-NIP, conventional MIP, conventional NIP and aptasensor). The progression of the study, starting from the aptasensor and finishing to the apta-MIP, demonstrates a continuous improvement in sensing of the challenging concentrations. All systems are using the model $R_s((R_{ct}W)Q_{dl})$ to characterise the circuit.

3.3.5 Characterisation of the apta-MIP

Characterisation of the apta-MIP system follows that described for the aptasensor in Chapter 2. A series of binding experiments were performed to provide insight into the sensitivity and specificity of the system, whilst also considering binding kinetics and detection range. Chronocoulometry was used to provide an estimation of the total number of possible binding sites on the sensor surface.

3.3.5.1 Stability, sensitivity and detection range (kinetics)

Stability is a key aspect of any biosensor. The corresponding section regarding the characterisation of the aptasensor in Chapter 2 has made clear that this factor directly affects both sensitivity and detection range. Apart from endurance and time lasting consistency, a physically stable polymer shows low levels of noise during testing, providing an opportunity to achieve lower LODs.

The apta-MIP system demonstrates good consistency in terms of recorded impedances following removal of the template molecule. All individual modified electrodes that have

been used in both the screening process and in dose-response experiments showed an average impedance of 27.1 kΩ, with an impressive standard deviation of 0.9 kΩ. This means that the CV is averaging ~ 3.3 %, which can be further reduced to ~ 1.75 % by the exclusion of potential outliers. Taking into consideration the small degree of error between replicates, the LOD can be calculated as the concentration that provides a signal greater than the baseline + 3 x SD (~10 %).

Chapter 2 demonstrated that the aptasensor's LOD was ~100 fg/ml, while the linear detection range spanned 1 pg/ml – 100 pg/ml. Given the improved performance seen in the early screening experiments, the apta-MIP was challenged with LPS concentrations from 1 fg/ml to 10 ng/ml (n=3 apart from the application of 10 ng/ml in which n=2). The control system (apta-NIP) was also challenged with the same concentrations. The results are shown in Figure 3.16.
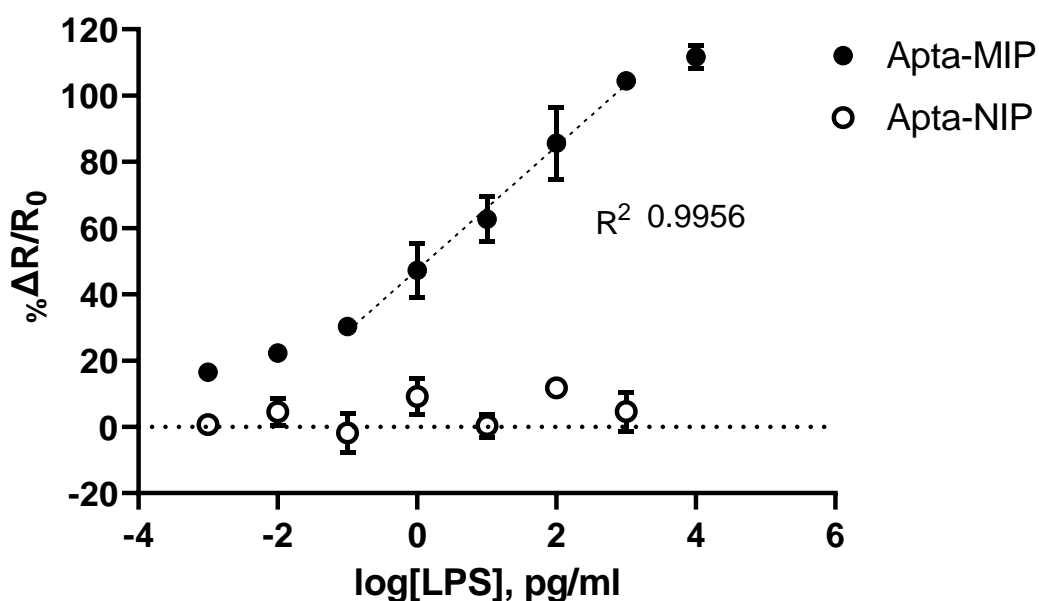
Figure 3.16: Dose-response graphs of the apta-MIP and apta-NIP when challenged with a variety of LPS concentrations, ranging from 1 fg/ml to 10 ng/ml. The sensor shows a linear response between 100 fg/ml and 1 ng/ml (R^2 = 0.9955) showing the best sensitivity so far in the study.

Figure 3.16 shows the schematic representation of a classic sigmoidal kinetics curve for the apta-MIP. The hybrid sensor shows a dose-dependent response with significantly larger changes in impedance observed at all concentrations when compared to the apta-

NIP. This is strongly supportive of the presence of imprinted sites. It is worth noting that the responses observed with the apta-NIP fall around zero and more specifically within the noise of the system; a maximum response of ~ +12% was seen when the apta-NIP system was challenged with 100 pg/ml of LPS.

Although when the apta-MIP is challenged with 1 fg/ml LPS an increase in impedance of 16.5 % is recorded (i.e. a value above the noise of the system and as such can be classified as the LOD) the difference between this observation and the response observed at 10 fg/ml (22.3 %) is small. On application of 100 fg/ml, the sensor records a ΔR value of 30.3 %, which is statistically different to the response observed with the application of 1 and 10 fg/ml according to student's two tailed t test (p = 0.001 and 0.0039 respectively). The R^2 within the response range obtained from the application of 100 fg/ml and 1 ng/ml equals to 0.9955, confirming the positive results. However, the linear range can be expanded from both sides, despite the fact the curve tends to form the two plateaus. More precisely, R^2 equals to 0.9829 when the response of 0.010 pg/ml is added in the linear range and improves at 0.9857 with the further addition of the response corresponding to 10,000 pg/ml. All of the observed R^2 values are still above the threshold of 0.97, confirming the strong correlation between the two variables.

According to the data provided in Chapter 2, the newly developed apta-MIP already outperforms the aptasensor, as its LOD is ~ 100 times lower. This directly leads to a more sensitive range of detection, as the system's linearity drops down to the femtogram scale. In comparison to other aptasensor based detection systems for LPS discussed in Chapter 2, the apta-MIP compares favourably in terms of LOD to the study of Bai *et al.* which reports a LOD of 0.087 pg/ml (50). It is only the study by Posha *et al.*, which reports a LOD of 7.94 zM, that exceeds the detection limit of the apta-MIP system (51).

Literature shows a very limited amount of information related to the development of molecularly imprinted systems targeting LPS. Although LPS is a biologically important molecule, its poor solubility coupled with its limited functionality (lipid chains and sugars), mean that it is a less than an ideal target from an imprinting perspective. Abdin *et al.* demonstrated the *in-silico* design of a nanoMIP based optical sensor for the monitoring of endotoxins. The sensitivity of the system was found to be in the ng/ml scale (52). A few years later, Altintas *et al.* attempted to produce computationally designed nano-MIPs to couple with SPR technology (33). The MIPs were constructed using various monomers such as itaconic acid, methacrylic acid and acrylamide, however, these

polymers also show LODs in the ng/ml scale. Buchegger *et al.* developed a thermo-nanoimprinted biomimetic probe for the immunosensing of LPS and LTA (53). Their study shows a lower LOD (LLOD) of 500 fg/ml for both LPS and LTA. Long *et al.* developed polymeric nanoparticles targeting the LPS of *Pseudomonas aeruginosa* (54). The information obtained from the study is limited and they don't report LOD values. Taking into consideration all the above information, it is apparent that utilising a hybrid imprinting approach allows for the development of system that outperforms conventional imprinted polymers in terms of sensitivity.

In order to characterise the performance of the sensing system further, GraphPad Prism was used. Unlike when analysing the apta-sensor system in Chapter 2, where it was assumed that only one type of binding site existed at the surface of the sensor, in the hybrid system, it is theoretically possible for LPS to interact with the aptamer, the polymer or the hybrid imprinted site. Although very little interaction was observed between LPS and the apta-NIP, suggesting that LPS preferentially binds to the imprinted site, it was decided to analyse the data using two models; a Langmuir-Freundlich model, describing specific and non-specific binding phenomena ("one site – total" model in GraphPad Prism version 8) and the Langmuir ("one site – specific" model in GraphPad Prism version 8) (55). Conversion of LPS concentrations (Figure 3.17) allows for calculation of an apparent K_d. When using the Langmuir-Freundlich model a good fit was observed ($R^2 = 0.9442$) and an apparent K_d of 1.7 pM (8.4 pg/ml) was calculated. Although a lower apparent K_d was obtained using the Langmuir model (0.18 pM, 875 pg/ml) the fit to the data is not as good ($R^2 = 0.7470$).
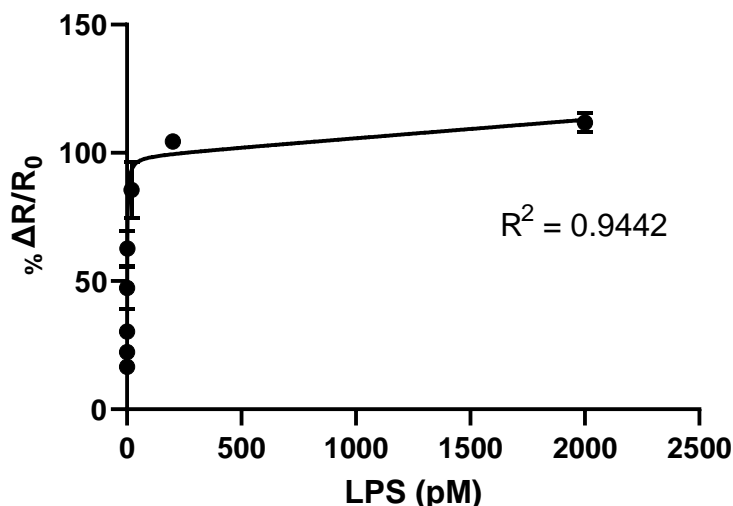
Figure 3.17: Dose response plot for the apta-MIP. The Langmuir-Freundlich ("one site – total") binding model used from GraphPad Prism shows a good fit, wih a R^2 value of 0.9442. The system displays an apparent K_d of 1.68 pM (8.4 pg/ml).

The existing MIP studies again provide a very limited amount of information to which the current data can be compared, with only Long and co-workers' reporting an apparent K_d of 22.4 nM for their MIP system (54).

3.3.5.2 Determination of active binding sites, chronocoulometric studies

As per Chapter 2, chronocoulometry was used to provide an estimation of the number of binding sites (aptamers) on the surface of the electrode. In Chapter 2, mixed aptamer-alkanethiol SAMs were generated, however in the current Chapter, the aptamer is immobilised on the surface of the electrode whilst complexed to LPS, without the addition of alkanethiol molecules. Therefore, in the present study, electrodes were modified with the aptamer-LPS complex before being split into two sets (n = 1). The first electrode kept the aptamer-LPS complex intact, while the other subjected to the washing process to remove LPS prior to performing chronocoulometry. In this way, any potential changes in the number of bound aptamers due to washing can be determined, assuming that RuHex does not interact with LPS. Chronocoulometry is extensively reported in the literature as the technique to allow determination of the the immobilisation densitiy of DNA on surfaces, since RuHex specifically interacts with its backbone, resulting in changes of charge (56,57). The results of this study are shown in Table 3.2.

137

Aptamer SAM	Number of aptamers	LPS needed to saturate (pg)
Washed	5.46×10^{10}	480
Unwashed	6.37×10^{10}	560

Table 3.2: Chronocoulometric results obtained from washed and unwashed aptamer-LPS SAMs (n=1). The differences between the two SAMs, one with and one without the presence of LPS are small, suggesting that the washing process has a minimal effect on aptamer presentation.

The difference between the washed and unwashed electrodes is insignificant (~ 10% difference), with ~ 500 pg of LPS estimated to saturate the system. This variation could be down to small differences in the working electrode in terms of surface area or cleanliness prior to SAM deposition.

The apparent negligible loss of aptamer during washing is encouraging as it would suggest that polymer formation should be similar when generating the apta-MIP and apta-NIP systems. It should be recognised however, that the chronocoulometric data only provides an estimation of maximum binding capacity for an aptamer only surface. When producing the hybrid system, it is possible that this capacity is affected either by some of the aptamer-LPS complexes becoming permanently entrapped within the polymer layer, by overgrowth of aptamer not complexed with LPS or by the polymer (non)specifically interacting with LPS on re-challenge.

The data presented in Figure 3.14, suggests that the apta-MIP system starts to reach saturation between 1 and 10 ng/ml. Given that the electrodes are incubated with 100 μl of this solution, this would suggest that the system is saturating when exposed to between 100 pg and 1 ng of LPS, which supports the chronocoulometry findings.

3.3.5.3 Specificity Studies

This section is divided into two parts. The first part focuses on evaluating the response of the apta-MIP when challenged with other pathogen associated molecular patterns such as lipoteichoic acid (LTA) and (1→3)-β-D glucan (GLU). The second part of this section examines the system's behaviour in the presence of human serum albumin (HSA), the most dominant protein in blood (58). LTA, GLU and HSA are all molecules that the

138

sensor will likely encounter when challenged with complex biological fluids, such as plasma or serum.

3.3.5.3.1 Challenging apta-MIPs with LTA and GLU

Both the introductory and second chapters of the thesis has made clear the need to produce a sensing system that is highly specific to LPS, thus overcoming the limitations of current commercially available tests that largely rely on the LAL assay or versions thereof. In Chapter 2 it was shown that the aptamer displayed good selectivity when challenged with LTA and GLU. It is important to ensure that this recognition specificity has not been compromised by the addition of the polymer to create the hybrid system. The sensor was therefore challenged with these two related molecules.

It is well established that apart from its presence in fungal sepsis, GLU can potentially interfere with LAL assay, generating false positive results (59). Digby *et al.* have demonstrated that patients in and outside of intensive care settings with fungal infections, can have serum glucan concentrations of up to ~200 pg/ml (60). For completeness, it was decided to challenge the apta-MIP with the range of concentrations as was used when evaluating the response to LPS i.e. 1 fg/ml to 1 ng/ml (n=3). The results are shown in Figure 3.18.
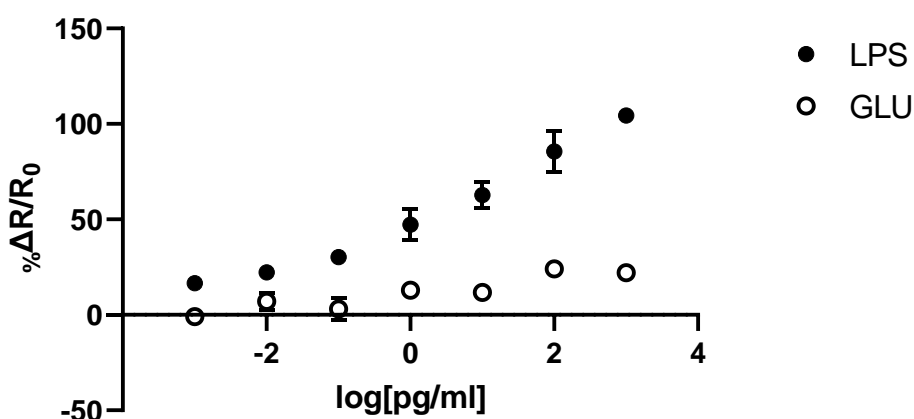
Figure 3.18: Dose-response graphs obtained following incubation of the apta-MIP with either LPS or GLU (n=3). The hybrid system clearly favours binding to LPS, since the responses to GLU all fall below 25%.

The performance observed with the apta-MIP follows that seen with the aptasensor in Chapter 2, with very low-level responses recorded when the system was challenged with GLU. More precisely, the apta-MIP response to GLU concentrations between 1 fg/ml and 100 fg/ml are falling either close to zero or within the system's noise. LPS at concentrations over this range all produce significant changes in impedance, well above the noise of the system. Following incubation with 1 and 10 pg/ml GLU, a ΔR of 12.9 and 11.8 % is observed for the respective concentrations. However, these signals are barely above the system's noise. The difference between GLU and LPS at these concentrations is clear, since the corresponding changes in impedance following incubation with LPS are greater than 50 %. The same observation appears following incubation with the higher concentrations; an increase of impedance of ~ 20 – 25 % for 100 pg/ml and 1 ng/ml GLU, whereas the same LPS concentrations result in changes of 104.4 and 111.8 %. The non-dose-dependent response to GLU across the concentration range tested suggests that the interaction with the sensor is non-specific in nature. Given the aptasensor reported small negative (within noise) changes in impedance when challenged with 1, 50 and 100 pg/ml GLU, it would seem likely that the increased interaction observed with the apta-MIP is caused by non-specific binding of GLU to the PAPBA polymer. As glucans are essentially linear polymers of glucose, it is unsurprising that some interaction with the polymer is observed (61). The relatively low responses observed, coupled with the observation that maximum concentration in sera would rarely exceed 200 pg/ml are encouraging (60). It should be noted that due to the nature of the experiment, this specificity assay was performed in a non-competitive manner i.e. target molecule added to the sensor in isolation, and therefore the observed interaction between GLU and the polymer may be disfavoured by the binding of LPS in samples containing both analytes.

Less information is available regarding LTA levels in blood despite the vast number of publications supporting a pathogenic nature similar to that of LPS (62–64). Without such information, it was decided that the apta-MIP system would be challenged with LTA at concentrations between 1 pg/ml and 1 ng/ml (n=3). The results of this challenge are presented in Figure 3.19.
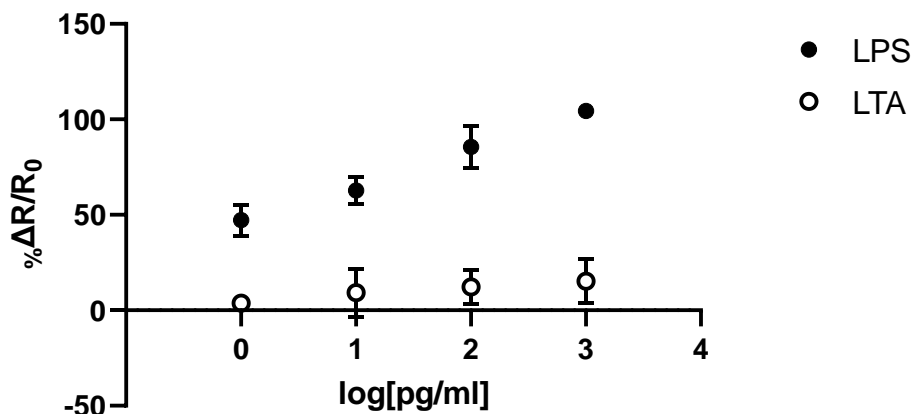
Figure 3.19: Dose-response graphs obtained after the apta-MIP's challenge with LPS and LTA (n=3). Similarly to Figure 3.16, the hybrid system clearly favours the binding to LPS; a low response to LTA at all concentrations is observed.

As observed with GLU, the sensor response following incubation with 1 and 10 pg/ml of LTA are insignificant (3.7 and 9.3 % respectively). Even at higher concentrations, the apta-MIP shows limited interaction with a maximum change in impedance sitting at ~15 %. LTAs are alditolphosphate-containing polymers meaning that they contain long chains of ribotol or glycerol phosphate rather than the repeating sugar units seen in LPS and GLU (65). It would therefore be expected that smaller interactions with a boronic acid containing polymer (used to target diol functionality) would be observed. The small responses observed are likely a consequence of hydrophobic interactions between LTA and the polymer surface (64).

3.3.5.3.2 Challenging the hybrid systems with HSA

As outlined in earlier Chapters, the ultimate goal would be to use the developed sensor to detect LPS in clinical sample matrices. Whilst low cross-reactivity has been observed with other pathogen associated molecules, the sensor will need to deal with a variety of other interferants if it is to be used clinically. HSA is the most dominant protein in blood - concentrations range from 35 to 50 mg/ml – and it is known to cause problems in sensing (66). Proteins are prone to non-specifically adsorb to many surfaces by virtue of their

multiple of hydrogen bond donors and acceptors. Protein biofouling of sensors is a common challenge that needs to be overcome (67).

In an attempt to minimise interference from blood components such as HSA, extensive sample preparation is often performed prior to introducing the sample to the sensor. As a minimum, samples are diluted with a physiological buffer. The degree of dilution depends on the sensitivity of the sensing platform as one has to be mindful that each dilution step not only dilutes out interferents but also dilutes the analyte of interest. For the purposes of this study, it was assumed that a minimum dilution of 1/10 would be employed; the improved sensitivity of the apta-MIP system easily accommodates this. The apta-MIP and NIP were therefore challenged with 5000 μg/ml (1/10), 500 μg/ml (1/100), 5 μg/ml (1/10,000) and 0.5 μg/ml (1/100,000) HSA (n = 3). The results are shown in Figure 3.20.
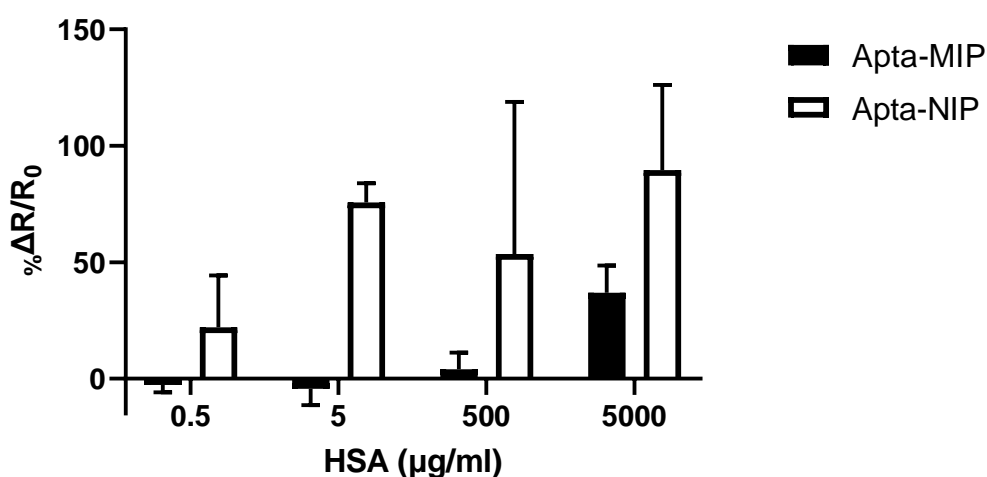
Figure 3.20: Dose-response graphs obtained following challenge of the apta-MIP with HSA. The apta-MIP interaction with HSA is extremely low up to a concentration of 500 μg/ml but increases considerably at 5000 μg/ml. The apta-NIP response to HSA is considerably higher at all concentrations, suggesting biofouling of the polymer surface.

As is evident from Figure 3.20, there is a marked difference in the response of the apta-MIP versus the apta-NIP. Whilst the response of the apta-MIP to HSA at concentrations of 0.5, 5 and 500 μg/ml is very low (+/- 4 %), the change in impedance in the apta-NIP system varies between ~22 and 76 % across the same concentration range. Although when challenged with 5000 μg/ml HSA the responses of both systems were shown to increase, the response from the apta-NIP (~90%) is still more than double that of the apta-MIP (~37

%). Furthermore, the degree of error across replicates is much greater in the apta-NIP system. It is also important to mention that the apta-MIP's response to the highest HSA concentration, corresponds to almost the half of the maximum response recorded when the sensor was challenged with LPS (Figures 3.16 & 3.20).

In the absence of LPS as a templating molecule in the apta-NIP system, it is highly likely that the aptamer becomes overgrown by the PAPBA polymer, thus creating a sensor surface which is essentially just polymer. Non-specific adsorption / biofouling is therefore to be expected. The difference in response between the two systems provides further evidence of the imprinting phenomenon. When LPS is bound to the aptamer, as in the case of the apta-MIP, growth of the polymer from the electrode surface occurs around these complexes such that once LPS is washed from the system, the aptamer groups remain accessible for rebinding of the target analyte. Given the strong negative charge of HSA at physiological pH, it is unlikely to interact as strongly with the apta-MIP surface in which areas of exposed aptamer, which also possesses a negative charge, exist (68).

Although a larger-than-wanted response was observed at 5000 μg/ml HSA – equivalent to a 1/10 dilution of serum – it is not clear how the binding of LPS to the aptamer would influence the interaction of HSA (and other blood / serum components) with the sensor surface. LPS is known to form complexes with such components, hence the current difficulty of detecting LPS in clinical matrices using existing tests. However, the superior sensitivity of the hybrid system would allow 1/100 dilutions to be used if required. Indeed, dilution is an approach used to try and improve responses from more complex endotoxin containing samples in current assay formats (69).

3.3.6. Recovery of LPS from spiked blood serum

Following completion of the LTA, GLU and HSA challenges, it was decided to challenge the apta-MIP system with serum samples spiked with LPS to assess the ability of the system to detect the analyte of interest when present in a complex matrix.

Samples were prepared as described in Section 3.2.2.8. The stock serum sample contained LPS at a concentration of 100 pg/ml. The stock solution was diluted to 10 fg/ml using 10 mM PBS pH 7.4. A blank serum sample (no spike, same dilution) was also prepared using the exact same approach. Despite the large dilution of the serum (1 in 100,000), a significant change in impedance (~ 160%, CV ~ 25%) was observed when the blank

sample was introduced to the apta-MIP system. Given the lack of response observed when an equivalent concentration of HSA was tested (0.5 µg/ml), this observation is concerning and suggests that other components in the sample matrix are able to interact with the sensor. During sample preparation, the serum was treated with acid and also subjected to a short, high temperature heating step. These conditions would have resulted in protein denaturation, however as the sample was not centrifuged nor filtered, protein fragments (peptides) will remain in the sample. It would appear that these perhaps interact more strongly with the sensor surface, resulting in a higher level of biofouling that would have been anticipated from the HSA study.

Despite this large background level, when the spiked sample (10 fg/ml) was introduced, a further increase in impedance of ~ 20% was observed. Although it is recognised that this value falls within the error reported for the blank, a relatively small CV of ~8 % was observed across repeats of this sample. Assuming, the increase in impedance observed with this sample was due to LPS, then it would suggest that ~ 90% of the target molecule was able to be recovered from the sample.

Unfortunately, due to time constraints and sample availability, it was not possible to test the system with other concentrations of LPS in serum. Testing higher concentrations using the stock serum sample employed in this study, would have meant less dilution of serum and therefore higher levels of interference would have been likely. The study needs to be repeated with further sample preparation (e.g. addition of a centrifugation step). The aptasensor should also be challenged with serum samples to try and establish which element of the hybrid system is responsible for the high background responses seen.

3.4 Apta-MIP performance in comparison to other available analytical tests and concluding remarks

The successful development and full characterisation of the apta-MIP brings Chapter 3 to its end. Before making the conclusive remarks, the system's performance will be compared to other existing analytical tests. The comparison will start with the commercially available 'gold-standard' LAL assay.

The LAL assay is able to sensitively detect 0.5 pg/ml of LPS, while the maximum detected concentration is around 5 ng/ml (70,71). However, as discussed and highlighted before, despite the good sensitivity, the LAL assay displays a number of serious

drawbacks. The first point focuses on the interference of glucans to the test, generating false positive results (40). The other point focuses on the fact that the LAL assay not able to readily detect LPS in biological samples. The complexity of biological fluids impedes the assay's performance, with several serum components e.g. proteases etc., directly interfering with the Factor C initiated coagulation cascade. As a consequence extensive sample preparation is required prior to testing (73). Other commercially available endotoxin assays e.g. the monocyte activation test (MAT) and recombinant Factor C (rFC) assay, generally lack the sensitivity shown by the LAL based systems, are time consuming to perform and in the case of the MAT suffer from inconsistencies due to the reliance on human cells (74).

The generated apta-MIP out-performed the commercially available assays in most aspects. The system successfully demonstrates an LOD of 1 fg/ml while the linear detection range lies between 100 fg/ml and 100 pg/ml, with possible expansion to 10 fg/ml to 1 ng/ml. Additionally, the apta-MIP showed little response when challenged with common, pathogen-associated, cross-reactants (GLU and LTA). However, less than optimal results were observed when the system was challenged with biological samples. Studies performed with HSA in buffer showed that concentrations $\geq$ 5,000 μg/ml (equivalent to 1/10 dilution of serum) resulted in considerable biofouling of the apta-MIP sensor. However, when the system was challenged with a spiked serum sample, diluted 1 in 100,000, a larger than anticipated 'background' response was observed. Despite this, a further increase in response was observed when the apta-MIP was challenged with a serum sample (same dilution) spiked with 10 fg/ml LPS. This observation suggests that perhaps with further optimisation / refinement of the sample preparation approach, the apta-MIP could provide the much-needed solution for detection of LPS in clinical samples.

Chapter 3 built upon the success of the aptasensor development described in Chapter 2. Indeed, both systems perform similarly across many of the performance characteristics; the selectivity shown by both sensors towards LPS is remarkable. The present Chapter showcases a true expansion of the objectives exploited in Chapter 2, providing more sensitive results with a reduction in LOD from 100 fg/ml to just 1 fg/ml. The linear range has also expanded, with good linearity demonstrated up to 1 ng/ml (cf. 1 pg/ml for the aptasensor). The newly developed system shows performance that very few sensing systems can demonstrate, when the applied solution is a buffer and not a biological sample.

Finally, the paucity of reports in the literature demonstrating the successful imprinting of LPS shows how difficult a target it is to work with. The development of an artificial recognition site for a molecule with poor solubility, variable chemical functionality and less defined molecular size / conformation remains one of the greatest challenges in the field of molecular imprinting. The use of the hybrid imprinting approach described in this body of work not only shows how integrating biorecognition elements within synthetic materials allows such challenges to be overcome, but how the combination is able to produce a sensing system with far superior performance when compared to the individual counterparts.

3.5 Bibliography

1.   Pauling L. A Theory of the Structure and Process of Formation of Antibodies. J
        Am Chem Soc [Internet]. 1940 Oct [cited 2020 Feb 4];62(10):2643–57.
        Available from: https://pubs.acs.org/doi/abs/10.1021/ja01867a018

2.   Mujahid A, Dickert FL. Molecularly Imprinted Polymers: Principle, Design, and
        Enzyme-Like Catalysis. Principle, Design, and Enzyme-Like Catalysis. In:
        Molecularly Imprinted Catalysts: Principles, Syntheses, and Applications.
        Elsevier Inc.; 2016. p. 79–101.

3.   Polyakov MV. Adsorption properties and structure of silica gel. Zh Fiz Khim.
        1931;2:799–805.

4.   Pauling L. Nature of forces between large molecules of biological interest.
        Nature. 1948;161(4097):707–9.

5.   Molecularly imprinted polymer - Wikipedia [Internet]. [cited 2020 Apr 14].
        Available from: https://en.wikipedia.org/wiki/Molecularly_imprinted_polymer

6.   Patrikeev V, Smirnova Z, Maksimova G. Some Biological Properties of
        Specifically Formed Silica. Dokl Akad Nauk SSSR. 1962;146:707–9.

7.   Wulff G, Sarhan A, Zabrocki K. Enzyme-analogue built polymers and their use
        for the resolution of racemates. Tetrahedron Lett. 1973;14(44):4329–32.

8.   Andersson L, Sellergren B, Mosbach K. Imprinting of amino acid derivatives in
        macroporous polymers. Tetrahedron Lett. 1984 Jan 1;25(45):5211–4.

9.   Alexander C, Andersson HS, Andersson LI, Ansell RJ, Kirsch N, Nicholls IA, et
        al. Molecular imprinting science and technology: a survey of the literature for the
        years up to and including 2003. J Mol Recognit [Internet]. 2006 Mar [cited 2020
        Feb 4];19(2):106–80. Available from: http://doi.wiley.com/10.1002/jmr.760

10.   Cormack PAG, Mosbach K. Molecular imprinting: recent developments and the
        road ahead. React Funct Polym [Internet]. 1999 Jul [cited 2020 Feb 4];41(1–
        3):115–24. Available from:
        https://linkinghub.elsevier.com/retrieve/pii/S1381514899000243

11.   Turner NW, Jeans CW, Brain KR, Allender CJ, Hlady V, Britt DW. From 3D to
        2D: A review of the molecular imprinting of proteins. Vol. 22, Biotechnology
        Progress. NIH Public Access; 2006. p. 1474–89.

12.   Nishino H, Huang C-S, Shea KJ. Selective Protein Capture by Epitope
        Imprinting. Angew Chemie Int Ed [Internet]. 2006 Apr 3 [cited 2020 Apr
        14];45(15):2392–6. Available from:
        http://doi.wiley.com/10.1002/anie.200503760

13.   Ding X, Heiden PA. Recent Developments in Molecularly Imprinted
        Nanoparticles by Surface Imprinting Techniques. Macromol Mater Eng
        [Internet]. 2014 Mar 1 [cited 2020 Apr 14];299(3):268–82. Available from:
        http://doi.wiley.com/10.1002/mame.201300160

14.   Bowen JL. Detection of Lipopolysaccharide Pyrogens by Molecularly Imprinted
        Polymers. 2011.

15.   Dechtrirat D, Gajovic-Eichelmann N, Bier FF, Scheller FW. Hybrid Material for

Protein Sensing Based on Electrosynthesized MIP on a Mannose Terminated Self-Assembled Monolayer. Adv Funct Mater [Internet]. 2014 Apr [cited 2020 Feb 5];24(15):2233–9. Available from: http://doi.wiley.com/10.1002/adfm.201303148

16.   Jolly P, Tamboli V, Harniman RL, Estrela P, Allender CJ, Bowen JL. Aptamer-MIP hybrid receptor for highly sensitive electrochemical detection of prostate specific antigen. Biosens Bioelectron [Internet]. 2016;75:188–95. Available from: http://dx.doi.org/10.1016/j.bios.2015.08.043

17.   Chen L, Xu S, Li J. Recent advances in molecular imprinting technology: Current status, challenges and highlighted applications. Vol. 40, Chemical Society Reviews. 2011. p. 2922–42.

18.   Hussain M, Rupp F, Wendel HP, Gehring FK. Bioapplications of acoustic crystals, a review. Vol. 102, TrAC - Trends in Analytical Chemistry. Elsevier B.V.; 2018. p. 194–209.

19.   Wang H-J, Zhou W-H, Yin X-F, Zhuang Z-X, Yang H-H, Wang X-R. Template Synthesized Molecularly Imprinted Polymer Nanotube Membranes for Chemical Separations. J Am Chem Soc [Internet]. 2006 Dec 20 [cited 2020 Feb 9];128(50):15954–5. Available from: https://pubs.acs.org/doi/10.1021/ja065116v

20.   Widayani, Yanti, Wungu TDK, Suprijadi. Preliminary Study of Molecularly Imprinted Polymer-based Potentiometric Sensor for Glucose. In: Procedia Engineering. Elsevier Ltd; 2017. p. 84–7.

21.   Wallace GG. Conductive electroactive polymers : intelligent polymer systems. CRC Press; 2009. 263 p.

22.   Sharma PS, Pietrzyk-Le A, D'Souza F, Kutner W. Electrochemically synthesized polymers in molecular imprinting for chemical sensing. Anal Bioanal Chem. 2012 Apr 1;402(10):3177–204.

23.   Tominaga Y. Ion-conductive polymer electrolytes based on poly(ethylene carbonate) and its derivatives. Vol. 49, Polymer Journal. Nature Publishing Group; 2017. p. 291–9.

24.   Rikukawa M, Sanui K. Proton-conducting polymer electrolyte membranes based on hydrocarbon polymers. Vol. 25, Progress in Polymer Science (Oxford). Elsevier Science Ltd; 2000. p. 1463–502.

25.   Sriwichai S, Baba A, Phanichphant S, Shinbo K, Kato K, Kaneko F. In situ study of electropolymerized poly(3-aminobenzoic acid) thin film on BD-R and DVD-R grating substrates by electrochemical-transmission surface plasmon resonance spectroscopy. Int J Polym Sci. 2015 Feb 25;2015.

26.   Haque SU, Inamuddin, Nasar A, Rajender B, Khan A, Asiri AM, et al. Optimization of Glucose Powered Biofuel Cell Anode Developed by Polyaniline-Silver as Electron Transfer Enhancer and Ferritin as Biocompatible Redox Mediator. Sci Rep. 2017 Dec 1;7(1):1–9.

27.   Chen S, Yau S. Self-organized electropolymerization of aniline on au (111) electrode in hydrochloric acid. J Electrochem Soc. 2014 Jan 1;161(10):H612–8.

28.   Pan D, Chen J, Nie L, Tao W, Yao S. Amperometric glucose biosensor based on immobilization of glucose oxidase in electropolymerized o-aminophenol film at

Prussian blue-modified platinum electrode. Electrochim Acta. 2004 Feb 25;49(5):795–801.

29. Wulff G. The covalent and other stoichiometric approaches. In: Yan M, Ramström O, editors. Molecularly Imprinted Materials, Science and Technology. New York: Marcel Dekker; 2005. p. 59–92.

30. Golabi M, Kuralay F, Jager EWH, Beni V, Turner APF. Electrochemical bacterial detection using poly(3-aminophenylboronic acid)-based imprinted polymer. Biosens Bioelectron. 2017 Jul 15;93:87–93.

31. Endotoxin MIP-SPR chip and its preparation method and use. 2013 Apr 26 [cited 2020 Feb 9]; Available from: https://patents.google.com/patent/CN103267745A/en

32. Ogawa KI, Hyuga M, Okada T, Minoura N. Development of lipid A-imprinted polymer hydrogels that selectively recognize lipopolysaccharides. Biosens Bioelectron [Internet]. 2012 Oct [cited 2020 Feb 9];38(1):215–9. Available from: http://www.ncbi.nlm.nih.gov/pubmed/22709936

33. Altintas Z, Abdin MJ, Tothill AM, Karim K, Tothill IE. Ultrasensitive detection of endotoxins using computationally designed nanoMIPs. Anal Chim Acta. 2016 Sep 7;935:239–48.

34. Otero TF, Cantero I. Electropolymerization of acrylamide at high current density in aqueous media. J Electroanal Chem. 1995 Oct 10;395(1–2):75–81.

35. Yoon SH, Mofrad MRK. Cell adhesion and detachment on gold surfaces modified with a thiol-functionalized RGD peptide. Biomaterials. 2011 Oct 1;32(30):7286–96.

36. Manesiotis P, Riley A, Bollen B. Polymerisable squaramide receptors for anion binding and sensing. J Mater Chem C. 2014 Nov 14;2(42):8990–5.

37. Cadoni E, Ferino G, Pitzanti P, Secci F, Fattuoni C, Nicolò F, et al. Halogen and Hydrogen Bonding Benzothiophene Diol Derivatives: A Study Using ab initio Calculations and X-Ray Crystal Structure Measurements. ChemistryOpen. 2015 Apr 1;4(2):161–8.

38. Rick J, Chou T-C. Amperometric protein sensor – fabricated as a polypyrrole, poly-aminophenylboronic acid bilayer. Biosens Bioelectron [Internet]. 2006 Sep 15 [cited 2017 Dec 1];22(3):329–35. Available from: http://www.ncbi.nlm.nih.gov/pubmed/16757163

39. Nikitina VN, Zaryanov N V, Karyakina EE, Karyakin AA. Electropolymerization of 2-Aminophenylboronic Acid and the Use of the Resulting Polymer for Determination of Sugars and Oxyacids. 2017;53(3):352–8.

40. Belarb E, Blas-Ferrando VM, Haro M, Maghraoui-Meherzi H, Gimenez S. Electropolymerized polyaniline: A promising hole selective contact in organic photoelectrochemical cells. Chem Eng Sci. 2016 Nov 2;154:143–9.

41. Zoshki A, Rahmani MB, Masdarolomoor F, Pilehrood SH. Room temperature gas sensing properties of polyaniline/ZnO nanocomposite thin films. J Nanoelectron Optoelectron. 2017;12(5):465–71.

42. Brett CMA, Thiemann C. Conducting polymers from aminobenzoic acids and

aminobenzenesulphonic acids: Influence of pH on electrochemical behaviour. J Electroanal Chem. 2002 Dec 13;538–539:215–22.

43.   Wang J lei, Li B chao, Li Z jun, Ren K feng, Jin L jiang, Zhang S miao, et al. Electropolymerization of dopamine for surface modification of complex-shaped cardiovascular stents. Biomaterials. 2014 Sep 1;35(27):7679–89.

44.   Thiemann C, Brett CMA. Electropolymerisation and properties of conducting polymers derived from aminobenzenesulphonic acids and from mixtures with aniline.

45.   He Y, Wang X, Huang H, Zhang P, Chen B, Guo Z. In-situ electropolymerization of porous conducting polyaniline fibrous network for solid-state supercapacitor. Appl Surf Sci. 2019 Mar 1;469:446–55.

46.   Springsteen G, Wang B. A detailed examination of boronic acid-diol complexation. Tetrahedron. 2002;

47.   Yan M, Ramström O. Molecularly imprinted materials : science and technology. New York: Marcel Dekker; 2005. 734 p.

48.   Badhulika S, Tlili C, Mulchandani A. Poly(3-aminophenylboronic acid)-functionalized carbon nanotubes-based chemiresistive sensors for detection of sugars. Analyst [Internet]. 2014 May 19 [cited 2020 Feb 15];139(12):3077–82. Available from: http://www.ncbi.nlm.nih.gov/pubmed/24776682

49.   Nantasenamat C, Isarankura-Na-Ayudhya C, Naenna T, Prachayasittikul V. Quantitative structure-imprinting factor relationship of molecularly imprinted polymers. Biosens Bioelectron. 2007 Jun 15;22(12):3309–17.

50.   Bai L, Chai Y, Pu X, Yuan R. A signal-on electrochemical aptasensor for ultrasensitive detection of endotoxin using three-way DNA junction-aided enzymatic recycling and graphene nanohybrid for amplification. Nanoscale. 2014 Mar 7;6(5):2902–8.

51.   Posha B, Nambiar SR, Sandhyarani N. Gold atomic cluster mediated electrochemical aptasensor for the detection of lipopolysaccharide. Biosens Bioelectron. 2018 Mar 15;101:199–205.

52.   Abdin MJ, Altintas Z, Tothill IE. In silico designed nanoMIP based optical sensor for endotoxins monitoring. Biosens Bioelectron. 2015 May 5;67:177–83.

53.   Buchegger P, Lieberzeit PA, Preininger C. Thermo-nanoimprinted biomimetic probe for LPS and LTA immunosensing. Anal Chem. 2014 Feb 4;86(3):1679–86.

54.   Long Y, Li Z, Bi Q, Deng C, Chen Z, Bhattachayya S, et al. Novel polymeric nanoparticles targeting the lipopolysaccharides of Pseudomonas aeruginosa. Int J Pharm. 2016 Apr 11;502(1–2):232–41.

55.   Umpleby RJ, Baxter SC, Chen Y, Shah RN, Shimizu KD. Characterization of Molecularly Imprinted Polymers with the Langmuir−Freundlich Isotherm. Anal Chem [Internet]. 2001 Oct 1 [cited 2020 Feb 19];73(19):4584–91. Available from: https://pubs.acs.org/doi/10.1021/ac0105686

56.   Zhang J, Song S, Wang L, Pan D, Fan C. A gold nanoparticle-based chronocoulometric DNA sensor for amplified detection of DNA. 2007;

57.   Satjapipat M, Sanedrin R, Zhou F. Selective desorption of alkanethiols in mixed

self-assembled monolayers for subsequent oligonucleotide attachment and DNA hybridization. Langmuir. 2001 Nov 27;17(24):7637–44.

58. Fanali G, Di Masi A, Trezza V, Marino M, Fasano M, Ascenzi P. Human serum albumin: From bench to bedside. Mol Aspects Med. 2012;33:209–90.

59. Wong J, Zhang Y, Patidar A, Vilar E, Finkelman M, Farrington K. Is Endotoxemia in Stable Hemodialysis Patients an Artefact? Limitations of the Limulus Amebocyte Lysate Assay and Role of (1→3)-β-D Glucan. Jha V, editor. PLoS One [Internet]. 2016 Oct 20 [cited 2017 Apr 21];11(10):e0164978. Available from: http://dx.plos.org/10.1371/journal.pone.0164978

60. Digby J, Kalbfleisch J, Glenn A, Larsen A, Browder W, Williams D. Serum glucan levels are not specific for presence of fungal infections in intensive care unit patients. Clin Diagn Lab Immunol. 2003 Sep;10(5):882–5.

61. Wright WF, Overman SB, Ribes JA. (1–3)-β-D-Glucan Assay: A Review of its Laboratory and Clinical Application. Lab Med. 2011 Nov 1;42(11):679–85.

62. Hartung S, Knapp S, Von Aulock K, Triantafilou M, Triantafilou TS, Bunk S, et al. Blood of Lipoteichoic Acid in Human Peripheral Are Critical for TLR2-Mediated Recognition Internalization and Coreceptor Expression. J Immunol [Internet]. 2010 [cited 2020 Feb 22];185:3708–17. Available from: http://www.jimmunol.org/content/185/6/3708http://www.jimmunol.org/content/185/6/3708.full#ref-list-1

63. Ginsburg I. Role of lipoteichoic acid in infection and inflammation. Vol. 2, Lancet Infectious Diseases. Lancet Publishing Group; 2002. p. 171–9.

64. Poxton IR. Teichoic Acids, Lipoteichoic Acids and Other Secondary Cell Wall and Membrane Polysaccharides of Gram-Positive Bacteria. In: Molecular Medical Microbiology: Second Edition. Elsevier Ltd; 2014. p. 91–103.

65. Percy MG, Gründling A. Lipoteichoic Acid Synthesis and Function in Gram-Positive Bacteria. Annu Rev Microbiol [Internet]. 2014 Sep 8 [cited 2020 Apr 6];68(1):81–100. Available from: http://www.annualreviews.org/doi/10.1146/annurev-micro-091213-112949

66. Wang RE, Tian L, Chang YH. A homogeneous fluorescent sensor for human serum albumin. J Pharm Biomed Anal. 2012 Apr 7;63:165–9.

67. Pan S, Zhang H, Liu W, Wang Y, Pang W, Duan X. Biofouling Removal and Protein Detection Using a Hypersonic Resonator. ACS Sensors. 2017 Aug 25;2(8):1175–83.

68. Alvarez B, Carballal S, Turell L, Radi R. Formation and reactions of sulfenic acid in human serum albumin. Vol. 473, Methods in enzymology. Academic Press; 2010. p. 117–36.

69. Reich J, Weyer FA, Tamura H, Nagaoka I, Motschmann H. Low endotoxin recovery—Masking of naturally occuring endotoxin. Int J Mol Sci. 2019 Feb 2;20(4).

70. Park CY, Jung SH, Bak JP, Lee SS, Rhee DK. Comparison of the rabbit pyrogen test and Limulus amoebocyte lysate (LAL) assay for endotoxin in hepatitis B vaccines and the effect of aluminum hydroxide. Biologicals [Internet]. 2005 Sep [cited 2020 Feb 23];33(3):145–51. Available from:

http://www.ncbi.nlm.nih.gov/pubmed/16055344

71.   Sondhi P, Maruf MHU, Stine KJ. Nanomaterials for Biosensing
      Lipopolysaccharide. Biosensors [Internet]. 2019 Dec 21 [cited 2020 Feb
      23];10(1):2. Available from: https://www.mdpi.com/2079-6374/10/1/2

72.   Wong J, Zhang Y, Patidar A, Vilar E, Finkelman M, Farrington K. Is
      endotoxemia in stable hemodialysis patients an artefact? Limitations of the
      limulus amebocyte lysate assay and role of (1???3)-??-D Glucan. PLoS One.
      2016;11(10):1–16.

73.   Laugerette F et al. Endotoxemia Analysis by the Limulus Amoebocyte Lysate
      Assay in Different Mammal Species Used in Metabolic Studies. J Anal Bioanal
      Tech. 2015 Jul 4;6(4):1–6.

74.   Dullah EC, Ongkudon CM. Current trends in endotoxin detection and analysis of
      endotoxin–protein interactions. Crit Rev Biotechnol [Internet]. 2017 Feb 17
      [cited 2020 Feb 23];37(2):251–61. Available from:
      https://www.tandfonline.com/doi/full/10.3109/07388551.2016.1141393

Development of CRP and PCT aptasensors

4.1   Introduction

4.1.1. General overview

The successful development and characterisation of a hybrid recognition system able to detect LPS in low concentrations has been demonstrated in Chapters 2 and 3. However, the original aim of the project was the development of a multiplex platform to enable the rapid and accurate diagnosis of sepsis. It has been widely accepted that a panel of biomarkers will be needed in order to achieve the requisite clinical specificity and sensitivity.

The present study therefore chose to add c-reactive protein (CRP) and procalcitonin (PCT) to the diagnostic panel. Both biomarkers have been widely used to monitor and diagnose patients with sepsis in a clinical setting. CRP is the longest serving biomarker that has been used to diagnose sepsis [1,2]. CRP is an acute phase protein, with levels rising quickly during periods of infection and/or inflammation. PCT was initially proposed as a good prognostic biomarker for sepsis during the 1990s and is considered a more specific biomarker than CRP.

A number of analytical assays for CRP exist, including electrochemical sensors. On the other hand, detection of PCT mainly relies on ELISA based assays. In the NHS, testing for both of these markers takes place in centralised laboratories which means that there is often a delay in diagnosis and/or monitoring of patients. Furthermore, the cost of PCT testing is such that testing is limited to critical care settings [3,4]. A cost-effective and rapid sensor, capable of testing for both markers simultaneously in a near-patient setting could revolutionise patient care.

The current Chapter describes the development of aptasensors for PCT and CRP. Following a similar approach to that presented in Chapter 2, the individual aptasensors were developed using thiolated aptamers in combination with alkanethiol molecules, which were screened for their interaction with the respective biomarker. The final sensors were characterised in terms of sensitivity, dynamic range and selectivity, prior to being challenged with spiked serum samples

4.1.2 C reactive protein (CRP)

C-Reactive Protein is one of the most common markers of systemic inflammation, alongside erythrocyte sedimentation rate (ESR) and white blood cell count (WBC) (5). Its synthesis takes place in the liver, but extrahepatic expression has also been documented (6,7). Tillet and Francis were the first to detect CRP in 1930, identifying a substance in the sera of patients with acute *pneumococcal* pneumonia that formed a precipitate when exposed to polysaccharides of *Streptococcus pneumoniae* (8). It was later found that this reaction was not limited to *pneumococcal* pneumonia, being observed for a variety of acute infections.

CRP is considered an "acute phase protein" indicating the body's chemical response to inflammatory states (9,10). CRP is normally present at low levels (~ 10 μg/mL) in serum but shows a rapid and dramatic elevation (350-400 μg/mL) in response to a variety of infectious or inflammatory conditions (11–13). Since 1930, CRP has been used as a screening tool for occult inflammation, as a marker of disease activity and as a diagnostic test (14). Several detection methodologies / assays exist for CRP. These are mainly immunoassay based, reporting a wide range of detection limits. Clinical testing is largely still carried out in central testing laboratories rather than at point-of-care, although several near-patient testing systems are available commercially. Testing methodologies will be discussed in Section 4.1.2.3.

4.1.2.1 Molecular structure and recognition

Regarding its biological function, CRP recognises pathogens and damaged cells and mediates their elimination via recruitment of the complement system (via C1q) and phagocytic cells (via the membrane receptor Fcγ (FcγR)) (15). CRP can bind to phosphocholine (PCh), which is widely distributed in teichoic acids and lipopolysaccharides (16). PCh's presence has been reported in various bacteria and micro-organisms (16).

The CRP gene lies between 1q21 and 1q23 loci of chromosome 1, containing 2,263 nucleotides and only one intron (17). Its transcript consists of a long 3' untranslated region (1.2 kb), which mediates its degradation after the pause of the inflammatory response and restoration of the homeostasis (16).

CRP belongs to the highly conserved "pentraxin" family of proteins (16). Its structure has been determined by X-ray crystallography at 3 Å resolution (18,19). Five noncovalently associated protomers are arranged symmetrically around a central pore to create the CRP molecule. In other words, this pentamer forms a "ring" structure, with an outside diameter approaching 102 Å. Its central pore diameter approaches 30 Å. The protomers are slightly bigger than the central pore, as their diameter is around 36 Å. As described in the review by Volanakis, "each protomer consists of 206 amino acids folded into two antiparallel β sheets with a flattened jellyroll topology" (Figure 4.1) (16).
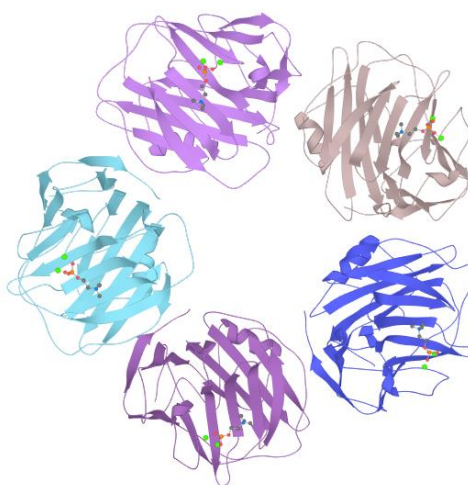
Figure 4.1: Three-dimensional structure of human C-Reactive Protein (CRP). CRP consists of 5 protomers, noncovalently assembled to form a "ring" structure (20).

Residues 168-176 form a long α – helix, which lies against one of the two β-sheets. In addition, residues 177-182 create a loop and with the carboxyl terminal end of the aforementioned helix, form one of the two sides of an unusual split. This split connects the protomer's centre with its edges at the central pore. The other split's terminal is formed by parts of the protomer's amino and carboxyl terminals. This unique structure, apart from characterising the protomer, facilitates binding to C1q and efficiently activates the classical pathway of human complement (21,22). In addition, this protomer's site can bind to cell-surface Fcγ receptors (FcγR) and activate leukocyte-mediated phagocytosis (15).

On the other side of the protomer, two Ca^{2+} ions are located at close distance between the side and main chain carbonyls (Figure 4.2). These ions are very important as CRP possesses Ca^{2+}-dependent binding specificity for phosphocholine (PCh), a constituent of many bacterial and fungal polysaccharides and of most biological cell membranes (16).
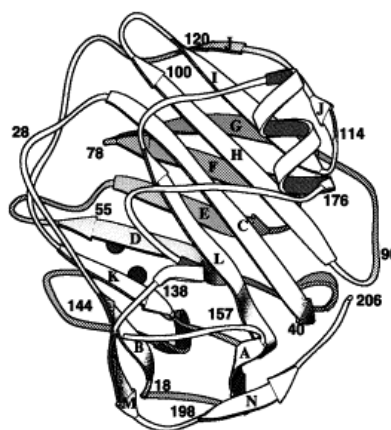
Figure 4.2: CRP protomer structure. The β-Strands are labelled A–N and the two Ca^{2+} are shown as spheres (16).

Electron microscopy and crystallographic data suggest that when the pentamer is assembled, all protomers have the same orientation (23). This characteristic helps CRP to demonstrate a dual activity; recognising the five PCh-binding sites and then transferring the signal by binding to C1q and FcγR.

In addition, the protomers are able to rotate around their axis, allowing the pentamer to multivalently bind to cell surfaces that expose various distributions of PCh (24). CRP's multipoint attachment could lead to a disposition of C1q- and FcR-binding sites more suitable for reactivity with their corresponding ligands. This explains the fact that only ligand-complexed CRP can activate the complement system (16).

Focusing on the PCh-binding site, it consists of the two Ca^{2+} ions (as previously mentioned) and an adjacent hydrophobic pocket (Figure 4.3). The two Ca^{2+} binding sites display equal affinity for those calcium ions, when the protomer is in solution (25). These CRP-bound Ca^{2+} ions are able to directly co-ordinate with two of the PCh's phosphate groups. At the same time, the choline group inserts itself the hydrophobic pocket. The binding between CRP and PCh is further boosted by the hydrophobic interaction of the

Phe66 residue and the three choline methyl groups, while Glu81's side chain (the residue is located on the other side of the pocket) interacts with the positively charged quaternary choline nitrogen (113).
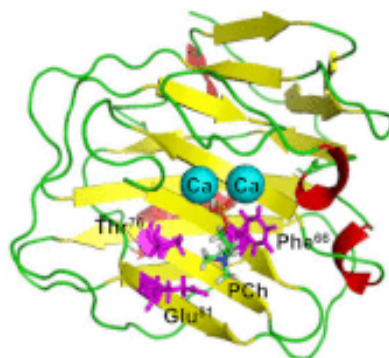
Figure 4.3: CRP displays a binding site for PCh consisting of two Ca²⁺ and an adjacent hydrophobic pocket, created by various neighbouring residues (26).

On the other hand, the "effector" face of CRP is able to bind to C1q through another pocket, formed by loops 86–92 and 112–114 on one side and the protomer's C-terminus and the residue of Tyr175 on the other (27). In addition, residues Asp112 and Tyr175 are thought to be contact sites, while Glu88 appears to change the conformations of C1q. With this change in the geometry, C1q can activate complement. Finally, the residues of Asn158 and His38 contribute to the stabilisation of the binding site (22).

4.1.2.2 CRP and sepsis

CRP has been ubiquitously associated with sepsis as a prognostic marker, due to its acute phase protein characteristics. The clinical cut-off concentration of CRP in sepsis is 50 µg/ml (28,29).

However, CRP's specificity as a marker for sepsis is low, sitting at around 75% (28). In addition, its peak plasma levels are unable to adequately show the severity of the systemic inflammation (29). Furthermore, CRP levels may also be significantly elevated in response to different types of trauma and inflammation, that may not be attributable to a

case of severe infection or sepsis; for example, CRP levels are often elevated following surgery (29,30).

On the other hand, evidence has showed that only a moderate increase in CRP levels (50-100 µg/ml or less) in patients with an acute onset of sepsis or even severe sepsis is sometimes observed, which can result in under-treatment with fatal consequences (29). In addition, CRP levels reach a peak in several days, while their decline can take up to two weeks. This suggests that this biomarker may be less appropriate for critically ill patients where a marker that allows timely diagnosis, and importantly close to real-time monitoring of the patient, is needed (29). Since there is no golden marker for the diagnosis of sepsis, it is widely accepted that multi-marker panels will be needed to provide sufficient clinical sensitivity and specificity. As CRP is in routine use in clinical care, it makes sense that it would be part of the platform under development.

4.1.2.3 CRP tests

CRP was discovered some 90 years ago by Tillett and Francis (8). Given its role in inflammatory and infectious conditions, it is perhaps unsurprising that a variety of analytical tests targeting the detection of CRP exist. Vashist *et al.* have reviewed such tests, highlighting varying performance characteristics with detection ranges from as little as fg/ml to as much as µg/ml (31).

The modern history of CRP assays starts with the development of turbidimetric assays in the late 1980s (32). The technology is quite simple, relying on the recognition properties of anti-CRP antibodies bound to latex particles (31). The interaction between antibody and biomarker leads to agglutination that can either be observed by measuring absorption or by the naked eye (32–34). Deegan *et al.* demonstrated a modified agglutination approach, as they relied on the binding between CRP and phosphocholine (35). Phosphocholine is conjugated with BSA and further bound to carboxy-modified microspheres. The turbidimetric assays can detect as little as 230 pg/ml, while the dynamic range of these assays lies between the micro- / nano- gram/ml scale (33).

As for many proteins, a high number of Enzyme Linked ImmunoSorbent Assay (ELISA) approaches have been described for CRP detection. Most of these immunoassays are sandwich type, meaning that the final signal of the analysis is obtained by the presence

of a second antibody, bound (mainly) to an enzyme that catalyses a specific reaction to produce a final product that can be detected via optical spectroscopy (color / fluorescence). Such assays have managed to showcase LOD values of 10 pg/ml (36). Punyadeera *et al.* demonstrated a one-step homogenous bead-based ELISA, employing the use of biotinylated antibodies with streptavidin beads (13).

The existence of CRP targeting antibodies, finding application in both ELISA and turbidimetric assays, opens the horizon to other techniques employing fluorometry or chemiluminescence. Fluorometric assays are often associated with detection ranges over the micro- / nano- gram/ml scale with a few exceptions (31). Kim and co-workers developed a capillary-driven on chip fluorescent immunoassay relying on the use of a microfluidics. The reported dynamic range starts at 1.18 pg/ml, finishing at 11.8 ng/ml, with a LOD of ~ 940 fg/ml (37). Islam *et al.* have developed two sandwich fluorescence immunoassays with remarkable results (38,39). Both immunoassays utilise total internal reflection fluorescence microscopy (TIRF) for their observations (38,39).

The widespread development of diagnostic assays across the research sector has also been seen in the commercial world, with the launch of portable analysers such as CUBE and SMART (Eurolyser Diagnostica) (31). Both analysers use fingerprick blood samples to perform the analysis. Orion Diagnostica (Finland) developed the QuickRead Go instrument, while Alere (now part of Abbott) presented the Afinion™ AS100 and Roche brought the Cobas c702 to market (31,40). Other notable approaches utilise technologies such as lateral flow, chemiluminescence etc., with some even using smartphones for the development of rapid CRP-specific assays (8).

However, the lengthy list of methods exploited for detecting CRP does not end here. Literature demonstrates the existence of surface plasmon resonance (SPR)-based assays. Kim and co-workers developed a direct immunoassay using polythiophene SAMs crosslinked to CRP antibodies (41). The polythiophene SAMs were developed on gold chips and the sensor shows an LOD of 10 μg/ml. Yeom and co-workers experimented with localized surface plasmon resonance (LSPR) biosensors (42). They also used gold nanoparticles to overcome problems that may limit sensitivity, selectivity, and dynamic range. Indeed, their sensor displays an LOD of as little as 100 ag/ml. Vance and Sandros also demonstrate impressive results, as their SPR sensor can detect zeptomoles of CRP (43). Their study explored the development of a sandwich ELISA employing aptamers

instead of antibodies. More precisely, aptamers conjugated with quantum dots bind to the complex formed between CRP and biotinylated anti-CRP aptamers, enhancing the signal.

Electrochemical CRP detection assays mainly rely on the use of antibodies. Salvo *et al.* authored a review to expose the wide range of sensors and biosensors targeting CRP for wound healing purposes (44). Potentiometric, amperometric and impedimetric sensors have all been developed, in an attempt to produce a low cost and efficient diagnostic tool. However, both reviews authored by Salvo *et al.* and Vashist *et al.* locate the detection range of these sensors at the micro- / nano- gram/ml scale, as the vast majority of the described assays (31,44). The study of Zhang and co-workers shows impressive results (6). They developed a sandwich type assay using antibodies to capture CRP. Copper nanoparticles in association with hybridisation chain reaction (for DNA) were used to amplify the signal, allowing the sensor to detect as little as 0.33 fg/ml (linear range 1.0 fg/m to 100 ng/mL). One of the notable studies belongs to Johnson *et al.*, in which the antibody and affimer based EIS immunoassay showed an apparent detection range between 35.4 to 59 pg/ml (45). Affimers are non-antibody short scaffolds deriving from the optimisation of the phytocystatin protein (46). These molecules have been successfully utilised in diagnostics, since their binding affinity is normally located in the nanomolar level (46,47). Moreover, Bryan and co-workers developed a biosensor showing a LOD value of 322 pM (48). However, the dynamic range of the sensor sits between 10 and 50 nM. Notably as MIP system has been developed by Kumar and Prasad (49). The system utilises CV to detect changes on the "multiwalled carbon nanotubes embedded molecularly imprinted polymer-modified screen-printed carbon" electrode. Although the development of the sensor was demonstrated, the dynamic range was reported to be between 0.18 and 8.51 µg/ml, while the LOD was shown to be 0.04 µg/ml.

Lab-on-a-chip systems also demonstrate a rich list of approaches detecting CRP. One of the notable studies belongs to Christodoulides and co-workers who developed a sandwich ELISA (50). The format relies on the presence of two antibodies; the first is bound on agarose beads while the other is conjugated to a fluorescent dye (Alexafluor-488). The generated system is able to detect as little as 5 fg/ml, while the detection range spans 10 fg/ml to 10 pg/ml.

Literature reports a large number of studies based on aptamers. CRP's large size provides a wide variety of binding opportunities, allowing the development of a plethora of

aptamers. In fact, the aptamers targeting CRP can be divided into several distinct groups; the first group deals with the molecular nature, as both RNA and DNA aptamers have been reported as recognition elements in biosensors (51,52). On the other hand, aptamers have also been developed to either detect monomeric or pentameric forms of the CRP molecule (53).

Information about DNA aptasensors will be provided during the later sections of this chapter, being used as direct comparators for the present study. RNA aptasensors have demonstrated satisfactory results. Wang *et al.* demonstrated the development of a RNA-based electrochemical sensor, utilising functionalized silica microspheres as immunoprobes (51). The system achieved an impressive linear range between 5 pg/ml and 125 ng/ml, while its LOD sits at 1.7 pg/ml. Bini and co-workers created an optical RNA aptasensor that showed LOD values of 500 pg/ml (54). The aptasensor showed good selectivity when challenged with HSA. The study also showed some preliminary results focused on the detection of CRP in serum. Eid *et al.* have also extended their work to serum spiked with CRP (55). They developed a slow off-rate modified aptamer, called a SOMAmer, utilising the technology of isotachophoresis. The difference between a normal aptamer and a SOMAmer is that in the second case, the DNA / RNA libraries are modified with artificial riboses and nucleobases to generate the molecules (56). This approach combined with slow off-rate selection leads to the development of molecules with high specificity and high affinity towards the targeted molecule. The assay was coupled with an ionic spacer whose role was to separate the bound from free SOMAmers. The study accomplished an apparent LOD of 2 nM, while the test run time was 20 minutes.

Other notable works include the ones of Qureshi *et al.* and Pultar *et al.* The first study shows a dynamic range between 100 and 500 pg/ml (57). The second study focused on the development of an RNA aptamer-based lab on a chip (58). The detection of the bound CRP aptamer was achieved with optical means, recruiting a labelled secondary antibody, mimicking a sandwich format. A similar approach, utilising the advantages of an aptamer and an antibody, is presented by Bernard and co-workers, developing a system relying on a multiplexing bead-based platform (59). A CRP specific RNA aptamer was bound on beads, while an antibody coupled with a fluorescently labelled streptavidin was used for the quantification. The system showed an LOD of 400 ng/ml with its linear range falling

between 400 ng/ml and 10 μg/ml. The study of Bernard *et al.* is one of the few reports displaying CRP recovery data from diluted blood sera.

4.1.3 Procalcitonin (PCT)

Procalcitonin (PCT) was first identified by Deftos, Roos and Parthemore in the 1970s and is considered an important biomarker in the determination of bacterial infections (60,61). Since 1993, PCT has been characterised as a sepsis marker (62). PCT can be detected in the circulation of patients with severe systemic inflammation, especially when this response is caused by bacterial infection, however levels in healthy persons are incredibly low (29).

4.1.3.1 Molecular Structure and Function

PCT is categorised as a prohormone being expressed by the CALC-1 gene, and consists of 116 amino acids (61). During normal homeostasis, pre-procalcitonin (pre-PCT) undergoes an intracellular proteolytic process; a specific protease group breaks the original transcript into calcitonin, katacalcin and N-terminal residue of PCT (Figure 4.4) (63). Subsequently, the active calcitonin, consisting of only 32 peptides, is secreted by the C cells of the thyroid gland (143,144). Despite the common origin, PCT's function and induction are different from that associated with calcitonin (29).
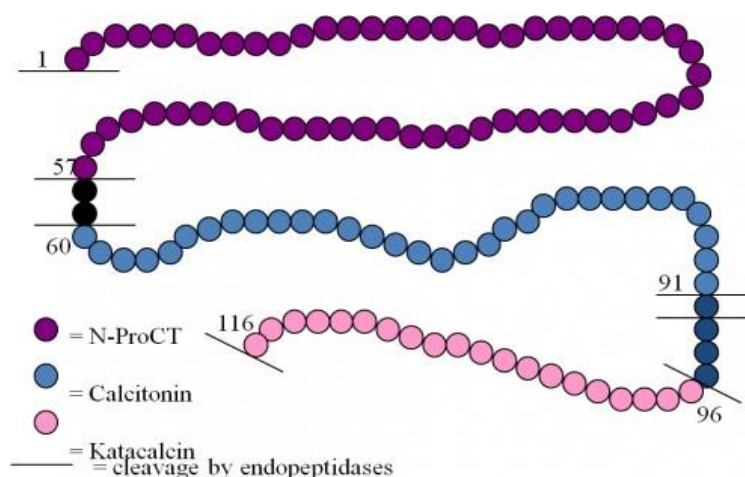
Figure 4.4: PCT is expressed by the CALC-1 gene. Following a proteolytic process, the molecule breaks into calcitonin, katacalcin and N-terminal residue (N-ProCT) (65).

This proteolytic cleavage means that the level of PCT in the blood of healthy humans is extremely low (typically less than 0.05 ng/ml). Its release is tightly controlled, being induced as a consequence of exposure to pathogen associated toxins (e.g. lipopolysaccharide) or other inflammatory molecules (e.g. TNF-α, IL-6) (66). Various tissues during sepsis are able to produce PCT (29). The elevated levels in blood are related to monocyte activation which occurs during sepsis, or generally during inflammatory responses, as research has shown that adherent monocytes and adipocytes can produce PCT, when exposed to activated monocytes (67). As is the case with CRP, the liver seems to regulate PCT responses as well, especially when these are triggered by the presence of endotoxin (68).

According to the literature, PCT demonstrates various biological functions, including the modulation of immunological functions and vasomotility (29). Some of these effects are time-dependent and differ according to cell types, e.g. the migratory response of monocytes is elevated by PCT's presence at first, and blocked after a long incubation period (69). Another example is the expression of inducible Nitric Oxide Synthase (iNOS) in vascular smooth muscle cells, which is controlled by PCT (70,71). This process is inhibited by PCT in native cells but promoted in prestimulated ones. Moreover, PCT influences cytokine expression by differentiating local and systemic response of tissue perfusion and inflammation (29).

4.1.3.2 PCT and sepsis

Diagnostic tests measure only a fragment of the 114-116 amino acid chain as they detect the calcitonin/N-ProCT section. As stated before, plasma levels of PCT in healthy individuals are low (< 0.1 ng/mL) (69). Plasma levels above 0.5 ng/ml are considered abnormal and provide a clinical cut-off for suspicion of sepsis. Elevated PCT levels are strongly correlated with the development of sepsis (0.5 ng/ml< PCT < 2 ng/ml) (29). Levels above 2 ng/ml are indicative of severe sepsis / septic shock (Figure 4.5).
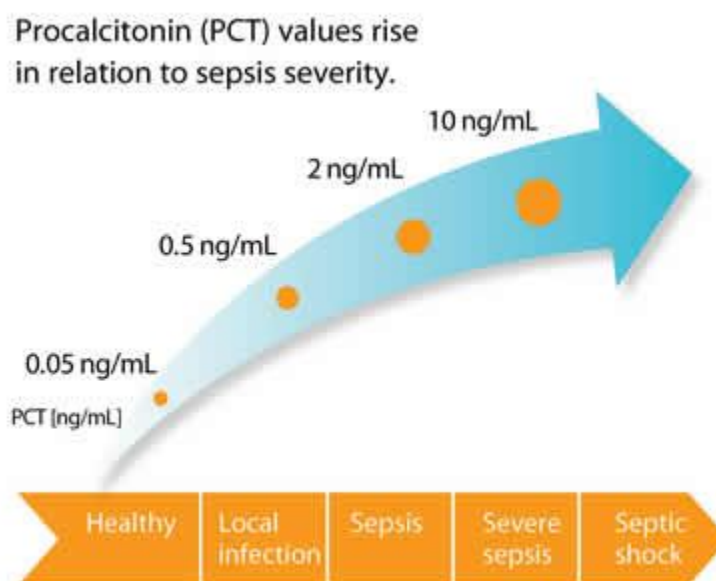
Figure 4.5: Variation of procalcitonin values during sepsis progression (72).

The common link between PCT's elevation and bacterial infection focuses on the severity of systemic inflammatory response. Bacterial infection can stimulate an excessive PCT production; something which is not observed in viral infections, where PCT expression remains low (73–76). Whilst PCT is induced in patients with SIRS, levels do not reach the concentrations observed when an infection is present.

Apart from bacterial infections, other conditions (e.g. trauma, endocarditis) can trigger PCT expression, and these levels can be normal or elevated, depending on the systemic inflammatory response. A similar response is acquired when there is no systemic inflammatory response in patients with bacteraemia, however, this is a very unlikely clinical scenario (77–79).

4.1.3.3 PCT tests

To date, there are no studies reporting on the development of aptasensors capable of detecting PCT. The biomarker of interest is detected mainly by a variety of sandwich-type immunoassays, that are fully automated (80–82). BRAHMS is the dominant franchise, as apart from their own instrumentation, the company collaborates with other

organisations such as Siemens, Roche, DiaSorin and Biomerieux in the development of PCT diagnostic systems (82). Here, the equally notable immunoturbidimetric assay from Diazyme has to be mentioned, since it is a part of clinical platforms provided by Roche, Abbott, Siemens and Beckman Coulter (82). However, this section focuses on the presentation of two point of care (POC) systems; KRYPTOR from BRAHMS and Radiometer's acute care AQT90 FLEX PCT assay.

BRAHMS has developed a series of instrumentation able to detect PCT (83). Its flagship POC device is called BRAHMS PCT direct and claims to provide results within 25 minutes (84). This feature is quite important, since some of the existing laboratory tests have a time to result of more than 2 ½ hours. The system uses a minimum of 20 μL of either venous or capillary blood. The BRAHMS PCT direct demonstrates a limit of quantitation (LOQ) of 0.22 μg/L with a linear range between 0.22 and 10 μg/L.

In addition to the direct assay, the company has developed an automated system, called sensitive KRYPTOR. More information about its mechanism is provided in the literature (85). The diagnostic tool is an immunoassay that uses TRACE (Time – Resolved Amplified Cryptate Emission) technology. The sample is incubated with a monoclonal antibody labelled with cryptate, which is a cage structure entrapping a europium ion. The cryptate possesses non-radioactive energy that donates to a part of the photo-receptive algal protein (XL665). This protein is chemically conjugated with monoclonal antibodies that recognise different epitopes of the PCT. The presence of PCT in the sample results in the binding of both monoclonal antibodies, bringing cryptate and XL665 in close proximity. Consequently, the emission spectrum provided by cryptate (donor) overlaps the absorption spectrum of the XL665 (acceptor). This action intensifies the donor's fluorescence signal and extends the duration of the acceptor signal, allowing the quantification of the time-delayed fluorescence. The signal is proportional to the PCT levels in the sample. The incubation time is as little as 19 minutes and the test needs 50 μL of blood (serum, plasma) to operate. The limit of quantitation is reportedly 0.06 μg/L while the linear range with automated dilutions is between 0.02 and 5,000 μg/L.

Radiometer has introduced to the market the acute care AQT90 FLEX PCT assay (86). Restricted information is provided by the website, regarding the system specifications and method of analysis. The assay claims to provide results in less than 21 minutes, using

whole blood or plasma samples (87). The test is also friendly to blood cultures and shows high correlation values to the KRYPTOR test (88).

In the research literature, a number of biosensors that rely on antibody-based detection of PCT are reported. For example, Chiang *et al.* developed a fibre optic biosensor, capable of detecting PCT at femtomolar concentrations (89). The method relies on the development of a sandwich immunoassay linked with gold nanoparticles. The reaction takes less than 15 minutes to complete, while the LOD is determined at 95 fg/ml. The above information suggests it would make an excellent POC system.

The work from Chen *et al.* demonstrates equally impressive results (90). Their electrochemiluminescent immunosensor shows great levels of sensitivity, since the LOD is determined at 33 fg/ml, with a reported linear detection range of 100 fg/ml to 10 ng/ml. The system uses CdS-MoS_2 nanocomposites.

Zhou and co-workers took advantage of fluorescence resonance energy transfer (FRET) technology to develop their sensor (91). Like all the other existing studies, the system relies on a sandwich immunoassay. The energy transfer occurs between quantum dots and upconversion nanoparticles. In comparison to the works presented from Chiang *et al. and* Chen *et al.*, the system's linear range lies in the nano scale and specifically at around 0.1 to 10 ng/ml. However, the LOD is located at 0.25 ng/ml.

The study of Lim *et al.* also shows results in the nano scale, as their electrochemical sensor demonstrated an apparent K_d of 0.39 ± 0.11 nM (92). This study is one of the few to use a recognition molecule that is not an antibody; the study explored the use of previously synthesised peptides to develop a sensor able to interact with PCT.

The last notable work comes from Sener *et al.*, which it describes the development of a surface imprinted polymer for use as a SPR sensor (93). A polyethylene glycol dimethacrylate – co – hydroxyethyl methacrylate MIP was created. The imprinted SPR sensor showed great selectivity to PCT over molecules such as myoglobin, human serum albumin (HSA) and cytochrome c, however the time to result was 1 hour. The system's linear range was reported to be between 20 and 1000 ng/ml, with an LOD of 9.9 ng/ml.

4.2   Materials and Methods

4.2.1 Materials

The vast majority of reagents and instrumentation have already been covered in the corresponding section of Chapter 2, since the aim of the present Chapter is to develop CRP and PCT aptasensors in a similar fashion to the one described for the development of the LPS aptasensor.

A CRP aptamer, capable of binding to the pentameric form of CRP was identified from patented work and a publication from Hwang *et al.* (52,94). The following sequence was synthesised by Sigma – Aldrich (UK):

5' – GGC AGG AAG ACA AAC ACA CAA GCG GGT GGG TGT GTA CTA TTG CAG TAT CTA TTC TGT GGT CTG TGG TGC TGT – 3'

The work of Hwang and co-workers describes the use of two aptamers of similar structure; one is bound on the surface of a microtitre plate, while the second sequence is used to bind to CRP following capture by the first. A washing step is included in the methodology which is designed to removal the aptamer II – CRP complex from the immobilised sequence. It was therefore believed that the second aptamer has higher affinity for the target molecule, and thus was selected for the current study.

A PCT aptamer was purchased from Base Pair Biotech (USA). The aptamers' sequence is unknown as it is protected by the company.

Both aptamers (CRP & PCT) are thiolated at the 5' prime end of the sequence, using the same six-carbon spacer as for the LPS aptamer.

Human CRP, recombinant human PCT (expressed in *E. coli* strains) and CRP depleted serum were purchased from HyTest (Finland). CRP was received as a solution containing 20 mM Tris pH 8.0, 0.3 M NaCl, 0.05 % sodium azide (NaN_3) and was kept at $2 - 8$ ºC. Human recombinant PCT was dissolved to the suggested concentration in deionised water, aliquoted and stored at -20 ºC.

4.2.2 Methods

All methods relevant to the developmental process have been described in the corresponding sections of Chapter 2, with the exception of chronocoulometry, the protocol for which was described in Chapter 3. Any minor modifications made to any of the protocols, along with justification / rationale are described in the results and discussion section of the present Chapter.

4.2.2.1 Cross-reactivity studies

Both CRP and PCT have a narrow selection of homologous molecules, or at least molecules showing a level of similarity. Therefore, it was decided to challenge the aptasensors with the target molecules of the present assay. More precisely, LPS and PCT were used to assess the selectivity of the CRP aptasensor, while CRP and LPS were the molecules of choice for the PCT aptasensor.

Three concentrations of each molecule were tested; LPS (0.01, 1 and 100 pg/ml), PCT (10, 75 and 150 pg/ml) and CRP (0.1, 1 and 25 pg/ml).

4.2.2.2 Challenging the CRP and PCT aptasensors with spiked serum

Initially the CRP aptasensor was challenged with 1/10 and 1/100 dilutions of CRP depleted serum (certified to contain less than 20ng/ml CRP) in order to establish a 'blank' reading. For studies involving spiked serum, human serum with a certified concentration of 41.2 ± 2.5 μg/ml of CRP was obtained from the Institute for Reference Materials and Measurements of the European Commission's Joint Research Centre. Dilution of this serum was performed with 10 mM PBS pH 7.4 to generate samples containing 100, 500, 1000 and 10,000 fg/ml CRP.

CRP depleted serum was also used for the experiments focused on the PCT aptasensor. The sensor was challenged with various dilutions (1:2, 1:10, 1:20, 1:100) of the serum to observe potential changes in impedance. The aptasensor was then challenged with serum spiked with 10, 50 and 100 pg/ml of PCT.

4.3   Results and Discussion

4.3.1 Evaluation of anti-CRP and anti-PCT aptamer functionality

The first and probably most crucial step of the developmental process explores the aptamer's suitability to the surface immobilisation approach and the electrochemical system in general. Literature has already shown that the CRP aptamer performs well following conjugation with biotin (52). However, this does not necessarily mean that the aptamer will perform equally well following addition of thiol functionality. A slight modification in the molecular structure might lead to unexpected interactions, different folding etc. which may be detrimental in terms of target recognition. Aptamer only SAMs were therefore developed for both CRP and PCT prior to further experimentation.

Figure 4.6 shows the response of the anti-CRP aptamer SAM monolayer. The modified electrodes (n = 3) were incubated with 1 μM of aptamer overnight at 2 – 8 °C and washed with 10 mM PBS pH 7.4 to remove non-chemisorbed molecules. The working electrodes were then dipped in 10 mM PBS pH 7.4 to determine the baseline readings before being challenged with 10, 100 and 1000 pg/ml of CRP.
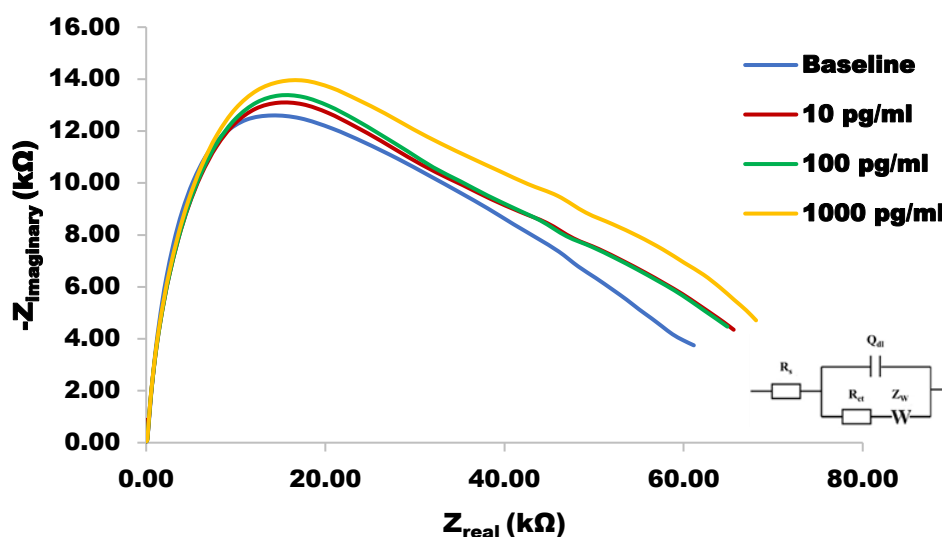
Figure 4.6: Development and characterisation of an aptamer-only SAM for CRP detection (n=3). The SAM resulted in impedances of around ~ 50 kΩ. A big increase in impedance was observed following incubation with 10 pg/ml CRP, however there was little difference between that response and the one seen when incubated with 100 pg/ml. A further increase was seen when the concentration of CRP was increased to 1,000 pg/ml.

The aptamer-only SAM produced high impedances, falling around 47 kΩ on average. Variation across repeats however was relatively high, similar to the response seen when the aptamer-only SAM was generated for the studies focused on LPS aptasensor development. Once again, this is likely due to the absence of alkanethiols, resulting in a disorganised surface layer. The high baseline impedance observed with the anti-CRP aptamer could be due to high density aptamer packing. This may also account for the inefficient recognition of the target analyte. As further work focused on improving the stability of the recognition layer and binding performance of the sensor would involve the generation of mixed aptamer-alkanethiol SAMs, it was decided to not explore this finding further unless similar data was generated in future experiments.

It is also worth noting that the Warburg effect is absent from the impedance spectra generated by the anti-CRP aptamer SAM. It appears that diffusion is rather limited due to high impedances, not allowing the observation of the Warburg impedance. This observation gives rise to finite diffusion behaviour, showing a different response from the expected pattern. This therefore reduces the fitting efficiency of the $R_s((R_{ct}W)Q_{dl})$ model. Again, it was decided to review the selection of equivalent circuit model once further optimisation of the system had been undertaken.

The aptamer was shown to be able to interact with CRP. An increase in impedance of ~4.5 kΩ was recorded following incubation with 10 pg/ml CRP, however there was no difference upon further addition of 100 pg/ml CRP (Figure 4.6). A slightly larger impedance was observed following incubation of the electrodes with 1000 pg/ml CRP, however a more significant response would have been expected; the difference in impedance between 10 and 1000 pg/ml was only ~ 3.5 kΩ, despite the 100 fold difference in concentration.

The same approach was followed for the development of the anti-PCT aptamer only SAM (n=4). The aptasensor was challenged with 10, 100 and 1000 pg/ml of PCT, with the results shown in Figure 4.7.
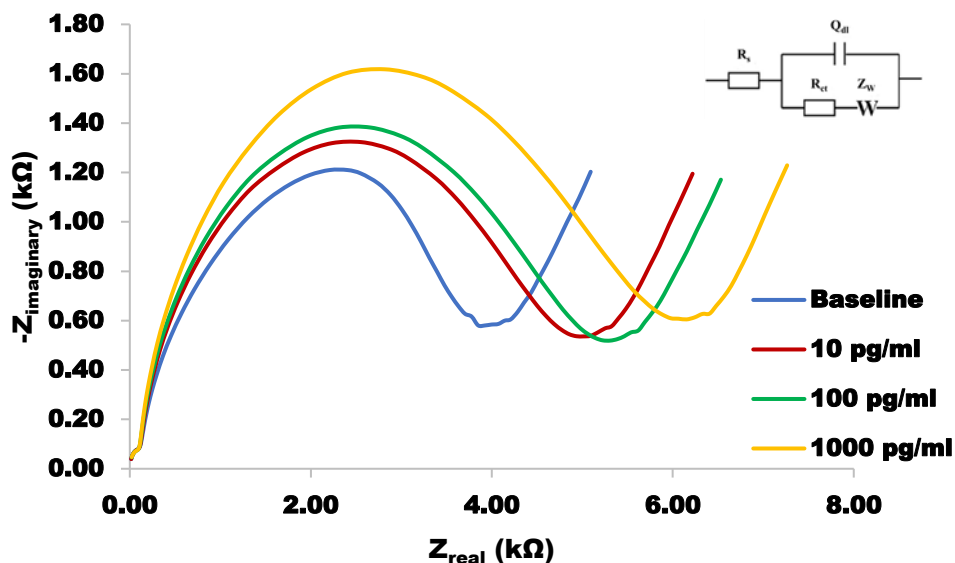
Figure 4.7: Development and characterisation of an aptamer-only SAM for PCT detection (n=4). The SAM demonstrated impedances of ~ 4 kΩ. A big increase in impedance was observed following incubation with 10 pg/ml PCT. Further increases were evident when the system was challenged with 100 pg/ml and 1,000 pg/ml PCT.

When compared to the CRP aptasensor, the anti-PCT aptamer only SAM produced relatively low impedances, more similar to the data obtained from the generation of the anti-LPS aptamer only SAM in Chapter 2 (Figure 2.7). The anti-PCT aptamer SAM produced average impedances of ~4 kΩ, however as per the other two aptasensor systems, reproducibility of these baseline readings across the replicates was less than ideal. Differences in impedance between consecutive readings of the same aptamer also suggest that perhaps the aptamer layer is not as stable as in the previous cases. Despite the relatively high noise of the system, the interaction between the aptamer and PCT was shown to be quite satisfactory; a dose-dependent response was observed across the range tested, with reasonable resolution between the impedances observed for consecutive PCT concentrations when compared to the data presented in Figures 4.6 (CRP) and 2.7 (LPS).

4.3.2 Development of the CRP-aptasensor

This section focuses on the development and optimisation of the CRP-aptasensor. As in Chapter 2, the initial studies aimed to explore selection of a suitable alkanethiol spacer molecule as well as the optimal ratio of aptamer to spacer when generating mixed SAMs. The optimised system was subsequently characterised using chroncoulometry to estimate the number of active binding sites and EIS to generate binding curves, assess specificity and evaluate the performance when challenged with clinical samples.

4.3.2.1 Screening of alkanethiols

As evidenced in Chapter 2, careful selection of an alkanethiol as a spacer molecule is necessary as they play a huge role in the overall performance of the aptasensor. In order to help narrow down the selection, it is useful to consider the physicochemical properties of the target marker of interest.

Studies have shown that CRP's isoelectric point is 6.3 ± 0.2 (95–97). More precisely, the calculated isoelectric point would be 5.3 when focusing on the molecule's primary amino acid sequence (95). Laurent and co-workers performed titration curves of CRP using electrophoretic methods (96). They demonstrated that CRP did not migrate inside the application trough within the pH range of 7.2 to 8.5, suggesting that the molecule is at its isoelectric point. In other words, the molecule would either be neutral or slightly negatively charged at physiological pH.

On the basis of this information, it was decided to screen a positively charged, negatively charged and neutral alkanethiol for interaction with CRP. The size of the alkanethiols was not considered important at this stage, as the study was focused simply on which functionality interacts to a greater or lesser extent with CRP. Keeping this in mind, SAMs comprising 6-mercaptohexanol (MCH), 4,4-dithiodibutyric acid (DTBA) and cysteamine (CYS) were developed and challenged with 10, 100 and 1000 pg/ml of CRP (n=2). The results of this screening process are presented in Figure 4.8.
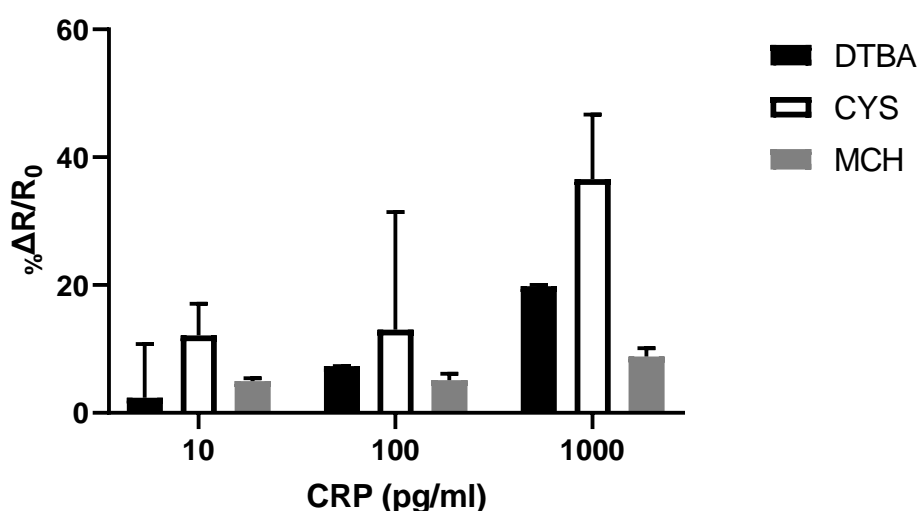
Figure 4.8: Alkanethiol SAMs were generated and challenged with 10, 100 and 1000 pg/ml of CRP (n=2). CRP appears to interact excessively with CYS, as a 40% increase in impedance was observed after incubation with 1 ng/ml CRP. DTBA and MCH SAMs displayed similar behaviours when challenged with 10 and 100 pg/ml, with ΔRs not exceeding 10 %. However, when challenged with 1 ng/ml CRP, the interaction with the DTBA SAM was more than double that seen with the MCH modified electrodes.

According to the generated data, CYS appears to be the least appropriate alkanethiol. CYS SAMs were associated with extremely low impedances (~230 Ω on average) since the positive molecular charges are attracting the electron flow, making the SAM easier to permeate. It is worth noting that a bare gold surface produces impedance of ~ 250 Ω. The above observations are confirmed by the work of Tolba and co-workers (98). For this reason, CV was used to validate modification of the electrode surface (Figure 4.9). The CYS modified electrodes were expected to show increased currents, when compared to bare gold electrodes, as a consequence of the electrostatic attraction between the positively CYS amino groups and the negatively charged redox probe (99). It was also observed that the voltammogram shifts towards electropositive potentials.
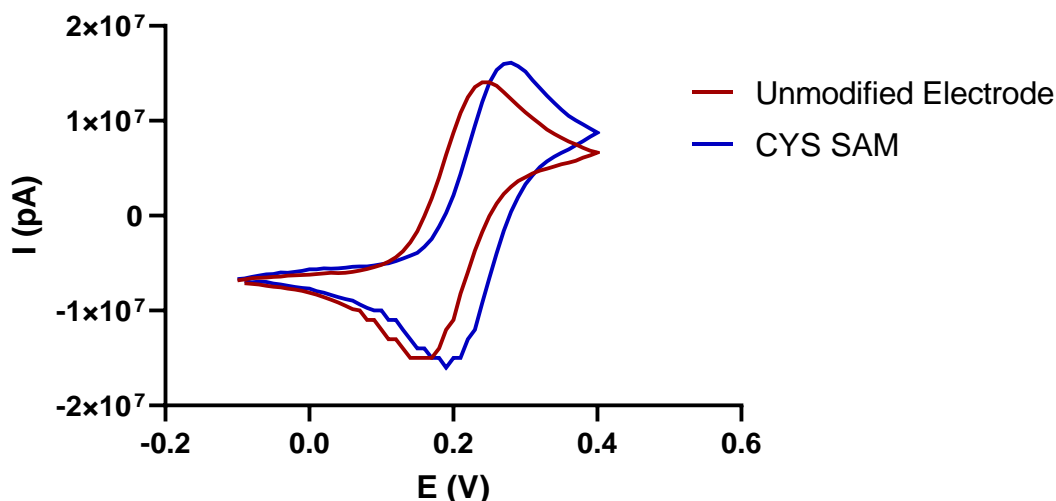
Figure 4.9: Cyclic Voltammograms obtained before and after the electrode modification with CYS. The modified electrode demonstrates an elevation in current, while the curve is shifted towards more electropositive potentials.

CYS was shown to interact excessively with CRP, with up to 40% increase in impedance recorded following incubation with 1 ng/ml CRP (Figure 4.8). Under physiological conditions, CYS will be positively charged and therefore may be electrostatically interacting with CRP. It's possible that CYS forms a rather weak SAM, potentially allowing CRP to adsorb to any regions of bare gold. For these reasons, CYS was not taken forward for further evaluation.

DTBA and MCH showed similar responses when challenged with 10 and 100 pg/ml of CRP, with all ΔR values sitting below 10 %. However, when the CRP concentration was increased to 1 ng/ml, the DTBA SAM showed an ~20 % increase in impedance, whilst the response observed with the MCH modified electrodes remained relatively low at ~9 %. It should also be noted that a clear dose-dependent response was evident for the DTBA modified electrodes, whereas MCH consistently showed low changes in impedance across all CRP concentrations tested. Consequently, MCH was selected as the alkanethiol of choice to take forward in the development of the CRP aptasensor. MCH's suitability as a blocking agent / spacer is also confirmed by the work of Jarczewska and co-workers (100).

4.3.2.2 Aptamer/MCH mixed SAMs: a screening process to investigate the best performing sensor

A screening process was undertaken to investigate the optimal ratio of anti-CRP aptamer to MCH. For the purposes of this study, various ratios of the two molecules were applied to working electrodes (Table 4.1). Three replicates of each SAM were produced and their performance when challenged with CRP evaluated.

SAM	CRP aptamer / MCH
1	1:1
2	1:3
3	1:5
4	1:10

Table 4.1: Examined ratios between aptamer and MCH to examine the best performing SAM.

Figure 4.10 shows the Nyquist plots obtained for the various SAMs. Several interesting observations are noted in the data. The MCH only SAM produces impedances of ~1.5 to 2 kΩ. When aptamer is introduced into the SAM but at a low level, as is the case of the 1:10 (aptamer: MCH), a small increase in impedance is observed. Further increasing the aptamer content to give a ratio of 1:5 (aptamer:MCH) results in a large increase in impedance (~9 kΩ), a pattern which continues with the generation of a 1:3 (aptamer:MCH) mixed SAM. However, once a ratio of 1:1 is reached the impedance was seen to fall back, sitting between that recorded for the 1:5 and 1:3 SAMs. This perhaps suggests that greater amounts of MCH are needed to form a well-organised self-assembled layer, possibly as a consequence of the lack of charge in the alkanethiol meaning that only steric effects influence aptamer immobilisation and spacing at the electrode surface.

As a result of these observations, it was decided to only challenge the 1:1, 1:3 and 1:5 mixed SAMs with CRP to evaluate their binding performance. The 1:10 SAM was not taken forward into further studies.
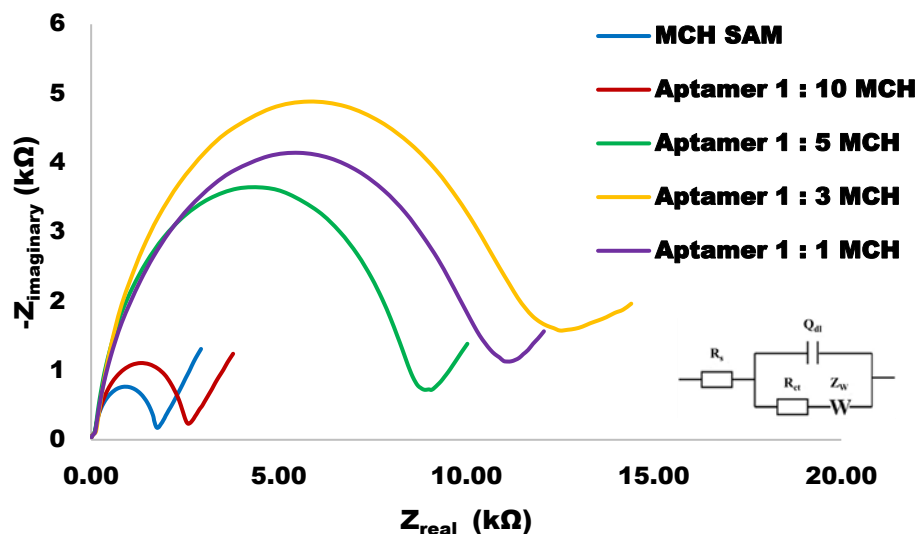
Figure 4.10: Nyquist plots obtained after the electrode modification with mixed SAMs of varying ratios (n=3). The SAM generated by the co-incubation of the CRP aptamer and MCH in ratio of 1:10 resembles an MCH-only SAM, whilst clear differences in impedances are seen with 1:1, 1:3 and 1:5 aptamer : MCH SAM systems.

Each mixed SAM aptasensor was challenged with 0.1, 0.5, 1, 5, 10, 15 and 20 pg/ml of CRP (n = 3). CRP is a lot larger molecule than LPS, since its molecular weight is approximately 120 kDa, while LPS' is around 5 kDa (101,102). It is also pentameric and so one molecule of CRP may be able to interact with more than one aptamer, depending on spacing at the surface. Consequently, when considering that all aptasensors created in this project use the same surface area for immobilisation of the aptamer, it should theoretically take fewer CRP molecules to fully saturate the available binding sites. Hence the choice of a relatively narrow concentration range in the first instance.

The screening process proved to provide important information, as both ratios 1:5 and 1:3 fail to deliver useful results (Figure 4.11). The changes in impedance when challenged with the biomarker did not correlate with the increase of concentrations, suggesting that the aptamers at the electrode surface are not able to interact sufficiently with CRP. The maximum change in impedance was a little over 1 kΩ. The random fluctuation and the high degree of variation in impedance across repeats gives the impression of non-specific binding phenomena dominating.
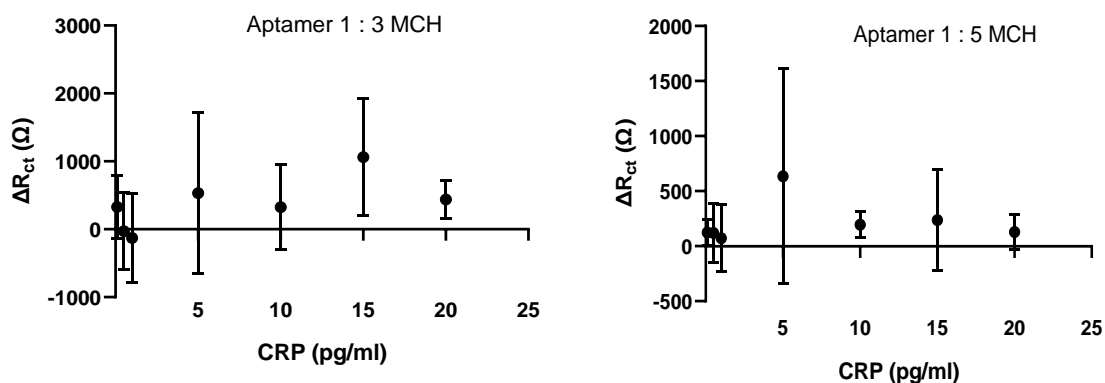
Figure 4.11: Dose-response graphs of 1:3 and 1:5 aptamer : MCH SAMs, when challenged with 0.1, 0.5, 1, 5, 10, 15 and 20 pg/ml CRP. Any increases in impedance are minimal, barely exceeding 1 kΩ, suggesting that the bound aptamers are failing to significantly interact with the target molecule.

Challenge of the 1:1 mixed SAM electrodes produced more promising results (Figure 4.12). A dose-dependent increase in impedance was observed across the concentration range tested, with good linearity between 1 and 20 pg/ml (r^2 0.998). However, the responses are somewhat shallow (maximum change ~ 2 kΩ) which, when coupled with large standard deviations, mean that some consecutive concentrations are found to not produce a significantly different response, statistically speaking (two-tailed t-test). For instance, the p value obtained following the comparison between 5 and 10 pg/ml is 0.444. The majority of the remaining comparisons are showing p values barely lower than 0.05, showing that the system is not performing well. The linear response suggests that saturation has not yet been achieved.
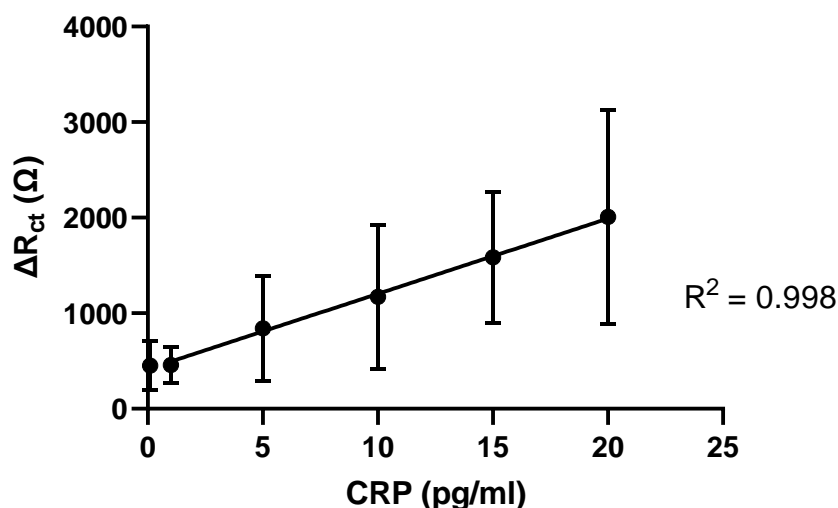
Figure 4.12: Dose-response plot of 1:1 SAM (n=3), when challenged with 0.1, 1, 5, 10, 15 and 20 pg/ml. The aptasensor displays a dose-dependent increase in impedance upon the application of varied CRP concentrations. Although good linearity is demonstrated across the range of 1 – 20 pg/ml, the shallowness of the response coupled with the high level of variability is problematic.

In order to try and increase the magnitude of response seen, an alternative approach to aptasensor development was explored. Instead of incubating the electrodes with a pre-mixed 1:1 aptamer:MCH solution, the aptamer was first allowed to assemble at the gold surface and then MCH was added to 'backfill' any gaps at the sensor surface, thus blocking any exposed regions of bare gold. This approach was used by Jarczewska *et al.* in the development of their CRP aptasensor.

When examining baseline impedances of aptasensors generated either via 1:1 co-incubation of aptamer and MCH, or via backfilling of an aptamer modified surface with MCH, little difference in response was noted (Figure 4.13). The sensors produced using the backfilling approach showed a slightly higher impedance (13.2 kΩ vs. ~11kΩ), suggesting perhaps a higher density of aptamers, or more complete coverage of the electrode surface.
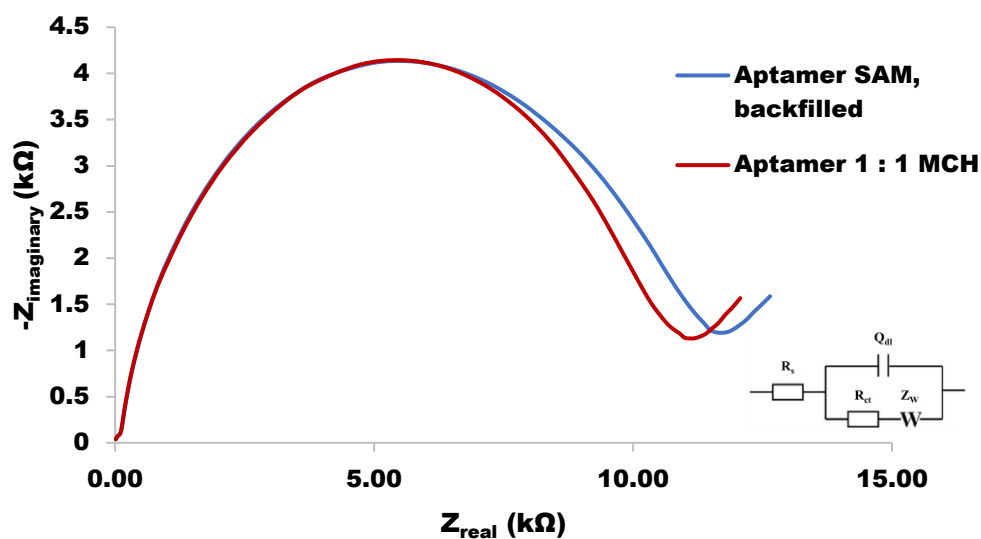
Figure 4.13: Nyquist plot obtained following the development of aptasensors using either co-incubation of 1:1 aptamer:MCH or the backfilling of an aptamer SAM with MCH (n=3). The two aptasensors displayed similar impedances. The slightly higher impedance obtained using the backfilling approach suggests either a higher number of aptamers bound on the area, or a more complete coverage of the electrode surface.

The backfilled aptasensor was then challenged with 1, 5 and 10 pg/ml of CRP to observe potential changes in impedance (n=3) (Figure 4.14). The changes in impedance are higher when compared to those of Figure 4.12 (e.g. 2 kΩ for 1 pg/ml cf. ~ 500 Ω), suggesting that the functionality has been improved. However, it seems that these concentrations are closing in on the maximum binding capacity of the sensor as there is no difference between the response observed with 5 and 10 pg/ml. Lower CRP concentrations need to be applied to the system to further determine its dynamic range.
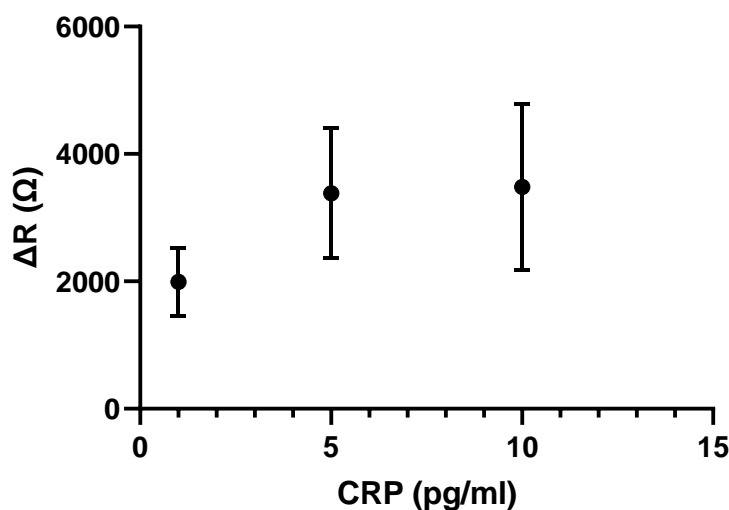
Figure 4.14: The CRP aptasensor was challenged with 1, 5 and 10 pg/ml of CRP (n=3). The changes of impedance are higher when compared to those of 1:1 aptamer/MCH mixed SAM (Figure 4.12), however it appears the response has saturated between 5 and 10 pg/ml.

4.3.2.3 CRP sensor characterisation

As per the previous chapters, the aptasensor was characterised using chronocoulometry to estimate the number of aptamers available on the electrode surface, and electrochemical impedance spectroscopy to evaluate binding kinetics, specificity and performance in clinical sample matrices.

4.3.2.3.1 CRP sensor characterisation: Stability and sensitivity

The first stage of the sensor characterisation is to explore and confirm the stability of the aptasensor and its response to challenges with CRP. Despite the aptamer only SAMs showing high impedances of 47 kΩ, as described in section 4.3.1. (Figure 4.6), the co-incubation with MCH provided lower impedances, which never exceeded 15 kΩ (Figures 4.10 and 4.13). Furthermore, the aptamer only SAM Nyquist plot was devoid of any features indicative of the Warburg effect; this effect was evident for all other SAMs generated in the ratio screening experiments.

The system's stability was not as good as in the case of the LPS aptasensor. It is likely that the formation of an aptamer-only SAM which is then backfilled with MCH, is

contributing to this. When the aptamer-only SAM is generated, some of the aptamers will lie on the surface in a non-canonical position, as depicted in Figure 2.6. The SAM is then washed to remove non-chemisorbed aptamers before being incubated with MCH. Despite the backfill, there potentially could still be bare areas of gold or aptamers changing their co-ordination between horizontal and vertical positions (and vice versa) through time, affecting the electron flow.

The relatively high variance between consecutive readings is a limiting factor for the sensing process, as the aptamer modified electrodes show an average standard deviation of 535 Ω. Considering the LOD must be greater than baseline impedance + 3 x SD, i.e. greater than ~ 1.5 kΩ, and the shallowness of the responses observed thus far, it would suggest that significant further optimisation will be needed to demonstrate a clinically useful sensor.

4.3.2.3.2 CRP sensor characterisation: Binding kinetics

In order to determine parameters such as LOD, K_d and dynamic range, the sensor was challenged with 0.1, 0.25, 0.5, 0.75, 1, 5, 10, 25 and 50 pg/ml of CRP – in other words with a range of concentrations starting from 0.83 and finishing up to 417 fM (Figure 4.15). A clear binding curve is evident, with an early rapid rise in response before plateauing out and reaching a maximum signal change between 50 and 100 pg/ml. As explained previously when analysing the data presented in Figure 4.7, the response to CRP is relatively shallow. Baseline impedances averaged 11 kΩ, however variation in response means that a change in signal of less than ~ 10% falls below the limit of detection. When the system was challenged with 0.1 pg/ml (100 fg/ml), a change in impedance equalling just over 5% was observed and as such this concentration falls below the LOD. The challenge with 0.25 pg/ml (250 fg/ml) was shown to produce a change in impedance of 9.9% and therefore this concentration is considered the LOD.
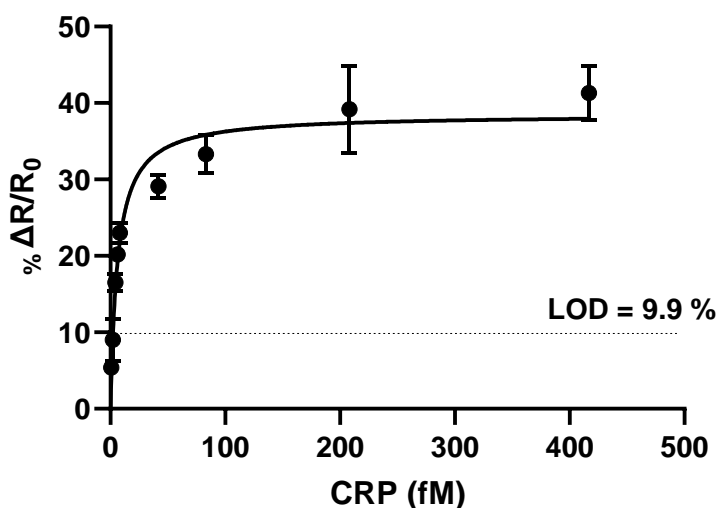
Figure 4.15: Dose-response curve of the aptasensor when challenged with 0.1, 0.25, 0.5, 0.75, 1, 5, 10, 25 and 50 pg/ml (0.83 – 417 fM) of CRP. The system's LOD is located at ~ 250 fg/ml (~2 fM), showing an apparent K_d of 6.17 fM (740 fg/ml).

As in previous Chapters, GraphPad Prism was used to further analyse the data and generate an apparent dissociation constant K_d. Using the "one site – specific binding" model, a good fit was achieved ($R^2 = 0.9357$) generating an apparent K_d of 6.17 fM (740 fg/ml). The sensor was shown to produce a linear, dose-dependent response over the range of 250 fg/ml to 1 pg/ml, with a R^2 of 0.9437 (Figure 4.16). The system's linear part can extend down to 100 fg/ml, producing better R^2 values, equalling to 0.9613, but unfortunately 100 fg/ml falls below the LOD under the present conditions.
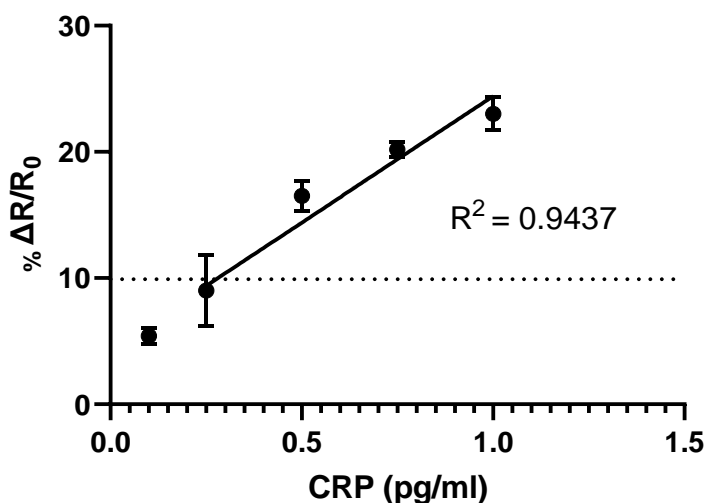
Figure 4.16: The linear part of the CRP dose-response curve spans from 250 fg/ml to 1 pg/ml, extending towards 100 fg/ml. However, the response of 100 fg/ml theoretically falls below the LOD (indicated by dotted horizonal line).

The aptasensor created in the present study shows competitive results when compared to other studies and tests from the literature. The reviews of Vashist *et al.* and Salvo *et al.* report that the vast majority of existing tests have affinities and LODs at the the micro / nano- gram/ml scale, whereas the current CRP aptasensor is able to detect concentrations in the range of fempto- / pico- gram/ml (31,44). It is preferable though to compare the system with other aptasensors. In fact, the CRP sensing field has been so extensively studied so that there are aptamers that specifically bind either the monomeric or pentameric form of the molecule (53). It is reminded that the aptamer of choice binds to the pentameric form as this is how CRP presents in clinical samples (52).

The work of Vance and Sandros has been already discussed in the introductory section. Their SPR sensor reportedly detects zeptomoles of CRP, with the LOD sitting at 5 fg/ml (43). It is possibly one of the best performing aptasensors found in the literature, with the exception of the work of Schulze *et al.* which demonstrates an aptasensor capable of detecting down to 80 ag/ml (103). Furthermore, the reported detection range of this sensor is quite wide, spanning from the LOD to 1.2 pg/ml. The system utilises the advantages of etched fiber Bragg gratings (eFBG) to generate a very sensitive optical-based aptasensor.

Wu *et al.* developed an aptamer/antibody sandwich assay, using nanoparticle-enhanced surface plasmon resonance (104). Sandwich assays have also been developed using RNA

aptamers (58,59). The study by Wu and co-workers presented three different strategies in their paper, with the best performing assay displaying a LOD of 10 pM. The sensor was challenged with diluted serum with CRP concentrations within the range of 10 pM to 100 nM.

Wu *et al.* have also demonstrated the development of an easy, label-free, fluorescent assay (105). The mechanism of detection relies on the use of Thioflavin T (ThT) – the fluorophore – conjugated to the CRP-specific aptamer. When the aptamer is not complexed to its target, the signal from ThT is strong, however that signal is quenched upon complexation with CRP. A linear response over the range 0.5 to 20 nM was reported, with a LOD of 380 pM.

Hwang *et al.* created a conjugate between an anti-CRP aptamer and human peripheral blood mononuclear cells (Apt-PBMCs) (52). The conjugation process relies on a series of modifications that take advantage of high affinities between molecules such as biotin and streptavidin. The generated system is a unique live cell-based biosensor, the mechanism of which is very smart. Lymphocytes (a type of peripheral blood mononuclear cells) possess the ability to migrate to sites of inflammation. The conjugation with aptamers will facilitate the visualisation of this *in vivo* trafficking. The quantification step relies on the binding of a CRP-specific antibody, which carries a fluorophore. The system's sensitivity is reasonable, reporting a LOD of 10 ng/ml.

Kao and co-workers created an integrated microfluidic system, using field effect transistors (FET) and aptamers (106). The aptamers were taken from the study of Hwang *et al.* with the FET based system demonstrating similar sensitivity with a reported detection range of between 625 ng/ml and 10 μg/ml.

Jarczewska and co-workers followed an approach quite similar to the one of the present study (100). They used thiolated aptamers to generate SAMs on gold surfaces. MCH was also selected as the alkanethiol of choice to cover the bare surface and prevent CRP from non-specifically binding. Their aptasensor showed a linear response over the range of 1 to 100 pM (120 pg/ml to 12 ng/ml). The study also demonstrates the efficiency of immobilisation of thiolated molecules on gold and the advantages of MCH over other blocking molecules.

Zhang and co-workers used the same oligonucleotide sequence as the study of Jarczewska *et al.* (107). Their experiment differs from Wu's study as they develop a 2D-porphrinic covalent organic framework-based aptasensor with enhanced photoelectrochemical response. The system's reproducibility was satisfactory, with a linear range is between 0.5 – 100 ng/ml, while the LOD was reported to be 0.1 ng/ml.

Finally, Zubiate *et al.* and Yang *et al.* used the same aptamer to develop their detection systems (108,109). Sorting the two studies in chronological order, Yang, Lin and co-workers developed a system using microfluidics. The system's LOD was reported to be 12.5 ng/ml. On the other hand, Zubiate and co-workers utilised the technology of lossy mode resonance based optical fiber devices. They report high reproducibility in results that demonstrate an apparent LOD of 62.5 ng/ml.

Table 4.2 summarises the different studies and contributes in the section's final conclusions.

Aptasensor Technology	Detection Range	LOD	Reference
SPR	-	5 fg/ml	43
Optical, etched fiber Bragg gratings	80 ag/ml – 1.2 pg/ml	80 ag/ml	100
SPR, aptamer/antibody	1.2 ng/ml – 12 µg/ml	1.2 ng/ml	101
Fluorescent	60 ng/ml – 2.4 µg/ml	45.6 ng/ml	102
Lymphocyte conjugate, fluorescence *	-	10 ng/ml	50
FET *	625 ng/ml - 10 µg/ml	-	103
Electrochemical	120 pg/ml - 12 ng/ml	-	97
Photoelectrochemical	0.5 – 100 ng/ml	0.1 ng/ml	104
Microfluidics	-	12.5 ng/ml	105
Optical, lossy mode resonance	-	62.5 ng/ml	106
Electrochemical	250 fg/ml – 1 pg/ml	250 fg/ml	Present study

* Studies using the same aptamer with the present study

Table 4.2: DNA aptasensors, their technology, detection range and LOD.

The aptasensor developed in the present study shows good sensitivity, with its LOD of 250 fg/ml (~2 fM) putting it in third place behind the works of Vance and Schulze. The

present study showed greater sensitivity when compared to the other electrochemical sensor, developed by Jarczewska *et al.* who report a detection range of 120 pg/ml – 12 ng/ml.

On the other hand, the current aptasensor shows one of the narrowest detection ranges. Similar issues are presented by another three aptasensors, however they display a range which spans one more order of magnitude than the sensor described herein (37, 41, 42).

4.3.2.3.3 CRP sensor characterisation: Chronocoulometric data

Chronocoulometric experiments were used to provide an estimate of the number of aptamers bound to the electrode surface. Following the same experimental process as described in previous chapters, the aptamer modified electrode, as developed and described in the preceding sections was estimated to display 6.63×10^9 molecules. This would mean that the SAM would be saturated by 27.5 ng of CRP. However, limitations such as steric hindrance and the pentameric nature of CRP meaning that it is able to interact with more than one aptamer, is likely to reduce the amount of CRP needed to fully cover all available sites.

A similar observation can be referred from the work of Jarczewska *et al* (100). They state that their aptasensor achieved a surface density of 4.55 pmol / cm^2. Considering that they also use gold disc electrodes, the calculations lead to the conclusion that 35.8 μg of CRP would be needed to completely saturate the available binding sites. However, the magnitude of their detection range is a lot lower, between 120 pg/ml - 12 ng/ml, showcasing a similar dichotomy to the present study.

4.3.2.3.4 CRP sensor characterisation: Spiked serum studies

As discussed previously, sensors often perform well when challenged with their target analytes in simple buffers however moving to a clinical sample such as serum often results in more significant 'background noise' in the system and dampened responses as a consequence of protein biofouling at the sensor surface. CRP-depleted serum (< 20 ng/ml CRP) is commercially available and so, given the differences in response between HSA and serum challenge in Chapter 3, it was decided to go straight to testing in serum.

Even the depleted serum contains relatively high amounts of CRP. Concentrations in healthy human serum would normally sit around 1 μg/ml, therefore depleting to the level of < 20 ng/ml would fall below the LOD of all commercially available assays (110). The sensitivity of the current aptasensor meant that the CRP-depleted serum would need to be diluted. The system was challenged with 1/10 and 1/100 dilution and the changes in impedance recorded (n=3) (Table 4.3).

CRP-depleted serum dilution	% $\Delta R / R_0$ (st. dev.)
1:10	42.0 (28.6)
1:100	10.2 (0.8)

Table 4.3: Responses of the CRP aptasensor when incubated with diluted CRP-depleted serum (n=3). The 1:10 dilution shows an increase in impedance of 42 %, with high degree of variability across the three repeats. On the other hand, the 1:100 dilution shows a limited increase with better standard deviation.

When challenged with 1/10 diluted serum, ΔR values were shown to be high (42 %) and were accompanied by equally high variation (standard deviation of 28.6 %). On the other hand, responses obtained after the incubation with 1/100 dilution shows improved results, with an increase in impedance of 10.2 % and much smaller degree of variation across the three repeats (0.8 %).

The results are similar to those described in Chapter 3 when the apta-MIP was challenged with various concentrations of HSA. However, the presence of CRP in the serum further complicates matters in the current studies. The actual concentration of CRP in the depleted serum is not known (a threshold value is simply provided), and therefore it's not possible to know whether the responses observed are due to the presence of CRP or because serum components are non-specifically interacting with the sensor. In order to be able to use CRP-depleted serum, more substantial dilutions would be needed; 1/100,000 would bring the concentration down to 0.2 pg/ml, sitting just below the LOD of the aptasensor.

The Institute for Reference Materials and Measurements of the European Comission's Joint Research Centre provides human serum with certified values of CRP. The certificate

of analysis denotes that the human serum used in the present study contained 41.2 ± 2.5 μg/ml of CRP. CRP was determined by immmunonephelometry and immunoturbidimetry, using EU certified calibrants.

Dilution of this serum was performed to generate samples containing 100, 500, 1000 and 10,000 fg/ml CRP. The results of the challenge of the aptasensors (n = 3) using these samples is presented in Table 4.4.

CRP (fg/ml)	Expected $_{\%}\Delta R/R_0$ (%)	Achieved $_{\%}\Delta R/R_0$ (%)	Recovery (%)	CV (%)
100	5.4	7.7	142.6	73.0
500	16.5	12.5	75.8	26.4
1000	23.0	13.1	57.0	8.2
10000	33.3	21.6	64.9	24.7

Table 4.4: Responses of the CRP aptasensor when incubated with known CRP concentrations (n=3). The extremely high CV values are highlighting the inability of the aptasensor to produce consistent results.

Although the aptasensor response is similar to that expected when incubated with 100 fg/ml, the % CV is huge (Table 4.4). It is the relatively small change in impedance (the shallowness of the response as described previously) at this concentration which results in such large deviations and high % recovery. The CV values improve upon the challenge with the higher concentrations, however they all still fail to reach the desired value of 5%. The recovery of the higher concentrations also fall below that expected, varying from 57 % to 76%.

It is worth noting that the EU standard was used roughly a year after its purchase, which is towards the maximum suggested period of handling. Even though every care was taken when preparing the samples, using a minimum of 20 μL of the standard for each experimental process, there's a chance that CRP concentration has depleted over time. Furthermore, the amount of dilution needed to drop down from 41.2 μg/ml to the fempto / picogram scale is enormous. Multiple dilution steps were required, potentially confounding any systematic analytical error.

Some of the previously discussed studies have challenged their aptasensors with spiked serum. Unlike the present study, they display a solid performance, generating reproducible results. For instance, the aptasensor of Zhang and co-workers shows CV values of less than 5 % and an average recovery of 100.4 % (107). Yang *et al.* even compared their system's performance with the Roche's autoanalyser E170, showing encouraging results (108). The aptasensor developed in this current study needs more development to improve stability / decrease noise to allow the sensitive detection of CRP from clinical samples.

4.3.3. Development of a PCT-aptasensor

The second part of this results and discussion section focuses on the development of the PCT-aptasensor. The rationale behind the PCT-aptasensor development follows the approaches used for the development of the LPS and CRP sensors. Unlike the other systems, there's nothing in the literature regarding the utilisation of the PCT aptamer, thus this section will just examine the results of the developmental process, with comparison to alternative detection methodologies when appropriate.

4.3.3.1 Screening of alkanethiols

The strategy of selecting an appropriate alkanethiol for incorporation into the SAM of the aptasensor has been extensively examined in the previous sections. Therefore, this section will jump to focus directly on the screening process.

Studies have reported the isoelectric points of N-procalcitonin fragment (3.98) and calcitonin (8.86 in non-mammalian species), however PCT's pI remains formally unknown (111,112). PCT distributors such as MyBioSource (USA) and Cloud-Clone (CCC, USA) indicate that its predicted pI is 6.5 and 5.7 respectively, bringing it quite close to the value reported for CRP (113,114).

As in previous cases, mixed SAMs were produced in triplicate using DTBA, MCH and CYS. Figure 4.17 shows the interaction of the generated SAMs with 10, 100 and 1000 pg/ml of PCT.
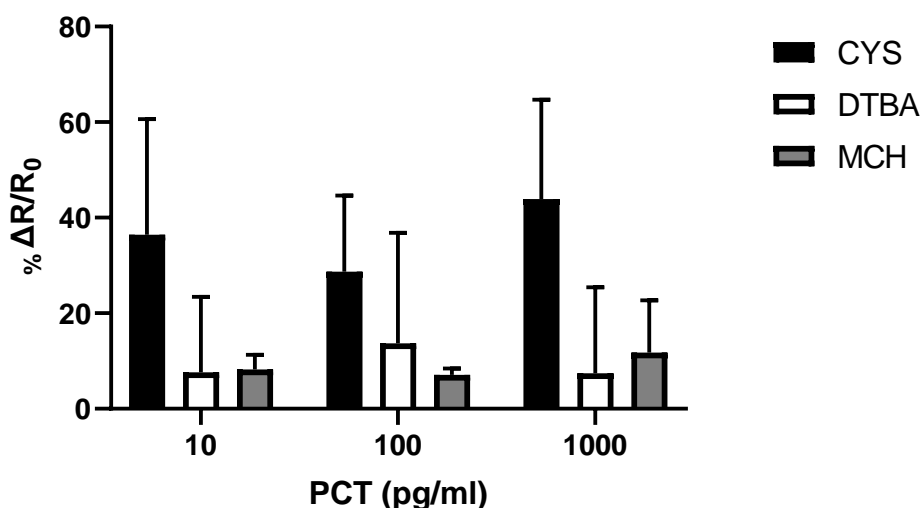
Figure 4.17: CYS, DTBA and MCH SAMs were incubated with 10, 100 and 1000 pg/ml of PCT to assess the degree of interaction. CYS shows the greatest binding across all concentrations, with DTBA and MCH performing similarly.

Despite the recruitment of all possible approaches to co-incubate the aptamer with any of the alkanethiols, the outcome was always either negative or resulted in the development of an alkanethiol-only SAM. However, the successful development of the aptamer-only SAM was shown in 4.3.1 and therefore it was decided to adopt the same approach as for the CRP aptasensor – create an aptamer-only SAM and then backfill with MCH since MCH is the only alkanethiol shown to have minimal interaction with both the PCT aptamer and the antigen itself.

4.3.3.2 PCT Aptamer/MCH SAMs: a screening process, sensor stability and sensitivity

The aptasensor characterisation begins as usual with the examination of the system's stability and determination of LOD. The aptasensor in its final form recorded an average impedance of 7,109 Ω. The SAM showed an impressive standard deviation of only 224 Ω, (CV 3.1%), meaning that any change of more than ~ 670 Ω (9%) will be considered to be above the LOD of the system.

It is worth noting that the impedance recorded from the PCT aptasensor was significantly lower than the CRP (13.2 kΩ) and LPS (31.3 kΩ) sensors, despite the lengths of all three

aptamers reportedly being quite similar (LPS: 86 nucleotides, CRP: 72 nucleotides and PCT: 70 nucleotides). This could mean that less PCT aptamers are bound to the surface of the electrode. This will be explored further during the chronocoulometry studies.

4.3.3.3 PCT sensor characterisation: binding kinetics

The promising stability and reproducibility of the backfilled aptamer SAM lead the process to the next level, to determine the sensor's sensitivity. The experience obtained from the development of both CRP and LPS aptasensors helped to guide the range of concentrations used for the binding study with PCT. PCT has a molecular weight of 14.5 kDa and is monomeric in nature (115). Therefore, from a binding capacity perspective, this makes it more similar to LPS than CRP, although it is recognised that ultimate binding performance is a function of the aptamer's affinity for its target. Consequently, the aptasensor was challenged with concentrations spanning 1 pg/ml to 250 pg/ml (0.7 – 17 pM) (n = 3). The results are shown in Figure 4.18.
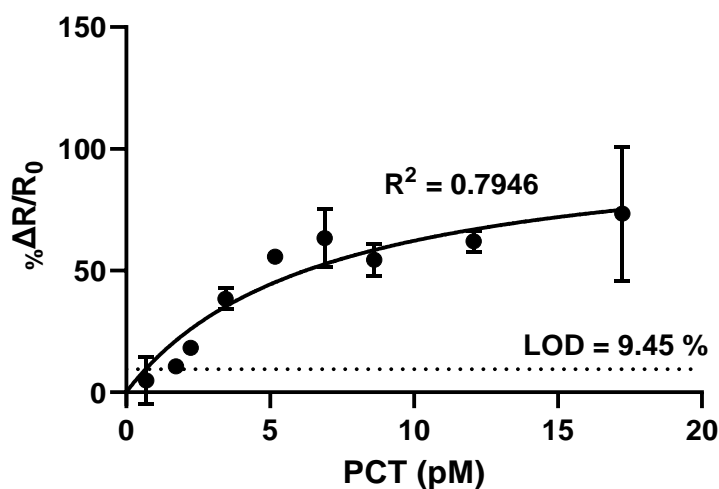
Figure 4.18: Dose-response curve of the PCT aptasensor when challenged with concentrations from 10 to 250 pg/ml (0.7 – 17 pM). According to the system's noise, LOD is equal to 25 pg/ml (1.7 pM). The linear range falls between 25 and 100 pg/ml. The system's response becomes saturated after the application of 100 pg/ml.

Using GraphPad Prism, the data was fitted to a "one-site, specific binding" (Langmuir) model as per the previous aptasensors. The fit in this case is not as good as the CRP / LPS

based systems, with an R^2 of 0.7946. The reason for this bad fit is quite obvious since the curve is not a 'curve' per se, more like two interconnecting straight lines that intersect at 100 fg/ml. Consequently, data extracted from this fit (e.g. K_d) is of poor quality / low confidence. A B_{max} value (which in turn influences the calculation of K_d) equivalent to a change in impedance of 104.6 % was estimated. However, it is evident from Figure 4.13, that the maximum response would sit much lower than that – all concentrations between 100 and 250 pg/ml resulted in responses of between 63 and 73 %. Although the spread of data for 250 pg/ml incubation is high, even on increasing the number of repeats for this particular concentration, all responses were found to fall around 70%. This over estimation of maximum response, results in a K_d of 6.82pM (98.85 pg/ml), which is unrealistic given this is the top end of the linear range. Significantly more development is needed before this aptasensor could be used with any confidence. Given the paucity of literature reports using aptamers to target PCT perhaps suggest that it is not an appropriate target for such sensing, however given the number of antibody-based tests available it is not obvious why this would be the case.

Figure 4.19 shows that the linear range of the sensor is extremely limited, spanning only 25 to 100 pg/ml. The incubation with 1 pg/ml PCT showed insignificant changes against the SAM baseline and for this reason, this data is excluded from Figure 4.19. The lowest concentration presented on the plot is 10 pg/ml, however this falls below the LOD established in the previous section, with a recorded change in impedance of 4.8 % and high variation across the replicate electrodes (9.8 %). The system's LOD was shown to be 25 pg/ml, as the observed ΔR values equal to 10.6 %, with a satisfactory standard deviation of 2.2 %.

The linearity of the aptasensor response is satisfactory ($R^2 = 0.9495$); it improves further by adding the response corresponding to 10 pg/ml ($R^2 = 0.9643$). Considering normal PCT levels would generally be at / below 50 pg/ml and that 2 ng/ml is the clinical cut off for indicating a high probability of systemic bacterial infection / sepsis, the top end of this range is unlikely to present a problem. Serum samples would need to be diluted prior to analysis to minimise non-specific effects arising from other matrix components and 1/100 dilution would still just about fall in the linear range of the sensor. The LOD however needs to be improved to allow definitive provision of 'healthy' results as 1/100 dilution

of a sample containing 50 pg/ml would mean an LOD of 0.5 pg/ml (or less) would be required.
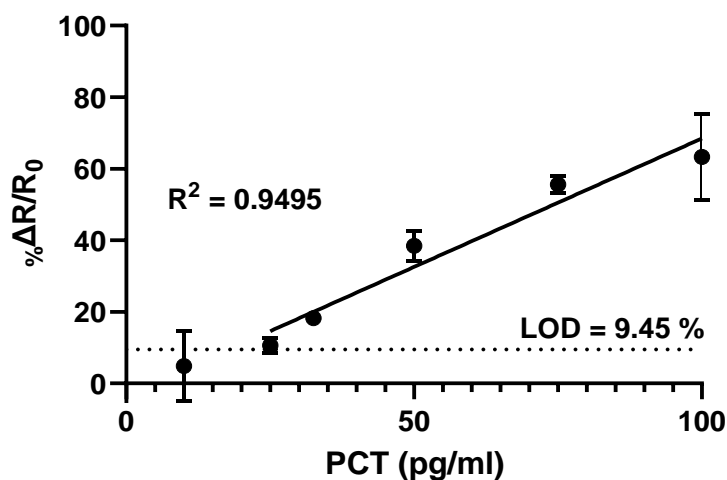
Figure 4.19: Dose-response curve of the PCT aptasensor when challenged with concentrations from 10 to 100pg/ml. According to the system's noise, LOD is equal to 25 pg/ml. Reasonable linearity across the concentration range tested is demonstrated.

4.3.3.4 PCT sensor characterisation: chronocoulometric data

As in previous Chapters, chronocoulometry has been used to estimate the number of aptamers bound to the electrode surface. It was hoped that such analysis may have shed some light on the limited detection range observed with the PCT aptasensor (assuming a 1:1 stoichiometric ration between aptamer and target).

Analysis suggest that the gold surface of the electrodes display 1.31×10^{10} molecules, which would mean that ~ 280 pg of PCT would be sufficient to fully saturate the aptasensor. This supports the binding data presented in Figure 4.13; given that occupancy is influenced by a number of factors such as the interaction between two surfaces (buffer / SAM), time of incubation, steric hindrance brought about by other interactions etc, then a observing a maximum response at ~ 100 pg/ml makes sense.

As stated previously, more work needs to be undertaken to decrease the LOD of the system. Due to time constraints, it was not possible to achieve such improvements within this project.

4.3.3.5 PCT sensor characterisation: recovery from spiked sera

Despite the demonstrated drawbacks and limitations, the aptasensor was tested with a number of serum samples. The system was first challenged with a series of dilutions of CRP depleted serum (n = 3, Table 4.5) with subsequent testing of samples spiked with PCT concentrations sitting within the linear range of the system (n = 3, Table 4.6).

A limited response was observed following incubation with diluted serum (Table 4.5). More precisely, the recorded elevation in impedances did not exceed 1.2 %, even when challenged with 50 % diluted serum. This suggests that a broad range of dilution steps could be used when testing clinical samples. The degree of variability in response across replicates decreases as the dilution increases, however all CV values are below 10%.

Dilution	Achieved $\%\Delta R/R_0$ (%)	SD (%)
1/2	0.3	9.8
1/10	- 0.5	2.2
1/20	1.2	3.5
1/100	1.2	2

Table 4.5: Responses of the PCT aptasensor following incubation with diluted human serum. Limited changes in impedance were observed across all samples tested.

The aptasensor was challenged with low (10pg/ml), mid (50 pg/ml) and high concentration (100 pg/ml) PCT serum samples. Taking into consideration the clinical PCT threshold for sepsis diagnosis / management (0.5 ng/ml < PCT levels < 2 ng/ml), it was decided that all final concentrations will comprise a 10-fold dilution of the spiked serum. Apart from the fact that the corresponding blank demonstrated encouraging results, the lower limit of the PCT clinical level is located exactly in the middle of the linear range of the aptasensor following such dilution.

Table 4.6 shows that all the responses are characterised by higher variances than were seen with the blank serum samples, showing similarities to the data presented from both the CRP aptasensor and LPS apta-MIP. The recoveries of both 10 and 100 pg/ml are

nowhere near the expected responses. When considering the response to the 10 pg/ml sample, an apparent recovery of ~265 % was observed. Whilst residual PCT in the serum may be considered a possibility, the fact that this was not evident in the blank serum study makes this very unlikely. On the contrary, the response after the incubation with 100 pg/ml shows a recovery of just 28.6 %. Good recovery was observed for the spike concentration falling in the middle of the linear range (50 pg/ml, ~88 %). This sample also showed the least amount of variance across the three repeats. With no other PCT aptasensor studies to compare to, the reasons behind the poor performance observed with the aptasensor are unclear at this stage.

PCT (pg/ml)	Expected $\%\Delta R/R_0$ (%)	Achieved $\%\Delta R/R_0$ (%)	Recovery (%)	CV (%)
10	4.8	12.6	265.6	21.03
50	38.4	33.9	88.2	13.55
100	63.3	18.1	28.6	28.36

Table 4.6: Responses of the PCT aptasensor when incubated with known PCT concentrations spiked in 1/10 diluted human serum (n=3). The high CV highlight the aptasensor's inability to produce consistent results. It is worth noting that the aptasensor showed a recovery of 88.2 % when incubated with 50 pg/ml.

4.3.4. Specificity studies

The characterisation studies are once again unified for the two sensors described in this chapter. The ultimate objective of the project was to create three individual sensors, that could be combined in one multiplex diagnostic platform. It is therefore important to show that each sensing system is not adversely affected by the other target analytes.

Starting with the CRP aptasensor, selection of appropriate cross-reactants in terms of proteins displaying high homology with CRP is difficult. CRP is a pentraxin, meaning that there's a limited pool of molecules belonging to this family. More precisely, serum amyloid P component protein (SAP), hamster female protein (FP), PTX3 and PTX4 are the other two molecules described as pentraxins (116,117). PTX3, also known as TSG-

14 shows a homology of 57 % to CRP (118,119). On the other hand, human SAP shows a similarity of up to 51 % to human CRP (119).

A look at other studies show that the use of the aforementioned molecules is widely avoided. Wu *et al.* demonstrate selectivity studies, in which they challenge their sensors with proteins such as myoglobin, HSA, IgG, haemoglobin, and transferrin, showing minimal binding (104,105). This observation is widely expected as none of these molecules show any level of homology to CRP and aptamers have already proved to be highly selective. The work of Jarczewska *et al.* seems to approve the above approach, as apart from the expected BSA, they challenge their sensor with yet another immunoglobulin, IgE (100). On the contrary, Zubiate and co-workers decided to adopt a completely different approach, by challenging the sensor with urea and creatinine (109). Zhang *et al.* tested the system's specificity by incubating their aptasensor with solutions containing human chorionic gonadotropin (HCG), prostate specific antigen (PSA), microcystin (MC–LR) and bovine albumin (BSA) (107).

The use of all previously mentioned molecules relies on the fact that they can be found at elevated concentrations during the development of the inflammatory phenomena and their presence might compete CRP for some of the sensors' available binding sites. Keeping in mind that the options to find a homologous molecule for CRP are limited, in association with the *de facto* selectivity of the aptasensors, the present study decided to challenge the CRP aptasensor with PCT and LPS.

Figure 4.20 shows the changes in impedance when the CRP aptasensor is incubated with LPS and PCT. LPS is known to adsorb to a high variety of surfaces, however the changes in impedance are in general minimal, with the exception of the response seen following the challenge with 1 pg/ml LPS. In fact, the aptasensor displays a response when challenged with this sample that is not dissimilar to that seen with 1 pg/ml of CRP. The response however falls back to zero on application of the 100 pg/ml LPS sample. Although high dose hook effects are not uncommon in bioassays, it would seem unlikely that the response with higher concentrations would fall that significantly. It should be noted that interaction between LPS and MCH was demonstrated in Section 2.3.2.2. It is possible that this may be responsible for the interaction seen in this cross-reactivity study. Further investigation is needed

On the other hand, the CRP aptasensor was shown to not interact with PCT; all values stayed within the error of the baseline value.
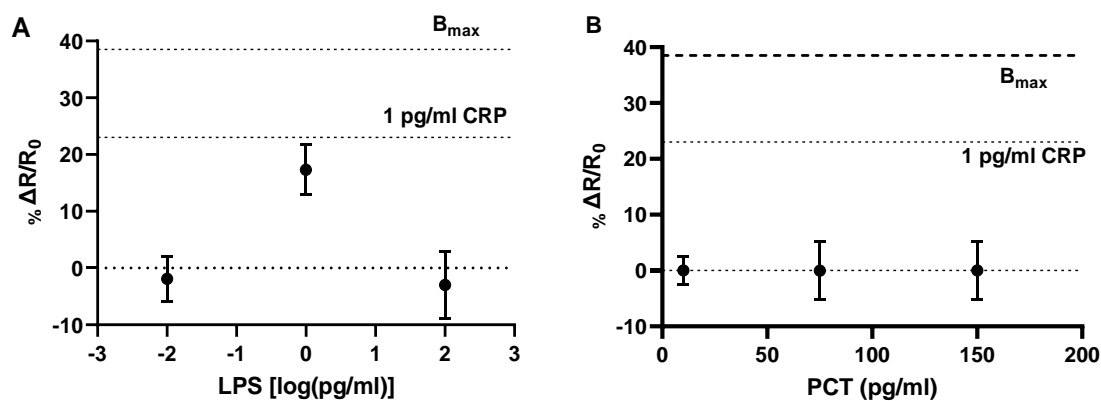
Figure 4.20: Specificity studies of the CRP aptasensor, when challenged with A) LPS (0.01, 1 and 100 pg/ml) and B) PCT (10, 75, 150 pg/ml). Both apparent B_{max} and $\%\Delta R/R_0$ corresponding to 1 pg/ml CRP (the highest point of the linear range) are indicated on the plots for reference.

Like CRP, PCT is a molecule with limited candidates to examine the specificity of the aptasensor. Apart from the components of blood serum that have already been used to challenge the sensor in the previous section, the only available molecules are the ones deriving from the CALC-1 gene; katalcin and calcitonin (63).

In keeping with the CRP specificity study, the PCT aptasensor was challenged with LPS and CRP. The results are shown in Figure 4.21.
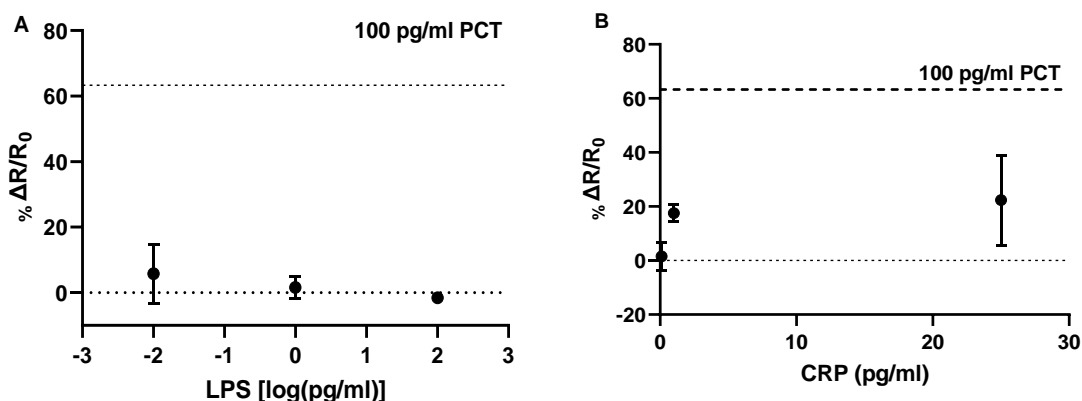
Figure 4.21: Specificity studies of the PCT aptasensor, when challenged with A) LPS (0.01, 1 and 100 pg/ml) and B) CRP (0.1, 1, 25 pg/ml). Both apparent B_{max} and the and $_{\%}\Delta R/R_0$ corresponding to 100 pg/ml PCT (the highest point of the linear range) are indicated on the plots for reference.

Unlike when the CRP aptasensor was challenged with LPS, the PCT aptasensor showed minimal response to this molecule across all concentrations tested, with a maximum average ΔR value of 5.8 % recorded following incubation with 10 fg/ml. This outcome is rather ambiguous as two electrodes recorded an approximate value of – 2 %, while the other two an average value of + 13 %, thus giving rise to the relatively high standard deviations. It does however support the suggestion that further investigation is needed with regard to the LPS interaction with the CRP aptasensor, as the aptamer-SAM of the PCT system was also backfilled using MCH, suggesting that the alkanethiol is not excessively interacting with the molecule.

On the other hand, CRP was shown to interact with the PCT aptasensor, showing significant changes in impedance following incubation with 1 and 25 pg/ml. A high degree of variance was observed for the electrodes challenged with 25 pg/ml CRP. Although perhaps such interaction could be considered 'expected' given protein interference is common in bioassays, the aptasensor performed exceptionally when incubated with serum, a biological fluid containing a wide variety of proteins. Additionally, CRP has shown minimal interaction with MCH; indeed, the molecule is also a component of the CRP aptasensor. As we have limited information on the PCT aptamer, as it was sourced commercially, it is difficult to know what causes this degree of cross-reactivity.

Of concern is the fact that the responses generated by 1 and 25 pg/ml CRP are significantly higher than those observed following application of PCT at the same concentration. CRP concentrations are significantly higher in serum regardless of disease state. The response following incubation with 1 pg/ml of PCT was shown to fall below the LOD (indistinguishable from baseline). The comparative response following incubation of the sensor with 25 pg/ml CRP and 25 pg/ml PCT is shown in Figure 4.22.
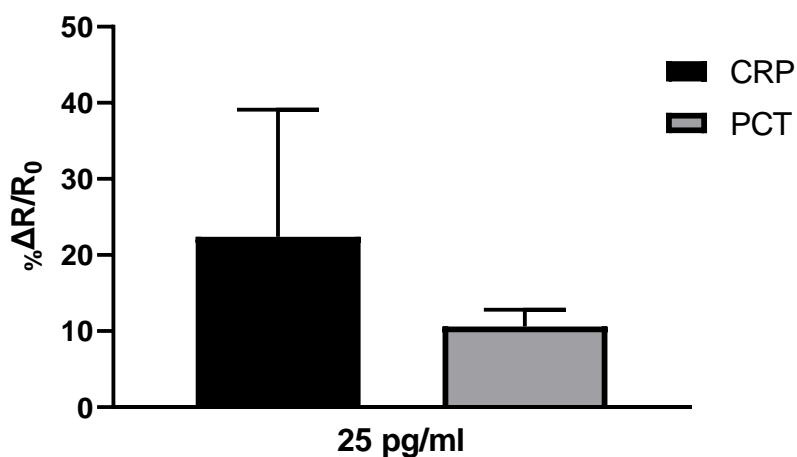
Figure 4.22: Specificity studies of the CRP aptasensor, when challenged with 25 pg/ml of CRP. The aptasensor shows ΔR values that are higher when compared to the ones generated after the incubation with 25 pg/ml of PCT, leading to biofouling.

It should be noted that this observation does not necessarily mean that the aptasensor would demonstrate similar cross-reactivity when challenged by both molecules in a competitive environment. Competitive assays would provide a more definitive answer, with regards to the true specificity of the system. Unfortunately, the experimental approach employed coupled with time restrictions meant that performing such an assay was not possible in this project.

4.4   Conclusions

The final Chapter of the present study described the development of two sensors able to detect biomarkers that have been routinely used for the detection of inflammation and monitoring of septic responses in clinical settings. Both sensors relied on the same approach i.e. immobilising the target specific aptamer on the electrode and blocking the remaining surface with MCH. The results obtained from both aptasensors are rather mixed, as the Chapter failed to deliver the results of the same level as Chapters 2 and 3.

Starting with CRP, the aptamer showed unconvincing results when co-immobilised with MCH, to develop mixed SAMs. Despite the change in strategy, by creating an aptamer – only SAM and then backfilling with MCH, the resulting system showed high levels of variance, making the baseline quite noisy. Consequently, the LOD of the system was determined as ~ 250 fg/ml. The linear detection range was shown to be quite narrow when compared to other studies. Still, the aptasensor is competitive since very few studies were able to reach the fempto scale during the characterisation of binding kinetics. The selectivity of the aptasensor was satisfactory however, the system's behaviour when challenged with spiked sera fell surprisingly short of expectations. Further work is needed to realise the true potential of this aptasensor.

The outcome for PCT was also mixed. The PCT aptamer employed in the present study is the sole oligonucleotide sequence claiming to interact with the biomarker of interest, with other reported sensing systems relying primarily on antibody-based recognition. The results obtained from the present study bring into questions its functionality. It was not possible to co-immobilise any of the alkanethiols alongside the aptamer, and so the same approach as for the CRP aptasensor, i.e. using MCH to backfill following immobilisation of the thiolated aptamer, was adopted. The resulting aptasensor demonstrated poor stability, with noisy signals, producing a binding isotherm which showed a poor fit when analysed using the traditional Langmuir model. Despite the issues, an LOD of 10 pg/ml was observed and so it is possible with a better understanding of the aptamer that further optimisation could be undertaken to generate a clinically useful sensing system for PCT.

Considering the results received from both aptasensors, it is evident that there is no need to develop MIP systems for the detection of the target molecules. CRP's concentration in blood during inflammatory phenomena is big enough to be detected from aptasensors

after the application of a certain amount of dilutions. The same principal applies for the PCT aptasensor, however, the MIP strategy might imply better results in terms of stability. Nevertheless, the top priority is to establish a reproducible way to immobilise the aptamer on the gold surface.

4.5   Bibliography

1.   Póvoa P, Teixeira-Pinto AM, Carneiro AH. C-reactive protein, an early marker of community-acquired sepsis resolution: a multi-center prospective observational study. Crit Care [Internet]. 2011 [cited 2017 Nov 23];15(4):R169. Available from: https://www.ncbi.nlm.nih.gov/pmc/articles/PMC3387609/

2.   Schmit X, Vincent JL. The Time Course of Blood C-reactive Protein Concentrations in Relation to the Response to Initial Antimicrobial Therapy in Patients with Sepsis. Infection [Internet]. 2008 Jun 10 [cited 2017 Nov 23];36(3):213–9. Available from: http://link.springer.com/10.1007/s15010-007-7077-9

3.   Procalcitonin (PCT) [Internet]. [cited 2020 Apr 16]. Available from: https://www.gloshospitals.nhs.uk/our-services/services-we-offer/pathology/tests-and-investigations/procalcitonin-pct/

4.   CEP10036 - Economic report: Procalcitonin to differentiate bacterial lower respiratory tract infections from non-bacterial causes. 2010.

5.   Nargis W, Ibrahim M, Ahamed BU. Procalcitonin versus C-reactive protein: Usefulness as biomarker of sepsis in ICU patient. Int J Crit Illn Inj Sci [Internet]. 2014 Jul [cited 2017 Nov 27];4(3):195–9. Available from: http://www.ncbi.nlm.nih.gov/pubmed/25337480

6.   Zhang J, Zhang W, Guo J, Wang J, Zhang Y. Electrochemical detection of C-reactive protein using Copper nanoparticles and hybridization chain reaction amplifying signal. Anal Biochem [Internet]. 2017 Dec 15 [cited 2017 Nov 27];539:1–7. Available from: http://www.sciencedirect.com/science/article/pii/S0003269717303834?via%3Dihub

7.   Dong Q, Wright JR. Expression of C-reactive protein by alveolar macrophages. J Immunol [Internet]. 1996 Jun 15 [cited 2017 Nov 30];156(12):4815–20. Available from: http://www.ncbi.nlm.nih.gov/pubmed/8648129

8.   Tillett WS, Francis T. Serological reactions in pneumonia with a nonprotein somatic fraction of pneumococcus. J Exp Med. 1930 Oct 1;52(4):561–71.

9.   Abernethy TJ, Avery OT. The occurrence during acute infections of a protein not normally present in the blood : i. Distribution of the reactive protein in patients' sera and the effect of calcium on the flocculation reaction with c polysaccharide of pneumococcus. J Exp Med [Internet]. 1941 Jan 31 [cited 2017 Nov 27];73(2):173–82. Available from: http://www.ncbi.nlm.nih.gov/pubmed/19871070

10.   Macleod CM, Avery OT. The occurrence during acute infections of a protein not normally present in the blood : ii. Isolation and properties of the reactive protein. J Exp Med [Internet]. 1941 Jan 31 [cited 2017 Nov 27];73(2):183–90. Available from: http://www.ncbi.nlm.nih.gov/pubmed/19871071

11.   Kolb-Bachofen V. A Review on the Biological Properties of C-Reactive Protein. Immunobiology [Internet]. 1991 Sep 1 [cited 2017 Nov 27];183(1–2):133–45. Available from: http://www.sciencedirect.com/science/article/pii/S0171298511801932

12.   Gewurz H, Mold C, Siegel J, Fiedel B. C-reactive protein and the acute phase response. Adv Intern Med [Internet]. 1982 [cited 2017 Nov 27];27:345–72. Available from: http://www.ncbi.nlm.nih.gov/pubmed/7041546

13.   Ballou SP, Kushner I. C-reactive protein and the acute phase response. Adv Intern Med [Internet]. 1992 [cited 2017 Nov 27];37:313–36. Available from: http://www.ncbi.nlm.nih.gov/pubmed/1558000

14.   Clyne B, Olshaker JS. The C-reactive protein. J Emerg Med [Internet]. 1999 Nov 1 [cited 2017 Nov 27];17(6):1019–25. Available from: http://www.sciencedirect.com/science/article/pii/S0736467999001353?via%3Dihub

15.   Lu J, Marnell LL, Marjon KD, Mold C, Du Clos TW, Sun PD. Structural recognition and functional activation of FcγR by innate pentraxins. Nature [Internet]. 2008 Dec 18 [cited 2017 Nov 30];456(7224):989–92. Available from: http://www.nature.com/doifinder/10.1038/nature07468

16.   Volanakis J. Human C-reactive protein: expression, structure, and function. Mol Immunol [Internet]. 2001 Aug 1 [cited 2017 Nov 27];38(2–3):189–97. Available from:

http://www.sciencedirect.com/science/article/pii/S0161589001000426?via%3Dih
ub

17.   Woo P, Korenbergs JR, Whiteheads AS. THE JOURNAL OF BIOLOGICAL
        CHEMISTRY Characterization of Genomic and Complementary DNA Sequence
        of Human C-reactive Protein, and Comparison with the Cornpiementary DNA
        Sequence of Serum Amyloid P Component*. 1985 [cited 2017 Nov
        30];260(24):13384–8. Available from:
        http://www.jbc.org/content/260/24/13384.full.pdf

18.   Shrive AK, Cheetham GM, Holden D, Myles DA, Turnell WG, Volanakis JE, et
        al. Three dimensional structure of human C-reactive protein. Nat Struct Biol
        [Internet]. 1996 Apr [cited 2017 Nov 30];3(4):346–54. Available from:
        http://www.ncbi.nlm.nih.gov/pubmed/8599761

19.   Thompson D, Pepys MB, Wood SP. The physiological structure of human C-
        reactive protein and its complex with phosphocholine. [cited 2017 Nov 30];
        Available from: https://ac-els-cdn-com.abc.cardiff.ac.uk/S0969212699800239/1-
        s2.0-S0969212699800239-main.pdf?_tid=be8e6026-d608-11e7-b8dd-
        00000aab0f27&acdnat=1512072050_d13950d40a83642d859ed70c956f8b3d

20.   CRP - C-reactive protein precursor - Homo sapiens (Human) - CRP gene &
        protein [Internet]. [cited 2020 Apr 13]. Available from:
        https://www.uniprot.org/uniprot/P02741

21.   Kaplan MH, Volanakis JE. Interaction of C-reactive protein complexes with the
        complement system. I. Consumption of human complement associated with the
        reaction of C-reactive protein with pneumococcal C-polysaccharide and with the
        choline phosphatides, lecithin and sphingomyelin. J Immunol [Internet]. 1974
        Jun [cited 2017 Nov 30];112(6):2135–47. Available from:
        http://www.ncbi.nlm.nih.gov/pubmed/4151108

22.   Agrawal A, Shrive AK, Greenhough TJ, Volanakis JE. Topology and structure of
        the C1q-binding site on C-reactive protein. J Immunol [Internet]. 2001 Mar 15
        [cited 2017 Nov 30];166(6):3998–4004. Available from:
        http://www.ncbi.nlm.nih.gov/pubmed/11238646

23.   Roux KH, Kilpatrick JM, Volanakis JE, Kearney JF. Localization of the

phosphocholine-binding sites on C-reactive protein by immunoelectron microscopy. J Immunol [Internet]. 1983 Nov 1 [cited 2017 Nov 30];131(5):2411–5. Available from: http://www.ncbi.nlm.nih.gov/pubmed/6195262

24.   Thompson D, Pepys MB, Wood SP. The physiological structure of human C-reactive protein and its complex with phosphocholine. Structure [Internet]. 1999 Feb 15 [cited 2017 Nov 30];7(2):169–77. Available from: http://www.ncbi.nlm.nih.gov/pubmed/10368284

25.   Kinoshita CM, Ying SC, Hugli TE, Siegel JN, Potempa LA, Jiang H, et al. Elucidation of a protease-sensitive site involved in the binding of calcium to C-reactive protein. Biochemistry [Internet]. 1989 Dec 12 [cited 2017 Nov 30];28(25):9840–8. Available from: http://pubs.acs.org/doi/abs/10.1021/bi00451a044

26.   Gang TB, Hammond DJ, Singh SK, Ferguson DA, Mishra VK, Agrawal A. The phosphocholine-binding pocket on C-reactive protein is necessary for initial protection of mice against pneumococcal infection. J Biol Chem. 2012 Dec 14;287(51):43116–25.

27.   Agrawal A, Volanakis JE. Probing the C1q-binding site on human C-reactive protein by site-directed mutagenesis. J Immunol [Internet]. 1994 Jun 1 [cited 2017 Nov 30];152(11):5404–10. Available from: http://www.ncbi.nlm.nih.gov/pubmed/8189060

28.   Póvoa P, Almeida E, Moreira P, Fernandes A, Mealha R, Aragão A, et al. C-reactive protein as an indicator of sepsis. Intensive Care Med [Internet]. 1998 Oct [cited 2017 Dec 1];24(10):1052–6. Available from: http://www.ncbi.nlm.nih.gov/pubmed/9840239

29.   Meisner M. Update on procalcitonin measurements. Ann Lab Med [Internet]. 2014 Jul [cited 2017 Dec 1];34(4):263–73. Available from: http://www.ncbi.nlm.nih.gov/pubmed/24982830

30.   Meisner M, Tschaikowsky K, Hutzler A, Schick C, Schüttler J. Postoperative plasma concentrations of procalcitonin after different types of surgery. Intensive Care Med. 1998;24(7):680–4.

31.   Vashist SK, Venkatesh AG, Marion Schneider E, Beaudoin C, Luppa PB, Luong
       JHT. Bioanalytical advances in assays for C-reactive protein [Internet]. Vol. 34,
       Biotechnology Advances. Elsevier Inc.; 2016 [cited 2020 Feb 24]. p. 272–90.
       Available from: http://www.ncbi.nlm.nih.gov/pubmed/26717866

32.   Collet-Cassart D, Van den Abbeele E, Poncelet S. A quantitative C-reactive
       protein assay using latex agglutination in microtiter plates. J Immunol Methods.
       1989 Dec 20;125(1–2):137–41.

33.   Thomas NE, Coakley WT. Measurement of antigen concentration by an
       ultrasound-enhanced latex immunoagglutination assay. Ultrasound Med Biol.
       1996 Jan 1;22(9):1277–84.

34.   Komoriya T, Inoue N, Yoshimune K, Ogawa M, Moriyama M, Kohno H. Use of
       a highly sensitive latex reagent with amino acid spacer for determination of C-
       reactive protein concentration in a variety of liver diseases. J Biosci Bioeng. 2012
       Nov 1;114(5):560–3.

35.   Deegan O, Walshe K, Kavanagh K, Doyle S. Quantitative detection of C-reactive
       protein using phosphocholine-labelled enzyme or microspheres. Anal Biochem.
       2003 Jan 15;312(2):175–81.

36.   Punyadeera C, Dimeski G, Kostner K, Beyerlein P, Cooper-White J. One-step
       homogeneous C-reactive protein assay for saliva. J Immunol Methods. 2011 Oct
       28;373(1–2):19–25.

37.   Kim SJ, Paczesny S, Takayama S, Kurabayashi K. Preprogrammed, parallel on-
       chip immunoassay using system-level capillarity control. Anal Chem. 2013 Jul
       16;85(14):6902–7.

38.   Islam MS, Lee HG, Choo J, Song JM, Kang SH. High sensitive detection of C-
       reactive protein by total internal reflection fluorescence microscopy on rapidly
       making nanoarray protein chip. Talanta. 2010 Jun 15;81(4–5):1402–8.

39.   Islam MS, Yu H, Lee HG, Kang SH. Molecular switching fluorescence based
       high sensitive detection of label-free C-reactive protein on biochip. Biosens
       Bioelectron. 2010 Nov 15;26(3):1028–35.

40.   Li R, Xue Y, Wang T, Gong L, Peng P, Xiong P, et al. A comparison study

between wide-range and high-sensitivity C-reactive protein assays (Roche Cobas c702) for low C-reactive protein concentration in patients with cardiovascular risk. J Clin Lab Anal [Internet]. 2019 Oct 1 [cited 2020 Mar 1];33(8):e22957. Available from: http://www.ncbi.nlm.nih.gov/pubmed/31218740

41.   Kim HC, Lee SK, Jeon WB, Lyu HK, Lee SW, Jeong SW. Detection of C-reactive protein on a functional poly(thiophene) self-assembled monolayer using surface plasmon resonance. Ultramicroscopy. 2008 Sep 1;108(10):1379–83.

42.   Yeom SH, Han ME, Kang BH, Kim KJ, Yuan H, Eum NS, et al. Enhancement of the sensitivity of LSPR-based CRP immunosensors by Au nanoparticle antibody conjugation. Sensors Actuators, B Chem. 2013 Feb 1;177:376–83.

43.   Vance SA, Sandros MG. Zeptomole detection of C-reactive protein in serum by a nanoparticle amplified surface plasmon resonance imaging aptasensor. Sci Rep. 2014 May 30;4(1):1–7.

44.   Salvo P, Dini V, Kirchhain A, Janowska A, Oranges T, Chiricozzi A, et al. Sensors and biosensors for C-reactive protein, temperature and pH, and their applications for monitoring wound healing: A review [Internet]. Vol. 17, Sensors (Switzerland). MDPI AG; 2017 [cited 2020 Mar 1]. Available from: http://www.ncbi.nlm.nih.gov/pubmed/29257113

45.   Johnson A, Song Q, Ko Ferrigno P, Bueno PR, Davis JJ. Sensitive affimer and antibody based impedimetric label-free assays for C-reactive protein. Anal Chem. 2012 Aug 7;84(15):6553–60.

46.   Arrata I, Barnard A, Tomlinson DC, Wilson AJ. Interfacing native and non-native peptides: using Affimers to recognise α-helix mimicking foldamers. Chem Commun [Internet]. 2017 Mar 2 [cited 2020 Sep 8];53(19):2834–7. Available from: https://pubs.rsc.org/en/content/articlehtml/2017/cc/c6cc09395g

47.   Carrington G, Tomlinson D, Peckham M. Exploiting nanobodies and Affimers for superresolution imaging in light microscopy [Internet]. Vol. 30, Molecular Biology of the Cell. American Society for Cell Biology; 2019 [cited 2020 Sep 8]. p. 2737–40. Available from: /pmc/articles/PMC6789155/?report=abstract

48.   Bryan T, Luo X, Bueno PR, Davis JJ. An optimised electrochemical biosensor

for the label-free detection of C-reactive protein in blood. Biosens Bioelectron. 2013 Jan 15;39(1):94–8.

49.   Kumar D, Prasad BB. Multiwalled carbon nanotubes embedded molecularly imprinted polymer-modified screen printed carbon electrode for the quantitative analysis of C-reactive protein. Sensors Actuators, B Chem. 2012 Aug 1;171–172:1141–50.

50.   Christodoulides N, Mohanty S, Miller CS, Langub MC, Floriano PN, Dharshan P, et al. Application of microchip assay system for the measurement of C-reactive protein in human saliva. Lab Chip. 2005 Feb 22;5(3):261–9.

51.   Wang J, Guo J, Zhang J, Zhang W, Zhang Y. RNA aptamer-based electrochemical aptasensor for C-reactive protein detection using functionalized silica microspheres as immunoprobes. Biosens Bioelectron [Internet]. 2017 Sep 15 [cited 2020 Mar 7];95:100–5. Available from: http://www.ncbi.nlm.nih.gov/pubmed/28431362

52.   Hwang J, Seo Y, Jo Y, Son J, Choi J. Aptamer-conjugated live human immune cell based biosensors for the accurate detection of C-reactive protein. Sci Rep. 2016 Oct 6;6.

53.   Wang MS, Black JC, Knowles MK, Reed SM. C-reactive protein (CRP) aptamer binds to monomeric but not pentameric form of CRP. Anal Bioanal Chem [Internet]. 2011 Sep [cited 2020 Mar 1];401(4):1309–18. Available from: http://www.ncbi.nlm.nih.gov/pubmed/21725632

54.   Bini A, Centi S, Tombelli S, Minunni M, Mascini M. Development of an optical RNA-based aptasensor for C-reactive protein. Anal Bioanal Chem [Internet]. 2008 Feb [cited 2020 Mar 7];390(4):1077–86. Available from: http://www.ncbi.nlm.nih.gov/pubmed/18066708

55.   Eid C, Palko JW, Katilius E, Santiago JG. Rapid Slow Off-Rate Modified Aptamer (SOMAmer)-Based Detection of C-Reactive Protein Using Isotachophoresis and an Ionic Spacer. Anal Chem [Internet]. 2015 Jul 7 [cited 2020 Mar 7];87(13):6736–43. Available from: http://www.ncbi.nlm.nih.gov/pubmed/26024067

56.   Duo J, Chiriac C, Huang RYC, Mehl J, Chen G, Tymiak A, et al. Slow Off-Rate
        Modified Aptamer (SOMAmer) as a Novel Reagent in Immunoassay
        Development for Accurate Soluble Glypican-3 Quantification in Clinical
        Samples. Anal Chem [Internet]. 2018 Apr 17 [cited 2020 Sep 8];90(8):5162–70.
        Available from: https://pubs.acs.org/sharingguidelines

57.   Qureshi A, Gurbuz Y, Kallempudi S, Niazi JH. Label-free RNA aptamer-based
        capacitive biosensor for the detection of C-reactive protein. Phys Chem Chem
        Phys [Internet]. 2010 Aug 28 [cited 2020 Mar 7];12(32):9176–82. Available
        from: http://www.ncbi.nlm.nih.gov/pubmed/20648264

58.   Pultar J, Sauer U, Domnanich P, Preininger C. Aptamer-antibody on-chip
        sandwich immunoassay for detection of CRP in spiked serum. Biosens
        Bioelectron [Internet]. 2009 Jan 1 [cited 2020 Mar 7];24(5):1456–61. Available
        from: http://www.ncbi.nlm.nih.gov/pubmed/18951012

59.   Bernard ED, Nguyen KC, DeRosa MC, Tayabali AF, Aranda-Rodriguez R.
        Development of a bead-based aptamer/antibody detection system for C-reactive
        protein. Anal Biochem [Internet]. 2015 Mar 1 [cited 2020 Mar 7];472:67–74.
        Available from: http://www.ncbi.nlm.nih.gov/pubmed/25481739

60.   Deftos LJ, Roos BA, Parthemore JG. Calcium and skeletal metabolism. West J
        Med [Internet]. 1975 Dec [cited 2017 Nov 30];123(6):447–58. Available from:
        http://www.ncbi.nlm.nih.gov/pubmed/1105981

61.   Baruti Gafurri Z, Pacarizi H, Zhubi B, Begolli L, Topciu V. The importance of
        determining procalcitonin and C reactive protein in different stages of sepsis.
        Bosn J basic Med Sci [Internet]. 2010 Feb [cited 2017 Nov 30];10(1):60–4.
        Available from: http://www.ncbi.nlm.nih.gov/pubmed/20192933

62.   Assicot M, Gendrel D, Carsin H, Raymond J, Guilbaud J, Bohuon C. High serum
        procalcitonin concentrations in patients with sepsis and infection. Lancet
        (London, England) [Internet]. 1993 Feb 27 [cited 2017 Dec 1];341(8844):515–8.
        Available from: http://www.ncbi.nlm.nih.gov/pubmed/8094770

63.   Jin M, Khan AI. Procalcitonin: Uses in the Clinical Laboratory for the Diagnosis
        of Sepsis. Lab Med. 2010 Mar 1;41(3):173–7.

64.   Jacobs JW, Lund PK, Potts JT, Bell NH, Habener JF. Procalcitonin is a glycoprotein. J Biol Chem [Internet]. 1981 Mar 25 [cited 2017 Dec 1];256(6):2803–7. Available from: http://www.ncbi.nlm.nih.gov/pubmed/7204375

65.   Morgenthaler NG, Struck J, Fischer-Schulz C, Seidel-Mueller E, Beier W, Bergmann A. Detection of procalcitonin (PCT) in healthy controls and patients with local infection by a sensitive ILMA. Clin Lab. 2002;48(5–6):263–70.

66.   Vijayan AL, Ravindran S, Saikant R, Lakshmi S, Kartik R, Manoj G. Procalcitonin: A promising diagnostic marker for sepsis and antibiotic therapy. Vol. 5, Journal of Intensive Care. BioMed Central Ltd.; 2017.

67.   Linscheid P, Seboek D, Schaer DJ, Zulewski H, Keller U, Müller B. Expression and secretion of procalcitonin and calcitonin gene-related peptide by adherent monocytes and by macrophage-activated adipocytes. Crit Care Med [Internet]. 2004 Aug [cited 2017 Dec 1];32(8):1715–21. Available from: http://www.ncbi.nlm.nih.gov/pubmed/15286549

68.   Meisner M, Müller V, Khakpour Z, Toegel E, Redl H. Induction of procalcitonin and proinflammatory cytokines in an anhepatic baboon endotoxin shock model. Shock [Internet]. 2003 Feb [cited 2017 Dec 1];19(2):187–90. Available from: http://www.ncbi.nlm.nih.gov/pubmed/12578130

69.   Wiedermann FJ, Kaneider N, Egger P, Tiefenthaler W, Wiedermann CJ, Lindner KH, et al. Migration of human monocytes in response to procalcitonin. Crit Care Med [Internet]. 2002 May [cited 2017 Dec 1];30(5):1112–7. Available from: http://www.ncbi.nlm.nih.gov/pubmed/12006810

70.   Hoffmann G, Czechowski M, Schloesser M, Schobersberger W. Procalcitonin amplifies inducible nitric oxide synthase gene expression and nitric oxide production in vascular smooth muscle cells. Crit Care Med [Internet]. 2002 Sep [cited 2017 Dec 1];30(9):2091–5. Available from: http://www.ncbi.nlm.nih.gov/pubmed/12352046

71.   Hoffmann G, Totzke G, Seibel M, Smolny M, Wiedermann FJ, Schobersberger W. In vitro modulation of inducible nitric oxide synthase gene expression and nitric oxide synthesis by procalcitonin. Crit Care Med [Internet]. 2001 Jan [cited

2017 Dec 1];29(1):112–6. Available from:
http://www.ncbi.nlm.nih.gov/pubmed/11176169

72.   Nasir IA, Mele HU, Babayo A, Yahaya F. Serum Procalcitonin Assay for
       Investigations and Clinical Management of Neonatal Sepsis: A Review. J Pediatr
       Infect Dis [Internet]. 2015 [cited 2020 Apr 12];10:3–11. Available from:
       http://dx.doi.org/

73.   Mathew B, Roy D D, Kumar TV. The Use of Procalcitonin as a Marker of Sepsis
       in Children. J Clin DIAGNOSTIC Res [Internet]. 2013 Feb [cited 2017 Dec
       1];7(2):305–7. Available from: http://www.ncbi.nlm.nih.gov/pubmed/23543035

74.   Moulin F, Raymond J, Lorrot M, Marc E, Coste J, Iniguez JL, et al. Procalcitonin
       in children admitted to hospital with community acquired pneumonia. Arch Dis
       Child [Internet]. 2001 Apr [cited 2017 Dec 1];84(4):332–6. Available from:
       http://www.ncbi.nlm.nih.gov/pubmed/11259234

75.   Gendrel D, Raymond J, Assicot M, Moulin F, Iniguez JL, Lebon P, et al.
       Measurement of procalcitonin levels in children with bacterial or viral
       meningitis. Clin Infect Dis [Internet]. 1997 Jun [cited 2017 Dec 1];24(6):1240–2.
       Available from: http://www.ncbi.nlm.nih.gov/pubmed/9195090

76.   Pfister R, Kochanek M, Leygeber T, Brun-Buisson C, Cuquemelle E, Machado
       MB, et al. Procalcitonin for diagnosis of bacterial pneumonia in critically ill
       patients during 2009 H1N1 influenza pandemic: a prospective cohort study,
       systematic review and individual patient data meta-analysis. Crit Care [Internet].
       2014 Mar 10 [cited 2017 Dec 1];18(2):R44. Available from:
       http://www.ncbi.nlm.nih.gov/pubmed/24612487

77.   van Nieuwkoop C, Bonten TN, van't Wout JW, Kuijper EJ, Groeneveld GH,
       Becker MJ, et al. Procalcitonin reflects bacteremia and bacterial load in urosepsis
       syndrome: a prospective observational study. Crit Care [Internet]. 2010 [cited
       2017 Dec 1];14(6):R206. Available from:
       http://www.ncbi.nlm.nih.gov/pubmed/21083886

78.   Liaudat S, Dayer E, Praz G, Bille J, Troillet N. Usefulness of procalcitonin serum
       level for the diagnosis of bacteremia. Eur J Clin Microbiol Infect Dis [Internet].
       2001 Aug [cited 2017 Dec 1];20(8):524–7. Available from:

http://www.ncbi.nlm.nih.gov/pubmed/11681430

79.   Peters RPH, Twisk JWR, van Agtmael MA, Groeneveld ABJ. The role of
       procalcitonin in a decision tree for prediction of bloodstream infection in febrile
       patients. Clin Microbiol Infect [Internet]. 2006 Dec [cited 2017 Dec
       1];12(12):1207–13. Available from:
       http://www.ncbi.nlm.nih.gov/pubmed/17121627

80.   Irwin AD, Carrol ED. Procalcitonin. Vol. 96, Archives of Disease in Childhood:
       Education and Practice Edition. Royal College of Paediatrics and Child Health;
       2011. p. 228–33.

81.   Lippi G, Salvagno GL, Gelati M, Pucci M, Lo Cascio C, Demonte D, et al. Two-
       center comparison of 10 fully-automated commercial procalcitonin (PCT)
       immunoassays. Clin Chem Lab Med. 2019 Dec 18;58(1):77–84.

82.   Dipalo M, Guido L, Micca G, Pittalis S, Locatelli M, Motta A, et al. Multicenter
       comparison of automated procalcitonin immunoassays. Pract Lab Med. 2015 Aug
       1;2:22–8.

83.   Home - B·R·A·H·M·S PCT (Procalcitonin) [Internet]. [cited 2020 Apr 15].
       Available from: https://www.procalcitonin.com/

84.   Kutz A, Hausfater P, Oppert M, Alan M, Grolimund E, Gast C, et al. Comparison
       between B·R·A·H·M·S PCT direct, a new sensitive point-of-care testing device
       for rapid quantification of procalcitonin in emergency department patients and
       established reference methods - A prospective multinational trial. Clin Chem Lab
       Med [Internet]. 2016 Apr 1 [cited 2020 Apr 7];54(4):577–84. Available from:
       http://www.ncbi.nlm.nih.gov/pubmed/26426890

85.   Dipalo M, Gnocchi C, Avanzini P, Musa R, Di Pietro M, Aloe R. Comparison of
       procalcitonin assays on KRYPTOR and LIAISON® XL analyzers. Diagnostics.
       2019 Sep 1;9(3).

86.   Procalcitonin test - PCT test - AQT90 FLEX immunoassay analyzer [Internet].
       [cited 2020 Apr 15]. Available from:
       https://www.radiometer.com/en/products/immunoassay-testing/aqt90-flex-
       immunoassay-analyzer/pct-on-the-aqt90-flex-immunoassay-

analyzer?addcanonical=true&

87.   Murasaki M, Nakanishi T, Kano K ichi, Shigemi R, Tanizaki S, Kono K, et al.
       Point-of-care procalcitonin may predict the need for surgical treatment in patients
       with small bowel obstruction. Am J Emerg Med. 2020;0(0).

88.   Mine L, Petit M, Nivet-Antoine V, Beaudeux JL, Hennequin C. Dosage de la
       procalcitonine (PCT) en microméthode sur analyseur AQT90 FLEX® et étude de
       la stabilité in vitro. Ann Biol Clin (Paris) [Internet]. 2018 Jan 1 [cited 2020 Apr
       7];76(1):53–9. Available from: http://www.ncbi.nlm.nih.gov/pubmed/29199155

89.   Chiang CY, Huang TT, Wang CH, Huang CJ, Tsai TH, Yu SN, et al. Fiber optic
       nanogold-linked immunosorbent assay for rapid detection of procalcitonin at
       femtomolar concentration level. Biosens Bioelectron. 2020 Mar 1;151:111871.

90.   Chen P, Xia F, Tian D, Zhou C. A Dual-Coreactants Electrochemiluminescent
       Immunosensor for Procalcitonin Detection Based on CdS-MoS 2
       Nanocomposites . J Electrochem Soc. 2018 Mar 27;165(5):B196–201.

91.   Zhou Y, Shao X, Han Y, Zhang H. Detection of procalcitonin (PCT) using the
       double antibody sandwich method based on fluorescence resonance energy
       transfer between upconversion nanoparticles and quantum dots. Anal Methods.
       2018 Mar 7;10(9):1015–22.

92.   Lim JM, Ryu MY, Kim JH, Cho CH, Park TJ, Park JP. An electrochemical
       biosensor for detection of the sepsis-related biomarker procalcitonin. RSC Adv.
       2017;7(58):36562–5.

93.   Sener G, Ozgur E, Rad AY, Uzun L, Say R, Denizli A. Rapid real-time detection
       of procalcitonin using a microcontact imprinted surface plasmon resonance
       biosensor. Analyst. 2013 Nov 7;138(21):6422–8.

94.   Lee G, Shiesh S, Huang C, Lin H. US8624008B2 - Aptamer and detection
       method for C-reactive protein - Google Patents [Internet]. [cited 2020 Feb 25].
       Available from: https://patents.google.com/patent/US8624008B2/en

95.   Potempa LA, Yao Z-Y, Ji S-R, Filep JG, Wu Y. Solubilization and purification
       of recombinant modified C-reactive protein from inclusion bodies using
       reversible anhydride modification. Biophys Reports. 2015 Aug 18;1(1):18–33.

96.   Laurent P, Potempa L, Gewurz H, Al E. The titration curve of native C reactive protein. Wiley Online Libr [Internet]. 1983 [cited 2020 Feb 29]; Available from: https://onlinelibrary.wiley.com/doi/abs/10.1002/elps.1150040414

97.   Potempa LA, Maldonado BA, Laurent P, Zemel ES, Gewurz H. Antigenic, electrophoretic and binding alterations of human C-reactive protein modified selectively in the absence of calcium. Mol Immunol. 1983;20(11):1165–75.

98.   Tolba M, Ahmed MU, Tlili C, Eichenseher F, Loessner MJ, Zourob M. A bacteriophage endolysin-based electrochemical impedance biosensor for the rapid detection of Listeria cells. Analyst. 2012 Dec 21;137(24):5749–56.

99.   Shervedani RK, Farahbakhsh A, Bagherzadeh M. Functionalization of gold cysteamine self-assembled monolayer with ethylenediaminetetraacetic acid as a novel nanosensor. Anal Chim Acta. 2007 Mar 28;587(2):254–62.

100. Jarczewska M, Rębiś J, Górski Ł, Malinowska E. Development of DNA aptamer-based sensor for electrochemical detection of C-reactive protein. Talanta [Internet]. 2018 Nov 1 [cited 2020 Mar 1];189:45–54. Available from: http://www.ncbi.nlm.nih.gov/pubmed/30086945

101. Moutachakkir M, Hanchi AL, Baraou A, Boukhira A, Chellak S. Caractéristiques immunoanalytiques de la protéine C-réactive et de la protéine C-réactive ultrasensible. Ann Biol Clin (Paris) [Internet]. 2017 Mar 1 [cited 2020 Mar 3];75(2):225–9. Available from: http://www.ncbi.nlm.nih.gov/pubmed/28377336

102. Lipopolysaccharide | C205H366N3O117P5 - PubChem [Internet]. [cited 2020 Mar 3]. Available from: https://pubchem.ncbi.nlm.nih.gov/compound/Lipopolysaccharide

103. Schulze S, Wehrhold M, Hille C. Femtosecond-pulsed laser written and etched fiber bragg gratings for fiber-optical biosensing. Sensors (Switzerland) [Internet]. 2018 Sep 1 [cited 2020 Mar 7];18(9). Available from: http://www.ncbi.nlm.nih.gov/pubmed/30154380

104. Wu B, Jiang R, Wang Q, Huang J, Yang X, Wang K, et al. Detection of C-reactive protein using nanoparticle-enhanced surface plasmon resonance using an aptamer-antibody sandwich assay. Chem Commun. 2016 Feb 28;52(17):3568–

71.

105. Wu B, Chen N, Wang Q, Yang X, Wang K, Li W, et al. A simple label-free aptamer-based method for C-reactive protein detection. Anal Methods. 2016 Jun 7;8(21):4177–80.

106. Kao WC, Chen YW, Chu CH, Chang WH, Shiesh SC, Wang YL, et al. Detection of C-reactive protein on an integrated microfluidic system by utilizing field-effect transistors and aptamers. Biomicrofluidics. 2017 Jul 1;11(4).

107. Zhang X, Chi KN, Li DL, Deng Y, Ma YC, Xu QQ, et al. 2D-porphrinic covalent organic framework-based aptasensor with enhanced photoelectrochemical response for the detection of C-reactive protein. Biosens Bioelectron. 2019 Mar 15;129:64–71.

108. Yang YN, Lin HI, Wang JH, Shiesh SC, Lee G Bin. An integrated microfluidic system for C-reactive protein measurement. Biosens Bioelectron. 2009 Jun 15;24(10):3091–6.

109. Zubiate P, Zamarreño CR, Sánchez P, Matias IR, Arregui FJ. High sensitive and selective C-reactive protein detection by means of lossy mode resonance based optical fiber devices. Biosens Bioelectron. 2017 Jul 15;93:176–81.

110. Salazar J, Martínez MS, Chávez M, Toledo A, Añez R, Torres Y, et al. C-Reactive Protein: Clinical and Epidemiological Perspectives. Cardiol Res Pract. 2014;2014.

111. Watts NR, Singh RP. Peptides as standards for denaturing isoelectric focusing. Electrophoresis [Internet]. 1995 Jan [cited 2020 Mar 12];16(1):22–7. Available from: http://www.ncbi.nlm.nih.gov/pubmed/7537658

112. Carr DA, Gómez-Burgaz M, Boudes MC, Peppas NA. Complexation hydrogels for the oral delivery of growth hormone and salmon calcitonin. Ind Eng Chem Res. 2010 Dec 1;49(23):11991–5.

113. Recombinant Procalcitonin (PCT) | RPA689Hu02 | Homo sapiens (Human) Cloud-Clone Corp.(CCC) [Internet]. [cited 2020 Mar 12]. Available from: http://www.cloud-clone.com/products/RPA689Hu02.html

114.   PCT recombinant protein | Procalcitonin (PCT) Recombinant Protein-
       NP_001029124.1 [Internet]. [cited 2020 Mar 12]. Available from:
       https://www.mybiosource.com/recombinant-protein/procalcitonin-pct/2018533

115.   Samsudin I, Vasikaran SD. Clinical utility and measurement of procalcitonin.
       Vol. 38, Clinical Biochemist Reviews. Australasian Association of Clinical
       Biochemists; 2017. p. 59–68.

116.   Martinez de la Torre Y, Fabbri M, Jaillon S, Bastone A, Nebuloni M, Vecchi A,
       et al. Evolution of the Pentraxin Family: The New Entry PTX4. J Immunol. 2010
       May 1;184(9):5055–64.

117.   Daigo K, Inforzato A, Barajon I, Garlanda C, Bottazzi B, Meri S, et al.
       Pentraxins in the activation and regulation of innate immunity. Vol. 274,
       Immunological Reviews. Blackwell Publishing Ltd; 2016. p. 202–17.

118.   Goodman AR, Cardozo T, Abagyan R, Altmeyer A, Wisniewski HG, Vilček J.
       Long pentraxins: An emerging group of proteins with diverse functions
       [Internet]. Vol. 7, Cytokine and Growth Factor Reviews. Elsevier Ltd; 1996
       [cited 2020 Apr 15]. p. 191–202. Available from:
       http://www.ncbi.nlm.nih.gov/pubmed/8899296

119.   Moalli F, Jaillon S, Inforzato A, Sironi M, Bottazzi B, Mantovani A, et al.
       Pathogen Recognition by the Long Pentraxin PTX3. J Biomed Biotechnol.
       2011;2011:15.

General discussion, concluding remarks and future outlook

5.1 General discussion

Despite symptoms of sepsis being first described more than 3000 years ago, the condition remains one of the leading causes of death worldwide (1). It is well established that sepsis results from an uncontrolled and prolonged activation of host immune system due to pathogenic insult (2,3). The immunopathogenesis of sepsis makes the condition hard to diagnose, as its starting point shows common symptoms of infection. The absence of a "gold-standard" clinically-useful, sepsis-specific, biomarker has resulted in a huge research effort to identify potential novel candidate biomarkers possessing the requisite sensitivity and specificity (4). However, at the time of writing, clinicians still have to use standard blood tests for the diagnosis and monitoring of patients. For some time, it has been postulated that a multiplex platform, able to sensitively detect a panel of biomarkers, will be needed. The present study therefore aimed to develop three individual biosensors targeting lipopolysaccharide (LPS), c-reactive protein (CRP) and procalcitonin (PCT). Although lipopolysaccharide has been ubiquitously connected with sepsis, it is not a frequently measured biomarker, due to a number of limitations associated with current testing methods. On the other hand, CRP and PCT have been extensively used to diagnose and monitor inflammatory phenomena in a clinical environment, although not in a near-patient format meaning blood samples are taken and sent for laboratory analysis, thereby presenting a delay to diagnosis and patient monitoring.

Chapters 2 and 3 focused on the development of a sensitive system for the detection of LPS. In Chapter 2, an aptamer sequence previously reported in the literature was selected and an aptasensor developed using mixed sensing surfaces comprising the aptamer and a range of alkanethiols (5). More precisely, a wide selection of alkanethiols were screened against LPS to observe binding interaction. Considering that LPS is negatively charged under physiological conditions (pH 7.4), the alkanethiols of choice were 4,4-dithiodibutiric acid (DTBA), 11-mercaptoundecanoic acid (MUA) and 6-mercaptohexanol (MCH). MCH was shown to interact most with LPS, and therefore in an attempt to minimise the amount of non-specific binding to the final aptasensor, this alkanethiol was discarded in favour of MUA and DTBA. Proposed steric hindrance effects observed with aptamer / MUA mixed SAMs (ratio 1:10) led to DTBA being selected as the final alkanethiol.

A programme of optimisation was undertaken to establish the ideal ratio of aptamer : DTBA. Six different mixed SAMs were developed (2:1, 1:5, 1:12.5, 1:25,1:32.5 & 1:50) and challenged with a variety of LPS concentrations. The molar ratios of 1:12.5 and 1:25 demonstrated the best results; ratios of 2:1 and 1:5 suggested that steric hindrance between the aptamers was a problem, whilst ratios of 1:32.5 and 1:50 resulted in too few aptamers bound to the surface, meaning small changes in impedance where observed when incubated with LPS. The screening study showed that a 1:20 molar ratio of aptamer:DTBA resulted in optimal performance.

The determination of the optimal ratio between aptamer and DTBA led to the full characterisation of the aptasensor. A baseline impedance of 31.3 kΩ, with a standard deviation of 0.699 (CV of 2.24%) was observed for the 1:20 mixed SAM. The system was shown to be able to detect as little as 100 fg/ml, with its linear range starting from between 1 and 5 pg/ml. The linear range reached its maximum when challenged with a concentration of 100 pg/ml ($R^2 = 0.9922$). Fitting of the binding data to a Langmuir model (based on binding to one specific site) indicated an apparent K_d of 17.62 pM (92.25 pg/ml).

Specificity studies followed. Unlike all existing studies, the newly developed aptasensor was challenged with (1→3)-β-glucan (GLU) and lipoteichoic acid (LTA). The rationale for picking these molecules as cross reactants was based on the fact the commercially available endotoxin test (LAL assay) provides false positive results in the presence of glucans, whilst LTA is a component of the outer membranes of Gram-positive bacteria and is therefore likely to be present in clinical sepsis samples. The aptamer proved its high selectivity to LPS, with minimal responses recorded when challenged with the cross-reactants. Finally, the aptasensor was shown to be regenerated by washing with 0.05 % Tween 20 for five minutes.

The ease of development in combination with the low LOD makes the aptasensor developed in Chapter 2 competitive when compared to existing studies, many of which employ complex chemistries or secondary transduction mechanisms that elongate the total assay time. The results obtained in this Chapter also provide an important baseline for moving on to developing the hybrid system in Chapter 3. Chapter 3 described the integration of the aptamer with an electropolymer in a hybrid imprinting strategy. In general, molecularly imprinted polymers (MIPs) perform poorly in aqueous environments

as many of the interactions between the target and polymer rely on hydrogen bonding. Furthermore, the generation of effective MIPs for molecules which lack defined chemical functionality, size and conformation is extremely challenging. LPS is only soluble in water, is made up of lipid chains and sugar moieties and even within bacterial species, displays a considerable amount of heterogeneity in terms of size and shape. Consequently, very few examples of MIP systems being successfully developed for the detection of LPS (and similar molecules) can be found in the literature.

Since the aptamer properties were already known from the proceedings of Chapter 2, Chapter 3 started with the evaluation of electropolymers and their level of interaction with LPS. A rational approach to electroactive monomer selection was applied, using literature to identify those most likely to interact strongly with LPS. Aniline (ANI), aminophenylboronic acid (APBA), dopamine (PDA) and aminobenzoic acid (ABA) were selected as monomers to be taken into a screening study. PANI showed excessive interaction with LPS, most likely as a consequence of its high porosity, while PABA showed high changes in impedance but high variance within the responses. For these reasons, these two monomers were dropped from the study.

APBA and DA were used to develop conventional surface imprinted MIPs in the absence of the aptamer. This experiment aimed to further explore the interaction with the target molecule. Although the conventional systems displayed similar imprinting factors, PAPBA showed slightly better results. The experimental process suffered from high standard deviations, showing how difficult it is to produce synthetic recognition systems for molecules such as LPS. Nevertheless, it was decided to progress with APBA as boronic acids are able to interact strongly with diols and it was thought this would confer better specificity to the final system than dopamine.

The second part of Chapter 3 focused on the development of the hybrid recognition system, comprising the aptamer and PAPBA. The aptamer / LPS complex was immobilised on the working electrodes and varying polymerisation cycles (from 4 to 10) were applied to determine the optimal polymer thickness for providing maximum target recognition. Polymers produced following the application of 3 or less cycles were unstable, whilst apta-MIPs produced using 5 polymerisation cycles or less, showed responses similar to those seen with the aptasensor (Chapter 2), suggesting negligible contribution from the polymer to target recognition. On the other hand, higher number of

polymerisation cycles (9 and 10) showed responses similar to those of bulk polymers, as the polymer overgrew the aptamer-LPS complex, making target exit from, and re-entry to, the imprinted cavity difficult. The apta-MIP showed optimal results when 7 polymerisation cycles were used. The apta-MIP showed significantly greater responses when compared to the non-imprinted counterpart (apta-NIP) at all LPS concentrations tested.

The optimisation of the apta-MIP led to the system's full characterisation, following the approaches elucidated in Chapter 2. The system's apparent K_d equals to 1.68 pM (8.4 pg/ml) obtained after the fitting the data to a "one site – total" (Langmuir-Freundlich) model ($R^2 = 0.9442$). The LOD was shown to be an impressive 1 fg/ml while the linear dynamic range falls between 100 fg/ml to 1 ng/ml (R^2 0.9955). The detection range could be further expanded from 10 fg/ml to 10 ng/ml without significant loss of linearity (R^2 0.9857).

The apta-MIP's selectivity results were shown to be in line with that demonstrated by the aptasensor in Chapter 2. Despite the addition of PAPBA, the apta-MIP showed limited interaction with GLU and LTA. The hybrid system showed limited changes in ΔR when challenged with up to 500 μg/ml human serum albumin (HSA), the most abundant protein in blood serum. However, changes in impedance of up to ~ 37 % were recorded when the system was challenged with 5,000 μg/ml (5 mg/ml) of HSA. Biofouling of the system resulted in less than ideal recovery of LPS from spiked serum.

The hypothesis of developing a hybrid MIP for the detection of LPS - covered in the proceedings of Chapter 3 – leaves Chapter 2 rather short when compared to all the other Chapters. For instance, the LPS aptasensor was not challenged with LPS spiked in blood serum, despite the acquisition of promising results in aquatic environments. The SAM's rigid packing might show better results than the hybrid MIP, based on the results obtained from Chapter 4. In fact, minimal interaction of a monolayer comprising aptamers and alkanethiols was demonstrated, meaning that the levels of biofouling could be less than the ones anticipated in the case of the hybrid MIP.

Both the systems developed in Chapter 2 and 3, show superiority when compared to the commercially available LAL assay, since they were able to detect LPS at the same (aptasensor) or lower levels (apta-MIP). As stated before, the biofouling observed with the apta-MIP when challenged with biological samples prevented the accurate detection

of spiked LPS, meaning that further optimisation of the system is needed. Therefore, the present study showcases the development of label-free bioassays displaying the same drawbacks with the existing commercial tests. The statement can be further supported considering that the study didn't challenge the aptasensor with (spiked) blood serum. Regarding the hybrid MIP performance, further sample preparation techniques should be explored; for example, centrifugation and / or filtering of the sample following heating and acid treatment.

Chapter 4 focused on the development of biosensors for c-reactive protein (CRP) and procalcitonin (PCT). Both biomarkers have been used extensively in clinical settings to diagnose and monitor patients in cases of sepsis and other inflammatory or infectious diseases. Although there are reports of CRP aptasensors in the literature, an aptasensor targeting PCT has not been described despite their being a commercially available sequence.

Chapter 4 tried to build up on the approaches established during the proceedings of Chapter 2 however, the development of the CRP sensor showed that deposition of mixed aptamer / alkanethiol SAMs resulted in poor responses. Consequently, a backfilling approach was used where MCH was added following aptamer modification of the electrode. The system showed a linear dynamic range over 250 fg/ml (LOD) to 1 pg/ml ($R^2 = 0.96$). Fitting the data to a Langmuir model ($R^2 = 0.9357$) an apparent K_d of 6.17 fM was determined.

The CRP sensor demonstrated satisfactory results when challenged with the other two targets of the present study (PCT, LPS), recording minimal responses over the vast majority of tested concentrations. A relatively large increase in impedance following the incubation with 1 pg/ml LPS was observed, however the response returned to just above baseline when the aptasensor was challenged with 100 pg/ml. Unfortunately, time constraints prevented further investigation of this outcome.

The CRP aptasensor was challenged with serum, in a similar way as described in Chapter 3. Although the blank readings of diluted serum (1/100) were encouraging, only the incubation with 500 fg/ml of CRP gave a response somewhat close to the expected value (75.8 %), showing the current inability of the aptasensor to deliver desirable data.

The PCT sensor demonstrated issues with its development from the very early stages. The selected aptamer was unable to form a mixed SAM with any of the alkanethiols. The only available scenario was to develop an aptamer-only SAM and backfill with MCH, as per the protocol evaluated for the development of the CRP aptasensor. The baseline readings of the aptasensor also demonstrated high standard deviations, resulting in an LOD of 10 pg/ml. This is also the start of the system's linear range. Unlike all other systems, the PCT aptasensor scored a relatively low R^2 value of 0.9495 when regressing the linear response region, despite the range being very narrow (10 pg/ml to 100 pg/ml). Application of the Langmuir model to the full binding isotherm data showed a poor fit ($R^2 = 0.7946$), giving low confidence in the determination of an apparent K_d of 6.82 pM (98.85 pg/ml).

Although the system behaved exceptionally well when challenged with a range of diluted serums, recovery of spiked PCT was far from optimal. Significant further work would be needed to generate a clinically useful PCT aptasensor.

The aptasensors designed for both CRP and PCT need to be further developed and optimised. The key to obtain reproducible results for both surfaces is mainly focused on their stability. The anti-CRP aptamer proved that it can co-immobilise with MCH in acceptable levels. However, the backfilling approach leaves gaps on the gold surface and favours steric hindrance effects between the aptamers. This makes the recognition of CRP more complicated, considering the size of the targeted molecule, which also favours steric hindrance.

It might be useful for future studies to find an alkanethiol able to co-immobilise with the aptamer and produce results similar to the level of the LPS aptasensor. A second scenario could be the utilisation of EDC /NHS chemistry, however this would not be ideal. The increase of the impedances due to the monolayer itself would decrease the system's sensitivity. This wouldn't be much of a problem, since the sensor's sensitivity can shift from the scale of femtogram/ml towards the picogram/ml, without affecting the accuracy of the detection, since the CRP concentration in blood samples is a lot higher. On the other hand, more than one aptameric sequences can be further explored to determine the molecule that performs the best in the system.

The PCT aptasensor shows the least promising results, meaning that its development needs to be reconsidered. Unfortunately, the Literature does not provide information about the development of PCT specific aptasensors, underlining its difficulty to develop

these recognition surfaces. Initially, the thiolation levels of the PCT aptamer need to be examined, in order to ensure the ability of the aptamer to bind to the surface of interest. If thiolation wouldn't enhance the aptamer's binding performance, then other immobilisation approaches would be explored (EDC / NHS chemistry). Unlike the case of CRP, only one aptameric sequence targeting PCT is available. Therefore, the approach needs to shift towards antibodies, if the aptamer is generally dysfunctional when used with the study's system parameters.

5.2 Development of a multiplex platform able to detect PCT, CRP and LPS

The concept of developing a multiplex diagnostic platform for the determination of sepsis biomarkers is not unique, with many research groups pursuing this common goal. The existence of such studies showcasing similar objectives further highlights the need to develop rapid and accurate point-of-care (POC) tests to enable rapid and accurate clinical decision making, thus improving patient outcomes.

Focusing on the biomarkers studied in the current work, Tanak *et al.* demonstrated the non-faradaic impedimetric profiling of PCT and CRP (6). The developed biosensor would serve a dual role in order to detect the biomarkers of interest during the early stages of sepsis. The present study shares the same technology as theirs, as EIS was employed to determine the levels of each biomarker. However, Tanak and co-workers used monoclonal antibodies to develop their sensors, immobilising them on gold surfaces with the aid of dithiobis (succinimidyl propionate) (DSP). The POC sensor shows a LOD of 100 pg/ml for PCT and 100 ng/ml for CRP when challenged with human serum and blood. From a personal point of view, the results obtained after the challenge of PCT are ambiguous, despite the high R^2 values (0.99 and 0.98), since the linear range has only been determined with 4 and 3 points for human serum and whole blood respectively. When testing CRP, 5 points have been used during the calibration process for both fluids. The range of applied concentrations spans 0.01 to 20 µg/ml when the system is challenged with human serum and 0.01 to 10 µg/ml with whole blood. The R^2 in the first case is 0.9, while in the second case the R^2 equals 0.98.

Rongbin and co-workers developed an immunosensor platform for POC testing of inflammatory biomarkers (7). The immunosensor is portable, resembling a pencil and the

platform is portable weighing less than 3 kg (Figure 4.6). Apart from PCT and CRP, the developed system is also able to determine the presence of interleukin-6 (IL-6) in human serum samples. The system's dynamics are quite impressive considering that the platform is designed to detect 3 different biomarkers. CRP's LOD is reported to be ~ 30 ng/ml with a linear range between 0.1 to 80 µg/ml ($R^2 = 0.9756$), whilst the LOD for PCT is determined to be ~10 pg/ml, with a linear range from 0.05 to 200 ng/ml ($R^2 = 0.9902$). Despite the minor interest, the IL-6 assay shows a linear response between 5 pg/ml and 10 ng/ml ($R^2 = 0.9832$), with a LOD of ~1 pg/ml.
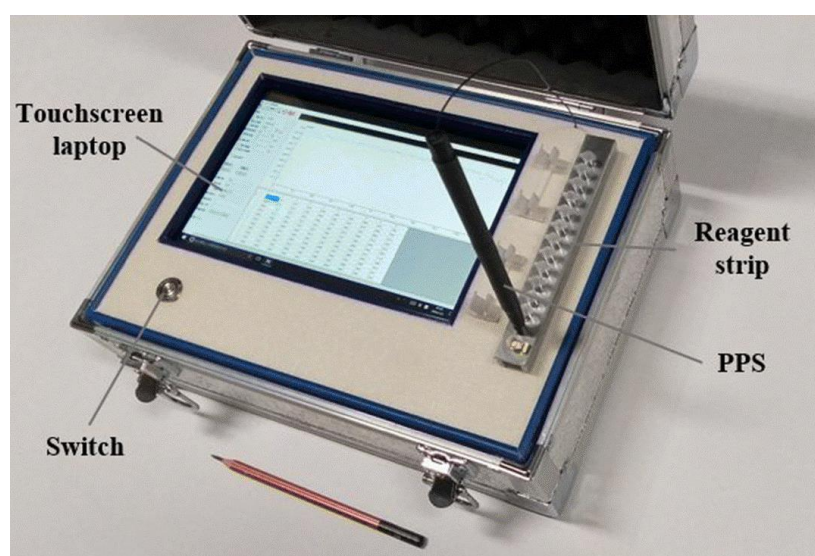

Figure 5.1: The portable platform designed from Rongbin et al. (7). The portable pencil sensor (PPS) can be seen in the picture.

Lastly, Selvam and Prasad published a work focusing on the development of a multiplex POC platform, aiming for the accurate and rapid diagnosis of sepsis. The study employs the use of EIS and target-specific antibodies that detect PCT, LPS and LTA. All three biomarkers were successfully detected in whole blood. The system's LOD was 1 µg/mL for both LPS and LTA (dynamic range: 1µg/ml to 1000 µg/ml) and 0.1 ng/ml for PCT (dynamic range: 01.1 ng/mL to 10 µg/mL).

Despite the differences in performance between the multiplex platforms and the present study, these studies cannot be directly compared due to two main reasons. The first reason has to deal with the fact that the biosensors of the present study are distant from the

optimal performance when challenged with biological fluids. The second and most important reason underlines the fact that all the generated systems were challenged as individual sensors and not as part of a multiplex platform.

The main question arising from the conclusions of the present study focuses on how far the present project is from developing a multiplex platform. The key limitation across all biosensors developed is the current poor performance observed when challenged with 'real-world' samples. With further optimisation of both sample preparation approaches and the sensor systems themselves, it would be possible to unify them in a single platform, for example, using impedance analysers able to measure multiple electrodes at the same time. Lab-on-a-chip approaches could help reduce the footprint and increase the automation of the system such that it would be attractive to both the commercial and clinical worlds. In the future, menu expansion could see other disease markers added to the platform. Such a multiplex platform, deployed at point-of-care, would not only decrease the costs and time of running these tests in standard laboratory settings but most importantly, it would save lives.

5.3 Bibliography

1.   World Sepsis Day Factsheet.

2.   Bhan C, Dipankar P, Chakraborty P, Sarangi PP. Role of cellular events in the pathophysiology of sepsis. Inflamm Res [Internet]. 2016 Nov 8 [cited 2019 Jun 22];65(11):853–68. Available from: http://www.ncbi.nlm.nih.gov/pubmed/27392441

3.   Delano MJ, Ward PA. The immune system's role in sepsis progression, resolution, and long-term outcome. Immunol Rev [Internet]. 2016 [cited 2019 Jun 22];274(1):330–53. Available from: http://www.ncbi.nlm.nih.gov/pubmed/27782333

4.   Pierrakos C, Vincent J-L. Sepsis biomarkers: a review. Crit Care [Internet]. 2010 [cited 2017 Apr 21];14(1):R15. Available from: http://www.ncbi.nlm.nih.gov/pubmed/20144219

5.   Kim SE, Su W, Cho M, Lee Y, Choe WS. Harnessing aptamers for electrochemical detection of endotoxin. Anal Biochem [Internet]. 2012;424(1):12–20. Available from: http://dx.doi.org/10.1016/j.ab.2012.02.016

6.   Tanak AS, Jagannath B, Tamrakar Y, Muthukumar S, Prasad S. Non-faradaic electrochemical impedimetric profiling of procalcitonin and C-reactive protein as a dual marker biosensor for early sepsis detection. Anal Chim Acta X. 2019 Nov 1;3:100029.

7.   Nie R, Huang J, Xu X, Yang L. A portable pencil-like immunosensor for point-of-care testing of inflammatory biomarkers. Anal Bioanal Chem. 2020 Mar 14;1–9.